

Université du Québec
INRS -Énergie, matériaux et télécommunications

Novel Silicate-based Membranes for Direct Methanol Fuel Cells

Par
Valeria Felice

Thèse présentée pour l'obtention du grade de
Philosophiae doctor (Ph.D.) en Science de l'Énergie et des Matériaux

Jury d'évaluation

Président du jury et examinateur interne:	Professeur Jean-Pol Dodelet INRS - Énergie, matériaux et télécommunications
Examineur interne:	Professeur Royson Paynter INRS - Énergie, matériaux et télécommunications
Examinatrice externe:	Docteure Asmae Mokrini Conseil National de Recherche du Canada
Examineur externe:	Professeur Enrico Traversa, International Center for Materials Nanoarchitectonics National Institute for Materials Science
Directrice de recherche:	Professeure Ana C. Tavares INRS - Énergie, matériaux et télécommunications

Abstract

Direct methanol fuel cells (DMFCs) attract a lot of interest, due to the high energy density of methanol and the simple and quick refill of the device. However, the DMFC performance is limited by the methanol crossover through Nafion, the state of the art electrolyte.

In this work zeolite-based materials are proposed as electrolyte for DMFCs.

Zeolites are aluminosilicates with a well-ordered pore system which could act as a barrier to the passage of methanol. However, an improvement of their proton conductivity ($\sim 10^{-4}$ S cm⁻¹) is required to be competitive with Nafion (~ 0.1 S cm⁻¹ at 25°C).

Three commercial Faujasites (CBV600, CBV720 and CBV780) with different Si/Al ratios (3.4 to 48.7) and surface areas (530 to 823 m² g⁻¹) were used as starting materials. In order to increase the proton conductivity and to make them suitable to be used in a fuel cell assembly, Faujasites were functionalized with sulfonic acid groups and blended with polymers.

The stability of Faujasite in acidic conditions was first tested by exposure to 6 mol dm⁻³ HCl for up to 7000 hours. Dealumination due to the acid exposure occurred within the first 24h but the zeolite structure remained intact. The dealumination induced secondary porosity and an increase of the water uptake at high relative humidity, which increased the proton conductivity.

The functionalization was carried out by grafting of mercapto-silane and subsequent conversion of the mercapto- groups into sulfonic acid groups by H₂O₂ treatment. The effect of the silane precursor concentration, and of the chemical and textural characteristics of the parent zeolites on the extent of functionalization were evaluated. In spite of a significant decrease of specific surface area and water uptake, the proton conductivity increased from 2.2×10^{-6} to 1×10^{-5} S cm⁻¹ for the CBV600 and by a factor of 3 for the CBV720 and CBV780 series (up to 3.4×10^{-4} S cm⁻¹). The difference in the extent of the increase and in the conductivity values are attributed to a H⁺ dilution effect and to different specific surface areas and water uptakes. Finally, water and methanol sorption measurements on parent and functionalized samples showed that the surface

functionalization improves significantly the zeolite selectivity in terms of water over methanol.

Selected zeolites (as-received and functionalized with sulfonic acid groups) were used in the fabrication of two types of composite membranes: Nafion/CBV780 (0-40 wt%) and CBV780 (up to 60 wt.%) blended with non-ionomer binders (Teflon, PVDF, HDPE, SEBS).

The Nafion/CBV780 composites with a zeolite loading below 2 wt%, show higher thermal stability, higher water mobility and proton conductivity compared to unfilled Nafion. An improvement of the DMFC performance was also observed, although at high methanol concentration (10 mol dm^{-3}) the effect of the methanol crossover through the composite membranes was still significant.

Among the non-ionomer composites, SEBS/60% functionalized CBV780 composite showed higher proton conductivity ($\sim 10^{-3} \text{ S cm}^{-1}$).

Although an improvement is still required, important criteria for the achievement of this goal, related to the zeolite surface modification, selectivity, composite fabrication and the effect of zeolite on the water mobility, are established and presented in this work.

Valeria Felice

Prof. Ana C. Tavares

Acknowledgments

There are many people I would like to thank for their contribution to this thesis.

I am most grateful to my advisor, Prof. Ana Tavares, because she gave me the opportunity to work on this project. During these years, I particularly appreciated her enthusiasm, patience, determination and constant presence and involvement in the research activity, even in the toughest moments of her private life.

A special thank to Dr. Barbara Mecheri for sharing with me her knowledge about ionomers and to Cesar Beatrice for his guidance on the polymer processing during his permanence at INRS-EMT.

I want also to thank Zhonghua Zhang, Francois Desilet and Fawzi Salama for their contribution to the work on the composites materials. Of course, I cannot forget Romain Dugas, for being always collaborative and supportive.

And yet, a thank to Christophe Chabanier for his professionalism and willingness, and all the technicians at INRS-EMT machine shop with whom I interacted almost daily during the first years of my Ph.D.

Finally I would like to thank INRS-EMT, MDEIE and the Laboratoire Conjoint «Advanced Nanostructured Materials for Energy, Catalysis and Biomedical Applications», MELS, CRSNG and CFI for the financial support.

Table of Contents

Abstract.....	ii
Acknowledgement.....	iv
Table of Contents.....	v
List of Figures.....	x
List of Tables.....	xvii
Preface.....	xix
1. Introduction.....	1
1.1 A general overview of fuel cell technology.....	1
1.2 Proton Exchange Membranes Fuel cells and Direct Methanol Fuel Cells.....	3
1.2.1 Polymer Electrolyte Membranes.....	6
1.2.1.1 Nafion®: the state of the art membrane for PEMFC and DMFC.....	7
1.2.1.2 Alternative approaches: Nafion modification and innovative materials.....	11
1.3 Objectives of the work.....	12
1.4 Structure of the thesis.....	14
1.5 References.....	15
2. Zeolites and their composites.....	19
2.1 Zeolites.....	19
2.1.1 Chemical and structural properties.....	19
2.1.2 Zeolite proton conductivity.....	22
2.2. State of the art of the use of zeolite as electrolyte material for fuel cells.....	24
2.3 Starting material.....	25
2.4 Zeolite Modification.....	26
2.4.1 Dealumination.....	27
2.4.1.1 Dealumination: Experimental Procedure.....	28
2.4.2 Surface functionalization.....	29
2.4.2.1 State of the art of functionalized zeolites.....	31

2.4.2.2 Experimental procedure.....	33
2.5 Composite membranes.....	34
2.5.1. Polymeric matrix: Nafion and non-conductive binders.....	35
(a) Polyvinylidene fluoride.....	35
(b) Polytetrafluoroethylene.....	36
(c) High Density Polyethylene.....	37
(d) Styrene-ethylene butylene-styrene.....	38
2.5.2 Composite fabrication methods.....	39
(a) Solution Casting.....	39
(b) Extrusion.....	39
2.5.2.1 Experimental procedure for the membrane fabrication.....	40
(a) Nafion-zeolite composites.....	40
(b) Nafion-functionalized zeolite composites.....	41
(c) PVDF-zeolite composites.....	42
(d) PTFE-zeolite composites.....	42
(e) PE-Zeolite, SEBS-zeolite and HDPE/SEBS (50/50)-zeolite composites.....	43
2.6 References.....	44
3. Characterization techniques.....	52
3.1 Sorption measurements.....	54
3.1.1 N ₂ sorption measurements.....	58
3.1.1.1 Data analysis.....	58
a) Determination of the Specific Surface Area: Brunauer, Emmett, and Teller theory.....	58
b) Determination of the Total Pore Volume.....	59
c) Determination of the micropore volume: t-Plot de Boer Method.....	60
d) Determination of the mesopore volume: Barrett, Joyner and Halenda method.....	61
e) Micropore and Mesopore Volume determination:	

Non Local -Density Functional Theory.....	61
3.1.1.2 Experimental Procedure.....	63
3.1.2 Water and Methanol sorption measurements:	
Dynamic Vapor Sorption.....	63
3.1.2.1 Principle of the technique and description of the apparatus.....	63
3.1.2.2 Determination of the diffusion coefficients from DVS	
measurements.....	65
3.1.2.3 Determination of the different state of water.....	67
3.1.2.4 Experimental conditions.....	69
3.2 Water uptake from liquid water.....	71
3.3. Differential Scanning Calorimetry.....	71
3.3.1 Principles of the technique.....	71
3.3.2 Experimental procedure.....	73
3.4. Ion Exchange Capacity.....	74
3.5 Neutron Activation Analysis.....	74
3.5.1 Principles of the technique.....	74
3.5.2 Experimental conditions and equipment details.....	75
3.6 Thermogravimetric Analysis.....	75
3.7 Dynamic flash combustion method.....	75
3.8 Fourier Transform-Infrared Spectroscopy.....	76
3.8.1 Principle of the technique.....	76
3.8.2 Experimental Procedure.....	77
3.9 X-Ray Photoelectron Spectroscopy.....	78
3.9.1 Principle of the technique.....	78
3.9.2 Experimental.....	79
3.10 X-Ray-Diffraction.....	79
3.10.1 Principle of the technique.....	80
3.10.2 Experimental procedure.....	81
3.11 Electrochemical Impedance Spectroscopy.....	81
3.11.1 Theory.....	81
3.11.2 Experimental conditions.....	83

3.12 Ex-situ membrane proton conductivity measurements.....	85
3.12.1 Through – plane proton conductivity.....	85
3.12.2 In-plane proton conductivity.....	86
3.13 Direct Methanol Fuel Cell tests.....	87
3.14 References.....	88
4. Faujasite dealumination.....	91
4.1 Chemical and structural characterization of dealuminated samples.....	91
4.2. Textural characterization.....	97
4.3. Water sorption.....	101
4.4. Proton Conductivity.....	104
4.5. Concluding remarks.....	108
4.6. References.....	110
5. Sulfonic acid grafted Faujasites.....	111
5.1 Zeolite functionalization.....	111
5.1.1 Grafting of mercaptopropyl groups.....	111
5.1.2 Conversion of –SH into –SO ₃ H.....	114
5.2 N ₂ adsorption measurements.....	118
5.3 Water and methanol uptake.....	121
5.4 Proton Conductivity.....	126
5.5 Concluding remarks.....	129
5.6 References.....	130
6. Composite membranes.....	132
6.1 Nafion-Faujasite Composite Membranes.....	132
6.1.1. Effect of Nafion activation treatment on CBV780 zeolite.....	133
6.1.2 Thermogravimetric analysis.....	134
6.1.3. X-ray photoelectron spectroscopy.....	136

6.1.4. Water uptake, membrane porosity and ion exchange capacity.....	138
6.1.5 State of water and its mobility: DSC and DVS analysis.....	141
6.1.5.1 DSC.....	141
6.1.5.2 Dynamic Vapor Sorption measurements.....	144
6.1.6. Proton conductivity and Fuel cell performances.....	146
6.1.7 Concluding remarks.....	152
6.2 Polymer-zeolite composite membranes.....	153
6.2.1. Polyvinylidene fluoride-Zeolite composite membranes	153
6.2.2 Zeolite-Teflon.....	154
6.2.3 HDPE based and Kraton® based zeolite composite membranes.....	156
6.2.4 Concluding remarks.....	161
6.3 References.....	161
7. Conclusion.....	163
7.1 Future work.....	167
7.2 References.....	167
Résumé.....	169

List of Figures

Chapter 1

- Figure 1.1:** Schematic illustration of a fuel cell device using H₂ as a fuel and proton exchange electrolyte.....1
- Figure 1.2:** Cell voltage as a function of the current density for a state of the art hydrogen-fuelled PEMFC and DMFC(with permission from[1] Copyright 2003 John Wiley and Sons).....5
- Figure 1.3:** Chemical structure of Nafion® 117; where $x = 5-13.5$, $y = 1000$ and $z \geq 1$7
- Figure 1.4:** Illustration of the model of the structural evolution of Nafion as a function of λ (with permission from [17], Copyright 2003, The Electrochemical Society).....8
- Figure 1.5:** Illustration of the Cluster-Channel model (with permission from [20], Copyright 1983, Elsevier).....9

Chapter 2

- Figure 2.1:** Scheme of zeolite a) dealumination (in acid conditions) and b) desililation (in basic conditions) (with permission from [9] Copyright 2010, American Chemical Society).....20
- Figure 2.2:** Example of building units constituting one of many zeolite structure: 1. TO₄ tetrahedra (T=Al, Si), 2. Secondary building unit formed by 6 tetrahedra, 3. sodalite or β cage, 4. Sodalitic structure.....21
- Figure 2.3:** H⁺ transport mechanisms for (a) the Grotthuss (hopping) and (b) the vehicle mechanisms in a solid acid (adapted with permission from [18] Copyright 2006, American Chemical Society).....24
- Figure 2.4:** FAU structure model showing the size (in nm) of the super-cage and window.....25
- Figure 2.5:** Illustration of the FAU structure with mesoporosity induced by post-synthesis dealumination (with permission from [35] Copyright 1999, Elsevier).....27

Figure 2.6: Illustration of a grafting mechanism of a tryalkoxysilane onto a substrate in presence of water [39].....	30
Figure 2.7: Illustration of a grafting mechanism of a monoalkoxysilane onto a substrate in anhydrous conditions [39].....	31
Figure 2.8: Illustration of the grafting of 3-MPTMS onto the zeolite surface and conversion of the mercapto-group into sulfonic acid groups(adapted with permission from reference [57], Copyright 2005, Elsevier).....	33
Figure 2.9: Polyvinylidene fluoride.....	36
Figure 2.10: Polytetrafluoroethylene.....	37
Figure 2.11: Polyethylene.....	38
Figure 2.12: Styrene-ethylene butylene-styrene block copolymer.....	38
Figure 2.13: a) The extruder, b) open chambers and screws, c) closed chamber with hopper.....	40

Chapter 3

Figure 3.1: IUPAC classification of sorption isotherms (from [1]).....	56
Figure 3.2: IUPAC classification of hysteresis loops (from [1]).....	56
Figure 3.3: IUPAC classification of adsorption isotherms for materials with different hydrophilicity (with permission from [4] Copyright 2008, Elsevier).....	57
Figure 3.4: Kinetics of water sorption of CBV600 at 25°C and at different partial pressures.....	64
Figure 3.5: Illustration of the DVS apparatus interfaced with a personal computer.....	65
Figure 3.6: M_t/M_∞ versus $t^{1/2}$ at 25°C and at 97%P/P for Nafion recast.....	66
Figure 3.7: Typical curve fitting (Park's model) of experimental sorption isotherm data (unfilled Nafion recast, T=25 °C) and the corresponding fitting parameters. C_w [SA], C_w [NSA], C_w [C] refers to specific adsorbed water, non-specific adsorbed water and clustered water, respectively.....	68
Figure 3.8: DSC thermogram of Nafion recast.....	73

Figure 3.9: Scheme of the photoelectric effect (adapted with permission from [25], Copyright 1996, Elsevier).....	79
Figure 3.10: Illustration of the diffraction of X-rays by a crystal. The black dots represent the atoms while the lines represent the family of parallel planes with Miller index hkl and distant d from each other.....	80
Figure 3.11: Equivalent circuit diagram (adapted with permission from [29], Copyright 1994, Elsevier). C_g , geometric capacitance; R_b , ion conductivity within the bulk of the crystal, R_{gb} , grain-boundary resistance; C_{gb} grain-boundaries capacitance; C_{dl} , double layer capacitance, R_{pl} , polarization resistance.....	82
Figure 3.12: Nyquist diagram of CBV600 as-received.....	83
Figure 3.13: Illustration of the cell used for the EIS measurement.....	84
Figure 3.14: Four electrodes glass cell used for through-plane proton conductivity measurements.....	85
Figure 3.15: Four Pt electrodes cell.....	86

Chapter 4

Figure 4.1: Si/Al molar ratio as a function of the dealumination time, t_D , for CBV600, CBV720 and CBV780 series.....	91
Figure 4.2: X-ray diffraction patterns of the CBV600 zeolite, as received (black)) and after acid exposure for 24h (red)) and 7000h (blue))......	92
Figure 4.3: (a) Infrared spectra of CBV600 zeolite as-received and after 6h of acid treatment; (b) Peak wavenumber of the T-O-T asymmetric stretching band of CBV600, CBV720 and CBV780 as a function of the Si/Al ratio.....	94
Figure 4.4: Correlation between the Si/Al molar ratio determined by XPS and by NAA for the CBV600 series; as-received ($t_D = 0$) and after $t_D = 0.5h$, 48h and 7000h.....	95
Figure 4.5: Evolution of the Al (2p) core level spectrum with the dealumination time for the CBV600 series, as received ($t_D = 0$) and after acid exposure for 0.5h, 48h and 7000h; Al _I - Al contribution ascribed to the framework Al; Al _{II} - Al contribution ascribed to the extraframework Al.....	96
Figure 4.6: N ₂ adsorption and desorption isotherms of CBV600 as received (black) and after 48h (red) and 7000h (blue).....	97

Figure 4.7: Comparison between micropore and mesopore volumes obtained by the t-plot de Boer method and the BJH method, respectively and by NL-DFT. Each column in the isograms is divided into two parts separating the micropore volume and the mesopore volume. Micropores on bottom, mesopores on top.....99

Figure 4.8: Pore volume as a function of the pore diameter in the range between 8 Å and 60 Å; a) CBV600 series, as received (black), after 6h (red), 168h (blue) and 7000h (green) of acid treatment; b) CB720 and c) CBV780 as received (black) and after 1.5h (red), 6h (blue) and 168h (green) of acid treatment. The inserts in each figure show the pore volume as a function of the pore diameter in a range between 8 Å and 20 Å.....100

Figure 4.9: Water adsorption and desorption isotherms recorded for CBV600 samples, as received (black) and dealuminated for 48h (red) and 7000h (blue) at 25°C.....101

Figure 4.10: Water uptake at a) 10% RH, b) 50% RH and c) 90% RH as a function of the Si/Al ratio; CBV600, CBV720 and CBV780 series.....102

Figure 4.11: Proton conductivity as a function of the relative humidity for a) CBV600, b) CBV720 and c) CBV780 as received (●) and dealuminated for $t_D = 0.5h$ (○), $t_D = 1.5h$ (×), $t_D = 6h$ (Δ), $t_D = 48h$ (▲), $t_D = 168h$ (◇), $t_D = 4500h$ (□) and $t_D = 7000h$ (■); 100% relative humidity on the x-axis corresponds to the conditioning of the samples by immersion in water104

Figure 4.12: Proton conductivity at 90% RH as a function of a) the Si/Al ratio, b) water uptake at 90%RH and c) the mesopore (20-60Å) volume for CBV600, CBV720 and CBV780.....106

Figure 4.13: Proton conductivity of samples immersed in liquid water as a function of (a) micropore (< 20Å) volume and (b) mesopore (20-60Å) volume for CBV600, CBV720 and CBV780.....107

Chapter 5

Figure 5.1: Thermograms (TG (black) and DTG (red)) of CBV600 a) as-received and b) grafted ((-SH) form) using 41 mmol g⁻¹ of 3-MPTMS.....112

Figure 5.2: Amount of silane (-SH form) determined by TGA as a function of the 3-MPTMS concentration.....113

Figure 5.3: X-ray photoelectron spectra of the S2p peak of the grafted samples prepared with 41 mmol g⁻¹ of silane precursor: before oxidation ($t_{ox} = 0$), after partial conversion ($t_{ox} = 3h$) of the mercapto group into sulfonic acid group and after complete conversion ($t_{ox} = 6h$). The oxidation treatment was carried out at 50 °C.....115

Figure 5.4: Conversion yield as a function of the oxidation time, t_{ox} , at 25°C and at 50°C.....116

Figure 5.5: Amount of silane after oxidation ((-SO ₃ H)-form) as a function of the amount of 3-MPTMS.....	117
Figure 5.6: Amount of silane (-SO ₃ H-form) after oxidation at 50°C and for 6h as a function of the amount of silane (-SH form) before the oxidation treatment.....	117
Figure 5.7: Specific surface area (S _{BET}) as a function of the amount of the silane grafted (SO ₃ H-form) onto the zeolite for the three series of functionalized zeolites.	119
Figure 5.8: Micropore a) and mesopore b) volume of functionalized samples as a function of the amount of grafted silane (-SO ₃ H form) for CBV600, CBV720 and CBV780 series.....	120
Figure 5.9: Water and methanol adsorption isotherms of as-received CBV600, CBV720 and CBV780.....	121
Figure 5.10: Water (a) and methanol (b) sorption isotherms of CBV600 as received and with 0.44 mmol g ⁻¹ and 1.2 mmol g ⁻¹ of grafted silane.	122
Figure 5.11: Volume of H ₂ O a) and MeOH b) adsorbed per gram of zeolite as a function of the amount of grafted silane at 10%RH.....	123
Figure 5.12: Volume of H ₂ O a) and MeOH b) per gram of zeolite as a function of the amount of grafted silane (-SO ₃ H form) at 97 %P/P ₀	124
Figure 5.13: Ratio between volume of methanol adsorbed and Volume of water adsorbed as a function of the grafted silane a) at 10%P/P ₀ and b) 97%P/P ₀	125
Figure 5.14: Proton conductivity as a function of the degree of functionalization for the CBV600, CBV720 and CBV780.....	127
Figure 5.15: Protons surface density as a function of the silane grafted for the three series of zeolites.....	127
Figure 5.16: λ (at 97%RH) as a function of the amount of grafted silane for CBV600, CBV720 and CBV780.....	128

Chapter 6

Figure 6.1: XRD patterns of a) CBV780 as-received and b) after activation treatment (DACBV780).....	133
--	-----

Figure 6.2: TGA (a) and selected DTG (b) diagrams for the recast Nafion and composite membranes with various zeolite contents prepared from 20 wt% Nafion dispersion.....	134
Figure 6.3: Zeolite wt% after the activation treatment vs the nominal wt% zeolite.....	135
Figure 6.4: O1s (a) and Si2p (b) core level spectra of the dealuminated zeolite, recast Nafion and composite membranes N20_4 and N20_5.....	136
Figure 6.5: Water uptake (wt%) vs zeolite content.....	138
Figure 6.6: Cross-section SEM images of (a) reference Nafion (N20_0) and (b) composite Nafion and 40% zeolite (N20_40). The scale bar and the magnification in the SEM images are 1 μm and 4000 \times , respectively.....	139
Figure 6.7: Water uptake of composite samples of the N20_n, as-prepared (AP) and after hot pressing (HP).....	139
Figure 6.8: IEC as a function of the zeolite content.....	141
Figure 6.9: DSC thermograms of (a) unfilled Nafion and (b) composite at 4.4 wt% of zeolite content (N20_10).....	142
Figure 6.10: θ_F , as a function of the zeolite content for non and hot pressed membranes prepared from a 20% Nafion solution.....	143
Figure 6.11: Water adsorption isotherms of N20_n composite membrane a) before and b) after hot-pressing.....	144
Figure 6.12: Non specific adsorbed water ($\theta_W[\text{NSA}]$) as a function of zeolite content at 97% P/P_0	145
Figure 6.13: D values of Nafion/zeolite composite membranes as a function of the zeolite content at 97% P/P_0	145
Figure 6.14: a) Through-plane and b) in-plane proton conductivity as a function of the zeolite content. The same values of in-plane proton conductivity were determined from both sides of the membranes.....	146
Figure 6.15: a) OCV as a function of the methanol concentration (C); b) maximum power density as a function of the methanol concentration, c) polarization curves and d) power density as a function of the current density of N20_4 before and after hot-pressing. T = 40°C.....	149
Figure 6.16: a) OCV as a function of the methanol concentration (C); b) maximum power density as a function of the methanol concentration; c) polarization curves, and d)	

power density as a function of the current density of commercial N115, N20_0, N20_2 and N20_4 hot-pressed. T = 40°C.150

Figure 6.17: Water uptake of PVDF-zeolite composites; as-prepared (AP), after hot-pressing (HP) and with functionalized zeolite (F).....154

Figure 6.18: a) measured and estimated water uptake and b) through-plane and in-plane proton conductivity of the Teflon-zeolite composite as a function of the zeolite content.....155

Figure 6.19: a) Water uptake of HDPE/CBV780 composite membranes measured after 48h at 97%P/P₀ and after 72h in direct contact with liquid water; estimated zeolite contribution for the water uptake is also included; b) Through-plane (TP) proton conductivity as a function of the zeolite content.....157

Figure 6.20: Water uptake at 97%P/P₀ of HDPE, SEBS and HDPE/SEBS composite membranes unfilled (0% ZEO) and prepared with 50 wt% and 60 wt% of unmodified and functionalized zeolite (ZEO_F).....158

Figure 6.21: Water uptake from liquid water of HDPE, SEBS and HDPE/SEBS composite membranes unfilled (0% ZEO) and prepared with 50 wt% and 60 wt% of unmodified and of functionalized zeolite (ZEO_F).....159

Figure 6.22: Through-plane proton conductivity of HDPE, SEBS and HDPE/SEBS composite membranes, unfilled (0% ZEO) and prepared with 50 wt% and 60 wt% of unmodified and functionalized zeolite (ZEO_F).....159

List of Tables

Chapter 2

Table 2.1: Si/Al molar ratio, specific surface area (S_{BET}), unit cell size, and micropore volume and mesopore (20-60Å) volume of the three commercial H^+ -form Faujasites.....	26
---	----

Chapter 3

Table 3.1: List of techniques used to characterize the zeolite after dealumination (DEA), after functionalization (FUNCT) and the composite membranes.....	53
---	----

Chapter 4

Table 4.1: Degree of crystallinity of CBV600 as-received and following acid exposure for 24h and 7000h, considering different regions of the diffraction patterns.....	93
---	----

Table 4.2: Binding energy, full width half maximum and relative peak area of the Al2p photoelectron lines recorded for CBV600 as-received and dealuminated samples.....	96
--	----

Table 4.3: Specific surface area and total pore volume of the CBV600, CBV720 and CBV780 Faujasite zeolites as a function of the dealumination tim.....	98
---	----

Chapter 5

Table 5.1: Hydrogen content and maximum silane grafted for CBV600, CBV720 and CBV780.....	114
--	-----

Chapter 6

Table 6.1: Composites membrane name, Nafion dispersion concentration and zeolite nominal content.....	133
--	-----

Table 6.2: Physicochemical properties of CBV780 as-received and after activation treatment.....	134
--	-----

Table 6.3: (S/F), (O/F) and (Si/F) atomic ratios of recast Nafion and composite membranes with 10.1 wt% and 21.4 wt% zeolite from XPS.....	137
---	-----

Table 6.4: Melting temperature of freezable water for all composite of the N20_n series before (Non HP) and after (HP) hot-pressing.....	142
---	-----

Table 6.5: Average membrane thickness.....148

Table 6.6: Zeolite content, solvent used during the casting, zeolite - silane form during the cast procedure, through-plane proton conductivity (σ_{TP}), water uptake (%WU) and degree of freezable water ($\theta_F/\%$).....151

Preface

Technological progress represents one of the main factors driving the development of a society, especially if directed to the development of means to exploit energy and put it to work. As affirmed by Leslie White, an American anthropologist known for his theories on cultural evolution, "the primary function of culture" is to "harness and control energy" and "culture evolves as the amount of energy harnessed per capita per year is increased, or as the efficiency of the instrumental means of putting the energy to work is increased" [1].

Beside any evolutionary theory, it is undeniable that an increased level of human comfort generally increases the dependence on external energy sources. Based on the increase in global world energy production in the past decades, the demand for energy is estimated to increase by about 50% in the next 20 years [2,3]. At the moment, most of the world's energy sources are based on the consumption of fossil fuels, which are non-renewable resources and therefore finite. By considering the present consumption rate, it has been estimated that the total petroleum reserve will be exhausted in the next 35 years. The scenario becomes gloomier when fossil fuel consumption is associated with its environmental impact and, in particular, to the increased CO₂ emission in the atmosphere and global warming [4]. The necessity to invest in possible alternatives to fossil fuels has spurred the development of fuel cells.

[1] W.J. Peace, 2007. Leslie A. White: Evolution and Revolution in Anthropology. USA, UNP, Nebraska Paperback.

[2] R.A. Kerr, 2007. "Even Oil Optimists Expect Energy Demand to Outstrip Supply". Science, Vol. 317 p. 437.

[3] Administration, E.I., International Energy Outlook 2010, U.S.D.O. Energy, Editor. 2010: Washington. p. 338.

[4] T.R. Karl, K.E. Trenberth, 2003. "*Modern Global Climate Change*". Science, Vol. 302 p. 1719-1723.

1. Introduction

1.1 A general overview of fuel cell technology

A fuel cell is an electrochemical device which converts the chemical energy of a fuel into electrical energy. The principle is similar to that of a battery although in a fuel cell the fuel and the combustive agent are externally supplied and the device will work continuously as long as there is enough of them, similarly to an internal combustion engine [1-3]. This clearly represents an advantage with respect to batteries, due to faster recharge and the absence of self-discharge. At the same time, fuel cells are a more efficient, non-polluting alternative to the internal combustion engine. A basic scheme of a fuel cell system using hydrogen as a fuel and a proton exchange electrolyte is shown in Figure 1.1.

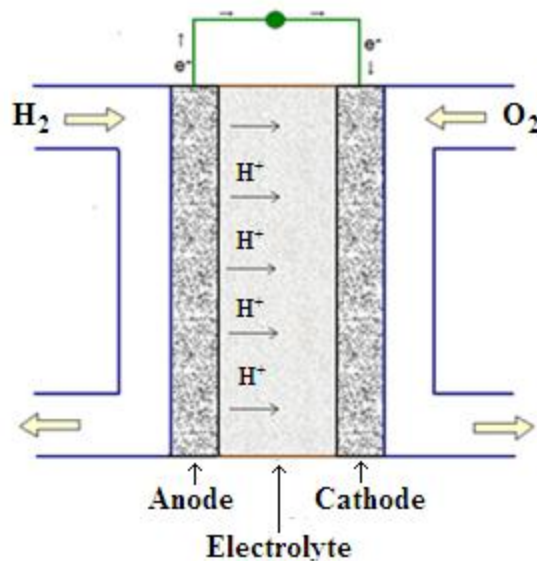


Figure 1.1: Schematic illustration of a fuel cell device using H_2 as a fuel and a proton exchange electrolyte.

As shown in Figure 1.1, the fuel is supplied at the anode where it is oxidized producing electrons and H^+ . The electrons travel through an external circuit to the cathode while the protons reach it through the electrolyte which separates the two electrodes. At the cathode

protons, electrons and O₂ (externally supplied or from air in air-breathing devices) react to produce water.

The anode and cathode reactions are shown in equation E1.1 and E1.2, respectively [1,2,4]:



The overall reaction in the cell is:



Two electrons pass through the external circuit for each molecule of hydrogen used and for each water molecule produced. Therefore, if -e is the charge on 1 electron, the charge that flows per mole of H₂ consumed is:

$$-2Ne = -2F \quad (\text{E1.4})$$

Where N is the Avogadro's number and F is Faraday constant.

If ΔE is the voltage of the fuel cell, then the electrical work done to move this charge round the circuit is -2FΔE. In an ideal system where there are no losses, the electrical work done is also equal to the Gibbs free energy released, ΔG:

$$\Delta G = -2F \cdot \Delta E \rightarrow \Delta E = \frac{-\Delta G}{2F} \quad (\text{E1.5})$$

ΔG = -237.2 kJ mol⁻¹ for the reaction E1.3 at 25 °C, so the electromotive force or reversible open circuit voltage (OCV) of the hydrogen fuel cell operating at 25 °C is 1.23 V [1]. In a real system this value is however never achieved because of energy losses due to several factors such as the slowness of the reactions taking place at the electrodes, the

resistance to the flow of electrons through the electrodes and interconnections and to the ions through the electrolyte. Of course, this is true for any type of fuel cell using hydrogen or any other fuel, although the losses and their extent can significantly vary from type to type. Indeed, among the several classes of fuel cells proposed as possible energy sources, different advantages as well as different drawbacks can be found.

The classification of fuel cells is based on the type of electrolyte and fuel used [1,2,5-7]. Electrolytes can be in a liquid state (such as KOH in alkaline fuel cells, H₃PO₄ in phosphoric acid fuel cells and molten carbonate in molten carbonate fuel cells), ionomer membranes (as in proton exchange membrane fuel cells) or ceramics (as in solid oxide fuel cells). Each class of fuel cell operates at different temperature, from 40°C-80°C (such as for proton exchange membrane fuel cells) up to 1000 °C (such as for solid oxide fuel cells), depending on the electrolyte. Each fuel cell finds application in different sectors, from space vehicles to small portable devices. Among the different types, proton exchange membrane fuel cells, using hydrogen or methanol as a fuel, have attracted great interest and they also represent the application target of the materials studied in the present research work. For this reason, a more detailed description of these devices will be presented in the following paragraphs, for a better understanding of their advantages over the other types of fuel cells and of the most important drawbacks which currently hamper their commercialization.

1.2 Proton Exchange Membrane Fuel cells and Direct Methanol Fuel Cells

Proton exchange membrane fuel cells (PEMFCs) were developed in the late 1950s by W. T. Grubb and L. Niedrach of the General Electric Company [5]. In this kind of device a polymer membrane is employed as the electrolyte and platinum based catalysts are used at both electrodes for H₂ oxidation and O₂ reduction. The membrane originally used in Grubb's work was sulfonated polystyrene, then replaced by Nafion ®, the DuPont trade name for a polyperfluorosulfonic acid ionomer. The use of an ionomer as the electrolyte represents an advantage compared to the use of a liquid electrolyte, due to less complex handling and assembling and security. [1,5]. PEMFCs are compact and robust and they are characterized by a high power density. They are being developed for various

applications, from stationary power generation systems to automotive and portable applications [2]. For fuel cell vehicles, in particular, PEMFCs seem the most suitable among the various types of fuel cells, thanks to the low temperature of operation, the CO₂ tolerance of the electrolyte and a combination of high power density and high energy conversion efficiency [8,2].

PEMFCs were originally designed to be used with hydrogen, which is a high energy density and non-polluting fuel. However, at present there are no sufficient infrastructures to support its widespread use. One very attractive alternative to hydrogen is methanol. Methanol, indeed, is a readily available and low-cost liquid fuel that has a high energy density. The net energy density of methanol (5.3 kWhKg⁻¹) is more than 26 times higher than that of H₂ at 300 bar pressure (0.2 kWhkg⁻¹) [1,2]. A device fed directly with methanol at the anode is simpler to use and very quick to refill. Fuel cells using methanol directly as a fuel are called Direct Methanol Fuel Cells (DMFCs). This kind of device lends itself very well to applications where the power density can be low but the energy density must be high, such as for applications for which the average power is only a few watts, but it must be provided for a very long time like in portable devices (mobile telephones, laptops).

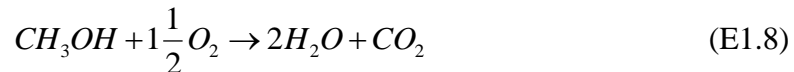
In a DMFC methanol is fed at the anode where it is oxidized [1,2]:



The electrons move through the external circuit while the protons move through the electrolyte to the cathode where the oxygen reduction reaction takes place:



The overall reaction in the DMFC is represented by the equation:



Six electrons are transferred for each molecule of methanol consumed and the reversible cell voltage (Equation E1.5) at 25°C is 1.21V in an ideal case where there are no losses. As for PEMFCs, the DMFC works at low temperature and platinum is used as a catalyst for the methanol oxidation, although an alloy with ruthenium is commonly used at the anode to reduce the poisoning effect of CO on the Pt catalyst site [9, 10]. As for a hydrogen fuel cell, the voltage of a real system is less than 1.21V but with even greater losses. In fact, the oxidation reaction of methanol is more complex and slower compared to the oxidation of hydrogen and the fuel crossover from the anode to the cathode through the electrolyte membrane is very significant for these devices. The **fuel crossover** occurs to some extent in all fuel cells but in a DMFC it is particularly severe and it represents one of the major problems affecting the DMFC performance. The reason for the high methanol crossover lays in the fact that methanol readily mixes with water, which is an essential part of the structure of hydrated Nafion.

The methanol crossover not only causes a waste of fuel but, when methanol reaches the cathode, two simultaneous electrochemical reactions, oxygen reduction and methanol oxidation, will compete for the Pt catalyst sites causing a mixed potential and the decrease of the cell efficiency. The effect induced by the methanol crossover can be easily seen from the comparison between PEMFC and DMFC polarization curves (Figure 1.2).

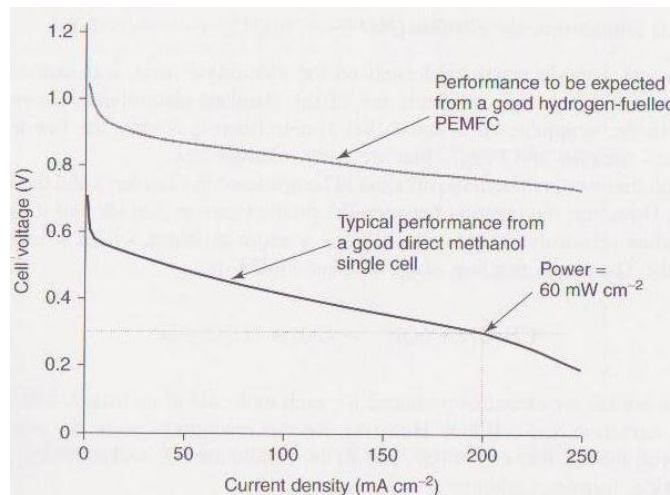


Figure 1.2: Cell voltage as a function of the current density for a state of the art hydrogen-fuelled PEMFC and DMFC (with permission from [1] Copyright 2003, John Wiley and Sons).

As shown in Figure 1.2, the voltage is considerably lower for a DMFC. The difference in OCV between the two types of fuel cells is due to the methanol crossover [11,12]. In order to reduce the effect of the methanol crossover through the electrolyte membrane, the methanol concentration fed at the anode is very low, typically 1M. An increase of the methanol concentration causes an increase of the crossover with a consequent decrease of the fuel cell performance [13].

At the moment a few strategies are used to reduce the fuel crossover, such as the use of a thick anode and thicker electrolyte membranes, or a controlled fuel feed to the anode in such a way that at low current no excess of methanol is fed. These approaches somewhat reduce the effective methanol permeability but at the same time they increase the cost, the cell resistance and the complexity of the system. Moreover, all these approaches do not provide a real solution to the problem, which is intrinsic to Nafion.

An overview of the characteristics, advantages and drawbacks of Nafion and the several approaches that have been proposed to improve its properties or find a better alternative material to replace it are presented in the next paragraphs.

1.2.1 Polymer Electrolyte Membranes

The electrolyte is an important component of a fuel cell, allowing the passage of the ions from the anode to the cathode and assuring the electronic insulation between the electrodes. The electrolyte should also be thermally, chemically and mechanically stable, impermeable to the reactants and preferably inexpensive [1,14]. All these requirements are necessary for the good performance of the fuel cell and for its fast commercialization.

At the moment, Nafion is the material that best fits all the requirements for a good electrolyte for PEMFCs and DMFCs. However, Nafion has very high methanol permeability and although a thicker membrane (Nafion 117, 180 μm) is usually used, the problem of methanol crossover still remains one of the major drawbacks affecting the performance of DMFCs.

1.2.1.1 Nafion®: the state of the art membrane for PEMFC and DMFC

First used as a membrane for chloro-alkali production, Nafion ® started to be employed as a membrane for PEMFC in 1967 and, with the introduction of DMFCs in 1990, it also became the most commonly employed proton exchange membrane for this kind of device [1].

Nafion shows excellent properties for fuel cell applications and these properties are due to its chemical structure (Figure 1.3): its hydrophobic tetrafluoroethylene backbone, in fact, provides a good thermal and chemical stability and its perfluorinated side chain with a terminal hydrophilic sulfonic acid group (-SO₃H) provides the good water sorption capacity and high proton conductivity [15].

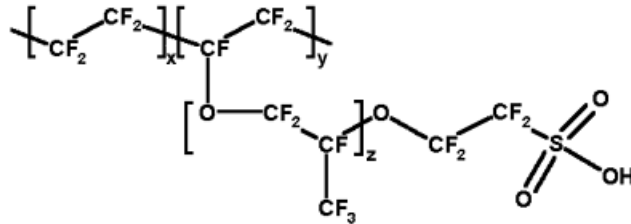


Figure 1.3: Chemical structure of Nafion®; where $x = 5-13.5$, $y = 1000$ and $z \geq 1$.

The high permeability of Nafion and Nafion-like ionomers to methanol is related to their morphological structure and the role played by water. For a better understanding of the main advantages and drawbacks of these materials and for a better design of possible alternative membranes, it is necessary to look at their morphology in more detail. Several models have been proposed to describe the morphology of Nafion [15] and the structural changes occurring in the membrane going from dehydrated to fully hydrated conditions.

One of the most popular models explains how Nafion morphology evolves as a function of the water content, expressed as the number of water molecules per sulfonic acid group, λ [16-18]. An illustration of the different stages proposed by the model as a function of λ is shown in Figure 1.4.

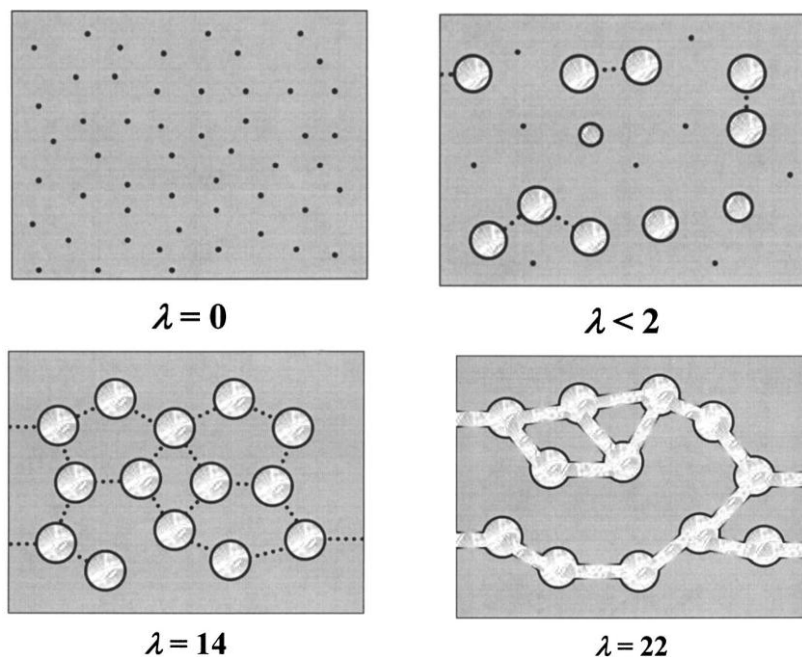


Figure 1.4: Illustration of the model of the structural evolution of Nafion as a function of λ (with permission from [17], Copyright 2003, The Electrochemical Society).

The dry membrane absorbs water which solvates the sulfonic acid groups. With further addition of water, the formation of clusters around the ions occurs, so that inverted interconnected micelles are formed. These clusters continue to grow and start to form interconnections with each other. When these clusters grow enough to be closely linked together by collapsed channels, a transport pathway is formed and this occurs at $\lambda \approx 2$. A complete cluster network is formed for membranes saturated with water vapour ($\lambda = 14$). In contact with liquid water, a structural reorganization occurs. The liquid water infiltrates and expands the channels, causing the formation of a porous structure ($\lambda = 22$) [17]. This model, therefore, also takes into consideration the Schroeder's paradox, first observed in 1903 by von Schroeder who reported a difference in solvent uptake (i.e. swelling) by a solid polymer sample (i.e., gel or membrane) between the sample exposed to a saturated vapor and in contact with a liquid [19].

Several models have been also proposed to describe the cluster geometry and distribution in hydrated Nafion. One of the first and most widespread models proposed to describe the Nafion morphology in its hydrated state is the Cluster-Channel or Cluster-Network model

[15, 20]. This model is based on the presence of ionic clusters approximately spherical in shape and about 4 nm in diameter with an inverted micellar structure, interconnected by short and narrow channels approximately 1 nm in size (Figure 1.5).

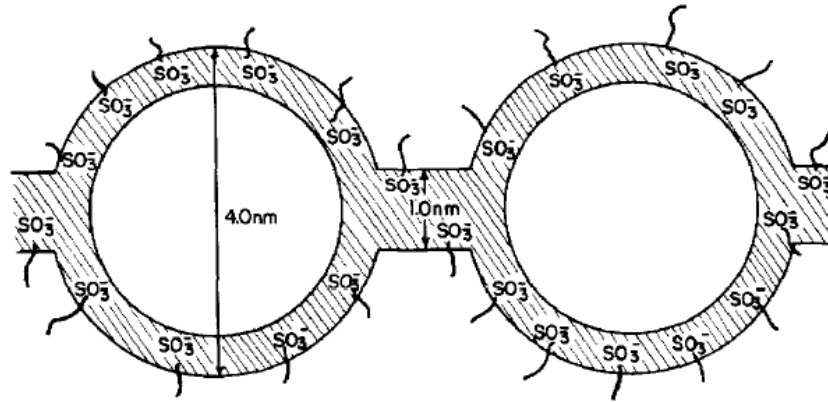


Figure 1.5: Illustration of the Cluster-Channel model (with permission from [20], Copyright 1983, Elsevier).

Successively, other models have been proposed to better fit the results obtained by a further extensive characterization of Nafion membranes. Yeager and Steck proposed a **three-phase model** [21]. Based on this model, the clusters do not have a strict geometrical definition and their geometrical distribution has a lower degree of order and there are transitional interphases between hydrophilic and hydrophobic regions.

The Cluster-Network model could be treated as an idealization of the Yeager and Steck model, where the pathways between the clusters are the interfacial regions.

Other models go from a **core-shell model**, where the ion-rich core is surrounded by an ion poor shell, and a **sandwich model**, where the polymer forms two layers whose sulfonic groups attract across an aqueous layer where transport occurs, [15] to a more recent **water channel model**, where the sulfonic acid functional groups self-organize into hydrophilic water channels of ~ 2.5 nm diameter through which small ions can be easily transported [22].

In spite of differences in the cluster geometry and distribution, most of the models agree on a structure where there is a separation between a hydrophobic domain (the fluorinated

backbone in Nafion) and a hydrophilic domain consisting of a network of ionic clusters comprising the sulfonic acid groups and the absorbed water.

The presence of water is very important because, by affecting the Nafion morphology, it affects the proton diffusion through the membrane and, consequently, its proton conduction properties. Water also plays an important role in the mechanism of proton transport itself and this is an important aspect to be considered.

Two main mechanisms are proposed to explain the proton transfer through Nafion: the Grotthuss mechanism and the vehicle mechanism [17, 18].

In the **vehicle mechanism**, the protons attach themselves to a vehicle, water, and the vehicles diffuse through the medium, carrying the protons along with them. On the other hand, the **Grotthuss mechanism** involves stationary vehicle molecules, the water molecules, (no translational motion of the vehicle molecules), with the proton itself moving from molecule to molecule, a process known as ‘hopping’. The proton transport in Nafion is caused by both the vehicle and Grotthuss mechanism, although the contribution of one mechanism over the other in the proton transport process can vary as a function of the humidification conditions [17, 18].

In both cases, water is a leading factor in the proton transport through the membrane and its presence is, therefore, essential to high proton conductivity. This requires a membrane that is constantly well-hydrated under operational conditions in order to achieve a good performance. Although of fundamental importance for the proton conduction, the presence of water in the membrane does contribute to the diffusion of methanol through it. In fact, other than the gradient in concentration and pressure (occurring at OCV), the methanol transport through the membrane is also due to the electro-osmotic drag effect [23, 24]. In fact, the proton flux through the membrane causes water transport in the same direction due to the hydration of the protons and the methanol molecules are also carried through the membrane by the same mechanism. In order to limit the methanol crossover, low concentration methanol solutions, typically 1-2M, are used, consequently lowering the efficiency of the DMFCs. However, a high methanol concentration causes an increase of the methanol concentration gradient and also of the electro-osmotic drag due to an increase of the channel diameter in the membranes through which the molecules can be carried along in the solvating envelope more easily [24].

1.2.1.2 Alternative approaches: Nafion modification and innovative materials

Several solutions have been proposed to overcome the problem of methanol crossover through the proton exchange membrane in DMFCs and/or to reduce its cost. Several alternative materials other than Nafion have been proposed in the last years including both other fluorinated materials (such as Flemion, Aciplex) and non-fluorinated materials such as ionomers based on polyphosphazene, polysiloxanes, polystyrene, polyimide, polyetherketones, polyether-ether-ketones, aromatic polysulfones and polyphenylsulfones [25,26]. However, these materials show either poor mechanical properties or chemical instability in fuel cell operating conditions.

A more recent approach consists of the fabrication of composite membranes obtained by adding inorganic/organic compounds to Nafion. Composite membranes using Nafion and several different inorganic fillers are reported in literature [27]. Many types of inorganic fillers such as SiO₂ [28-30], ZrO₂ [29], Al₂O₃ [29,31], TiO₂ [32,33], and zirconium phosphate [34-36,14] have been reported to decrease the methanol crossover in Nafion membranes. The filler is added to Nafion to increase the tortuosity of the methanol pathway. However, most of the composite membranes have a lower proton conductivity than pure Nafion, although an increase of the maximum working temperature is sometimes obtained [14], which could represent a benefit for PEMFCs.

Another approach is the use of proton conducting inorganic fillers, in order to avoid the decrease of proton conductivity when blended with Nafion. However, as Nafion is always the main component of the composite, the problems related to the methanol crossover are not completely eliminated. In an ideal case, the use of Nafion should be avoided. With a sufficiently high proton conductivity, the inorganic fillers could replace Nafion as a main component. The use of an inorganic material as the proton conductor could provide advantages in terms of selectivity towards methanol, as they are not subject to swelling as Nafion and Nafion-like ionomers commonly are.

1.3 Objectives of the work

The objective of the present work is to find an alternative membrane to Nafion, with the same high proton conductivity but impermeable to methanol, to be used in DMFCs. In the present research work, the use of an inorganic material having good proton conduction properties and a pore system of controlled size is proposed as a viable alternative to current electrolyte materials. Zeolites potentially meet all the requirements for this kind of application. These materials show, in fact, ion conduction properties due to the presence of mobile cations electrostatically bonded to their framework. Moreover, their ordered pore systems could work perfectly as a selective barrier towards methanol, without in principle hampering the water retention and the proton diffusion. In particular, the potential use of a type of zeolite, Faujasite, as a fuel cell electrolyte is evaluated. A description of the chemical and textural properties of zeolites is presented in Chapter 2.

• **Problems related to the use of zeolites as DMFC electrolytes.**

Although a potentially good material, zeolites need to be tailored for this specific application. In particular, the feasibility of their use as fuel cell electrolyte is related to several factors such as:

- 1) their **chemical stability in the acidic** fuel cell operational environment, depending on their chemical composition
- 2) their **proton conductivity**. The proton conductivity of zeolites varies from $\sigma = 10^{-8} \text{ Scm}^{-1}$ in dry conditions up to 10^{-3} - 10^{-2} Scm^{-1} at room temperature for fully hydrated materials [37]. Although they show good ion conduction properties, the zeolite proton conductivity is not high enough to compete with Nafion (0.1 S cm^{-1} at 25°C).
- 3) Their **selectivity towards methanol**. The barrier effect towards methanol offered by the zeolite pore system is effective only if it does not affect the proton transport through it (water sorption capacity, proton diffusion). The control of the

pore size is required to obtain the best compromise between proton conductivity and methanol selectivity.

- 4) A last issue is related to the **poor mechanical properties** of the zeolite films compared to those of a polymer film. It is necessary to process the zeolite powders into a film form able to withstand pressure and mechanical stress during the formation of the membrane electrodes assembly (MEA) and during the fuel cell operation. The use of a binder is therefore required. The choice of the binder, the blend proportion and the composite fabrication procedure are all important aspects to be considered in order to have good mechanical properties and still preserve the proton conductivity.

- **Strategies.**

The points listed above represent important issues that have to be solved in order to make zeolites good candidates for a fuel cell electrolyte. The ability of zeolites to lend themselves to modification of their chemical and textural properties over a fairly broad range is an important characteristic that can be used to this purpose. In fact, the versatility of zeolites allows the tailoring and tuning of their properties as a function of the specific application for which they are intended.

In order to tailor and to improve the zeolite properties, Faujasite was dealuminated and functionalized by grafting of sulfonic acid moieties.

Studies were made of the zeolite stability in a harsh acid environment, of the influence exerted by acid exposure on its chemical composition and textural properties and of the relationship between the degree of hydration and the proton conductivity.

Following an optimization of the functionalization procedure, a study of the effect of the extent of grafting on the zeolite textural properties, water and methanol uptake and proton conductivity was carried out. An important contribution to these studies was made by solvent sorption measurements carried out with a dynamic vapour sorption system. Criteria for the surface modification of Faujasites in order to optimize their properties as a low temperature fuel cell electrolyte were established.

Part of the work was also devoted to the fabrication of Faujasite-based composites with different materials (Nafion ionomer and polymeric binders) in order to obtain films with potential for use in low temperature direct methanol fuel cells.

1.4 Structure of the thesis

This **first introductory chapter** starts with a general description of the fuel cell devices and, in particular of PEMFCs and DMFCs, which represent the target application of this research work. A description of the state of the art membrane, Nafion, and its limitations was followed by a brief overview of the different alternatives already proposed in the literature to find a material with better performance. The approach and materials (zeolites) chosen in this work are introduced. the problematic related to the use of zeolites and the objectives of the work are included at the end of this first chapter.

Details about the chosen raw materials, the Faujasite-type zeolite, and its characteristics are described in the first paragraph of **Chapter 2**. In the same chapter, the methodology used to modify the zeolite, both by dealumination and by sulfonic acid grafting is presented through a brief introduction about each approach and a description of the experimental conditions. The last paragraph of Chapter 2 includes a description of the composite membrane fabrication techniques and procedures. For the composite membranes using a non-ionomer binder, the choice and properties of the polymers employed are also presented.

The zeolite samples before and after modification and the composite membranes were characterized by several techniques described in **Chapter 3**. Due to the large number of techniques used in this work, a summarizing table is presented at the beginning of the chapter. Only sorption techniques and proton conductivity measurements are described in more detail because they represent an important part of this work.

The results obtained from the zeolite modification through acid dealumination and surface grafting of sulfonic acid groups are presented and discussed in separate chapters: **Chapter 4** and **Chapter 5**, respectively.

Chapter 6 presents the results obtained from the characterization of the composite membranes. Each of these last three chapters contains a final paragraph where the main conclusions of the work are underlined.

A general conclusion about the main results obtained from this research work is presented in the last chapter of this thesis, **Chapter 7**. The perspectives on the work are also presented at the end of this chapter.

1.5 References

- [1] J. Larminie and A. Dicks, 2003. Fuel cell Systems Explained. 2nd Edition, England, John Wiley & Sons Ltd.
- [2] Fuel Cell Handbook. 7 ed. 2004, Morgantown: EG&G Technicals Services, Inc., Science Applications International Corporation.
- [3] M. Winter and R. J. Brodd, 2004. "What Are Batteries, Fuel Cells, and Supercapacitors?". Chemical Reviews, Vol. 104 p. 4245-4269.
- [4] L. Carrette, K. A. Friedrich and U. Stimming, 2001, "Fuel Cells-Fundamentals and Applications". Fuel Cells, Vol. 1 (1), p. 5-39.
- [5] J. M. Andu'jar and F. Segura, 2009. "Fuel cells: History and updating. A walk along two centuries". Renewable and Sustainable Energy Reviews, Vol. 13, p. 2309–2322.
- [6] A.K. Shukla, A.S. Aricò and V. Antonucci, 2001. "An appraisal of electric powersources". Renewable and Sustainable Energy Reviews, Vol. 5 p. 137–155.
- [7] A. Kirubakaran , Shailendra Jain and R.K. Nema, 2009. "A review on fuel cell technologies and power electronic interfaces". Renewable and Sustainable Energy Reviews, Vol. 13, p. 2430-2440.
- [8] S. Gottesfeld, T.A. Zawodzinski, Chapt. Polymer Electrolyte Fuel Cells, Advances in Electrochemical Science and Engineering, Vol. 5, R.C.
- [9] J.-M. Léger, 2001. "Mechanistic aspects of methanol oxidation on platinum-based electrocatalysts". Journal of Applied Electrochemistry, Vol. 31, p. 767-771.
- [10] A. S. Aricò, S. Srinivasan, and V. Antonucci, 2001. "DMFCs: From Fundamental Aspects to Technology Development". Fuel Cells, Vol. 1, p. 133-161.
- [11] A. Heinzl, V.M. Barragan, 1999. "A review of the state-of-the-art of the methanol

- crossover in direct methanol fuel cells”. Journal of Power Sources, Vol. 84, p.70–74.
- [12] V.M. Barragan, A. Heinzl, 2002. “Estimation of the membrane methanol diffusion coefficient from open circuit voltage measurements in a direct methanol fuel cell”. Journal of Power Sources, Vol. 104, p. 66-72.
- [13] J. Ge, H. Liu, 2005. “Experimental studies of a direct methanol fuel cell”. Journal of Power Sources, Vol. 142, p. 56–69.
- [14] V. Neburchilov, J. Martin, H. Wang and J. Zhang, 2007. “A Review of Polymer Electrolyte Membranes for Direct Methanol Fuel Cells”. Journal of Power Sources, Vol. 169, p. 221-238.
- [15] K. A. Mauritz and R. B. Moore, 2004. “State of Understanding of Nafion”. Chemical Reviews, Vol. 104, p. 4535-4585.
- [16] M. A. Hickner and B.S.Pivovar, 2005. “The Chemical and Structural Nature of Proton Exchange Membranes Fuel Cell Properties ». Fuel Cells, Vol. 5, p. 213-229.
- [17] A. Z. Weber and J. Newman, 2003. “Transport in Polymer-Electrolyte Membranes I. Physical Model”. Journal of Electrochemical Society, Vol. 150 (7), p. A1008-A1015.
- [18] A. Z. Weber and J. Newman, 2004. “Transport in Polymer-Electrolyte Membranes II. Mathematical Model”. Journal of Electrochemical Society, Vol. 151 (2), p. A311-A325.
- [19] C. Vallieres, D. Winkelmann, D. Roizard, E. Favre, P. Scharfer and M. Kind, 2006. “On Schroeder’s Paradox”. Journal of Membrane Science, Vol. 278 (1-2), p. 357-364.
- [20] W. Y. Hsu, T. D. Gierke, 1983. “Ion transport and clustering in Nafion pefluorinated membranes”. Journal of Membrane Science, Vol. 13, p. 307-326
- [21] H.L. Yeager and A. Steck, 1981. “Cation and water diffusion in Nafion ion exchange membranes: influence of polymer structure”. Journal of Electrochemical Society, Vol. 128, p. 1880-1884.
- [22] K. Schmidt-Rohr and Q. Chen, 2008. “Parallel cylindrical water nanochannels in Nafion fuel-cell membranes”. Nature Materials, Vol. 7 (1), p.75–83.
- [23] X. M. Ren, T. E. Springer, T.A. Zawodzinski and S. Gottesfeld, 2000. “Methanol Transport through Nafion Membranes - Electro-Osmotic Drag Effects on Potential Step Measurements”. Journal of Electrochemical Society, Vol. 147, p. 466-474.

- [24] T. Schaffer, T. Tschinder, V. Hacker and J. O. Besenhard, 2006. "Determination of methanol diffusion and electroosmotic drag coefficients in proton-exchange membranes for DMFC". Journal of Power Sources, Vol. 153, p. 210-216.
- [25] C. Iojoiu, F. Chabert, M. Maréchal, N. El. Kissi, J. Guindet and J.-Y. Sanchez, 2006. "From polymer chemistry to membrane elaboration: A global approach of fuel cell polymeric electrolytes". Journal of Power Sources, Vol. 153, p. 198-209.
- [26] M. A. Hickner, H. Ghassemi, Y. S. Kim, B. R. Einsla, J. E. McGrath, 2004. Alternative Polymer Systems for Proton Exchange Membranes (PEMs)". Chemical Reviews, Vol. 104, p. 4587-4612.
- [27] A. M. Herring, 2006. "Inorganic-Polymer Composite Membranes for Proton Exchange Membrane Fuel Cells". Polymer Reviews, Vol. 46 (3), p. 245–296.
- [28] B. Baradie, J. P. Dodelet and D. Guay, 2000. "Hybrid Nafion-inorganic membrane with potential applications for polymer electrolyte fuel cells". Electroanalytical Chemistry, Vol. 489, p.101-105.
- [29] A. S. Arico, V. Baglio, A. Di Blasi, P. Creti, P. L. Antonucci and V. Antonucci, 2003. "Influence of the acid-base characteristics of inorganic fillers on the high temperature performance of composite membranes in direct methanol fuel cells". Solid State Ionics, Vol. 161, p. 251-265.
- [30] W. L. Xu, T. H. Lu, C. P. Liu and W. Xing, 2005. "Low methanol permeable composite Nafion/silica/PWA membranes for low temperature direct methanol fuel cells". Electrochimica Acta, Vol. 50, p. 3280-3285.
- [31] K. A. Mauritz, 1998. "Organic-inorganic hybrid materials: perfluorinated ionomers as sol-gel polymerization templates for inorganic alkoxides". Materials Science and Engineering: C, Vol. 6, p. 121-133.
- [32] H. Uchida, Y. Ueno, H. Hagihara, M. Watanabe, 2003. "Self-Humidifying Electrolyte Membranes for Fuel Cells", Journal of Electrochemical Society, Vol. 150, p. A57-A62.
- [33] A. Sacca, A. Carbone, E. Passalacqua, A. D'Epifanio, S. Licocchia, E. Traversa, E. Sala, F. Traini and R. Ornelas, 2005. "Nafion-TiO₂ hybrid membranes for medium temperature polymer electrolyte fuel cells (PEFCs)". Journal of Power Sources, Vol. 152, p. 16-21.
- [34] F. Damay and L. C. Klein, 2003. "Transport properties of Nafion(TM) composite membranes for proton-exchange membranes fuel cells". Solid State Ionics, Vol.162-163, p. 261-267.

- [35] H. C. Kuan, C. S. Wu, C. Y. Chen, Z. Z. Yu, A. Dasari and Y. W. Mai, 2006. "Preparation of Exfoliated Zirconium Phosphate/Nafion Organic-Inorganic Hybrid Proton Exchange Membranes". Electrochemical and Solid-State Letters, Vol. 9, p. A76-A79.
- [36] A. K. Sahu, S. Pitchumani, P. Sridhar and A. K. Shukla, 2009. "Co-assembly of a Nafion-Mesoporous Zirconium Phosphate Composite Membrane for PEM Fuel Cells". Fuel Cells, Vol. 9, p. 139-147.
- [37] S.D.Mikhailenko, S.Kaliaguine, E.Ghali, 1997. "Water-assisted ionic conductance of zeolites with ZSM-5 structure". Microporous Materials, Vol. 11, p. 37-44.

2. Zeolites and their composites

2.1 Zeolites

Zeolites are a family of crystalline aluminosilicate materials that find application in several domains, including catalysts in the petrochemical industry or in the synthesis of chemicals, gas sensors and as recently proposed in drug delivery [1-4]. Such a widespread use of zeolites in different fields is due to their chemical and structural characteristics that make this class of materials very unique and versatile.

2.1.1 Chemical and structural properties

The chemical composition of zeolites can be expressed by the following formula:



where n is the valence of cation M , z is the number of water molecules per unit cell, and x and y are the total of AlO_4 or SiO_4 tetrahedra per unit cell.

The chemical composition of a zeolite is usually expressed as the ratio between x and y in the formula E2.1 i.e. SiO_2/Al_2O_3 ratio or the Si/Al ratio. The Si/Al ratio can vary from 1 to ∞ (silicalite) and it significantly influences the zeolite properties. The framework Al content, for instance, determines the number of exchangeable ions, M . The zeolite framework, in fact, can be described as four-connected AlO_4 and SiO_4 tetrahedra linked to each other by the sharing of oxygen atoms. The presence of aluminium, instead of silicon, at the center of the tetrahedron, introduces one negative charge in the lattice. The negative charges are balanced by an appropriate number of cations, usually mono- or dipositive. Typical cations include alkali metals, quaternary ammonium ions or protons. These cations are electrostatically bound to the framework and relatively free to move through it, giving rise to very good ion exchange and ion conduction properties [1].

The Al content also affects the hydrophilicity and the acidity of the zeolite surface. For each Al atom in the framework, in fact, a bridging hydroxyl group (Al...OH...Si) is present. This group is a hydrophilic site and the hydrophilicity of the zeolite surface increases as the Al content increases. The Al...OH...Si bridge is also characterized by Brønsted acidity, and the number of Al atoms in the framework determines the strength of the Brønsted acid sites [5-6].

The chemical stability of zeolites is also related to the framework Si/Al ratio, and the type of environment to which they are exposed. The zeolite chemical stability is related to the tendency of the aluminosilicate structure to dissolve in the presence of H^+ and OH^- in solution, in accordance with the Brønsted and Lewis theory.

In acid solutions Al can be progressively removed from the aluminosilicate framework because of proton binding on the Lewis basic sites according to: $(Al-OH + H^+ \rightarrow >Al-OH_2^+)$ [7-9]. The reaction is privileged at low pH values. Therefore, the stability of zeolites towards acid attack strongly depends on the Al content and thus Al-rich zeolites are less stable in acidic environments. Si-rich zeolites, conversely, are less stable in basic environments. A scheme of the dealumination and desilylation undergone by zeolites in acid and basic environment is reported in Figure 2.1.

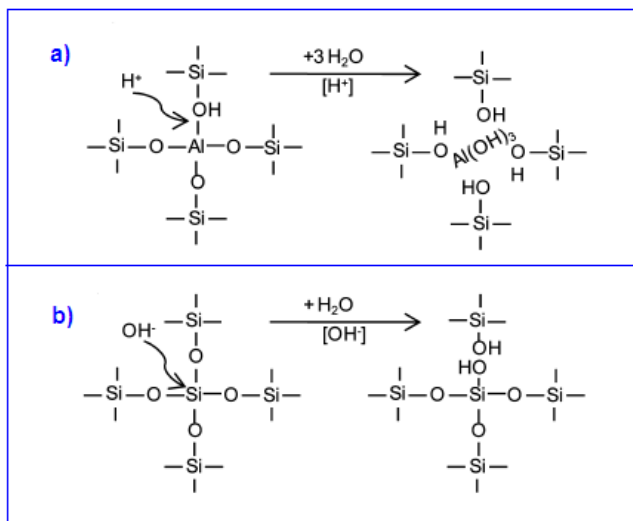


Figure 2.1: Scheme of zeolite a) dealumination (in acid conditions) and b) desilylation (in basic conditions) (with permission from [9] Copyright 2010, American Chemical Society).

The unique structural characteristics of a zeolite are also responsible for its properties. The four-connected AlO_4 and SiO_4 tetrahedra represent the primary building units of the zeolite framework and they are assembled together into secondary building units, which can be polyhedra such as cubes, hexagonal prisms or octahedra. These polyhedra are arranged in space to form more complex structures that repeat tridimensionally over a long-range.

Figure 2.2 shows an example of zeolite building units: starting from the SiO_4 and AlO_4 tetrahedra to form hexagonal secondary building units which are arranged together to form a sodalite unit (or β cage). The sodalitic cage is one of the most common units found in zeolites and it can give rise to many different structures. The assembly of sodalitic cages or other units to form a more complex structure gives rise to an open porous structure made of channels and voids of uniform molecular dimensions which are particularly effective for the diffusion of species. All atoms are accessible via the entire internal surface where the local coordination is unchanged.

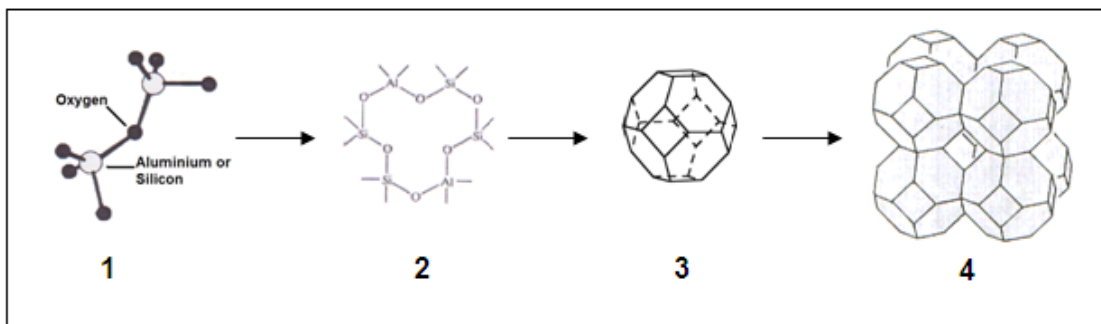


Figure 2.2: Example of building units constituting one of many zeolite structures: 1. TO_4 tetrahedra ($T=\text{Al}, \text{Si}$), 2. Secondary building unit formed by 6 tetrahedra, 3. Sodalite or β cage, 4. Sodalitic structure.

The size of the window and channels represents an important feature of the zeolite since it allows the diffusion of certain molecules rather than others, giving rise to shape selectivity. Through their dimensions, the zeolite pores can act as a physical barrier to the passage of molecules of larger size, allowing passage only to smaller molecules. The molecular sieve property of zeolites may play an important role in their use as fuel cell electrolytes, by hindering the passage of methanol without affecting water diffusion and

therefore the proton mobility: methanol and water have a different polarity and kinetic diameter (0.27 nm for water and 0.38 nm for methanol) [10].

2.1.2 Zeolite proton conductivity

Zeolites show ion conductivity due to the presence of mobile cations and the availability of paths provided by the channels [11,12]. A higher number of cations is clearly an important requisite for a good ion conductivity. However, other factors play a role in the proton conduction mechanism. In fact, the movement of ions is made possible by overcoming the electrostatic attraction to the zeolite pore wall; the activation energy of the charge transport is therefore correlated to factors such as cation size and charge [11, 13,14], cation distribution in different positions in the zeolite framework [12,13], and composition of the framework [15]. Water is another factor determining the ion conductivity in zeolites because it influences the interactions between cations and the framework, and is directly involved in the conduction mechanism by assisting the ion-transport process. In addition, water is an essential element for the functioning of DMFCs. The mechanism of proton transport in a H⁺-form zeolite is considered in more detail in this section.

As discussed in the previous paragraph, when protons are the cations, the so called Brønsted acid sites (bridged hydroxyl groups) are formed on each Al-site. The movement of protons through the lattice is made possible by overcoming the electrostatic attraction by thermal excitation. Two mechanisms of ion conduction can be distinguished: one which involves water absorbed in the pores of the zeolite and/or on its external surface (T < 200°C) and another one which occurs at higher temperature (> 200°C), when the water is all desorbed.

• Proton conduction in dehydrated conditions (> 200°C)

The activation energy of the local motion is a direct measure of the Brønsted acidity, which depends on the Al content in the framework. The mobility of these protons is related to the probability and energetics of proton jumps between the oxygen sites

surrounding the Al-centers (on-site motion) or between neighboring Al sites (inter-site motion). An inter-site jump requires the full deprotonation of the Si-O-Al group and consequently a high energy barrier (assumed to be ~ 13 eV) must be overcome. This implies that translational motion of protons in zeolites should not be observable at moderate temperature. However, evidence of proton conductivity in various dehydrated H-form zeolites were observed, indicating a long range motion which can be understood if the protons interact with bridging Si-O-Si groups between the Brønsted sites [11]. As also reported by Dekker and collaborators, the proton conduction above 200°C depends on the number of protons, meaning that protons migrate by hopping from one framework oxygen atom to another [16]. The role of the number of carriers in the proton conduction in the absence of water is evident from comparing an Al-rich zeolite before and after dealumination. As reported by Nischwitz and collaborators, between 220°C and 500°C the proton conductivity of the relatively Al-rich zeolite is substantially higher than that of dealuminated samples [12], because dealuminated samples have fewer counter-ions per unit cell.

• **Proton conduction under hydrated conditions (< 200°C)**

In the presence of water, the correlation between the number of carriers (protons) and the conductivity is not as obvious as in the absence of water. In fact, the influence on the conductivity of the framework charge density is only secondary compared to the primary effect of the solvation of the cations, which notably improves the cation mobility. By working in the presence of a constant number of water molecules, Mogensen et al. observed a decrease in the conductivity with an increase in the number of cations, explained by the reduced charge-carrier mobility due to the decrease of cation hydration number [17].

Similar to Nafion, in presence of water, the mechanism of proton transport in zeolites can be described by the Grotthuss model and the vehicular model. An illustration of the Grotthuss and vehicular mechanisms is shown in Figure 2.3.

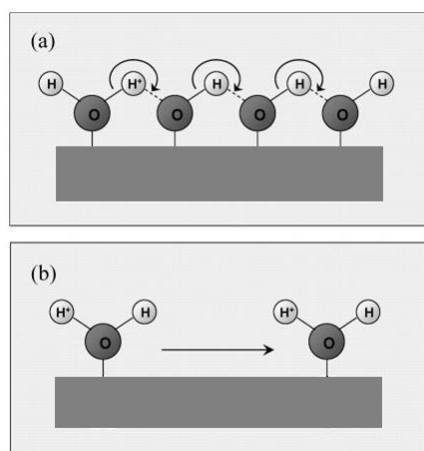


Figure 2.3: H^+ transport mechanisms for (a) the Grotthuss (hopping) and (b) the vehicle mechanisms in a solid acid (adapted with permission from [18] Copyright 2006, American Chemical Society).

2.2. State of the art of the use of zeolites as electrolyte materials for fuel cells

The zeolites' acid properties and their well-defined pore structures have motivated in recent years the use of these materials as a solid electrolyte in fuel cells. Different types of zeolites such as Mordenite, Chabazite, Clinoptilolite [19], Faujasite [20, 21] or H-ZSM5 [22, 23] have already been proposed as additives to Nafion[®]. In the specific case of DMFCs, the zeolites are dispersed within the ionomer membrane mainly to decrease the methanol permeation through tortuosity and barrier effects [24]. Some of the published studies confirmed that pristine zeolites and those functionalized with sulfonic acid groups can improve the performance of Nafion-based DMFCs operating typically at temperatures higher than 70°C, with O₂ fed at the cathode and diluted methanol (1 [22] to 5 mol dm⁻³ [25]). Moreover, it was found that they can increase the water retention of Nafion [19, 21], extending the operating temperature of Nafion based DMFCs up to 140°C [19].

In these composites, however, Nafion is always the main component (a maximum of 35% zeolite was reported) and the methanol crossover is still significant. In order to overcome this limitation, zeolites have been also proposed as the electrolyte material itself in novel

composite membranes and thus blended with a non-ionomer binder such as polytetrafluoroethylene, polyethyleneoxides and polyvinylalcohol [26-30]. These works reported low methanol diffusion across the composite membranes but proton conductivities (up to 10^{-2} S cm⁻¹) generally lower than Nafion [26-29].

Although promising, the use of zeolites as fuel cell electrolytes has to be researched further, requiring an improvement of the proton conductivity, the tailoring of shape selectivity and the identification research of a suitable binder for zeolite-based films for the fuel cell assembly. The mechanism of ion conduction in zeolites is quite complex, being controlled by several parameters such as the Si/Al ratio, the degree of hydration of the material and its porosity [11,14,17,31]. Therefore, all these parameters must be taken into consideration, and optimized, in the fabrication of zeolite based composite membranes for fuel cells.

Over 200 zeolite types are known, both natural and synthetic, characterized by different structures and composition, and consequently by different properties [1, 32]. The choice of the most suitable zeolite for fuel cell applications has to be dictated by specific criteria related to its stability, its selectivity towards methanol and its proton transport properties. Part of this research work aimed to establish these criteria.

2.3 Starting material

Faujasite-type (FAU) zeolite was chosen as a starting material for this research work. The FAU structure is characterized by spherical cages of 1.3 nm diameter with four smaller openings of 0.74 nm diameter. In Figure 2.4 the FAU structure model is shown.

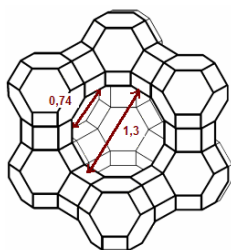


Figure 2.4: FAU structure model showing the size (in nm) of the super-cage and window.

The choice of FAUs over other types of zeolite was dictated by their large pore size, high surface area, the open three-dimensional pore system which allows a faster intra-crystalline diffusion, and by their commercial availability in a wide range of chemical compositions [1, 32]. Three commercial H⁺-form FAUs (supplied by Zeolyst International) were investigated. Their commercial names and characteristics are shown in Table 2.1.

Table 2.1: Si/Al molar ratio, specific surface area (S_{BET}), unit cell size, and micropore volume and mesopore (20-60Å) volume of the three commercial H⁺-form Faujasites.

FAU	Si/Al molar ^I	Unit cell ^{II} /Å	S_{BET} ^{III} /m ² g ⁻¹	Micropore Volume ^{III} (< 20Å) / cc g ⁻¹	Mesopores Volume ^{III} (20-60Å) / cc g ⁻¹
CBV600	3.4	24.35	530	0.163	0.052
CBV720	16.3	24.31	813	0.247	0.118
CBV780	48.7	24.24	823	0.238	0.132

^I obtained by Neutron Activation Analysis; ^{II} obtained by XRD; ^{III} obtained by N₂ adsorption measurements.

2.4 Zeolite Modification

In this work, two different types of modification were carried out in parallel on the Faujasites:

- **dealumination**
- **surface functionalization by grafting of sulfonic acid groups**

The two methods are presented in the following paragraphs, including their general mechanisms, the reason why these two modification methods were chosen and, finally, the specific methodology employed in this work.

2.4.1 Dealumination

The framework Si/Al ratio can be controlled during the zeolite synthesis (although it is not always feasible) and via post-synthesis treatments. The removal of Al from the zeolite framework by post-synthesis methods is known as dealumination, and this procedure is widely used in industry to improve the stability of Al-rich zeolite-based catalysts and to tailor their acidity. Dealumination can be carried out by a variety of techniques such as hydrothermal treatments, mineral acid treatment, a combination of both, or by using reagents such as SiCl_4 and EDTA [1].

In addition to the chemical composition, dealumination can also affect the textural characteristic of a zeolite. In fact, the removal of Al induces the formation of mesopores and a consequent increase of the zeolite surface area [31, 33-35], although at the expense of the number of charge carriers directly related to the framework Al. An illustration of mesopore formation induced by the dealumination on a Faujasite –type framework is shown in Figure 2.5.

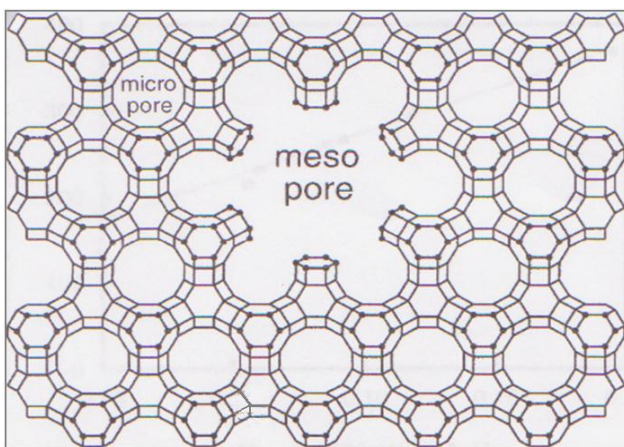


Figure 2.5: Illustration of the FAU structure with mesoporosity induced by post-synthesis dealumination (with permission from [35] Copyright 1999, Elsevier).

By controlling the dealumination conditions, it is then possible to use this technique as a tool to obtain zeolite samples with a wide range of Si/Al ratios and also with different textural properties. Indeed, one of the objectives of this work is to evaluate the sorption properties and proton conductivity as a function of the zeolite chemical composition and

porosity, to establish a correlation between these properties and the zeolite characteristics. This work would be the basis for a future optimization of the design of a zeolite system for the target application.

In this work the dealumination was carried out by acid leaching. Other than being a simple procedure requiring inexpensive chemicals, this technique was chosen for specific reasons:

- 1) firstly, the stability of the Faujasites in an acidic environment can be tested and, therefore, the feasibility of their use as electrolyte materials for PEMFCs and DMFCs;
- 2) secondly, the Al removed from the framework by acid treatment is dissolved in the solution. By using other techniques such as the hydrothermal method, extra-framework Al species are formed and remain trapped in the zeolite pore system [33, 36, 37, 38]. Because we are interested in the water and methanol diffusion and the proton conductivity, the accumulation of extra-framework Al in the pores is not desirable.

2.4.1.1 Dealumination: Experimental Procedure

In this work the dealumination of the three FAUs was carried out by suspending the solids in 6 mol dm^{-3} HCl aqueous solution (50 ml g^{-1} zeolite) at room temperature and under stirring. Samples were filtered, re-dispersed in deionised water under stirring and re-filtered twice. The dealumination time (t_D) was varied between 30 min and 7000 h for the CBV600 series, and between 30 min and 168 h for the CBV720 and CBV780 series. Each sample was dealuminated separately, thus corresponding to an independent batch. The solutions pH (< 1) was monitored and no significant variations could be detected during the dealumination process. All samples were characterized by elemental analysis and infrared spectroscopy, N_2 and water sorption measurements and by impedance spectroscopy. The results are presented in Chapter 4.

2.4.2 Surface functionalization

Although only recently applied to zeolites, the surface modification of a material by grafting of functional groups is widely used in industry, and two typical examples are the modification of the wetting or adhesion properties of materials. Essentially, with this technique it is possible to combine the properties of the material used as a substrate with the properties of the introduced functional group.

The grafted species have to form strong and stable bonds with the surface of the “host” material to become an integral part of the new hybrid material. Silane coupling agents usually have this ability, by forming durable covalent bonds between organic and inorganic materials, and by carrying the desired functional group [39].

The general formula of an alkyl silane coupling agent can be written as follows:



where F is the functional group and X the hydrolysable group (typically alkoxy, halogen or amine), R is a non hydrolysable group (such as $-CH_3$), and the number m of these groups can vary from 0 to 2. The alkyl chain $-(CH_2)_n-$ is the linker between the Si atom and the functional group, and n is the number of methylene groups in the chain. The linker, which can also be an aryl group, controls the final properties of the modified surface through its length by means of steric and hydrophobic effects.

In the silane grafting reaction, the hydrolysis of the alkoxy group forms reactive silanol groups which then condense with other silanol groups on the substrate surface to form siloxane covalent linkages. The grafting mechanism depends on the type of silane and on the conditions under which the grafting is performed [40-43]. When silanes have multiple hydrolysable substituents, the grafting mechanism involves multiple steps, shown in Figure 2.6. The first step consists of the hydrolysis of the silane followed by the formation of a self-assembled monolayer driven by Si-O-Si bond formation, hydrogen bonding and van der Waals interactions between alkyl chains. Then, the oligomers form hydrogen bonds with the OH of the substrate surface followed by the formation of a

covalent bond with the substrate concomitant with the expulsion of water molecules [39,44]. A surface coverage of this type is usually referred to as coating while, in anhydrous conditions and in the presence of a silane not capable of cross-linking, a so called silylation (Figure 2.7) is obtained [43].

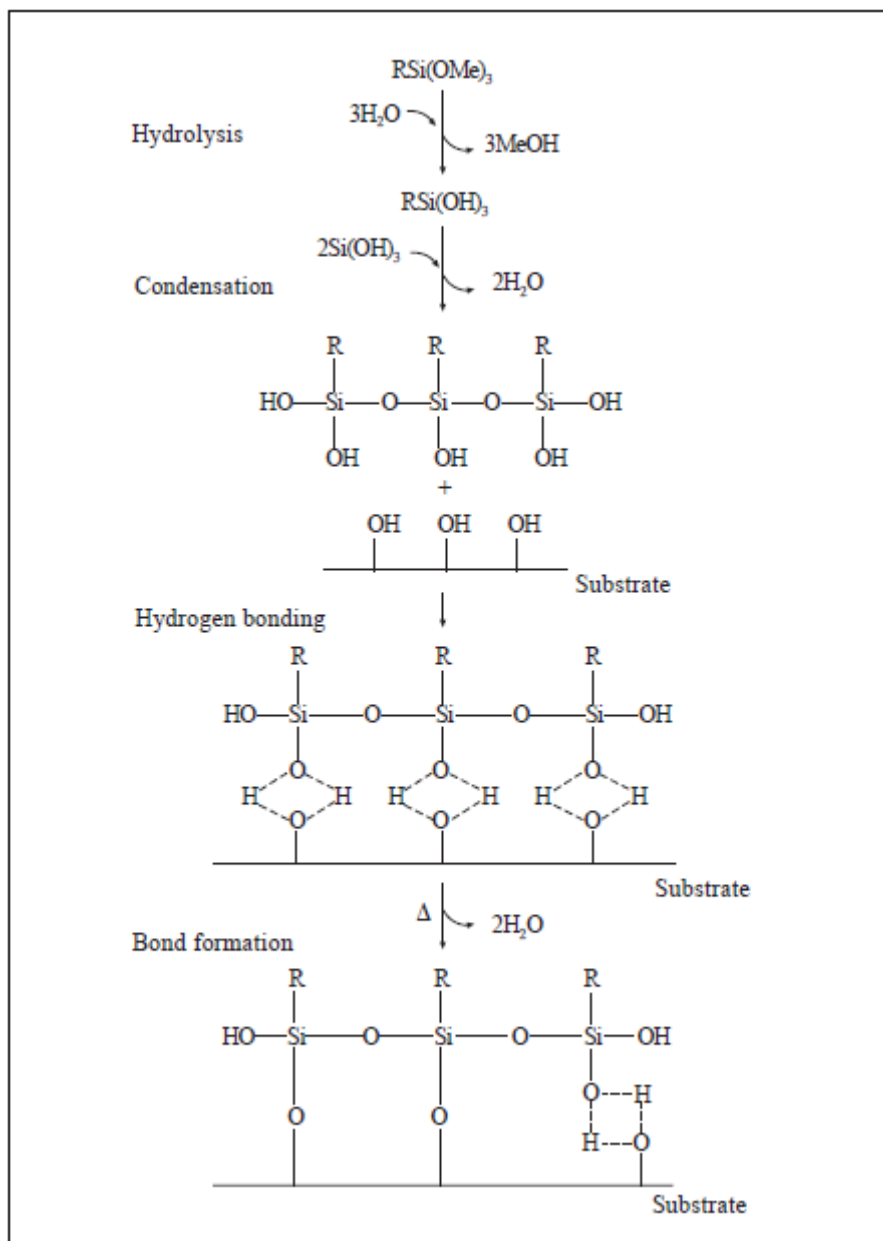


Figure 2.6: Illustration of the grafting mechanism of a trialkoxysilane onto a substrate in the presence of water [39].

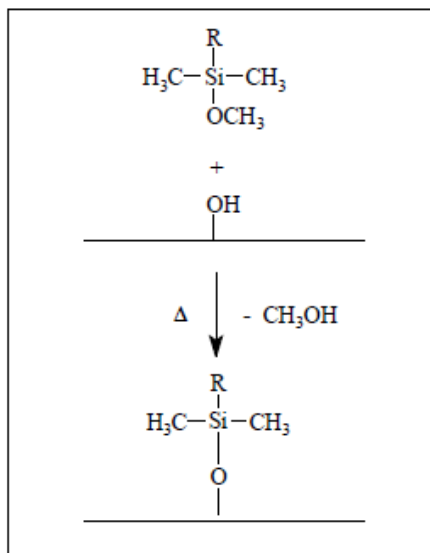


Figure 2.7: Illustration of a grafting mechanism of a monoalkoxysilane onto a substrate in anhydrous conditions [39].

Stable condensation products with the silane are formed not only with Si but with other oxides such as those of aluminum, zirconium, tin, titanium, and nickel [39, 45, 46].

The grafting of organosilanes is therefore an efficient way to introduce functional groups onto the zeolite surface. These compounds, in fact, can react with hydroxyl groups present on the zeolite surface and form strong covalent bonds while carrying the desired functional groups. If these functional groups are strongly acidic groups such as sulfonic acid groups, the proton conduction properties of the zeolite could be significantly enhanced.

2.4.2.1 State of the art of functionalized zeolites

Functionalization by alkyl- and aryl- organosilane grafting is reported on alumina [45] and silica in order to use them as catalysts for industrial applications or to improve their compatibility with other components in composites [47-55]. Sulfonic acid functionalization by silane grafting on silica is also reported to improve its proton conductivity. Mikhailenko et al. reported a proton conductivity of $\sim 10^{-2} \text{ S cm}^{-1}$ for porous silica functionalized with propyl sulfonic acid groups (20% of silicon atoms

connected to functional groups), almost 3 orders of magnitude higher than unmodified porous silica [55]. A similar improvement at $T \geq 60^\circ\text{C}$ of 2-3 orders of magnitude but only up to $\sim 10^{-5} \text{ S cm}^{-1}$ has been reported on Si-MCM-41 functionalized with 20 mmol g^{-1} of propylsulfonic acid groups [56] and up to $\sim 10^{-3} \text{ S cm}^{-1}$ on macroporous silica [57]. Mesoporous silica functionalized with arene-sulfonic acid groups was reported to have an appreciable proton conductivity as well ($\sim 10^{-2} \text{ S cm}^{-1}$) [58].

More recently, the functionalization procedure has been also applied to zeolites [59,60] in order to improve their catalytic properties [61-63], to improve their mechanical properties when blended with polymers in composites [64-68] to be used in gas permeation membranes [69] and for environmental applications [70,71]. Only a few works report the use of organo-functionalized zeolites as electrolytes for fuel cells. NaA zeolite was functionalized with 3-aminopropyltrimethoxysilane in order to improve the adhesion between the zeolite and Nafion ionomer to obtain a pinhole free composite membrane. This approach contributed to the reduction of the methanol crossover through the membranes but at the same it significantly reduced the proton conductivity due to the basic properties of the chosen organosilane [65]. Functionalization on beta zeolite with aryl sulfonic moieties and other organosilanes [61,72] was effective in improving the proton conductivity with respect to the parent zeolite: a proton conductivity of 1.2×10^{-3} - $1.2 \times 10^{-2} \text{ S cm}^{-1}$ was reported for BEA zeolite functionalized with phenylsulfonic acid groups, significantly higher than the unmodified zeolite $1.5 \times 10^{-4} \text{ (S cm}^{-1}\text{)}$ [72]. An improvement of more than one order of magnitude was also reported by John C. McKeen and collaborators [61]. A good improvement of the overall fuel cell performance due to the reduced methanol permeability is obtained as well when the functionalized beta zeolite is blended with Nafion, in spite of the small decrease of proton conductivity of the composite membranes compared to unmodified Nafion [66, 68].

Although a significant increase of the proton conductivity of functionalized zeolite powders has been reported, a further improvement is required in order to make these materials conductive enough to be competitive with Nafion. Up to now, none of the few works reported in the literature have focussed on the optimization of the functionalization conditions and on their influence on the functionalized zeolite textural properties, solvent uptake and diffusion, and on their correlation with the proton conductivity and methanol

selectivity. In order to establish correlations between the zeolite surface coverage and the properties of the functionalized samples (proton conductivity and selectivity towards methanol), in this work parameters such as the chemistry and texture of the Faujasite and the silane precursor concentration were varied. This part of the work aims to identify the most suitable functionalization conditions required to obtain a Faujasite-based electrolyte with a good proton conductivity and with a high selectivity towards water over methanol.

2.4.2.2 Functionalization: Experimental Procedure

In this work, 3-mercaptopropyltrimethoxysilane (3-MPTMS, 95% solution supplied by Alfa Aesar) was chosen as the silane coupling agent. This silane agent offers several advantages: it is non-toxic, it is commercially available, and it contains three hydrolyzable substituents, favoring coating over silylation and consequently a more highly ordered coverage of the surface [42]. Moreover, among the alkoxyxilanes, only methoxysilanes can be effectively grafted without a catalyst.

The zeolite surface modification was performed by grafting the 3-mercaptopropyltrimethoxysilane, followed by the conversion of the mercapto groups –SH into the sulfonic acid groups –SO₃H by oxidation with H₂O₂ [49,73-76]. An illustration of the 2-step process is shown in Figure 2.8.

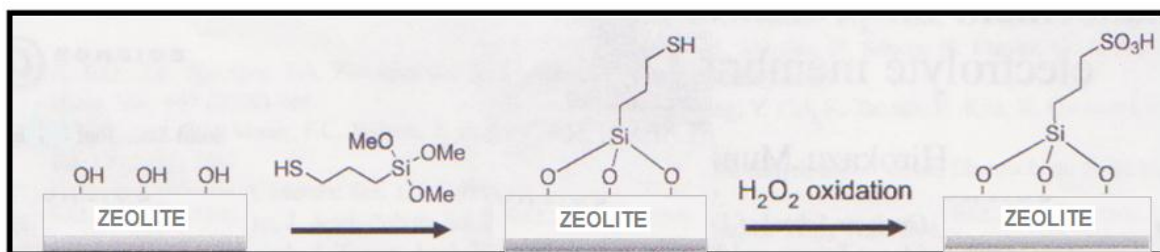


Figure 2.8: Illustration of the grafting of 3-MPTMS onto the zeolite surface and conversion of the mercapto-group into sulfonic acid groups (adapted with permission from reference [57], Copyright 2005, Elsevier).

Several samples were prepared using different silane/zeolite ratios (from 0.6 to 78 mmol g⁻¹ zeolite) and for a reaction time of 6h. The grafting was carried out in anhydrous toluene (98.9 %, Alfa Aesar) under continuous stirring. The volume of solvent was 2 ml for each 250 mg of starting zeolite. All samples were filtered and washed with toluene twice and dried at 50°C in a vacuum for 2h.

The conversion of -SH into -SO₃H was carried out using H₂O₂ as an oxidant agent. 20ml of 30% H₂O₂ aqueous solution (Aldrich) were added to each 70 mg of grafted sample. In order to establish the temperature and the time at which the conversion of -SH into (-SO₃H) is complete, the oxidation step was initially carried out on a series of CBV600 samples grafted with 41 mmol g⁻¹ 3-MPTMS, at room temperature and at 50°C, for a time between 1.5h and 9h. Then, all grafted samples of all series were oxidized at 50°C for 6h. Finally, all samples were filtered and washed with deionised water and dried at 50°C in a vacuum for 2h.

The samples were characterized by thermogravimetric analysis and x-ray photoelectron spectroscopy in order to quantify the amount of silane grafted and to follow the conversion of -SH into -SO₃H, respectively. N₂, H₂O and MeOH sorption measurements were carried out on all samples to evaluate the effect of the surface functionalization on the textural properties of the zeolite and to evaluate the solvent selectivity of the functionalized samples. The proton conductivity of all samples was also measured by impedance spectroscopy. The results are presented and discussed in Chapter 5.

2.5 Composite membranes

Although the use of a zeolite membrane would be desirable in order to overcome the methanol crossover, its mechanical properties are not ideal for this type of application. In fact, a membrane/pellet made of only zeolite is too brittle to resist any kind of stress. For this reason, it is necessary to use a composite made from the zeolite powder blended with a polymer binder or to disperse the zeolite within an ionomer matrix, in which a synergy between the two components should produce a material with the required characteristics. The choice of a good polymer matrix in the composite is dictated by several requirements: naturally, it has to be chemically and thermally stable enough to operate in

PEMFCs or DMFCs, and, ideally, it should be a material allowing proton mobility but not permeable to methanol.

2.5.1. Polymeric matrix: Nafion and non-conductive binders

The literature reports some works on Nafion composites fabricated with zeolites both as received and functionalized but the majority of the works focus on the fuel cell performance. Although the use of Nafion is not the main objective of this work, Nafion is still the state of the art material. Therefore, Nafion –Faujasite composite membranes were also prepared and characterized but a special emphasis was given to the study of the influence of the zeolite on the states of water in the composite membranes.

The preferential approach chosen in this work consists of the use of the zeolite as the main component of the composite and a polymer that is a non proton conductor and impermeable to methanol (although hydrophobic as well). Ideally, the amount of polymer used in the composite should be as small as possible. However, fabricating a composite where the polymer comprises only a small percentage is often simply not feasible. It is then important to consider several aspects, such as the compatibility between the inorganic and the organic components; the homogeneity of the composite, which means a good dispersion of the inorganic component in the polymer matrix, and the porosity, which is a characteristic particularly important for fuel cell applications, affecting the separation of the reactants. Considering these several issues, the right choice of the polymer and the fabrication method can play a very important role. A description of the selected polymers and the two methods used to fabricate the composites are presented in the following paragraphs. The experimental conditions used to prepare each type of composite membrane are presented at the end of this chapter.

(a) Polyvinylidene fluoride

Polyvinylidene fluoride (PVDF) is a thermoplastic fluoropolymer, and its structural unit is shown in Figure 2.9

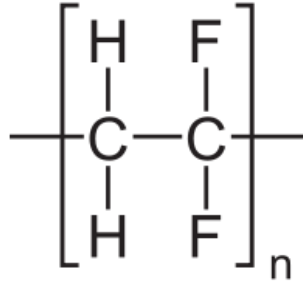


Figure 2.9: Polyvinylidene fluoride.

PVDF is a whitish solid showing a high resistance to corrosive reagents and to heat. Compared to other fluoropolymers, it has a low melting point ($\approx 177^\circ\text{C}$), low density (1.78 g cc^{-1}) and low cost [77, 78]. PVDF finds application as an insulator for electrical wires, and in biomedical and aerospace applications.

PVDF based composites are also fabricated with several inorganic fillers such as TiO_2 [79-82], SiO_2 [83,84], Al_2O_3 [85], antimonite acid derivative [86] and clay [87], to be employed as ultrafiltration membranes, antifouling materials or in permeation processes. Zeolites were also employed as fillers in PVDF-based composites in order to increase the polymer dielectric and thermal properties or for ultrafiltration applications [88, 89]. Sancho and collaborators also employed PVDF to fabricate fuel cell composites with four different zeolites mordenite, NaA zeolite, umbite and ETS-10[90]. Using a simple mixing and pressing procedure, they could obtain 90 wt% zeolite composite tablets of 13 mm diameter. However, the proton conductivity of the composites was lower than Nafion below 100°C except for the ETS_10 based composite and appreciable conductivity was measured at 150°C ($\approx 3 \times 10^{-2} \text{ S cm}^{-1}$) due to the significantly higher water retention of the composite compared to Nafion.

(b) Polytetrafluoroethylene

Polytetrafluoroethylene (PTFE) is a synthetic fluoropolymer, commonly known as Teflon®, the brand name registered by DuPont. Its structural unit is shown in Figure 2.10.

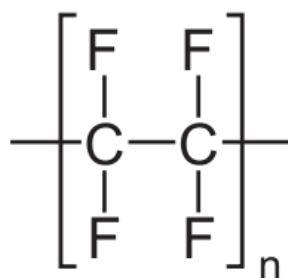


Figure 2.10: Polytetrafluoroethylene.

PTFE is a thermoplastic polymer, a white solid, with a density of about 2.2 g cc^{-1} and a melting point of $327 \text{ }^\circ\text{C}$. PTFE is a high-molecular-weight solid compound showing very high hydrophobicity. It is very resistant to reactive and corrosive chemicals and to heat. Teflon is commonly used as a non-stick coating for pans or for containers and parts of devices in contact with corrosive chemicals, as an insulator for electrical assemblies and for waterproof clothing [77, 78]. Due to its inertness and its impermeability to solvents, Teflon represents a good potential binder in composite for DMFCs.

Teflon composite membranes with 80 wt% Y-zeolite [91] and 90 wt% Zeolon 100H [26] loading were prepared by stirring a suspension of Teflon and zeolite in water and isopropanol, followed by drying and rolling of the composite on a heated flat surface. A proton conductivity on the order of $\sim 10^{-4} \text{ S cm}^{-1}$ at $80 \text{ }^\circ\text{C}$ and of $\sim 10^{-2} \text{ S cm}^{-1}$ at room temperature was reported for Y-zeolite and Zeolon based composites, respectively. The results reported are impressive, although the final proton conductivity depends on the type of zeolite employed and the mechanical properties need to be improved, as reported by the same authors.

(c) High Density Polyethylene

Polyethylene (polyethene, IUPAC nomenclature) is a thermoplastic polymer consisting of long chains of the monomer ethylene (ethene, IUPAC name). Polyethylene is non-polar and has a high resistance to solvents, being then ideal as a binder impermeable to methanol in DMFC electrolyte membranes. It is classified into several different categories based mostly on its density and branching. Its mechanical properties depend significantly on variables such as the extent and type of branching, the crystal structure and molecular weight.

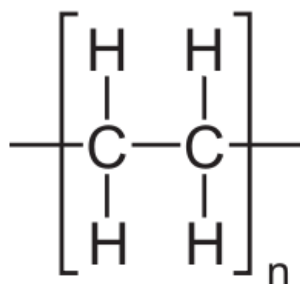


Figure 2.11: Polyethylene.

Polyethylene is widely used in industry, especially for packaging applications. It is also mixed with inorganic fillers, usually to control the permeation of water and various gases such as O₂ and CO₂ [92-95] especially when PE is employed in food packaging. Natural zeolites and ZSM-5 were also used as a filler to prepare PE based composites for the same application [93, 95, 96]. In general the amount of inorganic filler in this kind of composite is low (from 1 to 35 wt%) and low density polyethylene is used.

In this work high density (0.941 g cc⁻¹) polyethylene (HDPE) was chosen because it has a low degree of branching and thus stronger intermolecular forces and tensile strength. The melting temperature of HDPE is 130-140°C [77].

(d) Styrene-ethylene butylene-styrene

Styrene-ethylene butylene-styrene (SEBS), also known by its commercial name Kraton, is a non polar polymer offering many of the properties of natural rubber, such as flexibility and high traction but with increased resistance to heat and chemicals [77, 78].

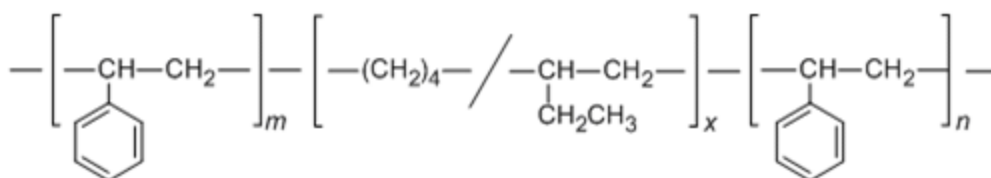


Figure 2.12: Styrene-ethylene butylene-styrene block copolymer.

The hydrogenated Kraton polymer (Kraton G) was also chosen in this work as a binder for the zeolite powders. Kraton G exhibits improved resistance to temperature (processing at 200-230°C is common) and to oxidation.

Only few works on SEBS-based composites are reported in literature. A blend of low density polyethylene (LDPE)/SEBS with ZSM-5 was proposed as material for food packaging. Having a higher flexibility and free volume than LDPE, SEBS was added to PE to improve the gas and water permeability of the composite while the zeolite provides gas selectivity [95].

2.5.2 Composite fabrication methods

Two methods were employed to fabricate the composite membranes: solution casting and extrusion.

a) Solution Casting

The solution casting technique consists of the fabrication of a membrane (composite or not) starting from a polymer in solution. The solution is poured into a mold, and when the solvent evaporates a polymer film is formed. In composite membranes the inorganic component is added to the solution before the casting.

This technique is simple and does not require any special equipment; however, the polymer has to dissolve well in a solvent and it requires a controlled procedure to eliminate the solvent in order to obtain a uniform defect-free film. In the case of composites, the inorganic component has to be well dispersed in the solution before casting, and it is often difficult to obtain homogeneous composites. The method can also induce porosity in the films due to the difficulty of controlling the solvent evaporation step.

(b) Extrusion

Extrusion is a technique used to process polymers [97]. A mixture of the polymer (in pellet or powder form) and the zeolite in the desired proportion is introduced through the feed screw into the mixing chamber (see Figure 2.13), heated above the melting temperature of the polymer.

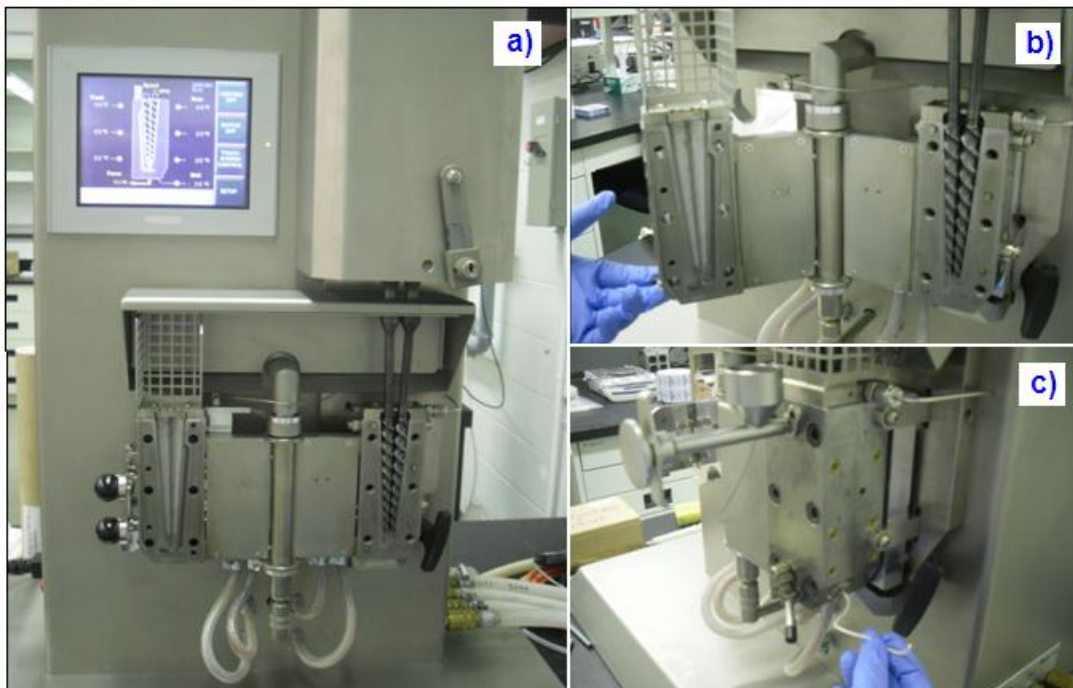


Figure 2.13: a) The extruder, b) open chambers and screws, c) closed chamber with hopper.

In the chamber the polymer melts and, under the action of the rotating screws, it is well mixed with the inorganic filler. By opening the valve connecting the mixing chamber and the die, the extrudate is then allowed to flow through the die at the bottom where it solidifies in air. The extrudate is cooled and solidified as it is pulled through the die.

Some of the composite membranes were prepared in a conical co-rotational twin screw extruder from DSM Xplore, model Micro 5cc, with 170 mm of length through a cylindrical die. A simple screw profile, designed only with transport elements was used.

2.5.2.1 Experimental procedure for the membrane fabrication

(a) Nafion-zeolite composites

Two series of composite membranes were prepared by casting a suspension formed by the desired amount of the CBV780 and 5 wt% or 20 wt% commercial Nafion® dispersions (DE521 and DE2021 Nafion® Polymer Dispersions, Ion Power Inc.). 2-

propanol was added to the 20 wt% Nafion® dispersion (1.66 g of 2-propanol for each 5 g of DE2021 dispersion). The suspensions were stirred for 30 minutes and kept in an ultrasonic bath for an additional 30 minutes to disperse the zeolite uniformly and then poured into a glass Petri dish. The solvent was evaporated in an oven at 50 °C for 6 hours, followed by a thermal treatment at 100 °C overnight and at 140 °C for 1 day. The membranes were peeled off by immersion in water.

Composites membranes with a zeolite loading from 2 to 40 wt% were prepared from the DE2021 Nafion dispersion and from 2 to 20 wt% from the DE521 Nafion dispersion.

Hot Pressing: A third series of composite membranes was obtained by additionally hot pressing the films prepared with the DE2021 Nafion dispersion. The hot pressing procedure consists of placing the membrane, protected by two Teflon sheets, between the plates of a Carver press (model 3851-0) heated at 140 °C for 1 minute and then hot pressing it under a pressure of 227 Kg cm⁻² for 40 s.

Activation procedure: All membranes were activated using the standard procedure for Nafion. They were boiled for 1 hour in 3 % H₂O₂ solution, then in deionized water for 1h, in 1.2 mol dm⁻³ H₂SO₄ solution for another hour and then stored in deionized water.

(b) Nafion-functionalized zeolite composites

Nafion-zeolite composites were also prepared using CBV780 functionalized with 12 mmol g⁻¹ of silane precursor, either in its -SH precursor form or in the -SO₃H form. The nominal wt% of zeolite was 10 wt%.

The procedure used to prepare the Nafion composite membranes with a functionalized zeolite is similar to the procedure used for the composites with unmodified zeolites. However, some of the composite membranes were prepared by using dimethylacetamide as a solvent instead of 2-propanol in order to improve the dispersion of the functionalized zeolite particles within the Nafion matrix.

The hot-pressing procedure and standard activation treatment for Nafion were also employed. It should be noted that the conversion of the silane from the –SH to SO₃H form is done when the membrane is treated with the boiling H₂O₂ solution.

(c) PVDF-zeolite composites

The PVDF-zeolite composite samples with a zeolite loading from 5 wt% to 80 wt% were prepared by solution casting. Composite membranes with a 5 wt% and 30 wt% of zeolite content were also prepared using CBV780 functionalized with 12 mmol g⁻¹ of 3-MPTMS.

PVDF pellets were milled to powder in a Retsch ZM 200 mill at a speed of 6000 rpm in order to accelerate the dissolution of the PVDF in the solvent. Prior to insertion in the milling chamber, the PVDF pellets were kept in liquid nitrogen for 5 minutes. The PVDF powder was dissolved in dimethylacetamide (15ml g⁻¹ PVDF) and the desired amount of zeolite was added to the solution. The total weight (PVDF pellets and zeolite powder) was kept constant at 1 g. The suspension obtained was magnetically stirred for 24h, then poured in a Petri dish of 5 cm diameter and dried overnight at 80°C. The same fabrication procedure was used for composites with unmodified and functionalized zeolites.

Hot Pressing: The membranes were hot-pressed using a Carver laboratory press at 130°C at 3 tons for 10 minutes.

Post-fabrication treatment: Composite samples fabricated with functionalized zeolite ((-SH) form) were treated in 3% H₂O₂ solution at 50°C, washed in deionized water and kept in 1.2M H₂SO₄ for 1 h. After treatment, the membranes were stored in deionized water. The treatment was necessary in order to convert the mercapto- groups of the grafted zeolite into sulfonic acid groups.

(d) PTFE-zeolite composites

The Teflon/zeolite composite were prepared by following the procedure reported by Z. Połtarzewski and collaborators [26].

Teflon - CBV780 composite membranes with a zeolite loading of 40 wt%, 70 wt% and 80 wt% were prepared by mixing a Teflon dispersion (60wt% in water, Aldrich) with a dispersion in water of zeolite, previously kept under ultrasonic stirring for 25 minutes at 50°C. The mixture was kept 25 minutes at 50°C in an ultrasonic bath and allowed to cool down. After addition of isopropanol (~30 vol.% of the suspension) and drying for 24h at room temperature, the mixture was dried at 70°C for 3h and then for 15 minutes at 150°C. To obtain a film, the paste was rolled on a flat surface with a small rolling pin.

(e) HDPE - Zeolite, SEBS - Zeolite and HDPE/SEBS (50/50) – Zeolite composites

Composites of CBV780/zeolite with HDPE, SEBS and with a HDPE/SEBS blend (50:50) were fabricated by extrusion. Both HDPE and SEBS pellets were pulverized using a cryogenic Retsch ZM 200 mill at a speed of 6000 rpm. The polymers and the zeolite powder in the desired proportions were always fed together. The barrel temperature was set between 190 and 200°C and the screw velocity was set at 100 rpm. The recirculation channels were used to set a residence time of approximately three minutes. The maximum shear rates in this extruder, using the conditions above, were approximately 1500 s⁻¹. The extruded composites were pressed in Carver press (model 3851-0), at 160°C and under 1 bar. All membranes had a thickness of approximately 200 µm.

The HDPE/Zeolite composites were prepared using a zeolite loading between 5 wt% and 60 wt% while the SEBS/zeolite and HDPE/SEBS/zeolite composites were prepared with 50 wt% and 60 wt% of zeolite.

Additional HDPE, SEBS and PE/SEBS composites were prepared using a 50 wt% loading of CBV780 grafted using 12 mmol g⁻¹ of silane precursor. The zeolite was added to the polymer in its –SH form. After being hot-pressed, the membranes were treated with 30% H₂O₂ at 50°C for 6 hours in order to convert the mercapto groups into sulfonic acid groups.

The results of the membrane characterization are presented in Chapter 6.

2.6 References

- [1] H. van Bekkum, E. M. Flanigen, J. C. Jansen, 1991. Introduction to Zeolite Science and Practice. Amsterdam, Elsevier Science Publishers B. V., 1991, p.18.
- [2] B. Smit, T. L. M. Maesen, 2008. "Towards a molecular understanding of shape selectivity". Nature, Vol. 451, p. 671-678.
- [3] K. Sahner, G. Hagen, D. Schönauer, S. Reiß, R. Moos, 2008. "Zeolites - Versatile materials for gas sensors". Solid State Ionics, Vol. 179, p. 2416-2423.
- [4] P. Horcajada, C. Márquez-Alvarez, A. Rámila, J. Pérez-Pariente, M. Vallet-Regí, 2006. "Controlled release of Ibuprofen from dealuminated faujasites". Solid State Sciences, Vol. 8, p.1459-1465.
- [5] A.L. Blumenfeld, J.J. Fripiat, 1999. "Characterization of Brønsted and Lewis acidity in zeolites by solid-state NMR and the recent progress in the REDOR technique". Magnetic Resonance in Chemistry, Vol. 37, p. S118-S125.
- [6] R.A. Van Santen, 1994. "Theory of Brønsted acidity in zeolites". Advanced Zeolite Science and Applications, Vol. 85, p. 273-294.
- [7] M. Rožić, Š. Cerjan-Stefanović, S. Kurajica, M. Rožmarić Maëfat, K. Margeta and A. Farkaš, 2005. "Decationization and dealumination of clinoptilolite tuff and ammonium exchange on acid-modified tuff". Journal of Colloid and interface Science, Vol. 284, p. 48-56.
- [8] A. De Lucas, P. Canizares, A. Durán and A. Carrero, 1997. "Dealumination of HZSM-5 zeolites: Effect of steaming on acidity and aromatization activity". Applied Catalysts A: General, Vol. 154, (1-2) p. 221-240.
- [9] R. M. Ravenelle, F. Schüßler, A. D'Amico, N. Danilina, J. A. Van Bokhoven, J. A. Lercher, C. W. Jones, C. Sievers, 2010. "Stability of zeolites in hot liquid water". Journal of Physical Chemistry C, Vol. 114, p. 19582-19595.
- [10] E.P. Ivanova, M.A. Kostova, B.K. Koumanova, 2010. "Kinetics of water and alcohol vapors adsorption on natural zeolite". Asia-Pacific Journal of Chemical Engineering, Vol. 5, p. 869-881.
- [11] M.E. Franke, U. Simon, 1999 "Proton mobility in H-ZSM5 studied by impedance spectroscopy". Solid State Ionics, Vol. 118 p.311-316.
- [12] P. Nischwitz, P. Amels, F. Fetting 1994. "Studies on the ionic conductivity of zeolitic solids". Solid State Ionics, Vol. 73, p. 105-118.

- [13] A. Abdoulaye, S.S. Soulayman, G. Chabanis, J.C. Giuntini, J.V. Zanchetta 1997. "Polarization conductivity in dehydrated zeolites NaY and HY". Microporous Materials, Vol. 8, p. 63-68.
- [14] S. D. Mikhailenko, S. Kaliaguine and E. Ghali, 1997. "Water-assisted Ionic Conductance of Zeolites with ZSM-5 Structure". Microporous Materials Vol. 11, p. 37-44.
- [15] M. S. Whittingham, A.J. Jacobson, 1982. Intercalation chemistry. New York, Academic Press.
- [16] M. Dekker, I. 't Zand, J. Schram, J. Schoonman, 1989. "NH₄Y and HY zeolites as electrolytes in hydrogen sensors". Solid State Ionics, Vol. 35, p. 157-164.
- [17] N. H. Mogensen, E. Skou, 1995. "Effect of solvation of charge carriers in hydrated zeolites". Solid State Ionics, Vol. 77, p. 51-54.
- [18] M. Saito, S. Tsuzuki, K. Hayamizu, T. Okada, 2006. "Alcohol and Proton Transport in Perfluorinated Ionomer Membranes for Fuel Cells". Journal of Physical Chemistry B, Vol. 110, p. 24410-24417.
- [19] V. Baglio, A. S. Aricò, A. Di Blasi, P. L. Antonucci, F. Nannetti, V. Tricoli and V. Antonucci, 2005. "Zeolite-based Composite Membranes for High Temperature Direct Methanol Fuel Cells". Journal of Applied Electrochemistry, Vol. 35, p. 207-212.
- [20] P. Kongkachuichay and S. Pimprom, 2010. "Nafion/Analcime and Nafion/Faujasite Composite Membranes for Polymer Electrolyte Membrane Fuel Cells". Chemical Engineering Research and Design, Vol. 88, p. 496.
- [21] Z. Zhang, F. Desilets, V. Felice, B. Mecheri, S. Licoccia, A. C. Tavares, 2011. "On the Proton Conductivity of Nafion-Faujasite Composite Membranes for Low Temperature Direct Methanol Fuel Cells". Journal of Power Sources, Vol. 196 (22), p. 9176-9187.
- [22] M. H. Yildirim, A. Roca Curoso, J. Motuzas, A. Julbe, D. F. Stamatialis and M. Wessling, 2009. "Nafion/H-ZSM-5 Composite Membranes with Superior Performance for Direct Methanol Fuel Cells". Journal of Membrane Science, Vol. 338, p. 75-83.
- [23] S.C. Byun, Y.J. Jeong, J.W. Park, S. D. Kim, H. Y. Ha, W. J. Kim, 2006 "Effect of solvent and crystal size on the selectivity of ZSM/Nafion composite membranes fabricated by solution-casting method". Solid State Ionics, Vol. 177 p. 3233-3243.
- [24] A. M. Herring, 2006. "Inorganic-Polymer Composite Membranes for Proton Exchange Membrane Fuel Cells". Journal of Macromolecular Science, Part C:

Polymer Reviews, Vol. 46, p. 245–296.

- [25] Z. Chen, B. Holmberg, W. Li, X. Wang, W. Deng, R. Munoz and Y. Yan, 2006. “Nafion/Zeolite Nanocomposite Membrane by in Situ Crystallization for a Direct Methanol Fuel Cell”. Chemistry of Materials, Vol. 18, p. 5669-5675.
- [26] Z. Połtarzewski, W. Wieczorek, J. Przyłuski and V. Antonucci, 1999. ”Novel Proton Conducting Composite Electrolytes for Application in Methanol Fuel Cells”. Solid State Ionics, Vol. 119, p. 301-304.
- [27] B. Libby, W.H. Smyrl and E.L. Cussler, 2003. ”Polymer-Zeolite Composite Membranes for Direct Methanol Fuel Cells”. AIChE Journal, Vol. 49, p. 991-1001.
- [28] J. Kjær, S. Yde-Andersen, N. A. Knudsen and E. Skou, 1991. ”Solid State Electrolyte Membranes for Direct Methanol Fuel Cells”. Solid State Ionics, Vol. 46, p. 169-173.
- [29] N. Rao, T. P. Andersen and P. Ge, 1994. ”Tin mordenite membranes for direct methanol fuel cells”. Solid State Ionics, Vol. 72, p. 334-337.
- [30] T. Sancho, J. Lemus, M. Urbiztondo, J. Soler and M. P. Pina, 2008. ”Zeolites and Zeotype Materials as Efficient Barriers for Methanol Cross-over in DMFCs”. Microporous and Mesoporous Materials, Vol. 115, p. 206-213.
- [31] V. Felice, A.C.Tavares, 2011. ”Faujasite zeolite as solid electrolyte for low temperature fuel cells”. Solid State Ionics, Vol. 194 (1), p. 53-61.
- [32] Database of Zeolite Structures (<http://www.iza-structure.org/databases>).
- [33] J. Lynch, F. Raatz, P. Dufresne, 1987. “Characterization of the textural properties of dealuminated HY forms”. Zeolite, Vol. 7, p. 333-33.
- [34] A. Zukal, V. Patzelova, U. Lohse, 1986. “Secondary porous structure of dealuminated Y zeolites”. Zeolites, Vol. 6 (2), p. 133-136.
- [35] T. Kawai and K. Tsutsumi, 1999. “A study on the surface silanol groups developed by hydrothermal and acid treatment of Faujasite type zeolites”. Journal of Colloid and Interface Science, Vol. 212, p. 310-316.
- [36] L. Aouali, J. Jeanjean, A. Dereigne, P. Tougne, D. Delafosse, 1988. “Structural evolution of dealuminated Y zeolites during various chemical treatments”. Zeolites, Vol. 8, p. 517-522.
- [37] W. Lutz, C.H. Rüscher, D. Heidemann, 2002. “Determination of the framework and non-framework [SiO₂] and [AlO₂] species of steamed and leached faujasites type

- zeolites: calibration of IR, NMR, and XRD data by chemical methods”. Microporous and Mesoporous Materials, Vol. 55, p. 193-202.
- [38] B. L. Meyers, T.H. Fleisch, C.L. Marshall, 1986. “Dealumination and Aluminum ion migration in faujasites”. Applied Surface Science, Vol. 26, p. 503-516.
- [39] B. Arkles, G. Larson, 2004. Silicon compounds: Silanes and Silicones. Morrisville Gelest.
- [40] A. Sayari, S. Hamoudi, 2001. “Periodic Mesoporous Silica-Based Organic-Inorganic Nanocomposite Materials”. Chemistry of Materials, Vol. 13, p. 3151-3168.
- [41] W. M. Van Rhijn, D. E. De Vos, B. F. Sels, W. D. Bossaert, P. A. Jacobs, 1998. “Sulfonic acid functionalised ordered mesoporous materials as catalysts for condensation and esterification reactions”. Chemical Communications, 3, p. 317-318.
- [42] D. L. Angst, G. W. Simmons, 1991. “Moisture absorption characteristics of organosiloxane self-assembled monolayers”. Langmuir, Vol. 7, p. 2236-2242.
- [43] W.D. Bossaert, D.E. DeVos, W. M. Van Rhijn, J. Bullen, P.J. Grobet, P.A. Jacobs, 1999. “Mesoporous Sulfonic Acids as selective heterogeneous catalysts for synthesis of monoglycerides”. Journal of Catalysis, Vol. 182, p. 156-164.
- [44] R. Helmy, A.Y.Fadeev, 2002. “Self-Assembled Monolayers Supported on TiO₂ Comparison of C₁₈H₃₇SiX₃ (X=H, Cl, OCH₃), C₁₈H₃₇Si(CH₃)₂Cl and C₁₈H₃₇PO(OH)₂”. Langmuir, Vol. 18, p. 8924-8928.
- [45] V. Smuleac, D.A. Butterfield, S.K. Sikdar, R. S. Varma, D. Bhattacharyya, 2005. “Polythiol-functionalized alumina membranes for mercury capture”. Journal of Membrane Science, Vol. 251, p. 169-178.
- [46] Y. Li, Y.Wang, T. Tran, A. Perkins, 2005. “Vibrational spectroscopic studies of (3-mercaptopropyl)trimethoxysilane sol-gel and its coating”. Spectrochimica Acta Part A, Vol. 61, p. 3032-3037.
- [47] S.-E. Park, Sujandi, 2008. “Green approaches via nanocatalysis with nanoporous materials: Functionalization of mesoporous materials for single site catalysis”. Current Applied Physics, Vol. 8, p. 664-668.
- [48] B. Sow, S. Hamoudi, M.H. Zahedi-Niaki, S. Kaliaguine, 2005. “1-Butanol etherification over sulfonated mesoporous silica and organosilica”. Microporous and Mesoporous Materials, Vol. 79, p. 129-136.
- [49] S. Sreevardhan Reddy, B. D. Raju, V.Siva Kumar, A.H. Padmasri, S. Narayanan,

- K.S. Rama Rao, 2007. "Sulfonic acid functionalized mesoporous SBA-15 for selective synthesis of 4-phenyl-1,3-dioxane". Catalysis Communications, Vol. 8, p. 261-266.
- [50] C. S. Gill, B. A. Price, C. W. Jones, 2007. "Sulfonic acid-functionalized silica-coated magnetic nanoparticle catalysts". Journal of Catalysis, Vol. 251, p. 145-152.
- [51] I. Diaz, C. Marquez-Alvarez, F. Mohino, J. Perez-Pariente, E. Sastre, 2000. "Combined alkyl and sulfonic acid functionalization of MCM-41-Type silica: Part 1. Synthesis and Characterization". Journal of Catalysis, Vol. 193, p. 283-294.
- [52] M. Boveri, J. Aguilar-Pliego, J. Pérez-Periente, E. Sastre, 2005. "Optimization of the preparation method of HSO₃-functionalized MCM-41 solid catalysts". Catalysis Today, Vol. 107-108, p. 868-873.
- [53] B. Rác, M. Nagy, I. Pálinkó, Á. Molnár, 2007. "Application of sulfonic acid functionalized MCM-41 materials—Selectivity changes in various probe reactions". Applied Catalysis A: General, Vol. 316, p. 152-159.
- [54] E. Cano-Serrano, G. Blanco-Brieva, J. M. Campos-Martin, J. L. G. Fierro, 2003. "Acid-Functionalized amorphous silica by chemical grafting-quantitative oxidation of thiol groups". Langmuir, Vol. 19, p. 7621-7627.
- [55] S. Mikhailenko, D. Desplantier-Giscard, C. Danumah, S. Kaliaguine, 2002. "Solid electrolyte properties of sulfonic acid functionalized mesostructured porous silica". Microporous and Mesoporous Materials, Vol. 52, p. 29-37.
- [56] R. Marschall, I. Bannat, J. Caro, M. Wark, 2007. "Proton conductivity of sulfonic acid functionalized mesoporous materials". Microporous and Mesoporous Materials, Vol. 99, p. 190-196.
- [57] H. Munakata, H. Chiba, K. Kanamura, 2005. "Enhancement of proton conductivity of inorganic-organic composite electrolyte membrane by addition of sulfonic acid group". Solid State Ionics, Vol. 176, p. 2445-2450.
- [58] S. Hamoudi, S. Royer, S. Kaliaguine, 2004. "Propyl- and arene-sulfonic acid functionalized periodic mesoporous organosilicas". Microporous and Mesoporous Materials, Vol. 71, p. 17-25.
- [59] W. Song, J. F. Woodworth, V. H. Grassian, S.C. Larsen, 2005. "Microscopic and Macroscopic Characterization of Organosilane-Functionalized Nanocrystalline NaZSM-5". Langmuir, Vol. 21, p. 7009-7014.
- [60] B.-Z. Zhan, M.A. White, M. Lumsden, 2003. "Bonding of organic amino, vinyl, and acryl groups to nanometer-sized NaX zeolite crystal surfaces". Langmuir, Vol. 19, p. 4205-4210.

- [61] J. C. McKeen, Y. S. Yan, M.E. Davis, 2008. "Proton Conductivity of Acid-Functionalized Zeolite Beta, MCM-41, and MCM-48: Effect of Acid Strength". Chemistry of Materials, Vol. 20, p. 5122-5124.
- [62] Y. Fong, A.Z. Abdullah, A. L. Ahmad, S. Bhatia, 2008. "Development of functionalized zeolite membrane and its potential role as reactor combined separator for para-xylene production from xylene isomers". Chemical Engineering Journal, Vol. 139, p. 172-193.
- [63] C.W. Jones, K. Tsuji, M. E. Davis, 1998. "Organic-functionalized molecular sieves as shape-selective catalysts". Nature, Vol. 393, p. 52-54.
- [64] D. Metin, F. Tihminlioglu, D. Balköse, S. Ülkü, 2004. "The effect of interfacial interactions on the mechanical properties of polypropylene/natural zeolite composites". Composite Part A, Vol. 35, p. 23-32.
- [65] X. Li, E. P. L. Roberts, S. M. Holmes, V. Zholobenko, 2007. "Functionalized zeolite A-nafion composite membranes for direct methanol fuel cells". Solid State Ionics, Vol. 178, p. 1248-1255.
- [66] B. A. Holmberg, X. Wang, Y. Yan, 2008. "Nanocomposite fuel cell membranes based on Nafion and acid functionalized zeolite beta nanocrystals". Journal of Membranes Science, Vol. 320, p. 86-92.
- [67] Y. Li, H. M. Guan, T.-S. Chung, S. Kulprathipanja, 2006. "Effects of novel silane modification of zeolite surface on polymer chain rigidification and partial pore blockage in polyethersulfone (PES)-zeolite. A mixed matrix membranes". Journal of Membranes Science, Vol. 275, p. 17-28.
- [68] Z. Chen, B. Holmberg, W. Li, X. Wang, W. Deng, R. Munoz, Y. Yan, 2006. "Nafion/Zeolite nanocomposite membrane by in Situ Crystallization for a direct methanol fuel cell". Chemistry of Materials, Vol. 18, p. 5669-5675.
- [69]. D. Sirikittikul, A. Fuongfuchat, W. Booncharoen, 2009. "Chemical modification of zeolite beta surface and its effect on gas permeation of mixed matrix membrane". Polymers Advanced Technologies, Vol. 20, p. 802-810.
- [70] P. Huttenloch, K. E. Roehl, K. Czurda, 2001. "Sorption of nonpolar aromatic contaminants by chlorosilane surface modified natural minerals". Environmental Science and Technology, Vol. 35 (21), p. 4260-4264.
- [71] W. Song, G. Li, V. H. Grassian, S. C. Larsen, 2005. "Development of improved materials for environmental applications: Nanocrystalline NaY zeolites". Environmental Science and Technology, Vol. 39, p. 1214-1220.

- [72] B.A. Holmberg, S-J. Hwang, M.E. Davis, Y. Yan, 2005. "Synthesis and proton conductivity of sulfonic acid functionalized zeolite BEA nanocrystals". Microporous and Mesoporous Materials, Vol. 80, p. 347-356.
- [73] M.Chidambaram, C.Venkatesan, A.P. Singh, 2006. "Organosilanesulfonic acid-functionalized Zr-TMS catalysts: Synthesis, characterization and catalytic applications in condensation reactions". Applied Catalysis A: General, Vol. 310, p. 79-90.
- [74] T. J. Horr, P.S. Arora, 1997. "Determination of the acid-base properties for 3-amino, 3-chloro and 3-mercaptopropyltrimethoxysilane coatings on silica surfaces by XPS". Colloids and Surfaces A: Physicochemical and Engineering Aspects, Vol. 126(2-3), p. 113-121.
- [75] C. Wu, T. Xu, W. Yang, 2003. "A new inorganic-organic negatively charged membrane: membrane preparation and characterizations". Journal of Membrane Science, Vol. 224, p. 117-125.
- [76] B. Rać, A. Molnar, P. Forgo, M. Mohai, I. Bertóti, 2006. "A comparative study of solid sulfonic acid catalysts based on various ordered mesoporous silica materials". Journal of Molecular Catalysis A: Chemical, Vol. 244, p. 46-57.
- [77] J. Brandrup, E.H. Immergut, 1975. Polymer Handbook, 2nd edition, New York, Wiley-Interscience
- [78] M.P. Stevens, 1999. Polymer chemistry and introduction, 3rd Edition, New York, USA, Oxford university press.
- [79] C. Liao, P. Yu, J. Zhao, L. Wang, Y. Luo, 2011. "Preparation and characterization of NaY/PVDF hybrid ultrafiltration membranes containing silver ions as antibacterial materials". Desalination, Vol. 272, p. 59-65.
- [80] S. J. Oha, N. Kimb, Y. T. Lee, 2009. "Preparation and characterization of PVDF/TiO₂ organic-inorganic composite membranes for fouling resistance improvement". Journal of Membrane Science, Vol. 345, p. 13-20.
- [81] D. S. Kim, H. B. Park, Y. M. Lee, Y. H. Park, J.-W. Rhim, 2004. "Preparation and characterization of PVDF/Silica Hybrid Membranes Containing Sulfonic Acid Groups". Journal of Applied Polymer Science, Vol. 93, p. 209-218.
- [82] K. Ebert, D. Fritsch, J. Koll, C. Tjahjawiguna, 2004. "Influence of inorganic fillers on the compaction behavior of porous polymer based membranes". Journal of Membrane Science, Vol. 233, p. 71-78.
- [83] Y.-J. Kim, C. Hyun Ahn, M. Bok Lee, M.-S. Choi, 2011. "Characteristics of electrospun PVDF/SiO₂ composite nanofiber membranes as polymer electrolyte".

- [84] S. Yu, X. Zuo, R. Bao, X. Xu, J. Wang, J. Xu, 2009. “Effect of SiO₂ nanoparticle addition on the characteristics of a new organic–inorganic hybrid membrane”. Polymer, Vol. 50, p. 553–559.
- [85] L. Yan, Y. S. Li,* , C. B. Xiang, 2005. “Preparation of poly(vinylidene fluoride)(pvdf) ultrafiltration membrane modified by nano-sized alumina (Al₂O₃) and its antifouling research”. Polymer, Vol. 46, p. 7701–7706.
- [86] A. Linares, J. L. Acosta, 2005. “Preparation and characterization of proton-exchange hybrid membranes”. Polymer International, Vol. 54, p. 972–979.
- [87] H.-Y. Hwang, D.-J. Kim, H.-J. Kim, Y.-T. Hong, S.-Y. Nam, 2011. “Effect of nanoclay on properties of porous PVdF membranes”. Trans. Nonferrous Met. Soc. China, Vol. 21, p. s141-s147.
- [88] C. Liao, P. Yu, J. Zhao, L. Wang, Y. Luo, 2011. “Preparation and characterization of NaY/PVDF hybrid ultrafiltration membranes containing silver ions as antibacterial materials”. Desalination, Vol. 272, p. 59–65.
- [89] A. C. Lopes, M. P. Silva, R. Goncalves, M. F. R. Pereira, G. Botelho, A. M. Fonseca, S. Lanceros-Mendez, I. C. Neves, 2010. “Enhancement of the Dielectric Constant and Thermal Properties of r-Poly(vinylidene fluoride)/Zeolite Nanocomposites”. Journal of Physical Chemistry C, Vol. 114, p. 14446–14452.
- [90] T. Sancho, J. Soler, M.P. Pina, 2007. “Conductivity in zeolite–polymer composite membranes for PEMFCs”. Journal of Power Sources, Vol. 169, p. 92–97.
- [91] Hidenori Yahiro, Yuuki Konda and Genji Okada, 2003 “Conductivity of zeolite/poly(tetrafluoroethylene) composite membrane in the presence of water vapor”. Phys. Chem. Chem. Phys., Vol. 5 p. 620–623.
- [92] K. Kim, S. Kwon, H. Kim, P. P. Kundu, Y.-W. Kim, Y.-K. Lee, K. J. Lee, B. H. Lee, S. Choe 2003. “Influence of Mixing Cycle on the Degree of Mixing of Calcite-Filled Polyethylene Upon Stretching”. Journal of Applied Polymer Science, Vol. 87, p. 311–321.
- [93] S. Nur Dirim, H. Özlem Özden, A. Bayındırlı, A. Esin, 2004. “Modification of water vapour transfer rate of low density polyethylene films for food packaging”. Journal of Food Engineering Vol. 63, p. 9–13.

- [94] P. P. Kundu, J. Biswas, H. Kim, S. E. Shim, S. Choe, D. S. Leek, 2004. "Effect of Calcite and Calcite/Zeolite Hybrid Fillers on LLDPE and PP Composites". Advances in Polymer Technology, Vol. 23, No. 3, p. 230–238.
- [95] P. Monprasit, C. Ritvirulh, T. Sooknoi, S. Rukchonlatee, A. Fuongfuchat, D. Sirikittikul, 2011. "Selective Ethylene-Permeable Zeolite Composite Double-Layered Film for Novel Modified Atmosphere Packaging". Polymer Engineering and Science, p. 1264-1272.
- [96] J. Biswas, H. Kim, S. Choe, P. P. Kundu, Y.-H. Park, D. S. Lee 2003. "Linear Low Density Polyethylene (LLDPE)/Zeolite Microporous Composite Film". Macromolecular Research, Vol. 11, No. 5, p. 357-367.
- [97] T.A. Osswald, G. Menges, 1996. Materials science of Polymers for Engineers. 2nd Edition, Cincinnati, Hanser-Gardner Publications.

3. Characterization techniques

This chapter contains descriptions of all the techniques used to characterize the samples under study. Several techniques were employed and they are listed in Table 3.1, together with the type of sample analyzed by each technique and the information obtained. This table aims to facilitate the reading of this chapter.

Table 3.1: List of techniques used to characterize the zeolite after dealumination (DEA), after functionalization (FUNCT) and the composite membranes.

Technique*	Type of sample	Information	Section
N₂ Sorption	Zeolites: DEA and FUNCT	Specific surface area Pore size distribution	3.1.1
H₂O and CH₃OH Sorption (DVS)	Zeolites: DEA and FUNCT Composite membranes	Water and Methanol uptake vs %P/P ₀ Water diffusion coefficient State of water	3.1.2
Water uptake and IEC	Composite membranes	Water uptake (contact liquid water) and number of protons (-SO ₃ H groups)	3.2 and 3.3
DSC	Composite membranes	State of water	3.4
NAA	Zeolites: DEA	%Si, %Al	3.5
TGA	Functionalized zeolites Composite membranes	Amount of grafted silane Zeolite content in composite membranes	3.6
CHNS Analysis	Zeolites: FUNCT	%S (amount of grafted silane)	3.7
FT-IR	Zeolites: DEA	Extent of dealumination	3.8
XPS	Zeolites: DEA and FUNCT, Nafion-zeolite composite membranes	1) Si/Al and extra-framework Al in DEA 2) Conversion -SH to -SO ₃ H 3) Interaction zeolite-Nafion	3.9
XRD	Zeolites: DEA and FUNCT	Structural changes	3.10
EIS	Zeolites: DEA and FUNCT	Proton Conductivity	3.11
DC (TP) and (IP)	Composite membranes	Proton Conductivity	3.12
Fuel Cell Testing	Composite membranes	Fuel cell performance	3.13

*The acronyms used in this table are explained at the beginning of the paragraph dedicated to each characterization method.

The principles of the techniques based on sorption measurements (N_2 , water and methanol) and the data analysis are presented first and in detail, due to the importance of these methods in this research work. Differential scanning calorimetry is also presented in more detail. For all the other techniques a brief description of the general principles and the experimental conditions applied to specific samples are presented afterwards.

3.1 Sorption measurements

In this work sorption measurements using three adsorbingspecies were carried out in order to obtain the following information:

- 1) N_2 sorption measurements were used to quantify the variation of the textural characteristics of the zeolites after dealumination and after functionalization by grafting of sulfonic acid groups.
 N_2 is a non polar molecule. Being quite inert, its adsorption behavior depends essentially on the number and size of the pores in the adsorbent material.
- 2) H_2O sorption measurements were performed on as-received, dealuminated and functionalized zeolites, and also on Nafion composite membranes and selected non-ionomer composites, in order to quantify the water sorption capacity of the samples as a function of the water partial pressure. Being a polar molecule, water can be used as a probe to estimate the hydrophilicity of the zeolite surface after modification. Information on the state of water and on the water diffusion through the composite membranes was also obtained from water sorption measurements.
- 3) CH_3OH sorption was measured as a function of the partial pressure on all zeolite samples, as-received and after functionalization in order to establish the effect of the functionalization on the methanol uptake.

As already discussed in Chapters 1 and 2, water plays an important role in the proton conduction in both Nafion-based membranes and zeolites. In the latter case, the extent of

porosity and the pore dimensions can determine the zeolite water sorption capacity and affect the proton diffusion through the channels, and they can also be the key factors to shape the selectivity between water and methanol in the zeolite.

Although N_2 , H_2O and CH_3OH are very different probe molecules, the sorption behavior of all species is based on common principles that are described below and prior to a discussion on the specific adsorptive properties.

The sorption mechanism is controlled by the interplay of several factors, such as the strength of the fluid - adsorbent wall and fluid - fluid interactions, and the textural properties of the adsorbent in relation to the size of the absorbing molecule.. For this reason, the sorption behavior of a specie depends on the adsorbent chemical and textural properties and in particular on the pore size. Based on the International Union of Pure and Applied Chemistry (IUPAC) classification, pores are classified based on their width: micropores, with internal width inferior to 2 nm; mesopores, with internal pore width between 2 nm and 50 nm; macropores, with an internal width greater than 50 nm [1,2].

The sorption behavior in micropores depends mainly on the interaction between the pore walls and the adsorbing molecules. In mesopores the interactions between the fluid molecules start to predominate. Macropores are so wide that they can be considered as flat surfaces.

The sorption behavior of adsorbents with different textural characteristics results in isotherms of different shapes. The IUPAC classification of six different sorption isotherms was published in 1985 and is reported in Figure 3.1. Each isotherm is characteristic of a material with specific textural characteristic.

The type I isotherm is typical of chemisorption or adsorption on microporous materials, while the type II isotherm is characteristic of non-porous or macroporous adsorbents. The type III isotherm arises from weak adsorbate-adsorbent interactions. In the case of a mesoporous material the type IV isotherm is typically observed and it is characterized by the presence of hysteresis loop between the adsorption and desorption curve. The type V isotherm reveals both a weak fluid-sorbent interaction and the presence of mesopores. The type VI isotherm is observed in the presence of stepwise multilayer adsorption on uniform non-porous surfaces by a spherically symmetrical non-polar absorbate [1].

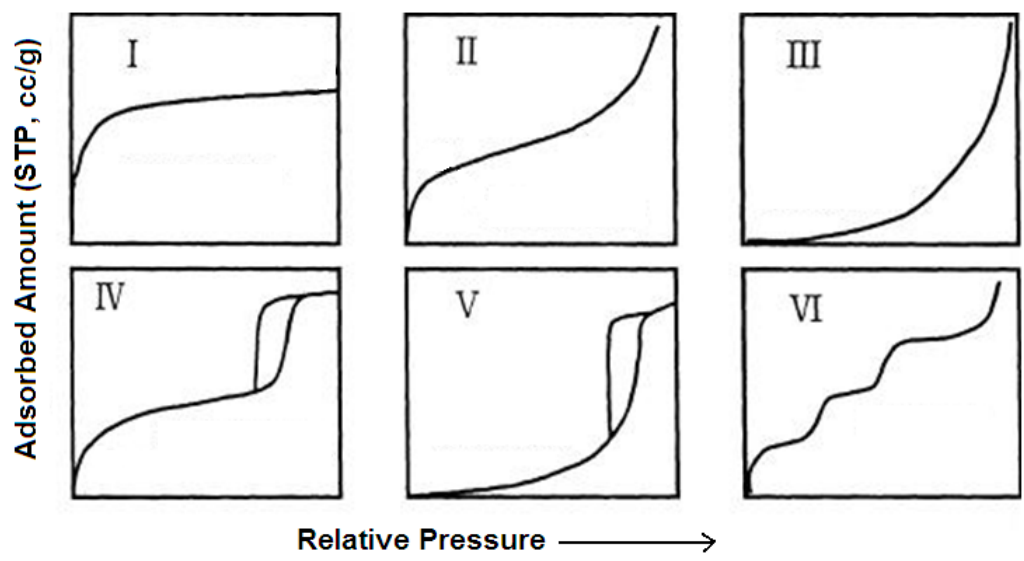


Figure 3.1: IUPAC classification of sorption isotherms (from [1]).

Information on the textural properties of the sample can be obtained from the shape and extent of the hysteresis loop [1,3]. The origin of the hysteresis loop is related to the difference between the nucleation and evaporation mechanisms inside the mesopores, further complicated by the presence of a more articulated pore structure [1,3]. A classification of the different types of hysteresis loops is also proposed by IUPAC and is reported in Figure 3.2.

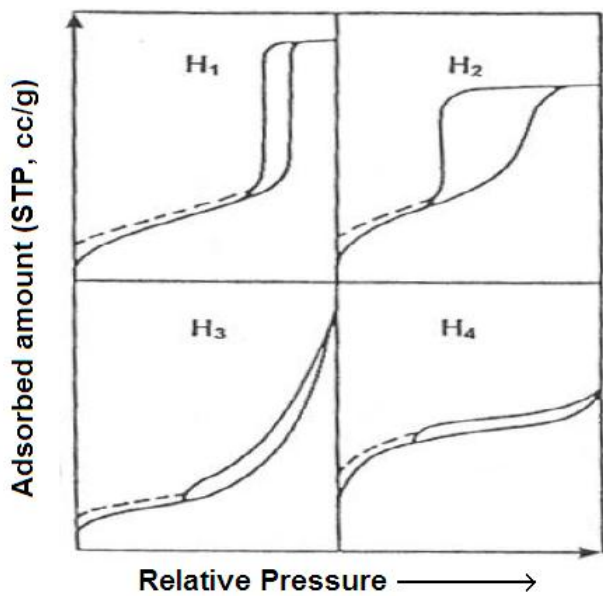


Figure 3.2: IUPAC classification of hysteresis loops (from [1]).

In figure 3.2 a correlation is made between the hysteresis loop shape and the type of porosity present in the sample. Hysteresis H1 is for porous materials with well-defined cylindrical-like pore channels or agglomerates of compacts of approximately uniform spheres; H2 is for poorly defined pore systems; H3 for non-rigid aggregates of plate-like particles giving rise to slit-shaped pores; and H4 is for narrow slit pores. The low pressure hysteresis (dashed curve) is observed in the case of a change in volume of the adsorbent i.e the swelling of non-rigid pores, or with the irreversible uptake of molecules in pores of about the same width as the adsorbate molecule, or in case of chemisorption.

Unlike nitrogen, water and methanol molecules are polar and their adsorption mechanism is influenced by their affinity for the adsorbent's surface.

In the case of a polar adsorbate the shape of the isotherm also reflects the hydrophilicity/hydrophobicity of the surface, and IUPAC proposed a classification scheme for such curves (Figure 3.3).

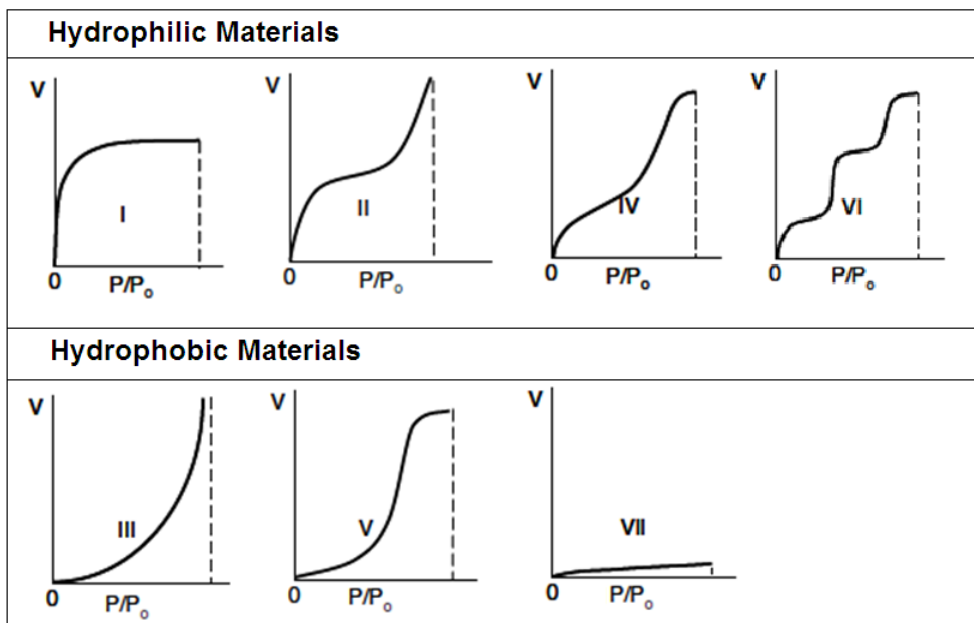


Figure 3.3: IUPAC classification of adsorption isotherms for materials with different hydrophilicities (with permission from [4] Copyright 2008, Elsevier).

Similar to the isotherm classification based on the textural characteristics of the adsorbent reported in Figure 3.1, each isotherm shape is ascribed to a material with specific hydrophilic characteristics [4]. Type I is characteristic of very hydrophilic materials. Type II and type IV isotherms are characteristic of moderately hydrophilic materials. Adsorbents with a low hydrophilicity will give rise to a type III or a type V isotherm. The type VI isotherm is typical of a hydrophilic material with multiple sorbent–water interactions and stepwise sorption while a type VII isotherm is characteristic of very hydrophobic materials.

3.1.1 N₂ sorption measurements

3.1.1.1 Data analysis

a) Determination of the Specific Surface Area: Brunauer, Emmett, and Teller theory

Brunauer, Emmett, and Teller (BET) theory explains the physical adsorption of gas molecules on a solid surface and it was used in this work to determine the specific surface area of the zeolite samples.

The BET theory is an extension to the multilayer adsorption of the Langmuir kinetic theory, which assumes that the coverage of a surface with an adsorbate is limited to a monolayer [1].

The BET theory is based on several assumptions such as that: the physisorption of gas molecules on a solid occurs infinitely, there is a dynamic equilibrium between the upper layer and the vapor, there is no interaction between each adsorption layer, and that the Langmuir theory can be applied to each layer. Taking into account these assumptions, the BET equation obtained in its final form is:

$$\frac{1}{W[P/P_0 - 1]} = \frac{1}{W_m C} + \frac{C - 1}{W_m C} \left(\frac{P}{P_0} \right) \quad (\text{E3.1})$$

where W is the weight of adsorbed gas, W_m is the weight of adsorbed gas in a completed monolayer, P is the equilibrium adsorbate pressure, P_0 is the pressure at saturation, and C is a constant related to the heat of adsorption and temperature.

From the equation E3.1, it is possible to obtain the surface area of the sample by plotting $1/W[P/P_0-1]$ as a function of P/P_0 . This plot usually yields a straight line in the range $0.05 \leq P/P_0 \leq 0.35$. From the slope and the intercept it is possible to obtain the W_m value and then the surface area S_t :

$$S_t = \frac{W_m N A_x}{MW} \quad (\text{E.3.2})$$

Where N is the Avogadro's number, A_x is the adsorbate cross-sectional area (for N_2 16.2 \AA^2) and MW is the adsorbate molecular weight.

To obtain the specific surface area S_{BET} , S_t is then divided by the mass of the sample.

b) Determination of the Total Pore Volume

The total specific pore volume, V_t , is determined from the volume of N_2 gas adsorbed at saturation ($P/P_0 \approx 1$), reflecting the adsorption capacity of the sample. V_t is calculated by converting the amount of gas adsorbed under standard conditions of temperature and pressure (STP), $V_{\text{ads, STP}}$, into a liquid volume V_{liq} , assuming that the density of the adsorbate is equal to the bulk liquid density at saturation:

$$V_t = V_{\text{liq}} = \left(\frac{PMW}{RT \rho_{\text{liq}}} \right) \cdot V_{\text{ads, STP}} \quad (\text{E.3.3})$$

where MW is the molecular weight, R is the gas constant, ρ_{liq} is the density of liquid nitrogen and P and T are the pressure and the temperature at standard conditions, respectively.

c) Determination of the micropore volume: t-Plot de Boer Method

The t-plot method was used to determine the micropore volume of the samples from the correlation with the statistical thickness, t , i.e. the film thickness on pore walls:

$$t = \frac{V_{liq}}{S} \quad (E3.4)$$

where S is the total surface area and V_{liq} is the adsorbed liquid volume[1].

By knowing the adsorbate diameter, t can be calculated by multiplying the number of monolayers by the adsorbate diameter as follows:

$$t = 3.54 \frac{W_a}{W_m} \quad (E3.4)$$

Where W_a is the weight adsorbed, W_m is the weight corresponding to the formation of a monolayer and 3.54 (in Å) is the nitrogen monolayer depth, assuming that the N_2 film has a close-packed hexagonal structure.

The thickness equation proposed by de Boer for nitrogen sorption at -196°C on adsorbents with oxide surfaces was used in this work:

$$t = \left[\frac{13.99}{\log \frac{P}{P_0} + 0.034} \right]^{1/2} \quad (E3.5)$$

By plotting the volume of adsorbed nitrogen V_{ads} at different P/P_0 values as a function of t , a straight line passing through the origin is obtained for a non-porous material. The slope (V/t) of this line gives the specific surface area. For a porous material, the line will have a positive intercept indicating the presence of micropores, or deviate from linearity,

suggesting the filling of mesopores. From this intercept it is possible to obtain the micropore volume.

**d) Determination of the mesopore volume:
Barrett, Joyner and Halenda method**

The Barrett, Joyner and Halenda (BJH) method is a procedure for calculating the pore size distribution from experimental isotherms using the Kelvin model of pore filling [1,5]. This method applies only to mesopores and small macropores.

The Kelvin equation relates the equilibrium vapor pressure of a curved surface, such as that of a liquid in a capillary or pore (P_p), to the equilibrium pressure of the same liquid on a planar surface (P_{ps}):

$$\ln \frac{P_p}{P_{ps}} = \frac{-2\gamma\bar{V}}{rRT} \quad (\text{E3.6})$$

Where γ surface tension of the liquid, \bar{V} is the molar volume of the condensed liquid contained in the narrow pore of radius r , R the gas constant and T the temperature.

In the BJH model, the relationship between N_2 desorption isotherms and the distribution of pore volumes with respect to pore radius is analyzed based on the assumption that the equilibrium between the gas phase and the adsorbed phase during desorption is determined by two mechanisms: (1) physical adsorption on the pore walls (occurring also in the case of a flat surface impenetrable to nitrogen), and (2) capillary condensation in the inner capillary volume [5]. By utilizing the Kelvin equation, the relationship between the volume of the capillary condensate and the relative pressure is defined.

**e) Micropore and Mesopore Volume determination:
Non Local -Density Functional Theory**

In this work Density Functional Theory (DFT) was used to determine the pore size distribution of the zeolite samples after dealumination. DFT is a microscopic method

based on statistical mechanics used to study and predict the properties of isolated molecules, bulk solids, material interfaces and condensed phases.

This theory is based on the density functional approach in which a functional $\Omega[\rho(r)]$ of the average density $\rho(r)$ is constructed and minimized with respect to $\rho(r)$ to obtain the equilibrium density (the local density $\rho(r)$ of the pore fluid). The grand potential $\Omega[\rho(r)]$ is given by the following expression:

$$\Omega[\rho(r)] = F[\rho(r)] - \int dr \rho(r)(\mu - V_{\text{ext}}(r)) \quad (\text{E3.7})$$

where $F[\rho(r)]$ is the intrinsic Helmholtz free energy functional in the absence of any external field, μ is the chemical potential and $V_{\text{ext}}(r)$ is the potential imposed by the walls. Once $\rho(r)$ is known, other thermodynamic properties, such as the adsorption isotherm, heat of adsorption, free energies and phase transitions, can be calculated.

The pore size analysis of the sample is based on a solution of the Generalized Adsorption Isotherm equation, which correlates the experimental sorption isotherm with a set of adsorption/desorption isotherms calculated for a set of pore sizes for a given adsorbate:

$$N(P/P_0) = \int_{W_p^{\text{MIN}}}^{W_p^{\text{MAX}}} N(P/P_0, W_p) f(W_p) dW_p \quad (\text{E3.8})$$

where $N(P/P_0)$ is the experimental adsorption isotherm data; W_p is the pore width, $N(P/P_0, W_p)$ is the isotherm on a single pore of width W_p and $f(W_p)$ is the pore size distribution function.

The set of theoretical isotherms, called the kernel, is calculated by integrating the equilibrium density profile, $\rho(r)$, of the fluid in the model pore. Because the equilibrium density profiles are known for each pressure along an isotherm, no assumptions about the pore filling mechanism are required as in the case of the macroscopic thermodynamic methods.

Particularly accurate in the analysis of the pore size distribution is the Non-Local Density Functional Theory (NLDFT), which differs from the Local DFT by taking into

consideration the short-ranged correlations between molecules [6]. The model takes in account that the density profile of a liquid near a wall usually exhibits oscillations on the scale of the molecular diameter and that the thermodynamics of the confined fluid is altered compared to the bulk fluid, affecting the pore condensation and hysteresis behavior.

In data analysis by the NL-DFT model the kernel for the N₂ sorption at -196 C on silica at equilibrium was used.

3.1.1.2 Experimental Procedure

N₂ sorption isotherms were measured at -196°C down to relative pressure P/P_o of 5x10⁻⁷ with a Quantachrome Instrument Autosorb-1. The samples were weighed and placed in the analysis port. Before the sorption measurement, each sample was heated at 60°C for 2h under vacuum. The sorption data were analyzed using Autosorb Software from Quantachrome Instrument. The data analysis can be carried out using different models depending on the system under study. A description of each model is given in the following paragraphs.

3.1.2 Water and Methanol sorption measurements: Dynamic Vapor Sorption (DVS)

Water and methanol DVS measurements were carried out on all zeolite samples as received, dealuminated and functionalized.

3.1.2.1 Principle of the technique and description of the apparatus

The Dynamic Vapor Sorption technique consists of determining the amount of solvent uptake by a sample exposed to a defined partial pressure by measuring the change in mass as a function of time up to equilibrium. An example of a typical diagram obtained from DVS measurements is shown in Figure 3.4.

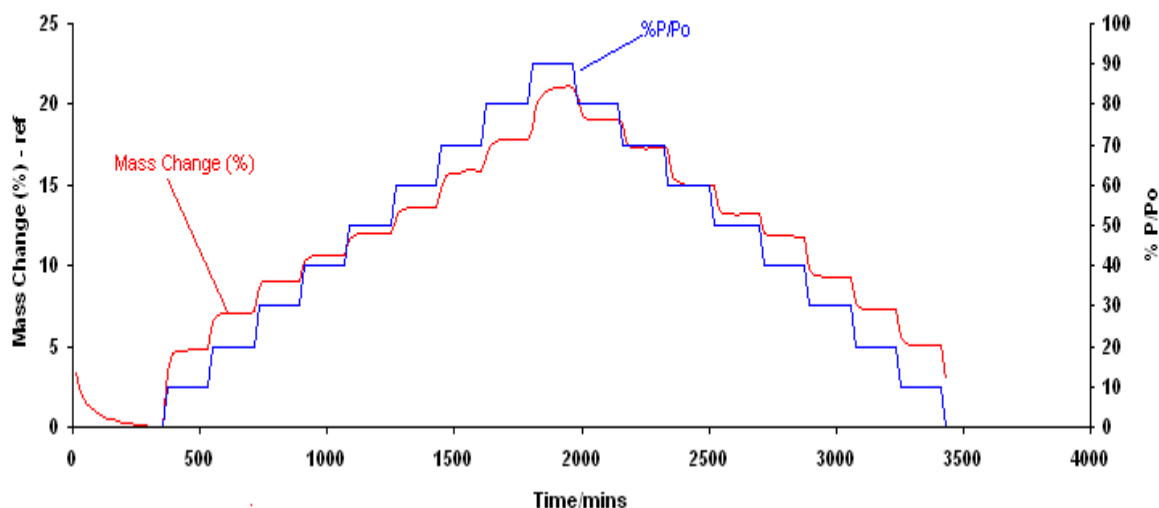


Figure 3.4: Kinetics of water sorption of CBV600 at 25°C and at different partial pressures.

From these measurements it was possible: 1) to quantify the variation of water and methanol sorption capacity between pristine and modified zeolites; 2) to evaluate the effect of zeolite addition on the composite membrane water sorption capacity; and 3) to determine the water diffusion coefficient and the state of the water in the Nafion-zeolite composite membranes.

Sorption isotherms were recorded with a DVS – High Throughput (HT) apparatus from Surface Measurement Systems, equipped with a Cahn ultra-microbalance with a mass resolution of 10 μg . A simplified scheme of the DVS apparatus is shown in Figure 3.5.

The DVS-HT is designed to perform dynamic vapor sorption measurements on up to 10 samples. The samples are placed on a rotating carousel, which enables the mass of all 10 pans to be sequentially measured whilst at all times maintaining their exposure to the % partial pressure and temperature-controlled environment.

The vapor partial pressure around the sample is controlled by mixing saturated and dry carrier gas steams using electronic mass flow controllers. The temperature is maintained constant $\pm 0.1^\circ\text{C}$, by enclosing the entire system in a temperature-controlled incubator.

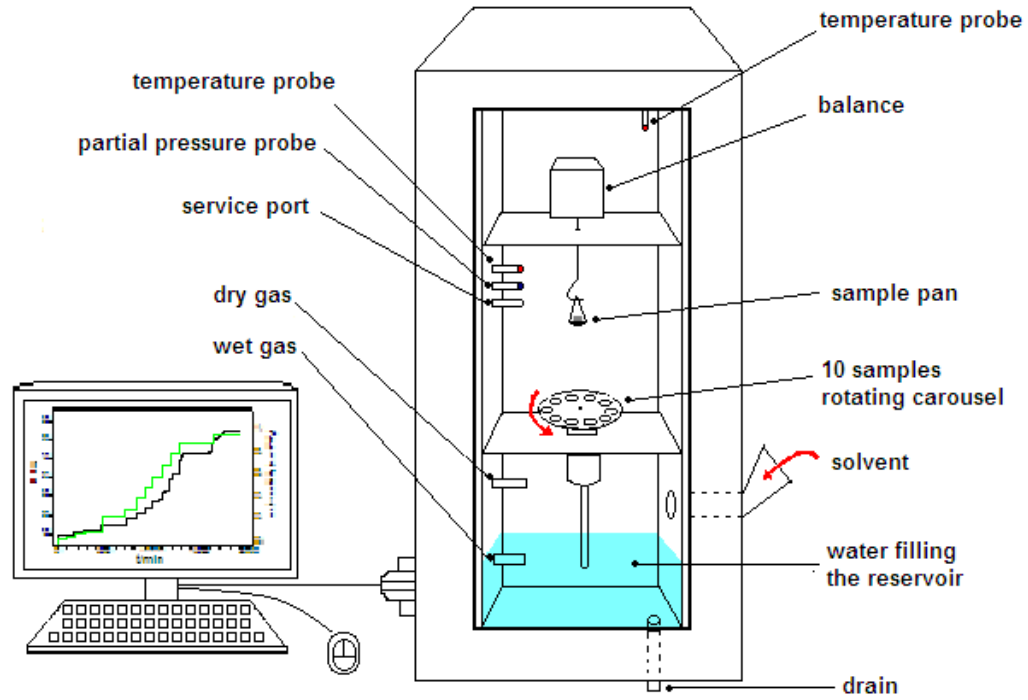


Figure 3.5: Illustration of the DVS apparatus interfaced with a personal computer.

3.1.2.2 Determination of the diffusion coefficients from DVS measurements

DVS measurements were also employed to evaluate the water diffusion coefficient in Nafion-zeolite composite membranes as a function of the zeolite content.

Assuming that the water sorption can be described by a Fickian behavior, the water diffusion coefficient, D , can be calculated from the relationship between the mass variation and the time of water vapor exposure up to equilibrium [7-9]. This relation is obtained by combining the first Fick's law (E3.9) (describing the transfer of solute atoms per unit area in a one-dimensional flow) and the conservation of mass relationship (E3.10) and is expressed by the second Fick's law (E3.11):

$$\mathbf{1^{st} Fick\ law} \quad J = -D \frac{\partial C(x,t)}{\partial x} \quad (\text{E3.9})$$

$$\mathbf{Conservation\ of\ mass} \quad \frac{\partial C}{\partial t} = -\frac{\partial J}{\partial x} \quad (\text{E3.10})$$

$$\mathbf{2^{nd} Fick law} \quad \frac{\partial C}{\partial t} = D \frac{\partial^2 C}{\partial x^2} \quad (\text{E3.11})$$

where: J is the particle flux; D is the diffusion coefficient; C is the concentration of the solute; x is the distance into the substrate, and t is the diffusion time

Assuming a constant diffusivity and that the water activity is constant across the membrane/vapor interface ($c=c_\infty$ at $x \pm d/2$), the solution of the equation E3.11 gives the relation between the normalized mass change and the time:

$$\frac{M_t}{M_\infty} = \frac{4}{d} \sqrt{\frac{Dt}{\pi}} \quad (\text{E3.12})$$

where: M_t is the mass of water adsorbed at time t , M_∞ is the mass of water adsorbed at equilibrium and d is the sample thickness

By plotting M_t/M_∞ for a sample exposed to a certain partial pressure P/P_0 as a function of the square root of time (Figure 3.6) and by fitting the curve to the equation E3.12, D can be obtained. This equation is valid for values of $M_t/M_\infty < 0.4$, where the plot of M_t/M_∞ against $t^{1/2}$ is linear.

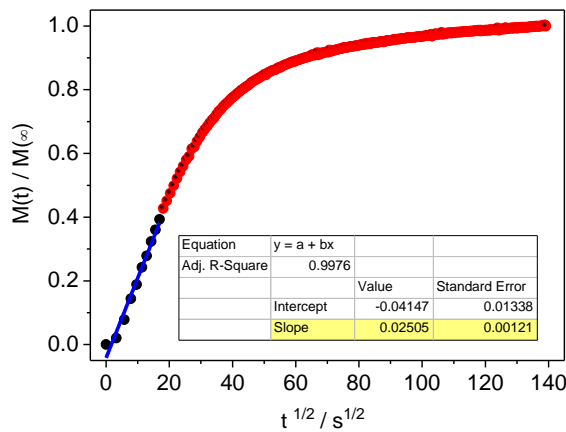


Figure 3.6: M_t/M_∞ versus $t^{1/2}$ at 25°C and at 97% P/P_0 for Nafion recast.

3.1.2.3 Determination of the different states of water

From the water sorption measurements it was also possible to obtain information about the effect of a zeolite on the water mobility (and consequently the proton transport) by investigating the state of water in the composite membranes.

This study was carried out by applying the multi-mode model proposed by Park [10-12] to the sorption isotherms of Nafion-zeolite membranes. The model hypothesizes the presence of three different mechanisms in the sorption process:

- a) specific adsorption at low water activity, described by the Langmuir model;
- b) non-specific adsorption, described by Henry's law;
- c) water clustering at high water activity.

All these contributions can be consolidated in the following equation:

$$C_w = \frac{a_L K_L a_w}{1 + K_L a_w} + K_H a_w + n K_A a_w^n \quad (\text{E3.13})$$

Where C_w is the water concentration, a_L is the specific site capacity, K_L is an affinity constant, K_H is the Henry's law coefficient, K_A is the aggregation equilibrium constant and n is the aggregate size, a_w is the water activity

According to this model, a distinct population of water adsorbed in the membrane can be associated with:

- a) specific adsorbed water [SA], consisting of the water molecules involved in strong hydrogen-bonding interactions with sulfonic acid groups in the Nafion membrane and residing in the hydration layers around the sulfonic acid groups (Langmuir population).
- b) non-specific adsorbed water [NSA] consisting of the molecules adsorbed in the polymer matrix by a dissolution mechanism (Henry population),

c) clustered water [C], due to the occurrence of an aggregation phenomena at high water activity.

Each water type is described by a term constituting the equation E3.13, as follows:

$$C_w [SA] = \frac{a_L K_L a_w}{1 + K_L a_w} \quad (\text{E3.14})$$

$$C_w [NSA] = K_H a_w \quad (\text{E3.15})$$

$$C_w [C] = n K_A a_w^n \quad (\text{E3.16})$$

Figure 3.7 shows a typical result of the curve fitting of a membrane sorption isotherm and the separation into the three contributions of sorbed water: $C_w[SA]$, $C_w[NSA]$ and $C_w[C]$.

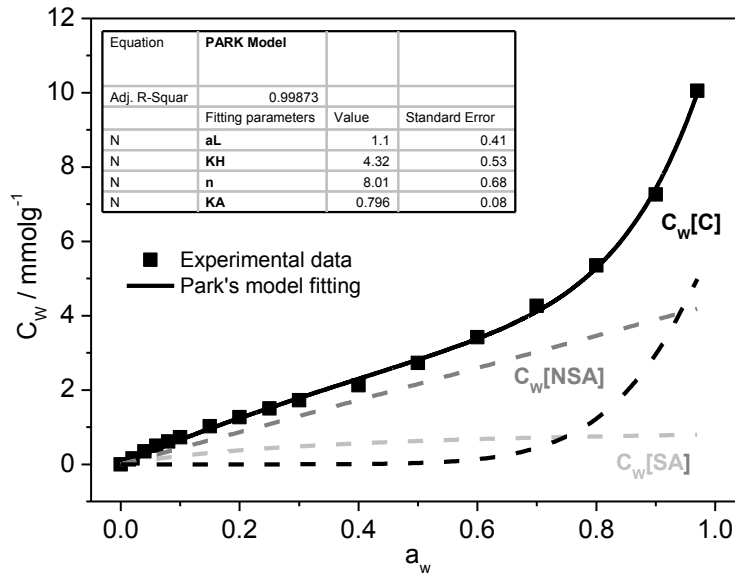


Figure 3.7: Typical curve fitting (Park's model) of experimental sorption isotherm data (unfilled Nafion recast, $T=25\text{ }^{\circ}\text{C}$) and the corresponding fitting parameters. $C_w[SA]$, $C_w[NSA]$, $C_w[C]$ refer to specific adsorbed water, non-specific adsorbed water and clustered water, respectively.

Each type of sorbed water is characterized by a different mobility. Being strongly bound to specific sites, the specific sorbed water is characterized by a low mobility, whereas the dissolved water molecules (Henry population) have a higher mobility. Then, the growth of water clusters reduces the mobility of the water aggregates. As a consequence, among the three types of water, the non-specific adsorbed water is characterized by the highest mobility.

The degree of mobility of water $\theta_w[NSA]$ in the membrane is calculated by normalizing the non specific sorbed water to the total amount of sorbed water:

$$\theta_w[NSA] = \frac{C_w[NSA]}{C_w} \times 100 \quad (E3.17)$$

The $\theta_w[NSA]$ parameter allows a comparison between the Nafion/zeolite composite membranes in terms of water mobility: the higher the value of $\theta_w[NSA]$, the greater the expected water mobility in the membrane.

3.1.2.4 Experimental conditions

In a DVS experiment, about 10 mg of zeolite powder or a section of $\approx 0.5 \text{ cm}^2$ of membrane film were placed in the stainless steel sample pans and dried under a stream of dry N_2 (5.0) at 25°C for 6 h. For each sample the loss of moisture during the drying stage is followed gravimetrically to ensure that all samples have reached a constant mass before the sorption measurements. Next, the partial pressure in the chamber is raised to a target value and the sample weight measured over time until constant mass (equilibrium). Depending on the type of sample (zeolite powders, ionomer and non-ionomer films) a different time is necessary to reach the equilibrium at each partial pressure and, for this reason, different sorption profiles were used as detailed below:

- a) Water and Methanol sorption profile for the zeolite powders:

Water and methanol sorption isotherms of as received, dealuminated and functionalized zeolite samples were recorded at 25°C by increasing the partial pressure (P/P_0) with a step size of 10 % P/P_0 and a step time of 3h in a full cycle from 0% to 97% P/P_0 and back down to 0% P/P_0 . The total gas flow used for each cycle was 400 sccm with water and 200 sccm with methanol.

b) Water sorption profile for Nafion-based composite membranes

Compared to the zeolite powder samples, the sorption profile of the Nafion-zeolite composite was modified by decreasing both the step size and increasing the step time in order to obtain a better fitting of the Park model to the experimental data and to obtain the diffusion coefficients (diffusion is usually a slower process than surface adsorption and requires longer steps at each relative humidity). The step size was shorter at low P/P_0 :

from 0 to 10% P/P_0 : step size: 2%, step time 3 h;

from 10 to 30% P/P_0 : step size 5%, step time 3 h;

from 30 to 80% P/P_0 : step size 10%, step time 3 h;

90% and 97% P/P_0 : step time 6 h.

For this series of measurements, each sample was run alone in order to record continuously the mass variation over time. The multi-sample mode is not suitable for the determination of the water diffusion coefficient.

c) Water sorption profile for non-ionomer composites

For these materials the interest was in measuring the water uptake at the highest partial pressure 97% P/P_0 (water sorption capacity). The partial pressure was varied from 0 to 97% P/P_0 with three short steps at 30%, 60% and 90% P/P_0 of 15 minutes each (necessary to avoid spikes in the P/P_0). The samples were kept 48h at 97% P/P_0 , as the adsorption process was much slower than in the Nafion based composites.

3.2 Water uptake from liquid water

The water uptake of the membranes was obtained from the difference between the weight of the sample completely hydrated and dry.

The sample was immersed in deionized water at room temperature for a time varying from 24h to 72h, depending on the time taken to reach a constant mass. Then the sample was removed from the water and the excess water eliminated from the membrane surface with wipe paper. The fully hydrated membrane was weighed. The membranes were then dried at 80 °C for 2 h in a vacuum oven and weighed. The percentage of water uptake was calculated as follows:

$$\text{Water uptake (\%)} = \left(\frac{W_w - W_D}{W_D} \right) \times 100 \quad \text{E3.18}$$

where W_D is the weight of the dried membrane and W_w is the weight of the wet membrane.

3.3. Differential Scanning Calorimetry

3.3.1 Principles of the technique

Differential Scanning Calorimetry (DSC) is a thermoanalytical technique generally used to determine the thermal transitions of polymers in a range of temperature between --180°C and +600°C [13,14]. It consists of measuring the difference between the amount of heat required to increase the temperature of a sample and of a reference with a well-defined heat capacity over the range of temperatures to be scanned. The sample and the reference will be maintained at the same temperature, and during a physical transformation (such as a phase transition), the heat flowing to the sample will be more or less than the heat flowing to the reference, depending on whether the process is endothermic or exothermic. The result of a DSC measurement is a curve of heat flux versus temperature or versus time. The area enclosed between the trend line and the base line is a direct measurement for the amount of heat, ΔH , needed for a transition. Useful

information can be obtained by DSC analysis of polymer samples such as the degree of crystallinity (from the ratio of the heat of fusion of a polymer sample and the heat of fusion of a 100% crystalline sample), specific heat capacity, the purity of the polymer and occurrence of oxidation, cross-linking and chain scission.

In this work, DSC was used to determine the state of water in the Nafion composite membranes. Water absorbed in a polymer shows, in fact, thermodynamic properties different from bulk liquid water due to the effect of capillary condensation, the presence of water clusters confined by the polymer chains and, above all, due to the interaction between the water molecules and the hydrophilic groups of the polymer. More than one type of adsorbed water differently bound to the polymeric matrix, and with different thermodynamic properties, can be distinguished [15-19].

- 1) **non-freezable bound water (W_{NF})**, strongly bound to the ionic groups present in the polymer. This type of water is characterized by the fact that it does not crystallize even when the swollen sample is cooled down to -100°C . These are water molecules in close proximity to an ionic group e.g. in hydration shells and which are highly polarized and unable to crystallize. W_{NF} water does not yield a characteristic thermal transition in DSC analysis.
- 2) **freezable bound water (W_F)**, weakly polarized. This type of water crystallizes at a temperature lower than 0°C .
- 3) **free water (W)**, crystallizes at 0°C

The freezable water, being more loosely bound, has a higher mobility than the non freezable water and it is supposed to play a more significant role in the proton transport mechanism. By performing a DSC analysis in the range between -50°C and 10°C , the freezable water can be quantified from the endothermic peak below 0°C . An example of a DSC thermogram obtained from a Nafion recast in the range -50°C to $+250^{\circ}\text{C}$ showing an endothermic peak ascribed to the melting of freezable water is shown in Figure 3.8.

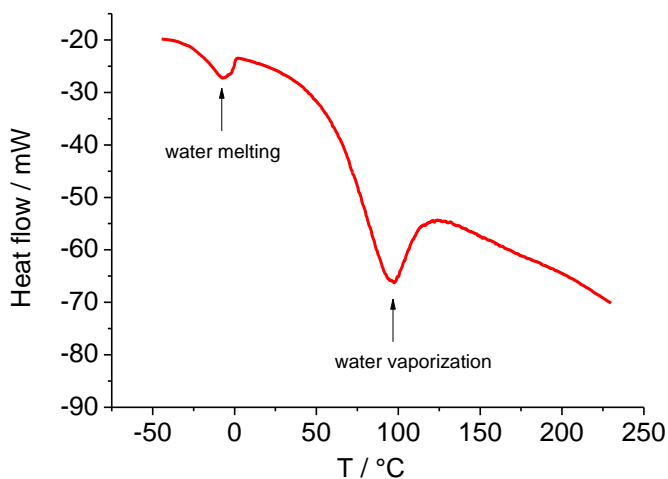


Figure 3.8: DSC thermogram of Nafion recast.

The percentage of freezable water in the sample was obtained from the following formula:

$$W_F (\%) = \left(\frac{A}{\Delta H_w} \frac{1}{m_d} \right) \times 100 \quad (\text{E3.20})$$

where A is the area of the endothermic peak, ΔH_w is the enthalpy of melting for bulk water (333 J g^{-1}) and m_d is mass of the dried sample.

3.3.2 Experimental procedure

The DSC measurements were carried out using a Perkin Elmer DSC 7 instrument at the Department of Chemical Science and Technology & NAST Centre, University of Rome “Tor Vergata”. The samples were equilibrated in liquid water at $25 \text{ }^\circ\text{C}$; then blotted with adsorbent paper and quickly sealed in aluminum DSC pans. In a typical run, the sample (two hydrated membrane disks of 6 mm in diameter) was cooled from $25 \text{ }^\circ\text{C}$ to $-50 \text{ }^\circ\text{C}$, then heated from $-50 \text{ }^\circ\text{C}$ to $10 \text{ }^\circ\text{C}$ at $10 \text{ }^\circ\text{C min}^{-1}$, under N_2 flow (20 ml min^{-1}). The DSC data reported in this work are the average values of quadruplicate analyses on different disks of the same sample.

3.4. Ion Exchange Capacity

The Ion Exchange Capacity (IEC) is expressed as the mmol of sulfonic acid groups for 1 g of dry polymer and it was determined by acid-base titration.

The membranes were dried at 80°C for 2 h in a vacuum oven, weighed and then immersed overnight into a 0.1 M NaCl solution to exchange the protons with Na⁺ ions. This solution was afterwards titrated with a 0.02 M NaOH solution until pH=7. IEC was calculated according to the following equation:

$$IEC(\text{mmol g}^{-1}) = \frac{V_{eq} \cdot C_{NaOH}}{W_D} \quad (\text{E3.19})$$

where W_D is the weight of the dry sample and V_{eq} and C_{NaOH} are the equivalent volume and the concentration of NaOH solution, respectively.

3.5 Neutron Activation Analysis

Neutron Activation Analysis (NAA) was used in this work to quantify the extent of dealumination of the samples, namely the variation of the concentration of Si and Al in samples after the acid treatment.

3.5.1 Principles of the technique

This technique is based on the activation of nuclei by bombarding them with neutrons [20]. The collision of the neutrons with the target nuclei of the elements constituting the sample causes neutron capture and the formation of compound nuclei in an excited state. The radioactive species will transmute into a more stable configuration by emitting gamma rays. This decay process depends on the unique half-life of the radioactive nucleus. The radioactive emission and radioactive decay paths are well known for each element. The number of gamma-rays detected at the specific energies is proportional to

the amount of the analysed elements in the sample. The exact amount of the elements is calculated by comparing with standards prepared from solutions of known concentration of each element.

3.5.2 Experimental conditions and equipment details

A sample amount between 50 mg and 100 mg was used for each analysis. The sample is weighed into a 1.4 mL polyethylene vial, and inserted in a polyethylene irradiation vial. A Slowpoke nuclear reactor (Atomic Energy of Canada Limited) with a pneumatic transfer system and a Germanium semiconductor gamma-ray detector (Ortec model GEM55185) was used for the analysis. The measurements were performed in the Slowpoke laboratory of the École Polytechnique de Montréal. The accuracy of the results is $\pm 5\%$.

3.6 Thermogravimetric Analysis

Thermogravimetric Analysis (TGA) was used to quantify the amount of grafted silane in functionalized samples and the zeolite content in composite membranes.

TGA provides quantitative measurements of mass change in materials, associated with dehydration, decomposition, and oxidation of a sample occurring with the increase of temperature [14, 21].

The thermogravimetric measurements were carried out with a Thermo-Gravimetric/Differential Thermal Analyzer (TG/DTA200, Seiko Instrument, Inc).

TGA measurements on pristine and modified zeolites were carried out under nitrogen flow, between 25°C and 650°C at a rate of 10°C min⁻¹. The same conditions were used for the Nafion and non-ionomer composite membranes.

3.7 Dynamic flash combustion method

The dynamic flash combustion method, also known as CHNS analysis, was carried out on

selected functionalized samples in order to quantify the amount of grafted silane from the percentage of S. This analysis was complementary to the thermogravimetric analysis. The CHNS analysis was also carried out on the three parent zeolites in order to quantify the hydrogen and, therefore, the number of hydroxyl groups present in each sample.

This technique is based on the complete oxidation of the sample [22]. About 2 mg of sample is weighed into a tin capsule and then introduced into a combustion reactor (a quartz tube) under a flow of He enriched with O₂. The sample and tin capsule react with oxygen and combust at temperatures of 1700-1800 °C, being broken into their elemental components, N₂, CO₂, H₂O and SO₂. The gases flow is carried through a gas chromatographic separation column, separated and detected sequentially by a thermal conductivity detector. The detector generates a signal, which is proportional to the amount of each element in the sample. The elemental peaks are compared to a known standard and a report for each element on a weight basis is generated.

The CHNS analysis was carried out at the Elemental Analysis Laboratory of the University of Montreal, and with the analyzer EAS1108, Fisons Instruments S.p.A. The accuracy of the results is $\pm 5\%$ for each element.

3.8 Fourier Transform-Infrared Spectroscopy

Fourier Transform - Infrared (FT-IR) spectroscopy was used to evaluate the extent of dealumination of acid treated zeolites.

3.8.1 Principle of the technique

IR spectroscopy gives information on the molecular structure through the frequencies of the normal modes of vibration of molecules [23]. The frequency of vibration is related to the strength of the bond and to the mass of the atoms involved in the bond; therefore, it can be associated with a particular bond type.

In a IR spectroscopy measurement, the sample is irradiated with infrared light. When the frequency of the IR radiation is the same as the vibrational frequency of a bond,

absorption and a transition between vibrational energy levels occur. The difference in energy between the two levels, E_1 and E_2 , is directly related to the frequency of the electromagnetic radiation by the following equation:

$$E_2 - E_1 = h\nu \quad (\text{E3.21})$$

in which h is Planck's constant and ν the vibrational frequency of the IR photon.

In a Fourier transform- infrared spectrometer, the infrared light is guided on the samples through an interferometer. A moving mirror inside the apparatus alters the distribution of infrared light that passes through the interferometer. The recorded signal, the light output as a function of mirror position, is then converted into light output as a function of infrared wavelength or wavenumber, $\bar{\nu}$, (i.e the frequency divided the velocity of light) by a data-processing technique called a Fourier transform. One of the advantages of the use of FTIR is that the information at all frequencies is collected simultaneously, improving both speed and signal-to-noise ratio.

The intensity of an infrared absorption peak is usually expressed as transmittance (T), i.e. the ratio of the radiant power or intensity (I) transmitted by a sample to the incident intensity (I_0):

$$T = I/I_0 \quad (\text{E3.22})$$

or as the logarithm in base 10 of its reciprocal, called absorbance (A):

$$A = \log_{10}(I_0/I) = \log_{10}(1/T) \quad (\text{E3.23})$$

3.8.2 Experimental Procedure

The powder samples were finely ground and mixed with KBr and the mixture was pressed in a mechanical press to obtain a pellet. FT-IR spectra were recorded over the range $650\text{-}4000\text{ cm}^{-1}$ for a total of 128 scans and with a resolution of 4 cm^{-1} using a NEXUS 670 FT-IR apparatus. Prior to each set of measurements, the spectrum of the background (air and KBr) was recorded and subtracted from the sample spectrum.

3.9 X-Ray Photoelectron Spectroscopy

X-Ray photoelectron spectroscopy (XPS) was used to obtain information about the concentration and state of Al at the surface of dealuminated zeolites and to follow the conversion of -SH into -SO₃H after the oxidation step during the zeolite functionalization. XPS was also employed to investigate the interaction between the zeolite and the polymer matrix in the Nafion composite membranes.

3.9.1 Principle of the technique

X-Ray photoelectron spectroscopy is based on the photoelectric effect, which occurs when an atom absorbs a photon of sufficient energy to cause the expulsion of an electron from its orbital [24,25]. The kinetic energy E_K of the expelled electron is equal to energy of the photon absorbed $h\nu$ minus the binding energy of the photoelectron E_b and the work function ϕ :

$$E_k = h\nu - E_b - \phi \quad (E3.24)$$

where h is Planck's constant and ν is the frequency of the exciting radiation. The work function ϕ is the energy required to bring an electron from the Fermi level to the vacuum level.

In XPS the sample is irradiated by a source of X-rays to produce the photoelectron effect.

An illustration of the photoelectric effect is shown in Figure 3.9.

Knowing the kinetic energy of the emitted photoelectron and the wavelength of the incident photon, it is possible to obtain the binding energy of the electron. A set of binding energies is characteristic of a certain element and its chemical environment.

A typical photoelectron spectrum consists of peaks distributed as a function of the binding energy: the position of the peaks gives information about the elements constituting the sample, their oxidation state and their bonding with other species, while from their intensity it is possible to quantify the elemental concentrations in the sample.

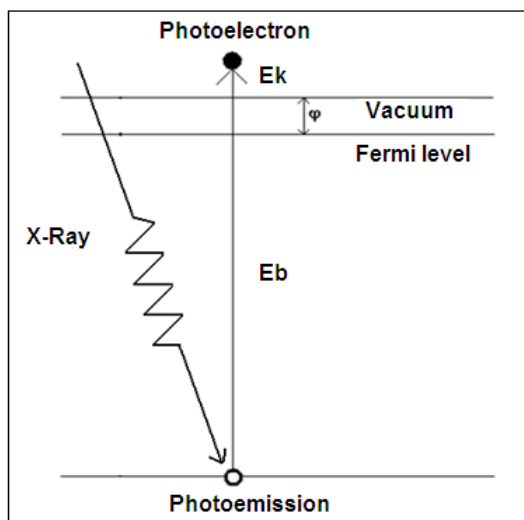


Figure 3.9: Scheme of the photoelectric effect (adapted with permission from [25], Copyright 1996, Elsevier).

3.9.2 Experimental

XPS spectra were recorded using a VG Escalab 220i-XL equipped with a achromatic Mg source ($\text{Mg K}_{\alpha} = 1253.6 \text{ eV}$) operating at 15 kV and 20 mA. The spectrum was acquired with a hemispherical analyser (pass energy = 20 eV) and the detection was performed with six single-channel detectors. The base pressure inside the spectrometer during the analysis was 3×10^{-10} Torr.

The samples were kept overnight in the preparation chamber before being transferred to the analysis chamber in order to reach the desirable pressure. The C1s photoelectron peak at 284.4 eV was used as an internal standard for the correction of the charging effect in all zeolite samples [25]. CasaXPS software was used to calculate the relative element concentrations.

3.10 X-Ray-Diffraction

X-ray diffraction (XRD) is a useful technique for the determination of the crystal structure of a sample. This technique was used to verify the effect of the acid treatment on the crystal structure of the zeolites.

3.10.1 Principle of the technique

Diffraction is a scattering phenomenon in which the regularly spaced atoms in a crystal act as scattering centers for an incident beam of X-rays, which have a wavelength about equal to the interatomic distance in crystals [26,27].

Based on the Bragg model, the diffraction phenomenon can be represented as a series of reflections from different families of atomic planes, characteristic of the crystal and identified by the Miller index (hkl) (Figure 3.10).

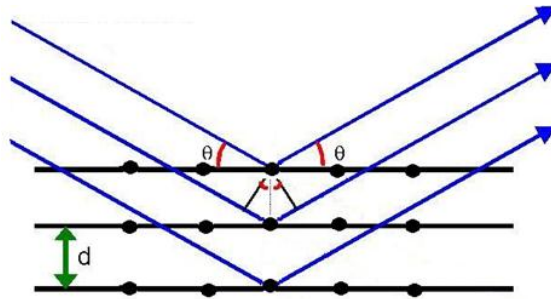


Figure 3.10: Illustration of the diffraction of X-rays by a crystal. The black dots represent the atoms while the lines represent the family of parallel planes with Miller index hkl and distance d from each other.

Diffraction occurs when the interference between the reflected rays is constructive and this condition is expressed by the Bragg equation:

$$n\lambda=2d \sin\theta \quad (\text{E3.25})$$

where n is an integer, λ is the X-ray wavelength, d_{hkl} is the distance between parallel planes of Miller index hkl and θ is the incident angle of the X-ray beam on the planes.

When the sample is a powder, XRD measurements are carried out by varying the incident angle of the X-ray beam, in order to consider all the possible orientations of the crystallites constituting the sample. The resulting diffraction pattern (intensity as a

function of 2θ) will present one or more series of peaks, characteristic of a specific crystalline phase present in the sample.

3.10.2 Experimental procedure

XRD characterization of the dealuminated zeolites was performed with a Bruker D8Advance diffractometer equipped with a $\text{CuK}\alpha$ source ($\lambda = 0.15406$ nm) operating at 40kV and 40mA, and data were collected between 2° and 40° (2θ) in a step mode of 0.02° and 1s duration. The unit cell parameter, a_0 , was calculated using EVA V14 software.

3.11 Electrochemical Impedance Spectroscopy

Electrochemical Impedance Spectroscopy (EIS) was used to determine the proton conductivity of zeolites as received, dealuminated and functionalized with sulfonic acid groups.

3.11.1 Theory

This technique consists of measuring the impedance of a system by applying a signal of alternating current as an excitation, over a wide range of frequency [28]. The excitation signal employed has a very low amplitude and the current–overpotential relation is virtually linear. The impedance Z of a system, i.e. its opposition to the flow of alternating current, is related to the current I and voltage V as follows:

$$I = V/Z \quad (\text{E3.26})$$

The impedance includes a real Z' and an imaginary part Z'' :

$$Z = Z' - jZ'' \quad (\text{E3.27})$$

where $Z' = R$ and $Z'' = 1/j\omega C$ and R is the ohmic resistance, ω is the angular frequency and C is the capacitance.

A system under study can be considered as an electrical circuit including both capacitive and resistive elements, in series or in parallel. For example, a system constituted of a powder compressed between two electrodes can be described by the equivalent circuit diagram shown in Figure 3.11.

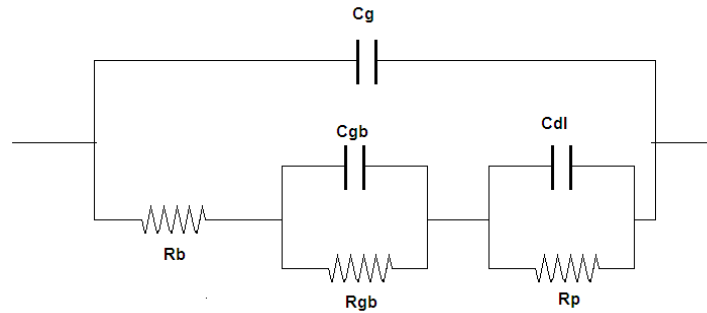


Figure 3.11: Equivalent circuit diagram (adapted with permission from [29], Copyright 1994, Elsevier). C_g , geometric capacitance; R_b , ion conductivity within the bulk of the crystal, R_{gb} , grain-boundary resistance; C_{gb} grain-boundaries capacitance; C_{dl} , double layer capacitance, R_p , polarization resistance.

The diagram (Figure 3.11) shows all the elements associated with processes taking place in the real system: the resistance to the passage of ions through the crystal bulk (R_b) and through the grain boundaries R_{gb} , the geometric capacitance C_g and the grain-boundaries capacitance (C_{gb}), double layer capacitance (C_{dl}) and polarization resistance (R_p). The total impedance of the system takes into account all these elements. However, the relaxation times characteristic of each process can differ of orders of magnitude and each process can be predominant at a different frequency. By measuring the impedance of the system as a function of the frequency, it is therefore possible to discern the different contributions.

One of the most common representations of the variation of the impedance with the frequency is the Nyquist plot, displaying Z'' vs Z' , with decreasing frequency from left to the right of the diagram. Ideally, each RC element in the equivalent circuit ascribed to the

system under study should appear in a Nyquist plot as a semicircle. However, the separation of the different contributions often requires a fitting of the plot. An example of a Nyquist plot recorded for a cell constituted of a zeolite (CBV600) pellet between two stainless steel electrodes is shown in Figure 3.12.

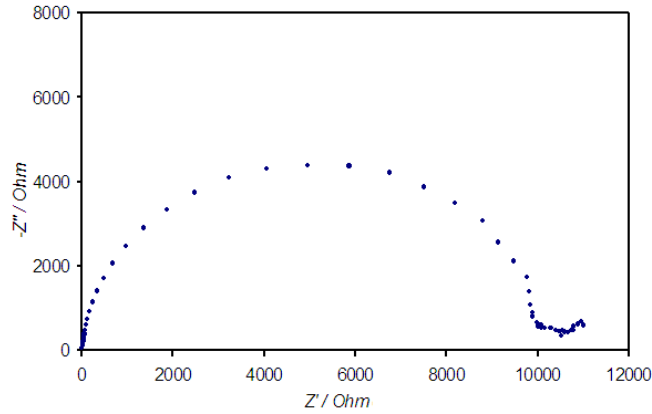


Figure 3.12: Nyquist diagram of CBV600 as-received.

3.11.2 Experimental conditions

EIS spectra were recorded with a SI 1260 impedance/gain-phase analyzer (Solartron) controlled by a PC through a GPIB interface, and by applying a sinusoidal signal with an amplitude of 10 mV over the frequency range 1Hz- 10MHz.

The pellets with a diameter of 7.2 mm were prepared by compacting ≈ 50 mg of zeolite powder under 12000 tons for 1 minute. The thickness of the pellets varies between 0.8 and 1 mm. The pellets were placed between the two stainless steel electrodes. An illustration of the cell used is shown in figure 3.13.

The impedance measurements were made at 25°C, at 10%, 50% and 90% relative humidity (RH) and for samples immersed in liquid water. The relative humidity control was achieved by equilibrating the pellets for 1 week in a hermetic box containing saturated salt solutions of LiCl, $Mg(NO_3)_2$ and $BaCl_2$ for 10, 50 and 90 % RH, respectively [30].

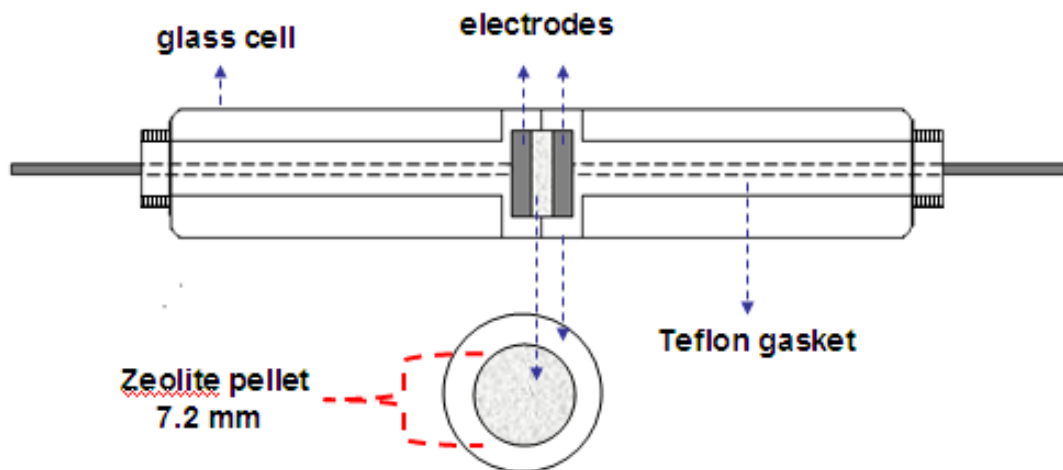


Figure 3.13: Illustration of the cell used for the EIS measurement.

The measurements on zeolite pellets in direct contact with water were carried out after 48h of immersion in deionised water. The pellets were dried under vacuum at 50°C for 2 hours before their exposure to each % water vapor.

The resistance of the electrolyte, R_e , was obtained from the Nyquist plot by considering the intersect of the semi-circle with the real Z' axis [31]. Knowing the R_e , it is possible to obtain the resistivity, ρ , and therefore the proton conductivity of the sample, σ , from the Ohm's law:

$$R_e = \rho l/S \rightarrow \sigma = 1/\rho \quad (\text{E3.28})$$

where l is the thickness of the pellet and S its surface area (0.41cm^2).

Analysis of the impedance spectra were carried out using Zview software.

3.12 Ex-situ membrane proton conductivity measurements

The proton conductivity of fully hydrated composite membranes was measured at room temperature and in two different directions of the membrane: in plane and through plane. Two different electrochemical cells were used.

3.12.1 Through – plane proton conductivity

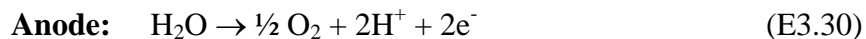
The membrane through-plane proton conductivity was determined from measurements of potential difference as a function of the current density flowing between two electrodes placed at the two sides of the membrane, according to the procedure reported by Slade et al. [32]. The electrochemical cell for this measurement is a four electrodes glass cell, shown in Figure 3.14, filled with 0.5M H₂SO₄ solution.



Figure 3.14: Four electrodes glass cell used for through-plane proton conductivity measurements.

Two Pt electrodes on the two sides of the membrane are connected to a galvanostat (AMEL Instruments Model 2051) and the current flowing between them is varied between 0 and 200 mA and back to 0 mA in 20 mA steps. The potential difference at each current value is measured by connecting two saturated calomel reference electrodes (SCE) to a digital voltmeter. The two SCEs are placed at a fixed distance from either face of the membrane using Luggin capillaries.

The net cell reaction (E3.29) is water electrolysis to produce hydrogen and oxygen at the cathode (E3.30) and at the anode (E3.31), respectively:



The potential difference is plotted against the current (measured over a wide range of current density) and the average cell resistance is obtained from the slope of the straight line. The membrane resistance is obtained by subtracting from the total cell resistance the cell resistance value determined when the cell is filled only with electrolyte. The membrane conductivity is calculated as in Equation (E3.28) in Paragraph 3.11, where, l is the thickness of the membrane and S is its surface area (0.79 cm^2).

3.12.2 In-plane proton conductivity

In-plane proton conductivity measurements were carried out using a Bekktech conductivity cell fixture with four Pt electrodes [33] shown in Figure 3.15.

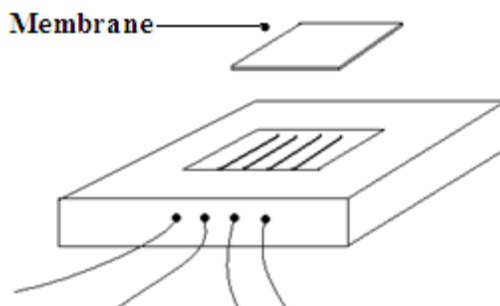


Figure 3.15: Four Pt electrodes cell.

The membrane is placed on the top of the four Pt electrodes. The two outer electrodes were connected to a galvanostat (AMEL Instruments Model 2051) and the two central platinum electrodes were connected to a digital voltmeter to measure the potential along the film section.

The current between the external electrodes was varied between 0 and 15 mA and back to 0 mA in steps of 1 mA, and the potential difference between the two inner Pt electrodes recorded. Similarly to the through-plane measurements, the slope on the E-I plot corresponds to the membrane resistance, from which the conductivity is obtained (Equation (E3.28), Paragraph 3.11).

Each membrane was soaked in water overnight before the measurement. The cell fixture was put inside a closed glass box with water in the bottom, and a water soaked filter paper was put on the top of the cell to keep the membrane fully hydrated. A full cycle was always recorded, and the overlapping of the two straight lines confirmed that the hydration was kept constant during the measurement. The in-plane conductivity measurements were carried out on both faces of the membranes.

3.13 Direct Methanol Fuel Cell tests

Unfilled Nafion and selected Nafion-zeolite composite membranes were tested in a DMFC. Both anode and cathode were purchased from Electrochem Inc; the anode catalyst layer contained 3 mg cm^{-2} PtRu alloy (from a 60 wt% PtRu/Vulcan XC-72 catalyst) and the cathode catalyst layer contained 3 mg cm^{-2} Pt (from a 60 wt% Pt/Vulcan XC-72 catalyst), and both electrodes were coated with 1 mg cm^{-2} Nafion. The membrane electrodes assembly (MEA) was hot pressed at $140 \text{ }^\circ\text{C}$ and installed in a fuel cell fixture of 5 cm^2 active area (Fuel Cell technologies). The single cells were connected to a fuel cell test station (model 850c from Scribner Associates) and equilibrated with the humidified gases at room temperature. For each MEA two cycles of galvanostatic polarizations were recorded at $40 \text{ }^\circ\text{C}$ with methanol solution fed to the anode chamber and with humidified air pre-heated at the same cell temperature fed to the cathode. The fuel cell tests were performed at different methanol concentrations: 1M, 2M, 5M and 10M. Atmospheric pressure in the anode and cathode compartments was used for all

experiments. The flow rates of methanol and air were 2.5 and 220 ml min⁻¹, respectively. The MEAs performance improved during the first two days of operation and reached steady-state behavior. Only the data set recorded under steady-state conditions is presented.

3.14 References

- [1] S. Lowell, J.E. Shields, M.A. Thomas, M. Thommes, 2004. Characterization of Porous Solids and powders: surface area, pore size and density, p. 148, Netherlands, Kluwer Academic Publishers.
- [2] B. D. Zdravkov, J. J. Čermák, M. Šefara, J. Janku, 2007. "Pore classification in the characterization of porous materials: A perspective". Central European Journal of Chemistry, Vol. 5(2), p. 385-395.
- [3] H. Liu, L. Zhang, N. A. Seaton, 1993. "Sorption Hysteresis as a Probe of Pore Structure". Langmuir, Vol. 9, p. 2576-2582.
- [4] E. Ng, S. Mintova, 2008. "Nanoporous materials with enhanced hydrophilicity and high water sorption capacity". Microporous and Mesoporous Materials, Vol. 114, p. 1-26.
- [5] E.P. Barrett, L.G. Joyner, P. P. Halenda, 1951. "The Determination of Pore Volume and Area Distributions in Porous Substances. I. Computations from Nitrogen Isotherms". Journal of American Chemical Society, Vol. 73, p. 373-380.
- [6] P. Tarazona, U. Marini, B. Marconi and R. Evans, 1987. "Phase equilibria of fluid interfaces and confined fluids: Non-local versus Local density functionals". Molecular Physics, Vol. 60, No. 3, p. 573-595.
- [7] J. Crank, G.S. Park, 1968. Diffusion in Polymers. , New York Academic Press.
- [8] Morris, DR; Sun, XD, 1993. "Water-sorption and transport properties of Nafion 117". Journal of Applied Polymer Science, Vol. 50, (8), p. 1445-1452.
- [9] T. Takamatsu, 1979. "Sorption phenomena in Nafion membranes". Journal of Applied Polymer Science, Vol. 24 (11), p. 2199-2220.
- [10] S. Ge, X. Li, B. Yi, and I-M. Hsing, 2005. "Absorption, Desorption and Transport of Water in Polymer Electrolyte Membranes for Fuel Cells". Journal of Electrochemical Society, Vol. 152, p. A1149.
- [11] P.W. Majsztzik, M. Barclay Satterfield, A.B. Bocarsly, J.B. Benziger, 2007. "Water

- sorption, desorption and transport in Nafion membranes”. Journal of Membrane Science, Vol. 301, p. 93-106.
- [12] M. Legras, Y. Hirata, Q. T. Nguyen, D. Langevin, M. Métayer, 2002. “Sorption and diffusion of water in Nafion 117 membranes with different counter ions”. Desalination, Vol. 147, p. 351-357.
- [13] T.A. Oswald, G. Menges, 2003. Materials Science of Polymers for Engineers. 2nd Edition, Cincinnati, USA, Hanser Gardner Publications.
- [14] B. Wunderlich, 2005. Thermal Analysis of Polymeric Materials. Berlin, Germany, Springer-Verlag.
- [15] A. Higuschi, T. Iijima, 1985. “DSC investigation of the sites of water in poly(vinyl alcohol) membranes”. Polymer, Vol. 26, p. 1207-1211.
- [16] Z. H. Ping, Q.T. Nguyen, S.M. Chen, J.Q. Zhou, Y.D. Ding, 2001. “State of water in different hydrophilic polymers-DSC and FTIR studies”. Polymer, Vol. 42, p. 8461-8467
- [17] T.L. Kalapos, B. Decer, H.A. Every, H. Ghassemi, T.A. Zawodzinski Jr, 2007. “Thermal studies of the state of water in proton conducting fuel cell membranes”. Journal of Power Sources, Vol. 172, p. 14-19.
- [18] A. Siu, J. Schmeisser, S. Holdcroft, 2006. “Effect of water on the low temperature conductivity of polymer electrolytes”. Journal of Physical Chemistry, Vol. 110, p. 6072-6080.
- [19] L. Guan, H. Xu, D. Huang, 2011. “The investigation on states of water in different hydrophilic polymers by DSC and FTIR”. Journal of Polymer Research, Vol. 18, p. 681-689.
- [20] S. J. Parry, 1991. Activation spectrometry in Chemical Analysis. Canada, John Wiley & Sons.
- [21] P. J. Haines, 2002. Principles of thermal analysis and calorimetry, Cambridge, UK, The Royal Society of Chemistry.
- [22] R. J. Errington, 1997. Advanced Practical Inorganic and Metalorganic Chemistry. 1st Edition, London, UK, Blackie Academic and Professional.
- [23] J. Mohan, 2003. Organic Analytical Chemistry: Theory and Practice, Pangbourne, UK, Alpha Science International.
- [24] D. Briggs and M.P. Seah, 1994. Practical Surface Analysis Volume 1-Auger and X-ray Photoelectron Spectroscopy, 2nd Edition, John Wiley & Sons.

- [25] M. Stöcker, 1996. "X-ray photoelectron spectroscopy on zeolites and related materials". Microporous Materials, Vol. 6, p. 235-257.
- [26] R. Jenkins and R.L. Snyder, 1996. Introduction to X-ray Powder Diffraction. New York: Wiley-Interscience.
- [27] B. D. Cullity, 1978. Elements of X-Ray Diffraction. 2nd Edition, MA: Addison-Wesley Publishing Company.
- [28] A. J. Bard, L. R. Faulkner, 2001. Electrochemical Methods. Fundamentals and Applications, 2nd Edition, New York, John Wiley & Sons.
- [29] P. Nischwitz, P. Amels, F. Fetting 1994. "Studies on the ionic conductivity of zeolitic solids". Solid State Ionics, Vol. 73, p. 105-118.
- [30] R. L. Opila, C.J. Weschler, R. Schubert, 1989. "Acidic vapors above saturated salt solutions commonly used for control of humidity" IEEE Transactions on Components, Hybrids and Manufacturing Technology, Vol. 12,p. 114.
- [31] S. D. Mikhailenko, S. Kaliaguine, E. Ghali, 1997. "Water-assisted ionic conductance of zeolites with ZSM-5 structure". Microporous Materials, Vol. 11, p. 37-44.
- [32] S. Slade, S.A. Campbell, T.R. Ralph, F.C. Walsh 2002. "Ionic Conductivity of an Extruded Nafion 1100 EW Series of Membranes". Journal of Electrochemical Society, Vol. 149, p. A1556.
- [33] Y. Sone, P. Ekdunge, D. Simonsson, 1996. "Proton conductivity of Nafion 117 as measured by a four-electrodes AC impedance method" Journal of Electrochemical Society, Vol. 143, p. 1254.

4. Faujasite dealumination

Part of this research work was dedicated to the tailoring of zeolite properties by dealumination. An intensive physicochemical characterization of the dealuminated samples allowed a correlation to be established between the zeolite chemical and textural properties and the proton conductivity.

4.1 Chemical and structural characterization of dealuminated samples.

The three FAUs with different Si/Al molar ratios were exposed to a 6 mol dm^{-3} HCl solution. The elemental analysis of all as received and acid treated samples was carried out by neutron activation analysis in order to quantify the extent of the dealumination. The variation of the Si/Al molar ratio as function of the acid exposure time, t_D , for from 0 to 168h is shown in Figure 4.1.

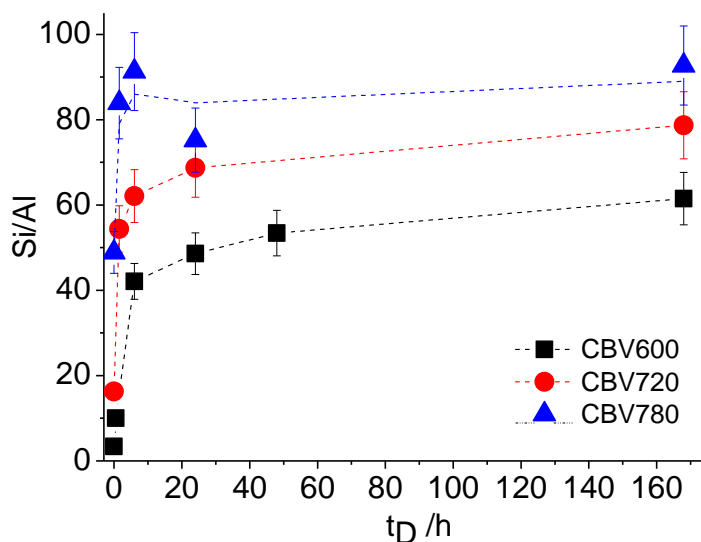


Figure 4.1: Si/Al molar ratio as a function of the dealumination time, t_D , for CBV600, CBV720 and CBV780 series.

The Si/Al ratio of all the three series increases rapidly within the first 24 hours, meaning that the Al removal by 6 mol dm^{-3} HCl solution is a very fast process. Subsequently, the dealumination rate is significantly lower, although not negligible for the CBV600 and

CBV720 series. As expected, the extent of dealumination is higher for the parent zeolite richer in Al (CBV600>CBV720>CBV780), and after 168 h the Si/Al ratio increased from 3.4 to 61.5 for the CBV600 series, from 16.3 to 78.7 for the CBV720 series and from 48.9 to 92.7 for the CBV780 series. The acid treatment of the CBV600 series was extended to 4500h and 7000h, and as revealed by NAA, the Si/Al ratio increased to 76.5 and 94.0 after 4500h and 7000h of acid treatment, respectively.

The structural integrity of each dealuminated sample was verified by X-ray diffraction, and the diffraction patterns of the CBV600 parent zeolite and of samples dealuminated for 24h and 7000h are shown in Figure 4.2.

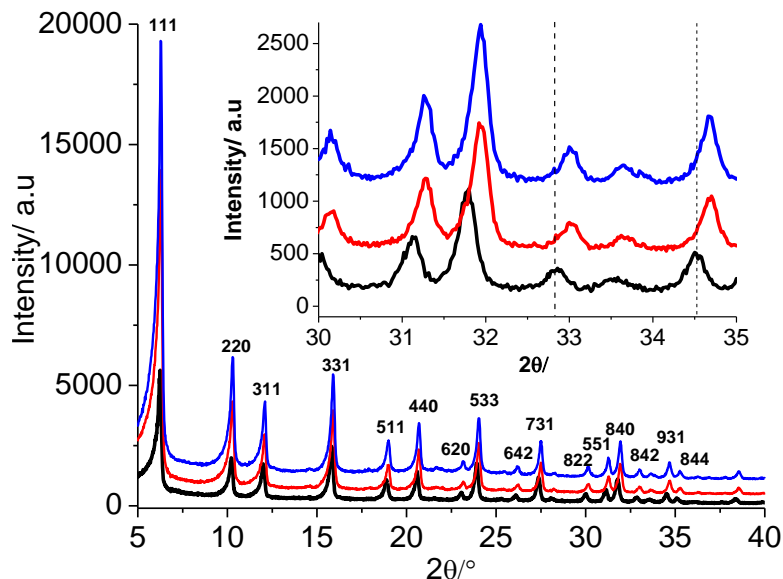


Figure 4.2: X-ray diffraction patterns of the CBV600 zeolite, as received (black) and after acid exposure for 24h (red) and 7000h (blue).

All diffraction peaks are related to the cubic Faujasite structure and no other crystalline phases were detected. Similar results were obtained for the other two zeolites series, CBV720 and CBV780 (XRD patterns not shown).

The degree of crystallinity of the as-received and dealuminated samples was estimated from the X-ray diffraction patterns. The degree of crystallinity was calculated as the ratio between the area of the peaks after subtraction of the background and the sum of the area of the peaks and the background in the same 2θ range. For the determination of the

degree of crystallinity two different 2θ regions of the diffraction pattern reported in literature were used: the region between 13° and 40° , as reported by Lynch[1], and the area of one single peak (corresponding to the 533 reflection) in the 2θ range between 23° and 25° , as reported by other authors[2].

Table 4.1 reports the degree of crystallinity for three zeolites of the CBV600 series: the as received CBV600 and the samples dealuminated for 24h and 7000h of acid exposure.

Table 4.1: Degree of crystallinity of CBV600 as-received and following acid exposure for 24h and 7000h, considering different regions of the diffraction patterns.

Sample	Reference [1]	Reference [2]
CBV600	0.37	0.64
Dealuminated for 24h	0.46	0.71
Dealuminated for 7000h	0.46	0.71

The as-received CBV600 sample has a lower degree of crystallinity (10% and 20% lower) than all the CBV600 dealuminated samples, for which the degree of crystallinity does not vary with the extent of dealumination. Although the absolute values are different, the same trend is observed in both the calculations. It is possible that the CBV600 as-received sample contains some amorphous residual phase from the synthesis procedure which is readily washed away during the acid treatment, although XPS data (as discussed in following paragraphs) does not show the presence of other species such as amorphous Al_2O_3 [3] or extra-framework Al [4]. No variation of the crystallinity (~ 0.42 based on Reference [1], ~ 0.70 based on Reference [2]), was observed between as-received and dealuminated samples of the CBV720 and CBV780 series.

As shown in the insert in Figure 4.2, the diffraction peaks of the dealuminated samples are shifted to higher 2θ values, which is consistent with the contraction of the cell parameter, a_o , after Al removal [5]. No further variation of the unit cell parameter was observed for all the three dealuminated series after 24h of acid treatment. The a_o values calculated for the CBV600, CBV720 and CBV780 as-received samples are 24.35 \AA , 24.31 \AA and 24.24 \AA , respectively, and 24.25 \AA , 24.24 \AA and 24.23 \AA after 24h of acid

exposure, respectively. As expected, the a_o reduction was higher for the CBV600 series, due to the higher extent of dealumination undergone by this Al-rich zeolite.

The dealumination process was also followed through the position of the T-O-T asymmetric stretching ($\omega_{\text{T-O-T}}$) band in the FTIR spectrum, because it shifts to higher wavenumber with a decrease of the Al content in the zeolite framework [5], as illustrated in Figure 4.3.a for the parent and dealuminated (for 6 hours) CBV600 samples.

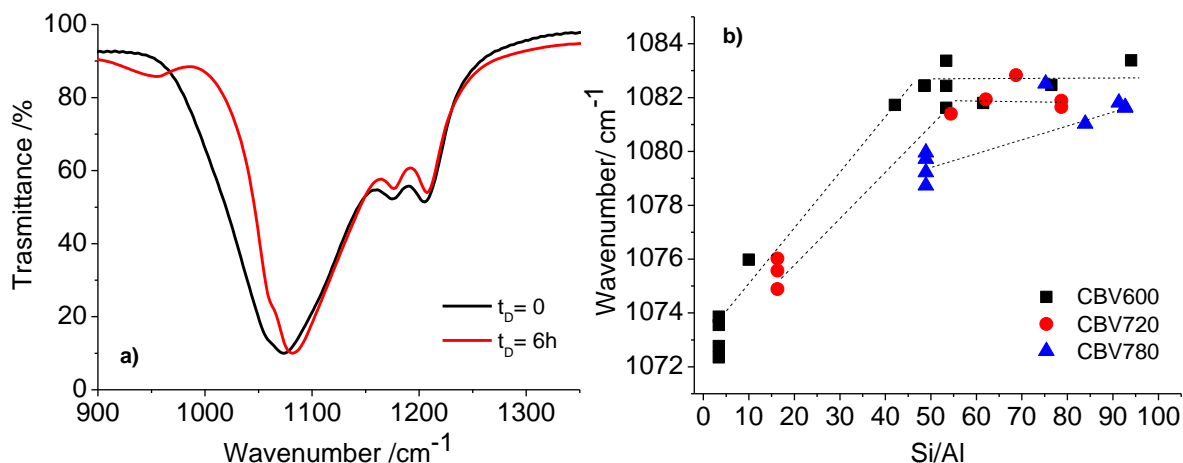


Figure 4.3: (a) Infrared spectra of CBV600 zeolite as-received and after 6h of acid treatment; (b) Peak wavenumber frequency of the T-O-T asymmetric stretching band of CBV600, CBV720 and CBV780 as a function of the Si/Al ratio.

As was found for the XRD patterns, no further variation in the T-O-T asymmetric stretching position is observed in the FTIR spectra after 24h of acid exposure, and for all the three series of Faujasites. Figure 4.3.b shows that the peak wavenumber of the T-O-T stretching band tends to level off for a Si/Al ratio higher than 55.

The infrared spectra and the diffraction patterns of the dealuminated samples suggest the end of the Al removal process after 24h of acid exposure. However, as determined by NAA, the Si/Al ratio continues to increase even after 24 hours for the CBV600 and CBV720 series.

The CBV600 series was further investigated by XPS analysis. As shown in Figure 4.4, for $t_D \geq 48$ h the surface Si/Al molar ratio is lower than the Si/Al ratio obtained from NAA analysis, thus pointing to a surface enrichment in Al; in addition, the difference

between the two values increases with the dealumination time.

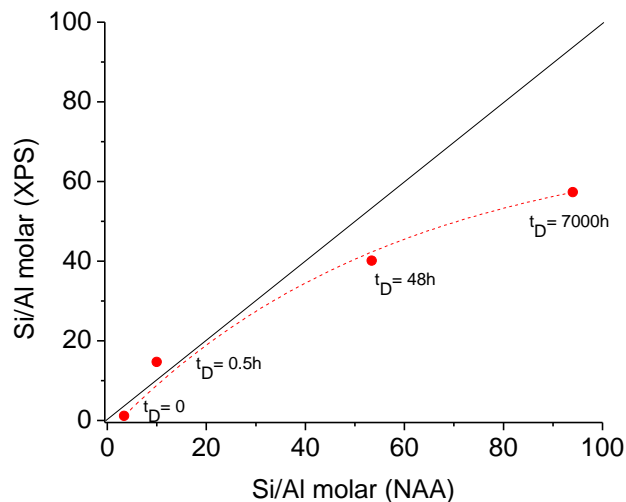


Figure 4.4: Correlation between the Si/Al molar ratio determined by XPS and by NAA for the CBV600 series; as-received ($t_D = 0$) and after $t_D = 0.5$ h, 48h and 7000h.

A surface enrichment in Al was not expected since the samples were dealuminated using concentrated hydrochloric acid. Nevertheless, Al surface enrichment on ferrierite type zeolites dealuminated by HCl leaching (0.25 to 11.4M for 4 hours at room temperature) has been also reported in the literature [6]. The deconvolution of the Al2p core level spectra reported in Figure 4.5 shows the presence of two different Al (III) species for all dealuminated samples, one at ca. 75 eV assigned to framework Al [4] and the other one at lower binding energy.

The binding energy (E_b), the full width at half maximum (FWHM) and the relative concentration of each Al species are reported in Table 4.2.

In spite of the surface enrichment in Al, the total amount of Al on the surface decreases significantly with the dealumination time, as expected. The Al species at lower binding energy could be due to non-framework Al species present on the surface as a thin film and not detected by XRD.

Hence, it can be concluded that the dealumination process for FAU zeolites exposed to HCl 6 mol dm⁻³ occurs mainly within the first 24 hours, and that for longer dealumination periods the variation on the total Si/Al ratio detected by NAA is due to the removal of

surface Al species formed during the first hours of acid treatment.

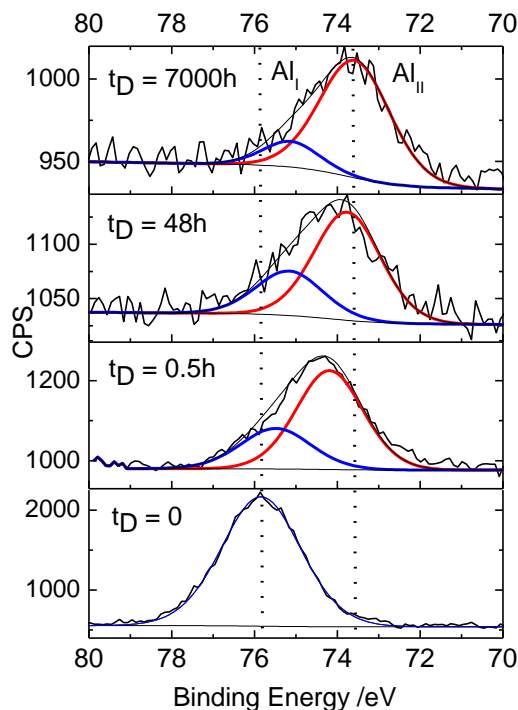


Figure 4.5: Evolution of the Al2p core level spectrum with the dealumination time for the CBV600 series, as received ($t_D = 0$) and after acid exposure for 0.5h, 48h and 7000h; Al_I- Al contribution ascribed to the framework Al; Al_{II}- Al contribution ascribed to the extraframework Al.

Table 4.2: Binding energy, full width half maximum and relative peak area of the Al2p photoelectron lines recorded for CBV600 as-received and dealuminated samples.

t_D / h	Al _I 2p			Al _{II} 2p		
	E_b / eV	FWHM/ eV	A_R / %	E_b / eV	FWHM/ eV	A_R / %
0	75.8	2.2	100	-	-	-
0.5	75.5	2.0	30.3	74.2	1.9	69.7
48	75.2	1.9	29.1	73.8	1.9	70.9
7000	75.1	1.6	14.8	73.6	2.0	85.2

t_D – dealumination time; E_b – binding energy; FWHM – full width at half maximum; A_R – Relative peak area; Al_I- Al contribution ascribed to the Al framework; Al_{II}- Al contribution ascribed to non- framework Al.

4.2. Textural characterization

N₂ isotherms were recorded for all samples in order to quantify the variation of the textural properties caused by the acid leaching and to correlate it with the water sorption and proton conductivity. Figure 4.6 shows the N₂ adsorption and desorption isotherms of the CBV600 sample as received, and after 48h and 7000h of acid treatment.

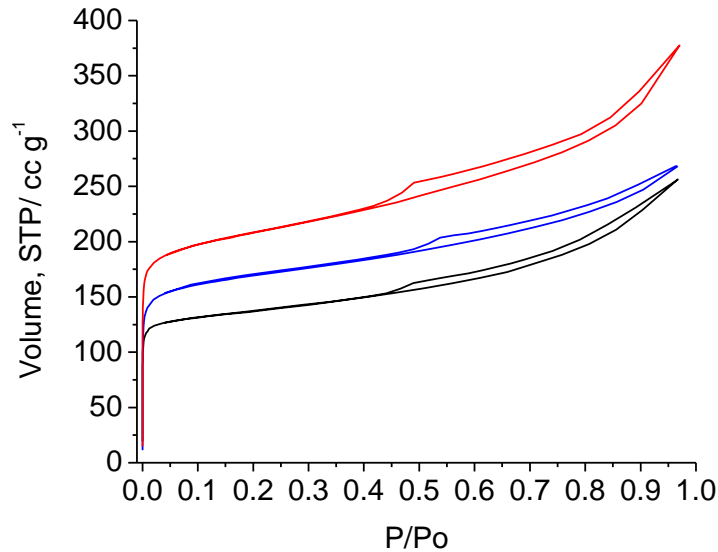


Figure 4.6: N₂ adsorption and desorption isotherms of CBV600 as received (black) and after 48h (red) and 7000h (blue).

The N₂ isotherms of all parent and dealuminated FAUs show similar shapes and are characteristic of this kind of materials [7]: they reveal the presence of micropores through the concave shape in the low relative pressure range, and the presence of mesopores through the hysteresis loop at high relative pressure and the steep increase close to the saturation pressure.

For the CBV600 series the increase of both the micropore and mesopore volume is clearly seen for an exposure time up to $t_D = 168$ h. For 4500h (isotherm not shown) there is a significant decrease of the volume in the low partial pressure interval, but the large hysteresis loop and steep increase at high partial pressure are still seen. By further extending the acid exposure to 7000h we see an additional decrease of the micropore

volume, a loss of the steep rising feature at high P/P_0 , a significantly smaller hysteresis loop, and thus a significant decrease of mesopore volume. The specific surface area (S_{BET}) and total pore volume (V_T) values are given in Table 4.3.

Table 4.3: Specific surface area and total pore volume of the CBV600, CBV720 and CBV780 Faujasite zeolites as a function of the dealumination time.

t_D / h	CBV600		CBV720		CBV780	
	$S_{BET} / m^2 g^{-1}$	$V_T / cc g^{-1}$	$S_{BET} / m^2 g^{-1}$	$V_T / cc g^{-1}$	$S_{BET} / m^2 g^{-1}$	$V_T / cc g^{-1}$
0	530	0.38	813	0.53	823	0.54
0.5	684	0.47	-	-	-	-
1.5	-	-	836	0.52	834	0.54
6	762	0.51	839	0.58	827	0.58
24	750	0.52	795	0.51	808	0.58
48	789	0.56	789	0.54	799	0.55
168	787	0.56	810	0.56	767	0.56
4500	627	0.58	-	-	-	-
7000	645	0.39	-	-	-	-

t_D – dealumination time; S_{BET} – specific surface area; V_T – total pore volume.

A noteworthy increase of the specific surface area and total pore volume by almost 50% is observed for the CBV600 series after dealumination for more than 6h. From 6h to 168h, the total surface area and pore volume do not show a significant variation. However, a drop of about 20% in the specific surface area occurs for samples dealuminated for 4500 and 7000h.

The micro- and mesopore distribution was assessed using the NL-DFT model. In order to corroborate the data obtained by the NL-DFT model, the micropore volume and the mesopore volume were also obtained by the t-plot de Boer method and the BJH method, respectively (Figure 4.7). The distribution of the pore volume as function of the pore diameter up to 60 Å is reported in Figure 4.8 for selected samples of the three Faujasite series.

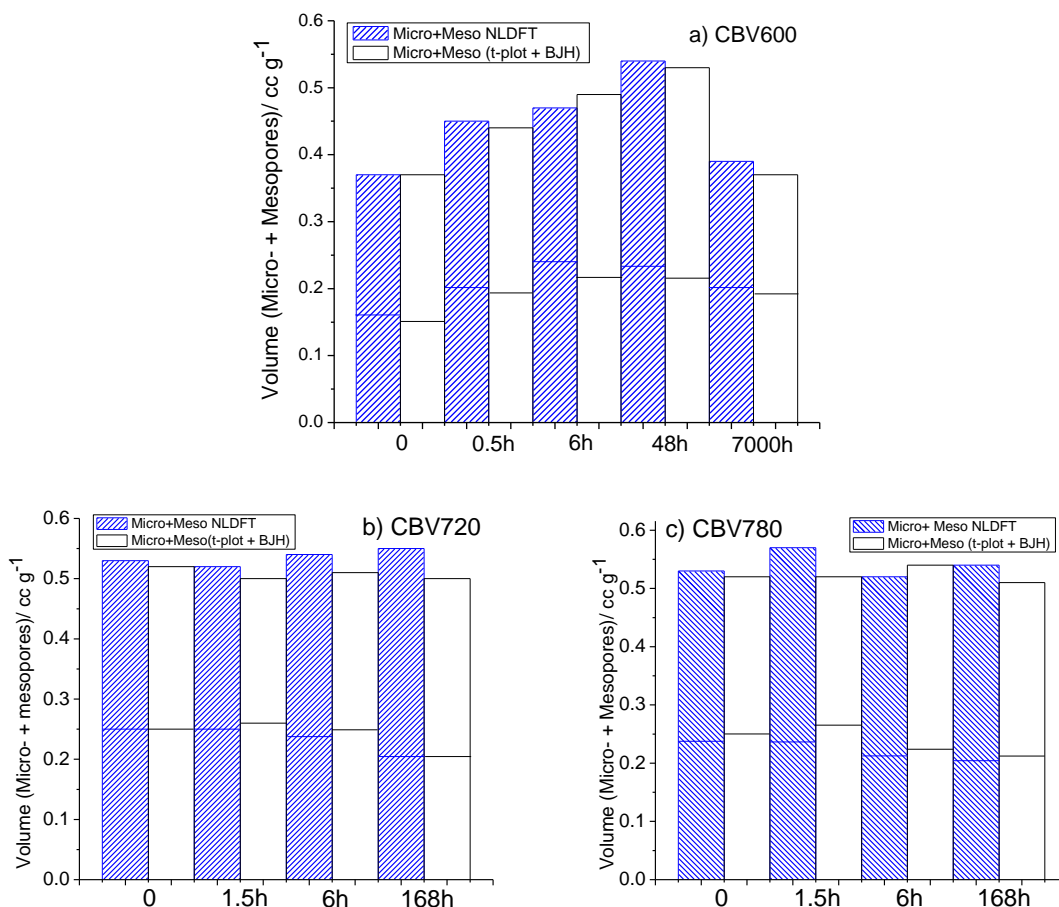


Figure 4.7: Comparison between micropore and mesopore volumes obtained by the t-plot de Boer method and the BJH method, respectively and by NL-DFT. Each column in the isograms is divided into two parts separating the micropore volume and the mesopore volume. Micropores on bottom, mesopores on top.

The analysis of the pore size distribution for the CBV600 series confirms the evolution anticipated from the variation of the shape of the isotherms (Figure 4.6): the volume of both micro- and mesopores increases by 45% after the first 24h of acid exposure and then remains constant until $t_D=168$ h, after 4500 h the micropore volume drops by 27 % while the mesopore volume is still high, and finally for the sample dealuminated for 7000 h both micro- and mesopore volumes decrease. The decrease of both micro- and mesopore volumes suggests a partial collapse of the zeolite pore structure for extended dealumination times (≥ 4500 h).

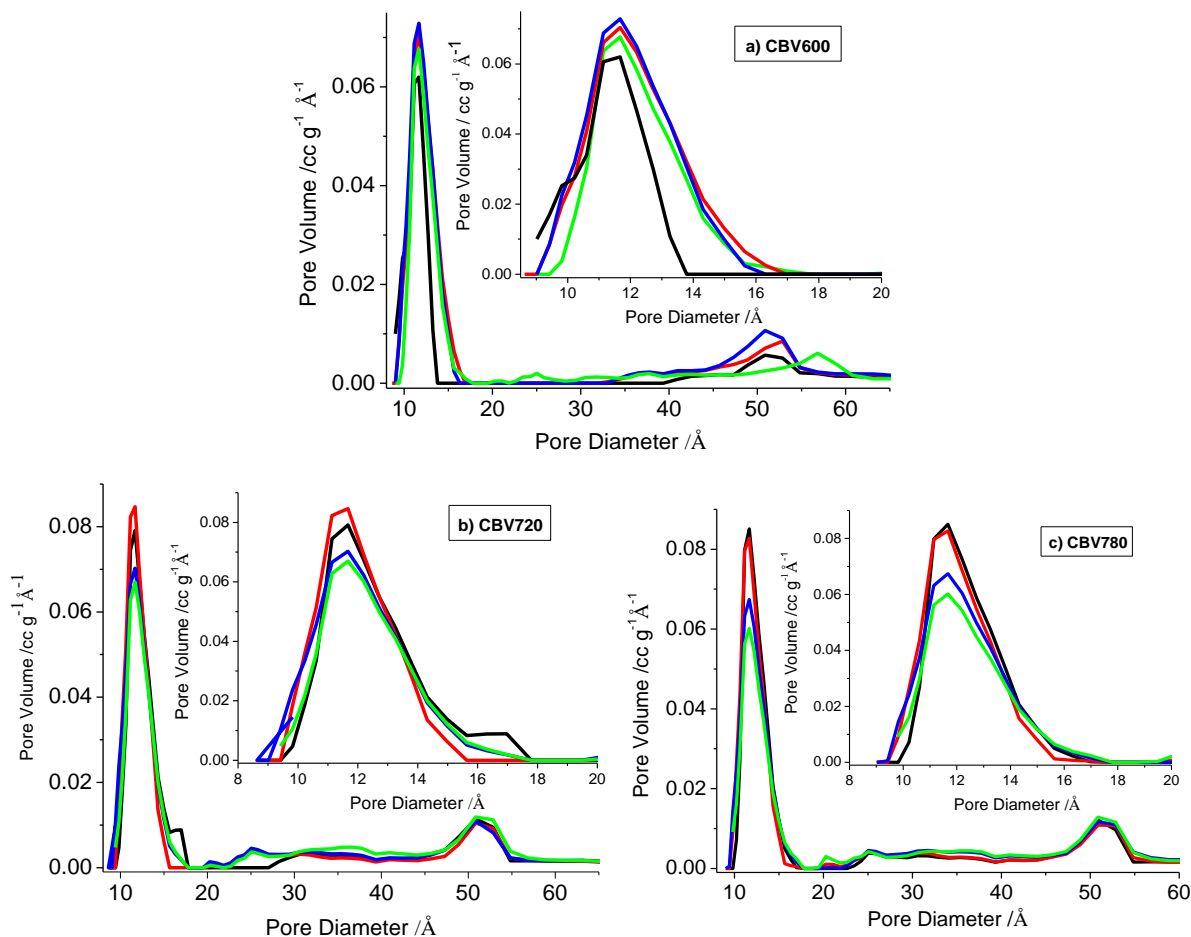


Figure 4.8: Pore volume as a function of the pore diameter in the range between 8 Å and 60 Å; a) CBV600 series, as received (black), after 6h (red), 168h (blue) and 7000h (green) of acid treatment; b) CBV720 and c) CBV780 as received (black) and after 1.5h (red), 6h (blue) and 168h (green) of acid treatment. The inserts in each figure show the pore volume as a function of the pore diameter in a range between 8 Å and 20 Å.

The N₂ sorption isotherms for the CBV720 and CBV780 parent zeolites (not shown) have similar shapes to those reported in Figure 4.6, differing only for the higher micropore volume and higher mesoporosity with respect to the CBV600 parent zeolite. No significant variations with the extent of dealumination were observed on the isotherms for these two Si-rich Faujasites, but the analysis of the pore size distribution displayed a slight rearrangement of the pore structure: after 168h of acid exposure there is a reduction of the micropore volume by about 10% and 20% for the CBV720 and CBV780 series, respectively, concomitant with an increase of the mesopore volume by about 20% and

10% respectively. What is observed is in accordance with the less extensive dealumination undergone by these two Si-rich Faujasites.

4.3. Water sorption

Water uptake measurements on all samples were carried out by dynamic vapour sorption at 25°C and as a function of the relative humidity. The water absorption and desorption isotherms recorded for CBV600 as received and after 48h and 7000h of acid exposure are shown in Figure 4.9.

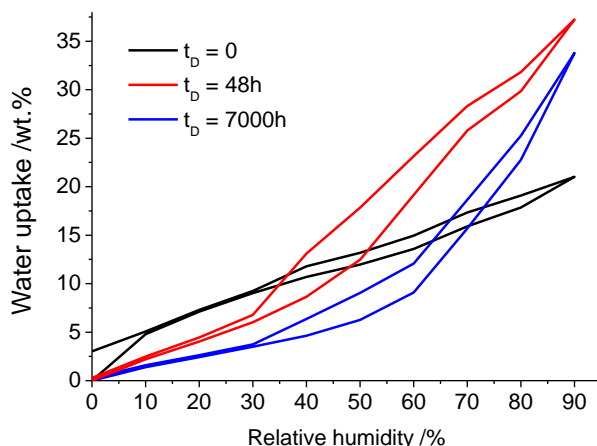


Figure 4.9: Water adsorption and desorption isotherms recorded for CBV600 samples, as received (black) and dealuminated for 48h (red) and 7000h (blue) at 25°C.

As observed in the figure, the shape of the isotherms can change significantly with the extent of dealumination when water is the adsorbate. Unlike nitrogen, which is a large and non-polar molecule, water is a small molecule that strongly interacts with the adsorbent surface due to its higher dipole moment and is therefore sensitive to the hydrophilic nature of the sorbent i.e. its chemical composition [7,8]. The CBV720 and CBV780 series show less pronounced variations in the shape of their isotherms (not shown) compared to CBV600, in accordance with the smaller extent of chemical and textural modification due to acid exposure. The water uptake values for the three Faujasite series at 10%, 50% and 90% relative humidity as function of the bulk Si/Al molar ratio are shown in Figure 4.10.

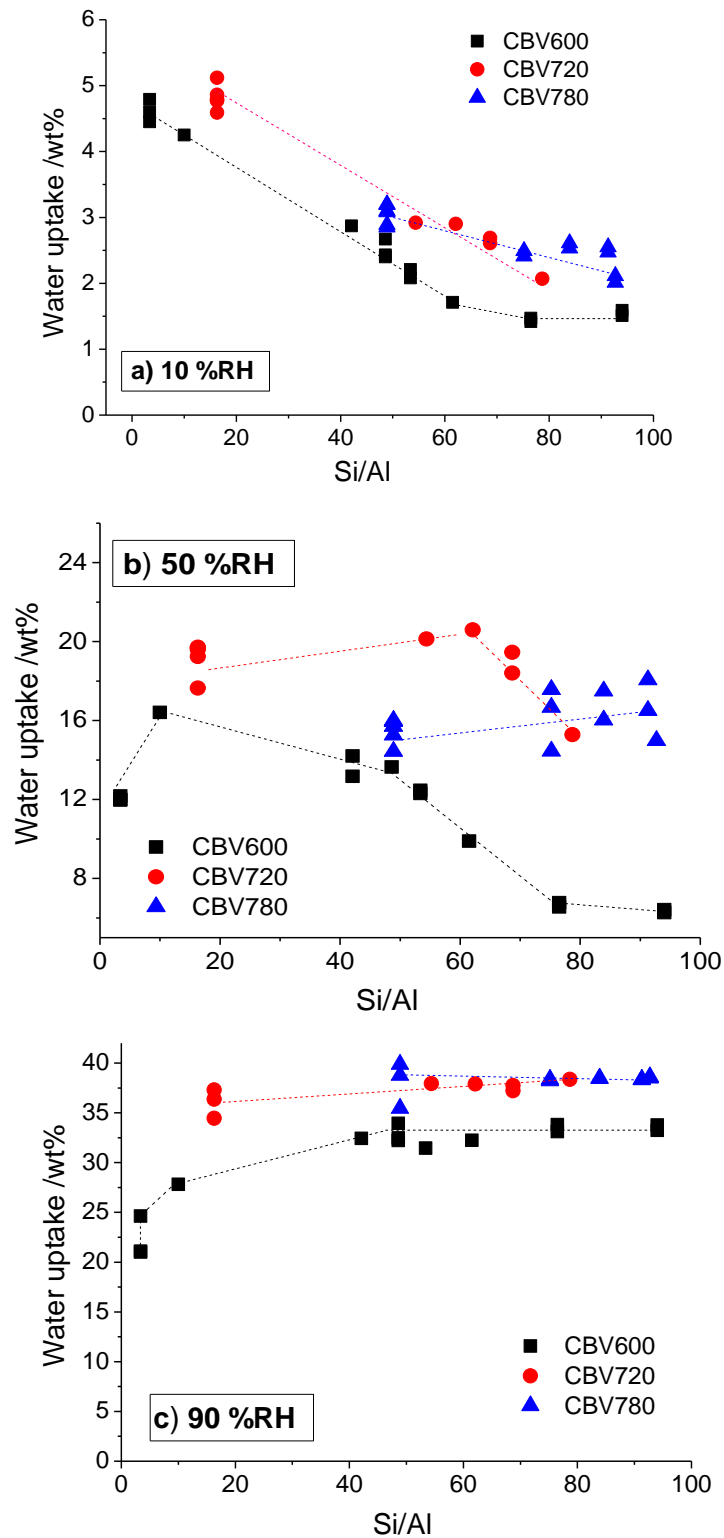


Figure 4.10: Water uptake at a) 10% RH, b) 50% RH and c) 90% RH as a function of the Si/Al ratio; CBV600, CBV720 and CBV780 series.

The CBV600 series shows the expected correlation between the water uptake and the Al content at low (10% RH), Figure 10.a: a decrease of the Al content causes a decrease of the water adsorption capacity because the number of hydrophilic sites formed by bridging hydroxyl groups Al-OH-Si decreases. At intermediate relative humidity (50% RH), the water adsorption shows an initial increase with the dealumination time up to 24 h (Si/Al=48.6) but then it decreases (Figure 10.b.). Such a variation indicates that two different effects are simultaneously responsible for the water adsorption at this RH.

The significant increase of the surface area (both micro- and mesopores) occurring within the first 24h of dealumination might be responsible for the initial increase of the water uptake, but for longer dealumination times the effect of the decreasing Al content becomes predominant.

At high relative humidity, an increase of the water sorption capacity and of the hysteresis are observed for CBV600 and this is due to an increase of the total pore volume and the mesoporosity induced by the dealumination (Figures 4.9 and 4.10.c). In accordance with the minor increase of pore volume after 6h and until 168h of dealumination, an equal water uptake at 90% RH is shown by all the samples of the CBV600 series dealuminated for more than 6h. This trend unexpectedly includes the samples dealuminated for 4500h and 7000h which have a much lower specific surface area, based on the N₂ adsorption measurements. It is possible that a partial pore collapse is hindering the ability of N₂ to fill all the volume available, which is instead filled by a smaller molecule like water.

Smaller variations were observed on the CBV720 and CBV780 series water sorption isotherms (not shown). The most marked effect is the slightly less concave shape and a decrease of water sorption at low RH (Figure 4.10.a). As expected, the variations are larger for the CBV720 series than for the CBV780 series. At high RH, the CBV720 and CBV780 series of samples have comparable water uptake, ranging between 36.4 wt.% and 39.9 wt.%, independent of the Al content. These samples have similar specific surface areas and pore size distributions but different Si/Al molar ratios, and the trends found for the water uptake emphasize the predominance of the surface area effect (pore filling adsorption mechanism) over the Al content (adsorbate-adsorbent affinity) at high relative humidity.

At equal Si/Al ratios and total pore volumes, a lower water uptake was found at high RH for the CBV600 samples with respect to the CBV720 and CBV780 samples. This difference can be ascribed to the higher volume of micro (<20 Å) and mesopores (between 20Å and 60Å) in samples of the CBV720 and CBV780 series.

4.4. Proton Conductivity

The proton conductivity measured at 25°C as a function of the relative humidity is reported in Figure 4.11.

As shown in the figure, an increase of 4 orders of magnitude, from 10^{-8} S cm⁻¹ up to 10^{-4} S cm⁻¹, was observed for the majority of the samples, when the relative humidity changed from 10% RH to direct contact with liquid water. The zeolites proton conductivity is significantly affected by the degree of hydration. Water, in fact, improves the proton mobility by weakening the interaction between the protons and the zeolite framework and through the exchange between the hydronium ion and water molecules [9,10,11].

At low RH, the proton conductivity values vary between 1×10^{-8} and 2.2×10^{-8} Scm⁻¹. For the CBV600 series, in particular, a decrease of the proton conductivity with a decrease of the Al content is observed.

Increasing the relative humidity to 50%, the proton conductivity of the dealuminated samples increases by 1 order of magnitude, whereas the conductivity of the parent zeolites remained unchanged and in the 10^{-8} S cm⁻¹ range. However, no evident correlation was found between the proton conductivity and the Al content, water content or textural characteristics of the samples, probably due to the concurrent role played by all these parameters at this relative humidity.

In Figure 4.12.a the proton conductivity measured at 90% RH is reported as a function of the Si/Al ratio. The proton conductivity of the as-received CBV600 zeolite is still low, 3.7×10^{-8} S/cm, although slightly higher than the proton conductivity measured at 10%RH. However, after dealumination, the proton conductivity is remarkably higher, 2.2×10^{-6} Scm⁻¹ after only 6h of acid exposure.

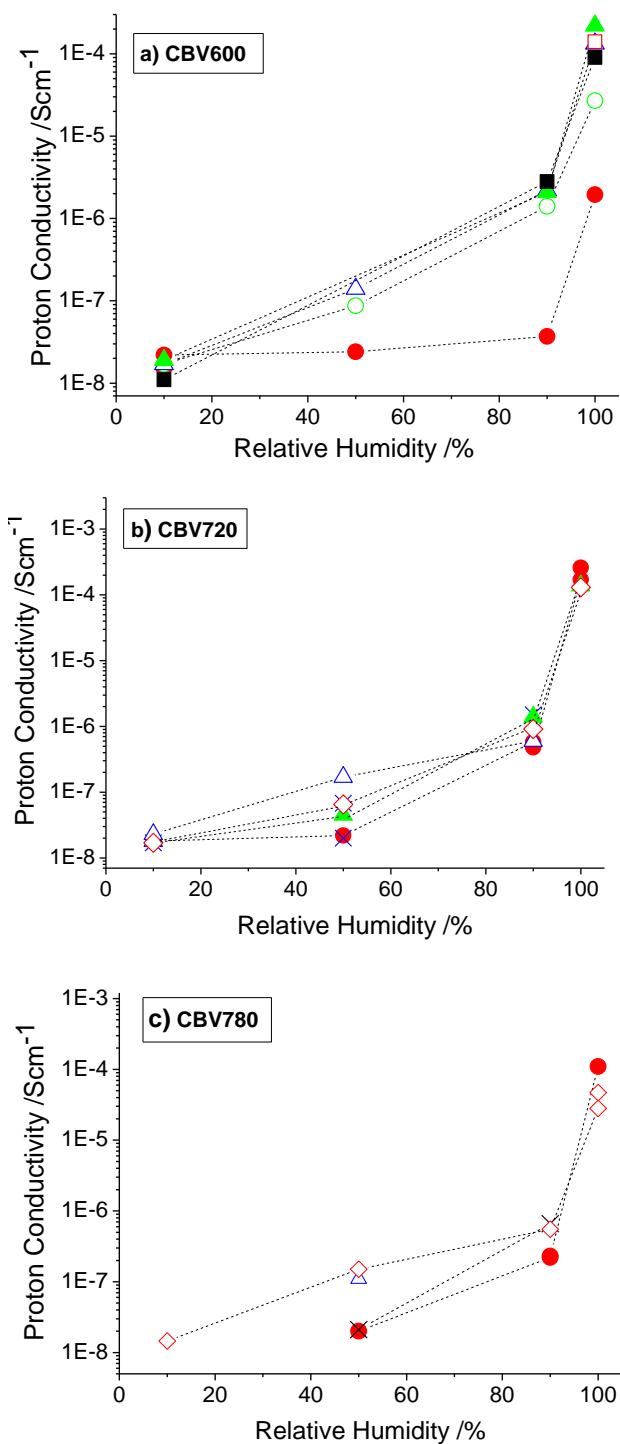


Figure 4.11: Proton conductivity as a function of the relative humidity for a) CBV600, b) CBV720 and c) CBV780 as received (●) and dealuminated for $t_D = 0.5h$ (○), $t_D = 1.5h$ (×), $t_D = 6h$ (Δ), $t_D = 48h$ (▲), $t_D = 168h$ (◇), $t_D = 4500h$ (□) and $t_D = 7000h$ (■); 100% relative humidity on the x-axis corresponds to the conditioning of the samples by immersion in water.

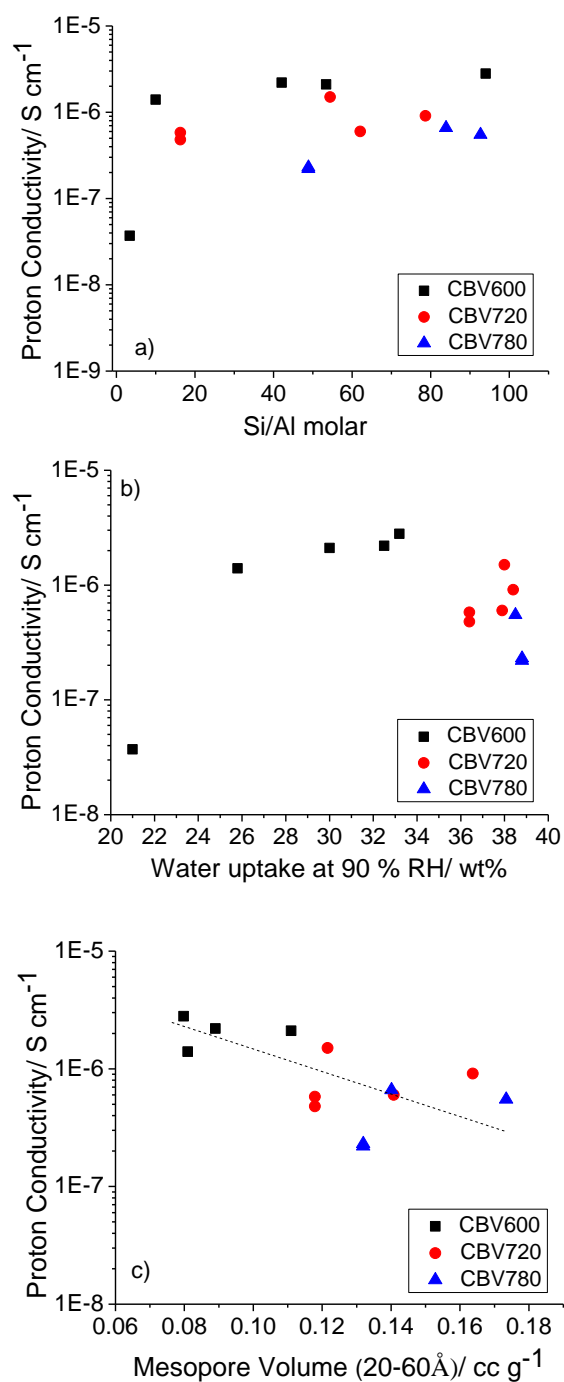


Figure 4.12: Proton conductivity at 90% RH as a function of a) the Si/Al ratio, b) water uptake at 90%RH and c) the mesopore (20-60Å) volume for CBV600, CBV720 and CBV780.

The higher proton conductivity of CBV600 dealuminated samples is mainly ascribed to the increase of water uptake, due to the increase of total surface area after acid treatment, as shown in Figure 4.12.b. The predominant effect of water content over the Al content at high degree of hydration has been observed by other authors on mordenite [11].

The variation of the proton conductivity between parent and dealuminated samples is less pronounced for the CBV720 series and even less for the CBV780 series, Figure 4.12.a, in accordance with the minor changes in surface area and porosity observed for these samples. Interestingly, the proton conductivity is higher for the CBV600 series, and it decreases in the order CBV600 series > CBV720 series > CBV780 series, Figure 4.12.a, regardless the higher water uptake of the CBV720 and CBV780 series, Figure 4.12.b. The conductivity was plotted against the micro and mesopore volume and rather surprisingly no correlation was found with the micropore volume. However, it was found that the conductivity decreases with an increase of the mesopore (20-60Å) volume, Figure 4.12.c.

A notable increase of the proton conductivity, to $\sim 10^{-4} \text{ Scm}^{-1}$ is observed for samples in direct contact with liquid water, Figure 4.11. This enhancement can be ascribed to a better hydration of the inner part of the zeolite pellets due to the direct contact with the liquid phase. A similar increase was reported by Mikhailenko and collaborators [9], who observed a variation of the proton conductivity of almost 2 orders of magnitude between pellets of H-ZSM-5 samples exposed to 100% water vapor (10^{-6} Scm^{-1}) and immersed into liquid water (10^{-4} Scm^{-1}). This behavior represents a clear advantage for certain applications such as DMFC for which direct contact with a water/methanol solution is required.

As was found for 90% RH, no effect of the Al content was observed on the proton conductivity when the pellet had been immersed in liquid water. The variation in proton conductivity can be related to the variation of the specific surface area, and in particular to the increase of the micropore volume, Figure 4.13.

For samples of the series CBV720 and CBV780, which have similar specific surface areas, the proton conductivity decreases with the mesopore (20Å-60Å) volume, Figure 4.13.b.

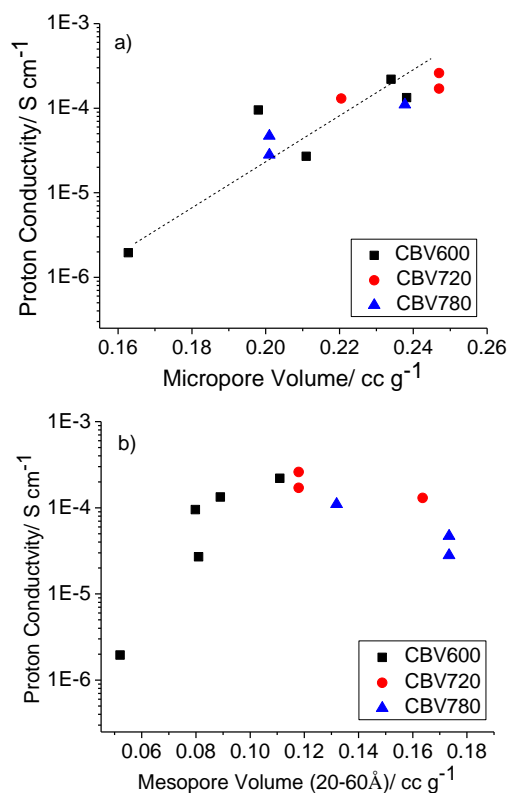


Figure 4.13: Proton conductivity of samples immersed in liquid water as a function of (a) micropore (<20Å) volume and (b) mesopore (20-60Å) volume for CBV600, CBV720 and CBV780.

Although the reasons for this are not clear, the increase of the mesopore volume does not positively affect the proton conductivity at a high degree of hydration, and Faujasite with a high surface area but with small pore size seems more suitable as an electrolyte in applications requiring high relative humidity or direct contact with a liquid aqueous phase.

4.5. Concluding remarks

In this work, the potential use of Faujasites as a solid electrolyte was evaluated, and particular attention was paid to their stability in an acid environment, and to the influence of the zeolite chemical and textural properties on the proton conductivity. Faujasite-type zeolites show a high resistance to acid attack, maintaining their crystal structure even

after extended acid exposure times up to 7000 h and significant removal of Al from the framework. Dealumination by 6 mol dm⁻³ HCl leaching occurs mainly during the first 24 h of acid exposure, with a major effect for Al-rich Faujasites (CBV600 (initial Si/Al=3.4)>CBV720(initial Si/Al=16.3)>CBV780 (initial Si/Al=48.7)). In accordance with the relative variation of the extent of dealumination, the surface area of the CBV600 Faujasite increases up to 50% due to an increase of both micro- and mesopores, while the specific surface area of CBV720 and CBV780 does not vary significantly.

Nevertheless, N₂ sorption measurements point to a partial collapse of the CBV600 zeolite pore structure for extended dealumination times (≥4500 h).

As expected, the chemical and textural modifications influence the water adsorption capacity of the zeolites. At 10%RH the water uptake decreases as the Al content decreases for all the three FAU series regardless of their surface area, while at high RH the effect of specific surface area becomes predominant. Moreover, at equal Si/Al ratio and total pore volume, samples with a higher mesopore volume (20–60 Å) show higher water adsorption at 90%RH.

The proton conductivity of Faujasites is considerably affected by the degree of hydration. At 90% relative humidity, the proton conductivity increases by up to 2 orders of magnitude compared to the values obtained at 10%RH, and a further notable increase of up to 4 orders of magnitude is observed for samples that were in direct contact with liquid water. This behavior represents a clear advantage for certain applications such as DMFCs for which direct contact with a water/methanol solution is required. Yet, the proton conductivity was also found to depend on the textural properties of the zeolites, and a higher percentage of small pores seems to favor the proton conductivity, although the reasons for this are not clear at this point.

The use of Faujasite as a solid electrolyte for DMFCs either with or without the use of an ionomer still requires an improvement in the proton conductivity. This improvement can be achieved by the functionalization of the Faujasite surface with sulfonic acid groups, research which is already being carried out by our group using Faujasites with a higher acid stability and a higher specific surface area.

4.6. References

- [1] J. Lynch, F. Raatz and P. Dufresne, 1987. "Characterization of the textural properties of dealuminated HY forms". Zeolites, Vol. 7, p. 333-338.
- [2] Q. Liu, A. Navrotsky, 2001. "An in situ calorimetric study of the synthesis of FAU zeolite". Microporous and Mesoporous Materials, Vol. 46, p. 137-151.
- [3] J. van den Brand, P. C. Snijders, W. G. Sloof, H. Terryn, and J. H. W. de Wit, 2004. "Acid-Base Characterization of Aluminum Oxide Surfaces with XPS". Journal of Physical Chemistry B, Vol. 108, p. 6017-6024.
- [4] M. Stöcker, 1996. "X-ray photoelectron spectroscopy on zeolites and related materials". Microporous Materials, Vol. 6, p. 235-257.
- [5] H. van Bekkum, E. M. Flanigen, J.C. Jansen, 1991. Introduction to Zeolite Science and Practice, Amsterdam, Elsevier Science Publishers B. V. p. 262 and 263.
- [6] R. Rachwalik, Z. Olejniczak, B. Sulikowski, 2005. "Dealumination of ferrierite type zeolite: Physicochemical and catalytic properties". Catalysis Today, Vol. 101, p. 147-154
- [7] J. Kornatowski, 2005. "Expressiveness of adsorption measurements for characterization of zeolitic materials - A review" Adsorption, Vol. 11, p. 275.
- [8] E. Ng, S. Mintova, 2008. "Nanoporous materials with enhanced hydrophilicity and high water sorption capacity". Microporous and Mesoporous Materials, Vol. 114, p. 1-26
- [9] S. D. Mikhailenko, S. Kaliaguine, E. Ghali, 1997. "Water-assisted ionic conductance of zeolites with ZSM-5 structure". Microporous Materials, Vol. 11, p. 37- 44
- [10] N.H. Mogensen, E. Skou, 1995. "Effect of solvation of charge carriers in hydrated zeolites". Solid State Ionics, Vol. 77, p. 51-54.
- [11] T. Hibino, T. Akimoto, H. Iwahara, 1993. "Protonic conduction of modernite-type zeolite". Solid State Ionics, Vol. 67, p. 71-76.

5. Sulfonic acid grafted Faujasites

The zeolite surface modification by grafting of propyl sulfonic groups was carried out on the three Faujasites in order to improve their proton conductivity.

The grafting of 3-mercaptopropyltrimethoxysilane silane followed by the oxidation of the mercapto group into a sulfonic acid group was performed for the functionalization, as described in Section 2.4.2, Chapter 2. The silane concentration was varied in order to determine the optimum silane coverage in terms of the number of grafted sulfonic groups, pore size distribution, and water and methanol sorption; all these parameters affect the proton conductivity and the selectivity towards methanol. The oxidation step was also optimized by varying the oxidation time and temperature in order to reach the complete conversion of the mercapto groups into sulfonic acid groups with the minimum loss of grafted silane.

The optimization of the zeolite functionalization procedure, the effect of the Si/Al ratio and textural properties of the parent zeolites are discussed in the first section of this chapter (Paragraph 5.1. Zeolite functionalization). The second section (Paragraph 5.2. Functionalized zeolite characterization) is centered on the effect of the functionalization on the textural characteristics of the modified zeolites, on their water and methanol sorption properties and the proton conductivity.

5.1 Zeolite functionalization

5.1.1 Grafting of mercaptopropyl groups

Thermogravimetric analysis was carried out on all samples before and after oxidation, in order to quantify the amount of silane grafted onto the Faujasite surface. The thermograms of CBV600 as-received and grafted using 41 mmol g⁻¹ of 3-MPTMS are reported in Figure 5.1. a) and b), respectively.

The thermograms show a first weight loss below 100 °C due to water desorption. The amount of silane grafted onto the zeolite surface was quantified from the weight loss between 200°C and 450°C [1-3].

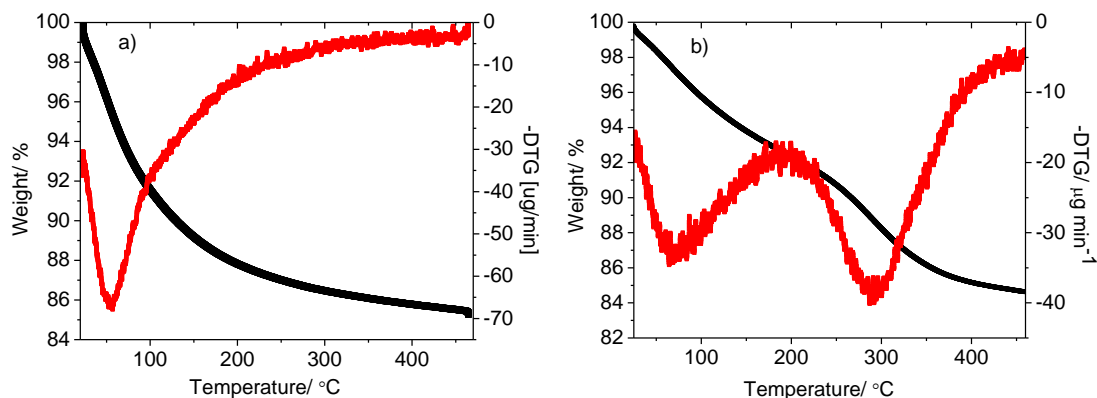


Figure 5.1: Thermograms (TG (black) and DTG (red)) of CBV600 a) as-received and b) grafted ((-SH) form) using 41 mmol g⁻¹ of 3-MPTMS.

The peak corresponding to the loss of the organic moieties is quite broad and, in order to verify the accuracy of the quantification from the thermograms selected samples were also analyzed by CHNS analysis. The values obtained by TGA and CHNS analysis were in good agreement.

An estimate of the surface coverage for each sample was made by calculating the degree of grafting, expressed as the amount of grafted silane obtained by TGA normalized for the specific surface area of the respective parent zeolite:

$$\text{degree of grafting} = \frac{\text{amount of silane(-SH)}}{S_{BET}(\text{as-received zeolite})} \cdot \left(\frac{\text{mmol}}{\text{m}^2} \right)$$

where S_{BET} is the specific surface area of the as-received zeolite (CBV600=530 m² g⁻¹, CBV720 = 813 m² g⁻¹ and CBV780 = 823 m² g⁻¹).

The degree of grafting as a function of the silane precursor concentration is reported for the three series in Figure 5.2. As shown in the figure, the amount of silane increases with the 3-MPTMS concentration up to a maximum and then it decreases for the CBV600 and CBV720 series and practically does not vary for the CBV780 series. The 3-MPTMS concentration for maximum degree of coverage is 12 mmol g⁻¹ for CBV600 and CBV720 and 2.2 mmol g⁻¹ for CBV780. In addition, the extent of grafting is higher in the following order CBV780<CBV720<CBV600, i.e. it increases with the Al content.

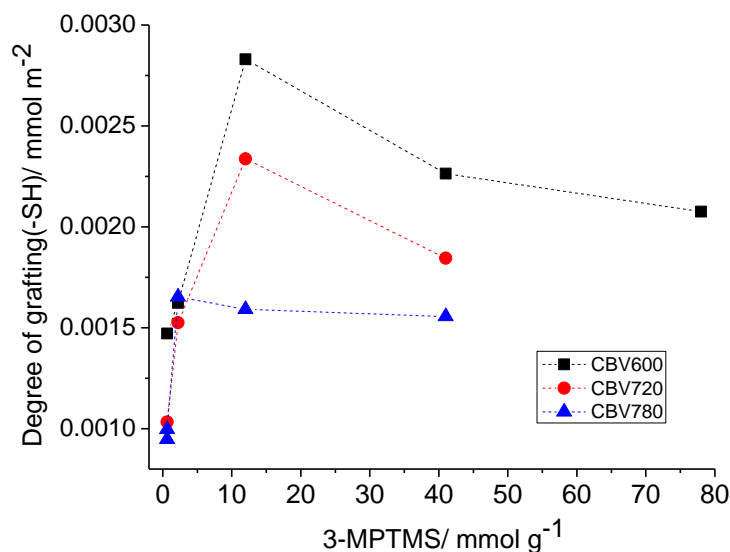


Figure 5.2: Amount of silane (-SH form) determined by TGA as a function of the 3-MPTMS concentration.

As expected, the hydrogen content on the three as-received Faujasites estimated from CHNS higher in the order CBV600>CBV720>CBV780 (Table 5.1), These numbers include the H⁺ counter-ions associated with each Al atom and also the hydrogen in hydroxyl groups present in the zeolite surface (-Si-OH). Moreover, there is also the contribution due to the hydrogen of physisorbed water and an estimate of its amount was made gravimetrically with the DVS apparatus. All these contributions are presented in Table 5.1. These data clearly suggests that samples with a higher Al content have a higher number of grafting sites available for the silane precursor and this would explain the higher degree of grafting for these samples.

Table 5.1: Hydrogen content and maximum silane grafted for CBV600, CBV720 and CBV780.

FAU	H (CHNS) (mmol g ⁻¹)	Al (NAA) (mmol g ⁻¹)	H _{water} (DVS) (mmol g ⁻¹)	H from Si-OH (mmol g ⁻¹)	Maximum silane grafted (mmol g ⁻¹)
CBV600	13.3	1.9	2.8	8.6	1.5
CBV720	10	0.9	1.4	7.7	1.9
CBV780	5.8	0.32	0.6	4.9	1.4

The amount of the hydrogen due to the hydroxyl groups (-Si-OH) reported in Table 5.1 is overestimated since it includes the contribution of water strongly bound and not desorbed during the drying step in DVS. However, this amount is expected to be negligible and, in any case, smaller in the order CBV600>CBV720>CBV780, due to the increased hydrophobicity of the zeolite with decreasing Al content.

The numbers reported in Table 5.1 also show that the saturation of all potential grafting sites is not reached, as the amount of silane grafted is much lower than the number of available grafting sites, assuming that all the hydroxyl groups are available for the grafting. Moreover, if the trend observed for the degree of grafting as a function of the 3-MPTMS concentration (Figure 5.2) were to depend on a saturation of the grafting sites on the zeolite surface, a plateau would be observed instead of a decrease after a maximum.

The observed trend points to an effect related to the conditions under which the grafting is performed, namely, the increase of precursor concentration, and to the possibility of cross-linking of the silane precursor (as described in Section 2.4.2, Chapter 2) and of self-polymerization [4,5]. It is suggested that at high concentration the self-polymerization reaction of the 3-MPTMS is preferred over the silane grafting reaction on the zeolite surface and the polymerized silane in the silanation solution is then washed away during the washing step of the grafting procedure.

5.1.2 Conversion of -SH into -SO₃H

All grafted samples were treated with an H₂O₂ solution to convert the mercapto-groups

into sulfonic acid groups¹. The temperature (25 and 50°C) and oxidation time (1-9 hours) were varied in order to establish the optimal conditions for complete conversion. For this study, the CBV600 sample grafted with 41 mmol/g of 3-MPTMS was chosen. The conversion of the mercapto-group into a sulfonic group was followed by XPS exploiting the significant difference (~ 5 eV) between the binding energy of S2p in a thiol group and in a sulfonic acid group [6], Figure 5.3.

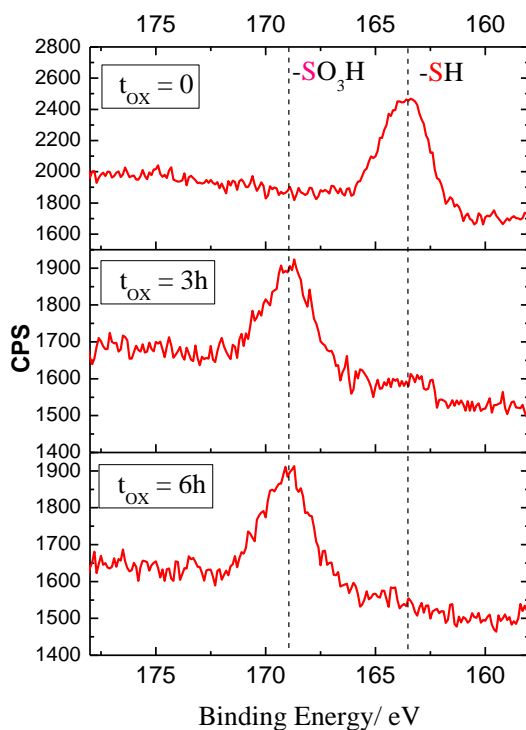


Figure 5.3: X-ray photoelectron spectra of the S2p peak of the grafted samples prepared with 41 mmol g⁻¹ of silane precursor: before oxidation (t_{ox}= 0), after partial conversion (t_{ox} = 3h) of the mercapto group into sulfonic acid group and after complete conversion (t_{ox} = 6h). The oxidation treatment was carried out at 50 °C.

The conversion yield as a function of the oxidation time for the two temperatures at 25°C and at 50°C is reported in Figure 5.4. As shown in the figure, the complete conversion of

¹ The CBV600 was also treated with 30% H₂O₂ at 50°C and characterized by X-ray diffraction. No variations were found in the diffraction pattern (crystallinity and Si/Al ratio).

the mercapto- groups into sulfonic acid groups is achieved only at 50°C and after at least 6h of oxidation treatment.

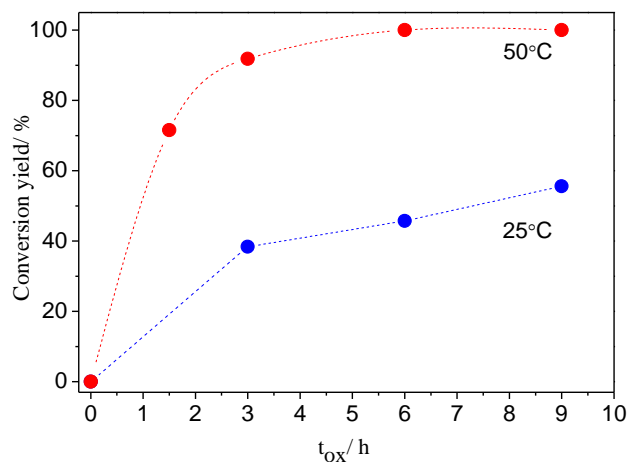


Figure 5.4: Conversion yield as a function of the oxidation time, t_{ox} , at 25°C and at 50°C.

The amount of silane in the $-SO_3H$ form grafted on the surface of the zeolite was determined by TGA. The thermograms are similar to those recorded for the samples functionalized with the silane in the $-SH$ form and show a weight loss between 180 °C and 450°C. However, the DTG peak is shifted of about 60°C to higher temperature as is also observed in the literature [2]. As for grafted samples before the oxidation, the amount of silane was also determined by CHNS analysis on selected samples and the results obtained with the two different analyses were in good agreement.

The degree of grafting ($-SO_3H$) was also calculated for samples after the oxidation treatment as follows:

$$\text{degree of grafting}(-SO_3H) = \frac{\text{amount of silane}(-SO_3H)}{S_{BET}(\text{as-received zeolite})} \cdot \left(\frac{\text{mmol}}{\text{m}^2} \right)$$

where the amount of silane ($-SO_3H$) is the amount of silane after conversion of $-SH$ groups into $-SO_3H$ groups.

As reported in Figure 5.5, the trend of the degree of grafting ($-\text{SO}_3\text{H}$) as a function of the silane precursor concentration (3-MPTMS) is the same as that obtained before the oxidation, and shown in Figure 5.2.

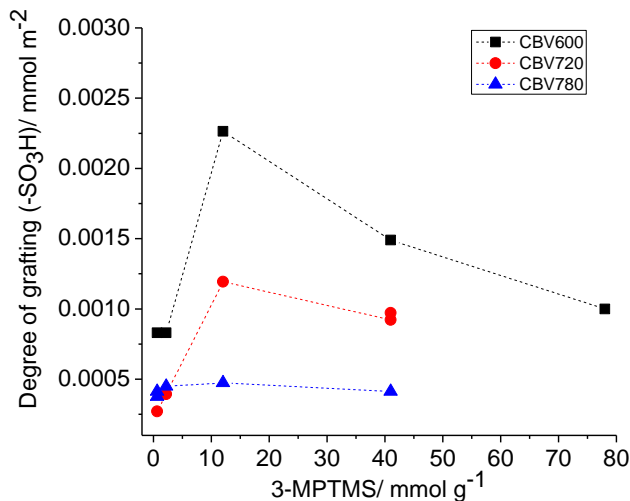


Figure 5.5: Amount of silane after oxidation ($-\text{SO}_3\text{H}$ -form) as a function of the amount of 3-MPTMS.

However, the amount of grafted silane after the oxidation is always inferior to the amount of silane present in the sample before the oxidation, as shown in Figure 5.6.

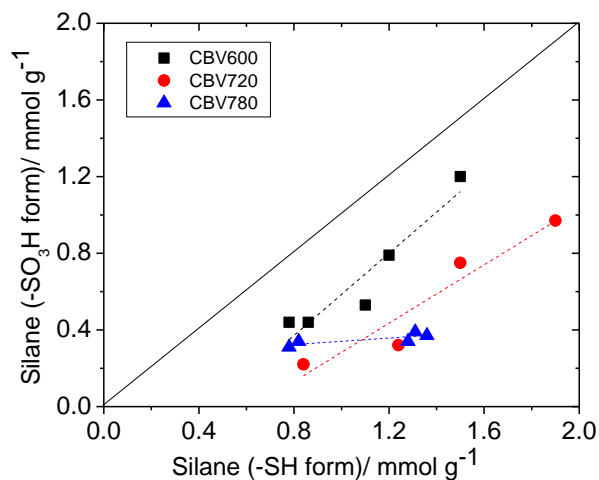


Figure 5.6: Amount of silane ($-\text{SO}_3\text{H}$ -form) after oxidation at 50°C and for 6h as a function of the amount of silane ($-\text{SH}$ form) before the oxidation treatment.

The loss of silane during the oxidation occurs at both room temperature and at 50°C, although a slightly higher loss was observed at the higher temperature. Moreover, longer exposure to H₂O₂ solution causes a higher loss of organosilane species, as established by comparing samples oxidized for 6h and 9h. A loss of organic moieties due to H₂O₂ treatment on propyl-mercapto- functionalized silica was also reported by other authors [6], who hypothesized a leaching of silane precursor giving soluble species (OH)₃Si(CH₂)₃SH or (OH)₃Si(CH₂)₃SO₃H.

In the present work, we observed that the loss is lower for samples with a higher Al content. One first hypothesis could be that a higher amount of polymerized precursor (not attached to the surface) is present in samples with a lower Al content (fewer grafting sites). If not completely removed during the washing step of the grafting procedure, the polymerized precursor remains trapped in the pores of the zeolite and is washed away during the second treatment. A second hypothesis involves the possibility that the silane anchored onto the surface is detached during the oxidation treatment due to the cleavage of the silane's Si-C bond by H₂O₂ at 50°C [7]. In the latter case, it is suggested that the framework Al could play a role in stabilizing the Si-C bond.

However, a further investigation is required to establish the truth of any of these hypotheses.

5.2 N₂ adsorption measurements

N₂ adsorption measurements were carried out on all samples as-received and after functionalization with -SO₃H groups.

In Figure 5.7, the specific surface area (S_{BET}) determined by BET analysis is reported as a function of the amount of the silane grafted (SO₃H – form) onto the surface for each series of Faujasite. As shown in Figure 5.7, the specific surface area undergoes a significant reduction after the functionalization. When about 1 mmol of silane per gram of zeolite is grafted, the specific surface area is reduced by 90% and 75% for CBV600 and CBV720, respectively. A small decrease of the specific surface area is observed for the CBV780 samples due to the lower silane loading (<0.4 mmol g⁻¹), and a trend similar to that of CBV720 can be anticipated. Nevertheless, for this series, samples with similar

degree of functionalization have different values of specific surface area, indicating a poorly-ordered coverage of the surface.

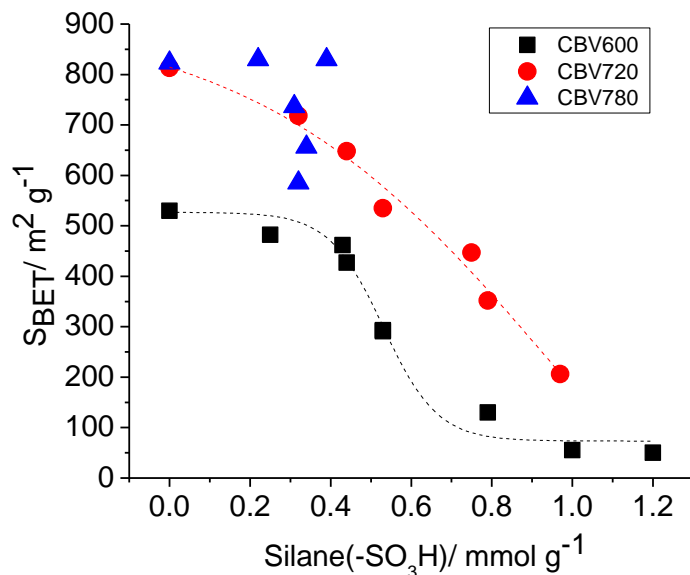


Figure 5.7: Specific surface area (S_{BET}) as a function of the amount of the silane grafted (SO_3H -form) onto the zeolite for the three series of functionalized zeolites.

An analysis of the pore size distribution with respect to the extent of functionalization was also carried out by using the BJH and t-plot method. The micropore and mesopore volumes for the three zeolite series are reported in Figure 5.8. As shown in the figure, the silane grafting causes a decrease of both micropore and mesopore volumes. The micropore volume reduction, however, occurs to a greater extent than the reduction in the mesopore volume. When 1 mmol of silane per gram of zeolite is grafted, the micropore volume is reduced to almost zero for both CBV600 and CBV720 while the mesopore volume is reduced by 50% and 40%, respectively.

The grafting of silane occurs on the external surface and also on the internal surface of the zeolite. The significant and steep decrease of the specific surface area (Figure 5.7), of the meso- and especially of the micropore volume at high amount of grafted silane (Figure 5.8), suggest the partial blockage of the access of N_2 through the smaller pores. This blockage could result from the formation of silane lumps in the opening of micropores when high concentration of 3-MPTMS is used.

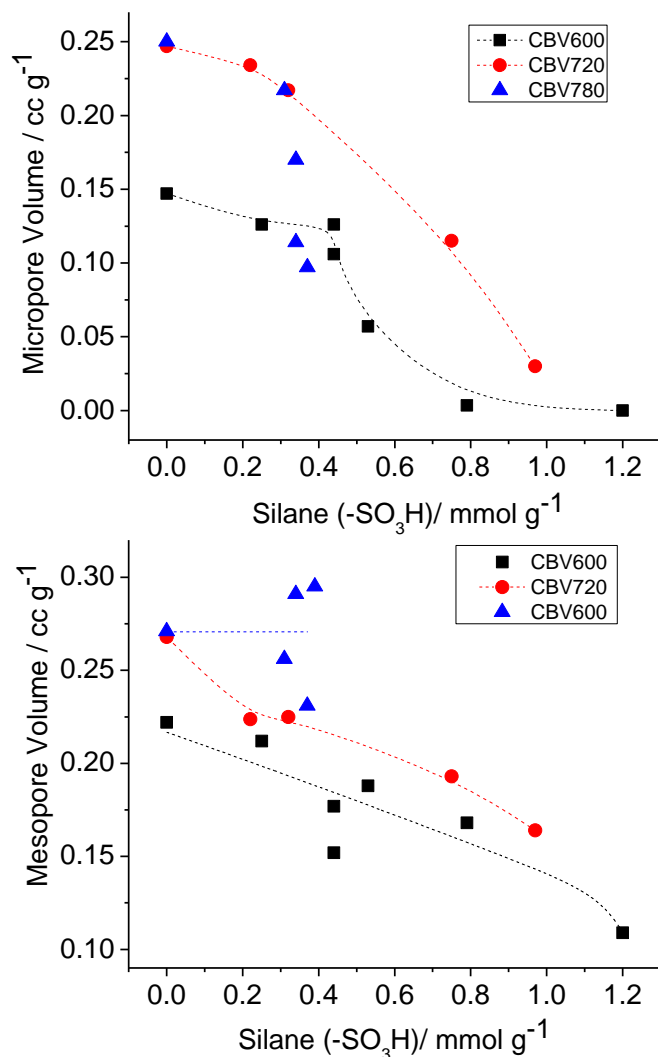


Figure 5.8: Micropore a) and mesopore b) volume of functionalized samples as a function of the amount of grafted silane (-SO₃H form) for CBV600, CBV720 and CBV780 series.

The presence of lumps of silane close to the openings to micropores due to the high concentration of silane in a small area can be also reason of the drastic decrease of porosity observed by N₂ adsorption measurements.

At equal amounts of grafted silane a much higher specific surface area is still available for the CBV720 compared to the CBV600. At 1 mmol g⁻¹, the S_{BET} of CBV720 is about 200 m² g⁻¹, four times higher than the CBV600 sample grafted with an equal amount of silane (S_{BET} ≈ 50 m² g⁻¹). The higher specific surface area of CBV720 and CBV780

available for accommodating water and for proton diffusion represents an advantage in terms of better proton conduction, as already reported and discussed in this work (Chapter 4). Therefore, the choice of starting material with certain textural properties becomes of fundamental importance, especially if its surface is to be coated with functional acid groups. The effect of the surface coverage on the water and methanol adsorption is reported and discussed in the following paragraph.

5.3 Water and methanol uptake

Water and methanol adsorption and desorption isotherms were recorded at 25°C and at different % P/P_0 values by dynamic vapor sorption. The water and methanol adsorption isotherms of the three parent zeolites and of selected functionalized samples of the CBV600 series are reported in Figure 5.9 and 5.10, respectively. As shown in figure 5.9, the shape of the water and methanol isotherms is significantly different and the relative trend (water vs methanol) varies with the partial pressure.

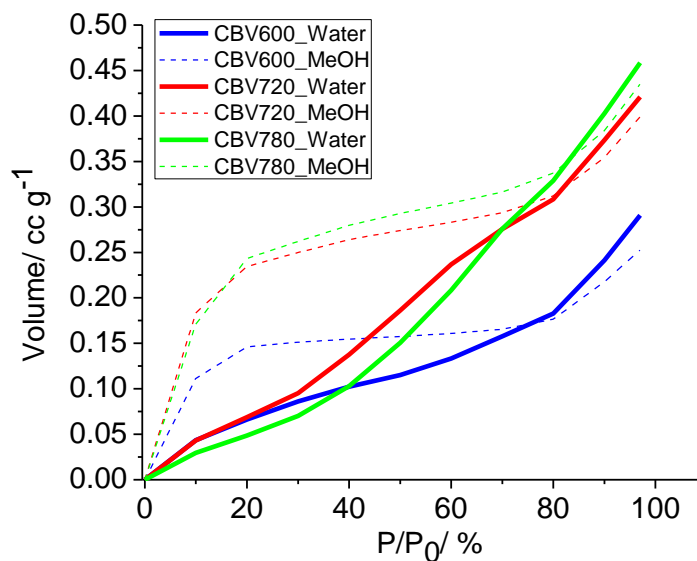


Figure 5.9: Water and methanol adsorption isotherms of as-received CBV600, CBV720 and CBV780.

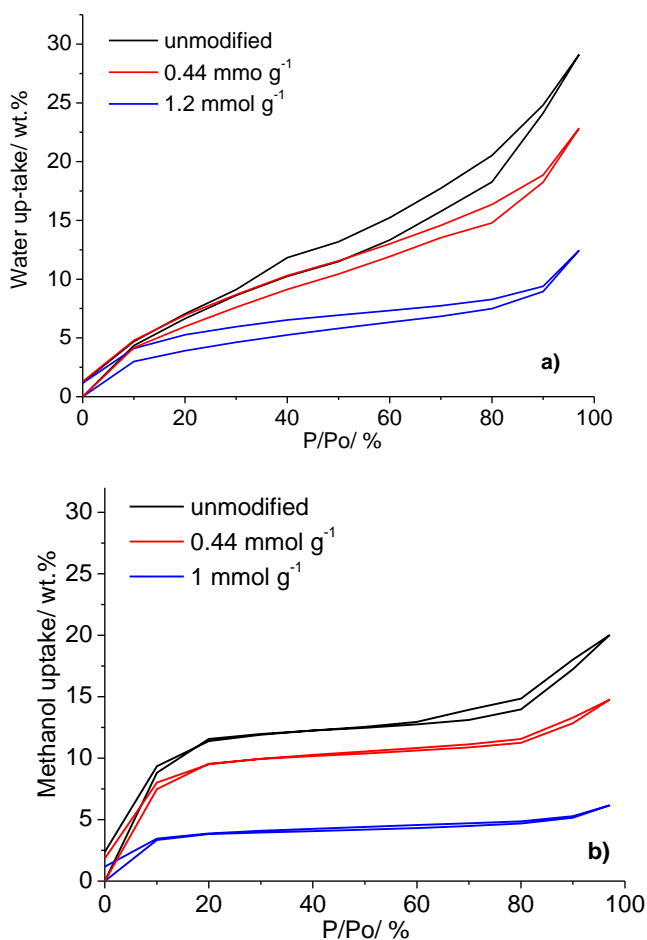


Figure 5.10: Water (a) and methanol (b) sorption isotherms of CBV600 as received and with 0.44 mmol g^{-1} and 1.2 mmol g^{-1} of grafted silane.

At low P/P_0 the methanol uptake is significantly higher than the water uptake for all samples. The same behavior at low P/P_0 was observed by other authors on a Si-rich Faujasite ($\text{Si}/\text{Al} \approx 40$) and was also predicted by a molecular simulation study on the adsorption of water and methanol on a metal-organic framework with a Rho-type zeolite topology characterized by a hydrophobic framework [8].

The behavior can be explained by considering the different polarity of water and methanol molecules in relation to the energy barrier for these molecules to access the pore structure of the three zeolites with different chemical and textural characteristics.

As already discussed in Chapter 3, water is a polar molecule with high dielectric constant ($\epsilon_{\text{H}_2\text{O}}=80$) and a partial charge on its oxygen, while the methanol dielectric constant ($\epsilon_{\text{CH}_3\text{OH}}=33$) is much lower. This permits an easier penetration of methanol molecules

into the zeolite pores compared to water at low P/P_0 , due to the fact that methanol is less affected by the repulsive barrier effect created by the oxygen ions with negative partial charges covering the pore surface [9,10].

The effect of the chemical composition of the zeolite surface on the different accessibilities of water and methanol at low P/P_0 is also seen in the adsorption trend with the Si/Al ratio. In fact, the water uptake at low P/P_0 decreases with the Si/Al ratio, while the methanol uptake increases (Figure 5.9), and the difference between water and methanol uptake increases with the Si/Al ratio. Moreover, the two Faujasites with higher Si/Al ratios also have larger pore sizes, further facilitating the access of methanol molecules.

As shown from the isotherms reported in Figure 5.10, the surface coverage with propyl sulfonic acid groups affects the water and the methanol sorption, due to the introduction of hydrophilic moieties ($-\text{SO}_3\text{H}$) and also to the significant variation of the specific surface area and pore size. The isotherms also show a hysteresis much more significant for water than for methanol.

The volume of water and methanol adsorbed per gram of zeolite, as a function of the amount of silane grafted onto the zeolite surface at 10%RH and 97%RH for CBV600, CBV720 and CBV780 is shown in Figure 5.11 and 5.12, respectively.

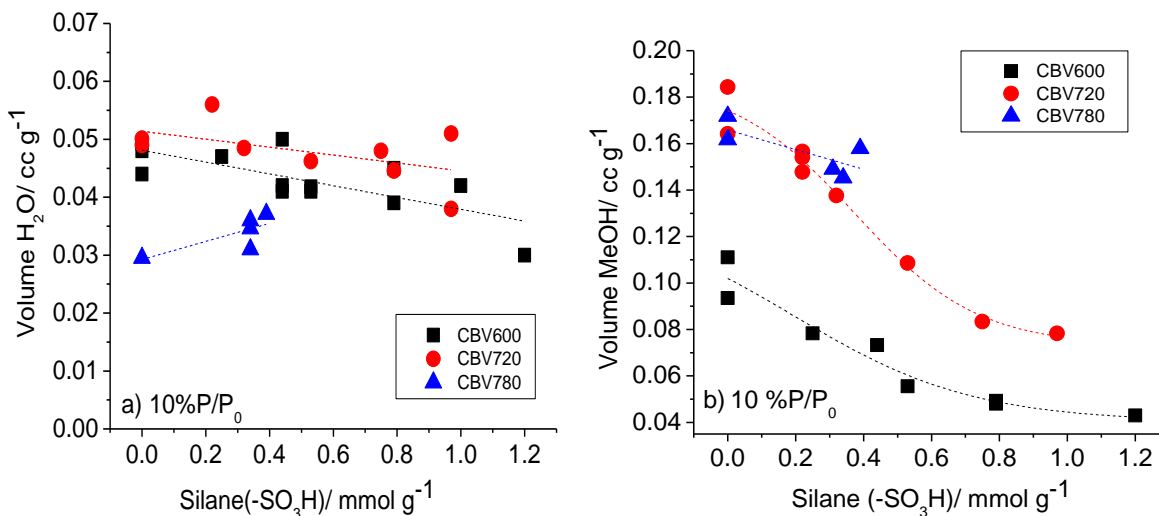


Figure 5.11: Volume of H₂O a) and MeOH b) adsorbed per gram of zeolite as a function of the amount of grafted silane at 10%RH

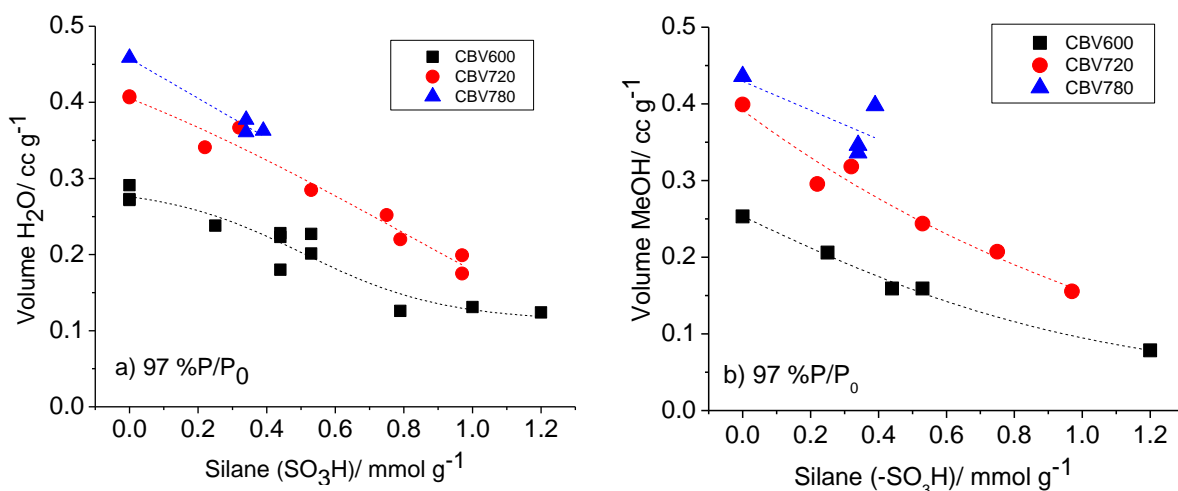


Figure 5.12: Volume of H₂O a) and MeOH b) per gram of zeolite as a function of the amount of grafted silane (-SO₃H form) at 97 %P/P₀.

As shown in the figures, it is possible to observe a marked dependence of both water and methanol uptake on the extent of silane grafting, both at low and high relative humidity.

At 10 %P/P₀, the functionalization does not significantly affect the water uptake. Only a small decrease of water uptake is observed in spite of the significant changes in the textural properties due to the surface coverage. Most probably the increase of hydrophilicity through the introduction of sulfonic acid groups compensates for the loss of porosity.

The methanol sorption at low P/P₀ of the three series of functionalized samples differs from the water sorption. Other than being higher than the water uptake, as already pointed out from an analysis of the shape of the isotherms, it is observed that the methanol uptake increases with the hydrophobicity of the zeolites: CBV600 < CBV720 < CBV780. Moreover, the difference in methanol uptake between CBV600 and CBV720 is greater than the difference in water uptake, further confirming the role of the textural characteristics of the zeolite in the methanol uptake even at low P/P₀. In fact, the larger average pore size of CBV720 implies an easier access of methanol in this zeolite compared to CBV600.

At high %P/P₀ the trend is reversed and a significant increase of water uptake, much steeper than the methanol increase in the same range of high P/P₀ is observed, Figure 5.10. Steric effects (kinetic diameter 0.38 nm and 0.27 nm for methanol and water

molecules, respectively [11]) can explain this difference at high partial pressure and close to saturation. The steeper increase of water adsorption compared to methanol could also be due to the greater tendency of water to form clusters compared to methanol [8,12].

In fact, studies on silica gel reported that the water is adsorbed as clusters on the hydroxyl groups of silica [12], and the same cluster-type adsorption is likely to occur on the hydrophilic sites of the zeolite.

As anticipated, due to the decrease in the specific surface area and the pore size, there is a significant decrease of water and methanol uptakes with the extent of the functionalization. The uptake of both water and methanol decreases in the order CBV780>CBV720>CBV600 for as-received and functionalized samples. The lower values found for the CBV600 functionalized samples were expected due to the significant decrease in the specific surface area with the functionalization.

The ratio between methanol and water uptakes for each sample also follows the same trend CBV780>CBV720>CBV600, as shown in Figure 5.13, where the ratio between the volume of methanol and water is reported as a function of the silane (-SO₃H form) content at 10 % P/P₀ and at 97 % P/P₀.

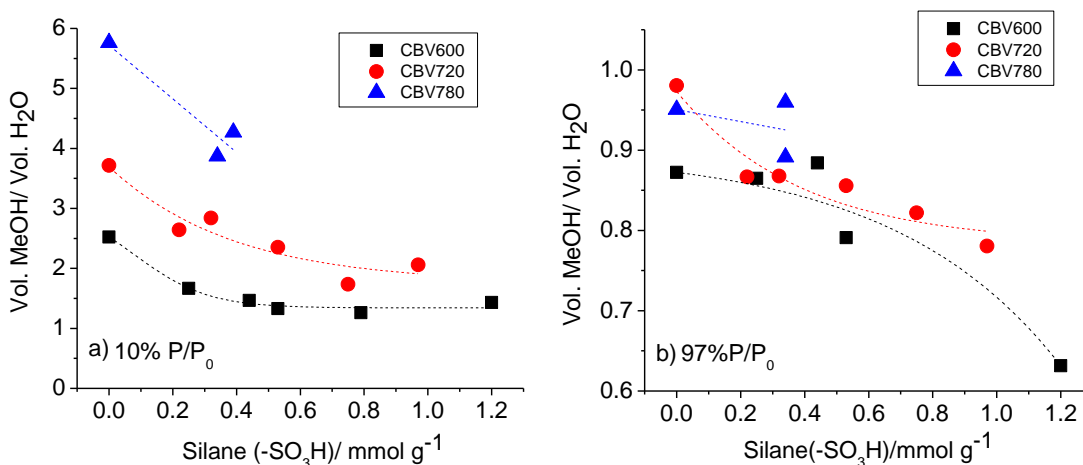


Figure 5.13: Ratio between volume of methanol adsorbed and Volume of water adsorbed as a function of the grafted silane a) at 10% P/P₀ and b) 97% P/P₀.

At 10 % P/P₀ the methanol uptake is 2.5, 3.7 and 5.8 times higher than the water uptake for the as-received CBV600, CBV720 and CBV780, respectively, but the ratio decreases

with the degree of functionalization. However, at high %P/P₀ the volume of water adsorbed is always higher than the volume of methanol and again the methanol to water volume ratio decreases with the extent of functionalization.

When the % P/P₀ is higher, in fact, water can fill all the remaining empty cavities of the zeolite pore system while the bigger methanol molecule does not have easy access. The molecular sieve effect of the functionalized zeolite pore system is then particularly effective. Indeed, the possibility of introducing a more hydrophilic group onto the surface and, at the same time, of physically reducing access to the methanol molecules represents a clear advantage for applications such as electrolyte materials for DMFCs.

For an equal amount of grafted silane, the samples of the CBV600 series have the lowest methanol/water volume ratio which could represent an advantage in terms of lower methanol uptake. However, as already discussed, a lower water uptake and a lower specific surface area might hamper the proton conductivity. The values of proton conductivity for the three series of functionalized samples and a correlation with their chemical/physical characteristics and properties are presented in the following paragraph.

5.4 Proton Conductivity

The proton conductivity of the zeolites before and after surface functionalization was measured by impedance spectroscopy at 25°C on fully hydrated pellets. The values of proton conductivity of all samples were correlated with the amount of acid sulfonic groups grafted onto the zeolite surface. Figure 5.14 reports the proton conductivity as a function of the amount of silane grafted onto the zeolite.

An improvement of proton conductivity is observed after the surface functionalization, in spite of a decrease of porosity and water uptake. However, the increase of proton conductivity does not occur to the same degree for the three series of FAU samples, being greatest on the CBV600 series. The proton conductivity increases by a factor of only 3 for the CBV720 and CBV780 series, while an increase up to one order of magnitude is achieved for CBV600.

The lower increase in the proton conductivity for CBV720 and CBV780 samples for equal amounts of grafted silane could be due to a H⁺ dilution effect since these samples

have a higher specific surface area and pore size with respect to CBV600 series.

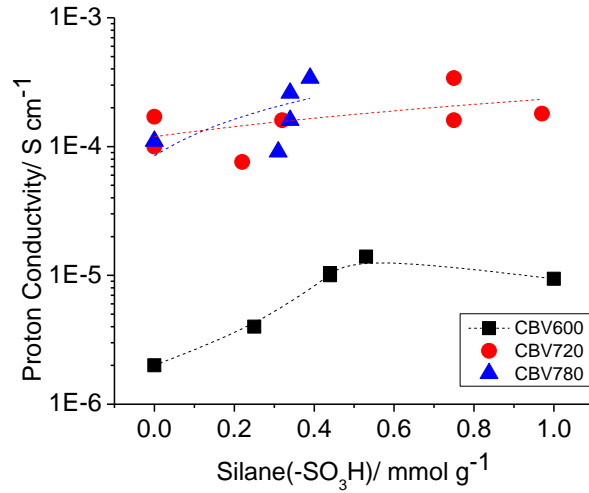


Figure 5.14: Proton conductivity as a function of the degree of functionalization for CBV600, CBV720 and CBV780.

The concentration of transport carrier H^+ is proportional to the number of sulfonic acid groups. In order to take into consideration the textural changes induced by the functionalization, the number of moles of silane ($-SO_3H$ form) (i.e. H^+) was normalized for the specific surface area of the sample after functionalization and plotted against the amount of silane ($-SO_3H$ form), Figure 5.13. As shown in the figure, the H^+ density on the surface increases more rapidly for CBV600.

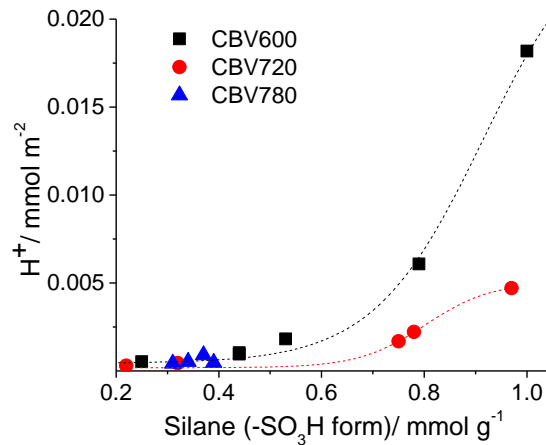


Figure 5.15: Protons surface density as a function of the silane grafted for the three series of zeolites.

In spite of the smaller improvement in proton conductivity achieved through the sulfonic acid functionalization, the CBV720 and CBV780 series show higher proton conductivities than the CBV600 samples for the same amount of grafted silane. Proton conductivities for CBV720 and CBV780 that were higher than for CBV600 were also observed on unmodified samples, in spite of the lower Al content, as already discussed in Chapter 4. The explanation might be that the proton conductivity not only depends on the density of carriers but also on their mobility. The mobility of the protons strongly depends on the water content and the state of the water in the pores, and also on the type of diffusion paths available for the proton transport. The CBV720 and CBV780 have higher specific surface areas and pore volumes available to accommodate water and for the proton diffusion compared to CBV600, and this is reflected in the higher proton conductivities.

An estimate of the effect of water content on the proton conductivity was made by calculating λ , i.e. the number of molecules of water for each sulfonic acid group (i.e. H⁺), as is usually done for ionomer membranes. A plot of λ as a function of the amount of grafted silane is reported in Figure 5.16.

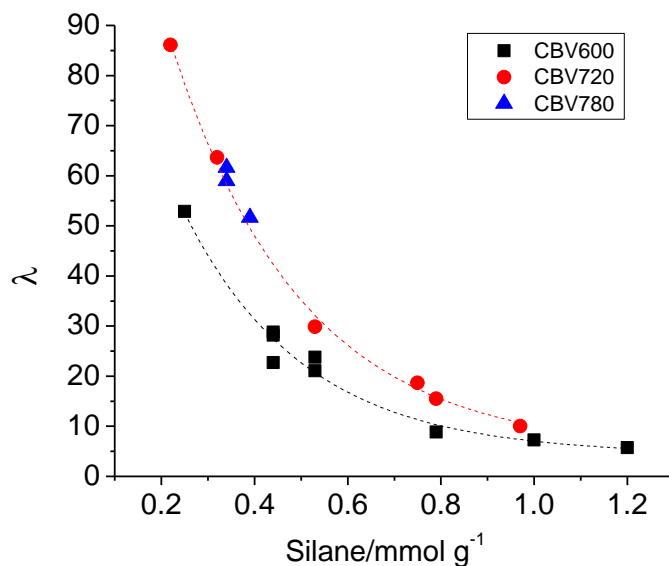


Figure 5.16: λ (at 97%RH) as a function of the amount of grafted silane for CBV600, CBV720 and CBV780.

As observed in the figure, the number of water molecules available for each sulfonic acid group is always higher for CBV720 and CBV780. However, the difference between the λ values decreases with the extent of grafting for the different series, although the difference in proton conductivity is still significant. This suggests that other factors such as the pore size (as shown in the previous chapter) and the type of water could play a role. In fact, as seen for the CBV600 series the proton conductivity decreases slightly when the amount of grafted silane increases from 0.53 mmol g⁻¹ to 1 mmol g⁻¹, Figure 5.14. This was accompanied by a significant loss in the surface area (from 291 m² g⁻¹ to 55 m² g⁻¹) and a reduction of the micropore and mesopore volumes (micropores: from 0.06 cc g⁻¹ to ~ 0, mesopores: 0.19 cc g⁻¹ to 0.11 cc g⁻¹), and a drop in the water uptake at 97% from 23% to 13.1%).

A further optimization of the functionalization on the Si-rich samples has to be done in order to succeed in grafting a higher amount of sulfonic acid groups onto their surfaces, at the same time preserving a higher specific surface area for the water uptake and proton mobility.

5.5 Concluding remarks

The functionalization of the zeolite surfaces with sulfonic acid groups is an effective way to improve the proton conductivity of CBV600 (1 order of magnitude, from ~ 10⁻⁶ S cm⁻¹ to from ~ 10⁻⁵ S cm⁻¹) only. Although the functionalization was not as effective for zeolites with higher Si/Al ratios and higher specific surface areas, the as-received and functionalized samples of these two series have the highest proton conductivity (~ 10⁻⁵ S cm⁻¹).

The work was valid in establishing the role of the zeolite surface chemistry on the grafting reaction and criteria for the further improvement of the zeolite proton conductivity.

The first consideration is the choice of the starting material, which should have a high specific surface area, a large pore size and a high Al content. In fact, it was found that Al affects the grafting yield and probably also the stability of the bond between the silane and the zeolite surface, although a further investigation is necessary.

An important aspect also evaluated in this work is the selectivity of the samples after functionalization. The water and methanol adsorption studies on as-received and functionalized samples showed that the zeolite offers an efficient water/methanol selectivity. The zeolite water vs methanol selectivity benefits from the silane surface coverage by hindering the access of methanol through steric effects and chemical affinity, without affecting to the same extent the adsorption of the smaller water molecules.

5.6 References

- [1] J.C. McKeen, Y.S. Yan, M. E. Davis, 2008. "Proton conductivity of Acid-functionalized zeolite beta, MCM-41, and MCM-48: effect of acid strength". Chemistry of Materials, Vol. 20, p. 5122-5124.
- [2] R. Marschall, I. Bannat, J. Caro, M. Wark, 2007. "Proton conductivity of sulfonic acid functionalized mesoporous materials". Microporous and Mesoporous Materials, Vol. 99, p. 190-196.
- [3] I. Diaz, C. Marquez-Alvarez, F. Mohino, J. Prez-Pariente, E. Sastre, 2000. "Combined Alkyl and Sulfonic Acid Functionalization of MCM-41-type Silica. Part1. Synthesis and Characterization". Journal of Catalysis, Vol. 193, p. 283-294.
- [4] M.HU, S. Noda, T. Okudo, Y. Yamaguchi, H. Komiyama, 2001. "Structure and morphology of self-assembled 3-mercaptopropyltrimethoxysilane layers on silicon oxide". Applied Surface Science, Vol. 181, p. 307-316.
- [5] P. Silberzan, L. Leger, D. Ausserré, J.J. Benattar, 1991. "Silanation of silica surface. A New Method of constructing pure or mixed monolayers". Langmuir, Vol. 7, p. 1647-1651.
- [6] E. Cano-Serrano, G. Blanco-Brieva, J. M. Campos-Martin, J.L.G. Fierro, 2003. "Acid-functionalized amorphous silica by chemical grafting-quantitative oxidation of thiol groups". Langmuir, Vol. 19, p.7621-7627.
- [7] D. L. Moore, M. P. Taylor, P. L. Timms, 2000. "Reaction of hydrogen peroxide with organosilanes under chemical vapour deposition conditions". Journal of the Chemical Society, Dalton Transactions, p. 2673–2677.
- [8] A. Nalaparaju, X.S. Zhao J.W. Jiang, 2010. "Molecular understanding for the adsorption of water and alcohols in hydrophilic and hydrophobic zeolitic metal-organic frameworks". Journal of Physical Chemistry C, Vol. 114, p. 11542-11550.
- [9] I. Halasz, S. Kim, B. Marcus, 2001. "Uncommon adsorption isotherm of methanol

on a hydrophobic Y-zeolite“. Journal of Physical Chemistry B, Vol. 105, p. 10788-10796.

- [10] I. Halasz, S. Kim, B. Marcus, 2002. “Hydrophilic and hydrophobic adsorption on Y zeolites“. Molecular Physics, Vol. 100, p. 3123-3132.
- [11] E. P. Ivanova, M.A. Kostova, B.K. Koumanova, 2010. “Kinetics of water and alcohol vapors adsorption on natural zeolite“. Asia-Pacific Journal of Chemical Engineering, Vol. 5, p. 869-881.
- [12] Y. I. Tarasevich, 2001. “Interaction of water and other polar substances with various sorbents according to calorimetric and chromatographic data“. Theoretical and Experimental Chemistry, Vol. 37 (4), p. 197-214.

6. Composite membranes

In this chapter, the results obtained from the characterization of zeolite based composite membranes are presented and discussed. The chapter is separated into two sections:

- 1) Section 6.1: focused on the **Nafion-zeolite composites**.
- 2) Section 6.2: focused on all composites obtained by blending the **zeolite** (as-received and functionalized) **with non-ionomer polymer binders**.

6.1 Nafion-Faujasite Composite Membranes

Nafion-zeolite composites were prepared and characterized in order to investigate the effect of the zeolite on the sorption and conductivity properties of composites membranes and on their DMFC performance. A study on composites using the zeolite prior to surface modification aims to obtain a baseline and an understanding of the interaction between Nafion and the filler, and to assess the stability of the zeolite under Nafion pre-treatment conditions. Moreover, being a reference material intensively studied for decades, Nafion was considered a good starting material for this study on composite membranes.

Several composite membranes were fabricated by solution casting, using a 5% or 20% Nafion dispersion and different loadings of as-received CBV780. As discussed in Chapter 4, CBV780 shows a higher stability and, at the same time, a higher porosity and proton conductivity.

The series of samples fabricated from 5% Nafion dispersion is indicated as N5_n, where N stands for Nafion, 5 for the Nafion dispersion concentration and n is the nominal zeolite wt.%. Similarly, the series of samples fabricated from 20% Nafion dispersion is indicated as N20_n. All the composite membranes and corresponding Nafion-zeolite proportions are listed in Table 6.1. All membranes underwent the standard activation procedure for unfilled Nafion in H₂O₂ and H₂SO₄ as described in Section 2.5.2.4, Chapter 2. However, since zeolites undergo dealumination, this treatment should affect the zeolite structure and properties and, for this reason, the Faujasite alone was subjected to the same treatment.

Table 6.1: Composites membrane name, Nafion dispersion concentration and zeolite nominal content.

Sample Name	% Nafion dispersion	wt% Nominal Zeolite Content
Nafion D521		
N5_0	5	0
N5_2	5	2
N5_4	5	4
N5_20	5	20
Nafion D2021		
N20_0	20	0
N20_2	20	2
N20_4	20	4
N20_10	20	10
N20_20	20	20
N20_40	20	40

6.1.1. Effect of Nafion activation treatment on CBV780 zeolite

The Faujasite powder before and after treatment was characterized by XRD, NAA and N₂ sorption measurements. The proton conductivity of the zeolite powder in pellet form, fully hydrated, was also measured. As shown by XRD, the zeolite structure remained intact after the activation treatment, Figure 6.1, although it underwent severe Al removal.

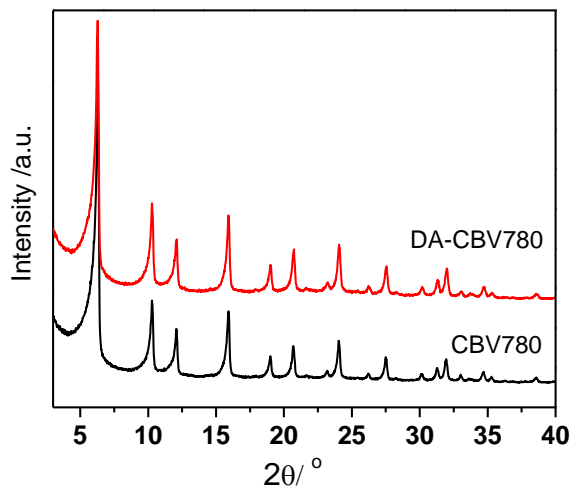


Figure 6.1: XRD patterns of a) CBV780 as-received and b) after activation treatment (DA-CBV780).

The elemental composition and physicochemical properties of CBV780 as-received and after the activation treatment are reported in Table 6.2.

Table 6.2: Physicochemical properties of CBV780 as-received and after activation treatment.

Sample	Si/Al	$A_0 / \text{\AA}$	$S_{\text{BET}} / \text{m}^2 \text{g}^{-1}$	$\sigma / \text{S cm}^{-1}$
CBV780	48.7	24.24	823	2.6×10^{-4}
CBV780 after treatment	103.7	24.21	735	7.8×10^{-5}

6.1.2 Thermogravimetric analysis

In order to determine the zeolite loading after the $\text{H}_2\text{O}_2/\text{H}_2\text{O}/\text{H}_2\text{SO}_4$ treatment, all composite membranes were characterized by TGA. In Figure 6.2a and 6.2b the TGA and selected DTG diagrams for the recast Nafion and samples from the N20_n series of composite membranes are shown. Similar curves were obtained for the N5_n series of samples.

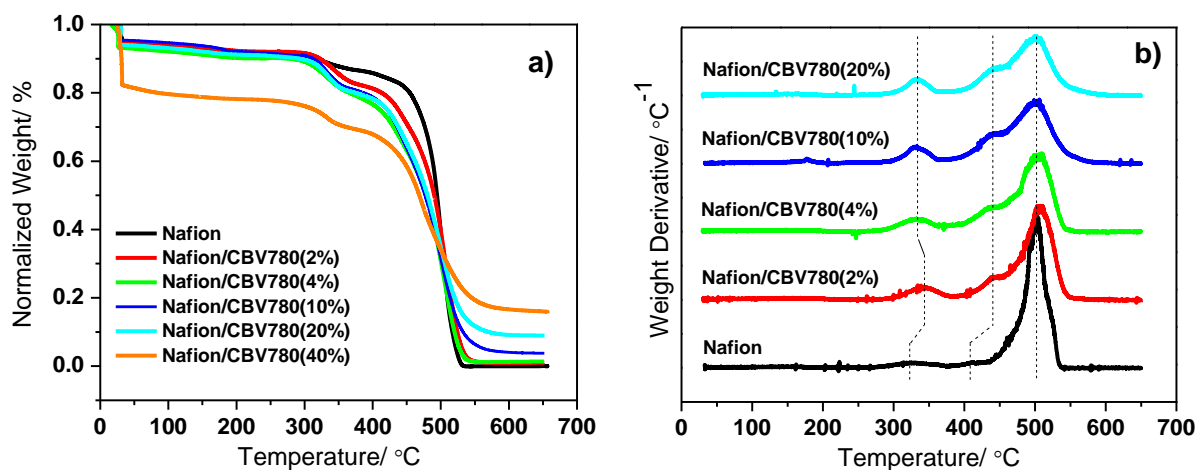


Figure 6.2: TGA (a) and selected DTG (b) diagrams for the recast Nafion and composite membranes with various zeolite contents prepared from 20 wt% Nafion dispersion.

In all thermograms there is an initial weight loss at 25°C due to water evaporation by the N₂ stream. The thermal degradation of all membranes occurs in three stages, as is commonly observed for Nafion in the H⁺ form [1-5]:

- a) a first stage between 250 °C and 380 °C, due to the decomposition of the sulfonic acid groups;
- b) a second stage between 380 °C and 450 °C, due to the ether side-chain decomposition;
- c) a third stage between 450 °C and 600 °C, due to the decomposition of the PTFE backbone.

The zeolite content is obtained from the residues found above 600°C, as CBV780 is stable in the scanned temperature range. By plotting the zeolite content after the activation treatment vs the nominal content (Figure 6.3), it was possible to observe a linear relation for both series of samples, with the slope close to 0.5 for the fitted line. The final wt% of filler is about half of the initially added zeolite wt%, the difference being due to the zeolite dealumination occurring during the treatment.

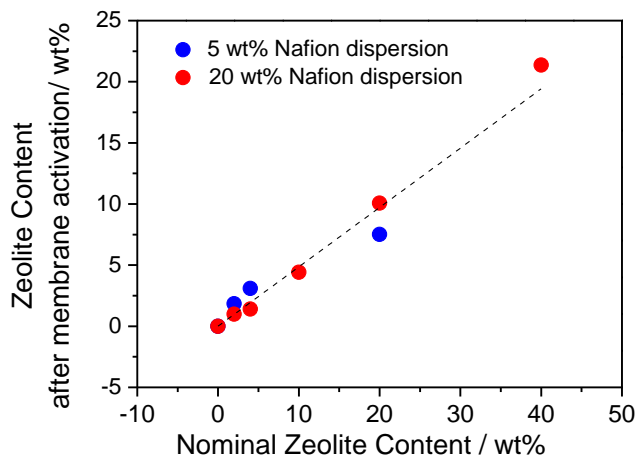


Figure 6.3: Zeolite wt% after the activation treatment vs the nominal wt% zeolite.

From the thermograms it was also possible to obtain information about the influence of the zeolite on the thermal stability of Nafion. In all composite membranes The DTG peaks (1st and 2nd stage) show a shift of between 10°C and 15°C to a higher temperature

(Fig. 6.2b). Such shift is attributed to the stabilizing H-bonding interaction between the polymer sulfonic acid groups and Si-OH functionalities on the zeolite surface [2, 3, 6]. The maximum shift is for a zeolite content of 1 wt% (nominal 2 wt%) (see Figure 6.2). This type of dependence was also observed by other authors on Nafion-SiO₂ composites [3] and it was explained by the fact that, at higher silica content, the effect of the SO₃H--SiO₂ interaction between would be more significant, weakening the C-S bond and favoring its cleavage and the decomposition of the sulfonic acid groups [7].

6.1.3. X-ray photoelectron spectroscopy

In order to complement the information obtained by TGA analysis, an XPS analysis was carried out on unfilled Nafion membranes and on the two composite membranes with the highest zeolite loading (N20_20 and N20_40).

The shape, width and number of peaks of the C1s, F1s and S2p peaks are typical of Nafion membranes and did not vary in presence of the zeolite, but the shape of the O1s and Si2p spectra of the composite membranes with the highest loading did change. The O1s and Si2p spectra of unfilled Nafion, composite membranes and dealuminated zeolite are reported in Figure 6.4 (and discussed below).

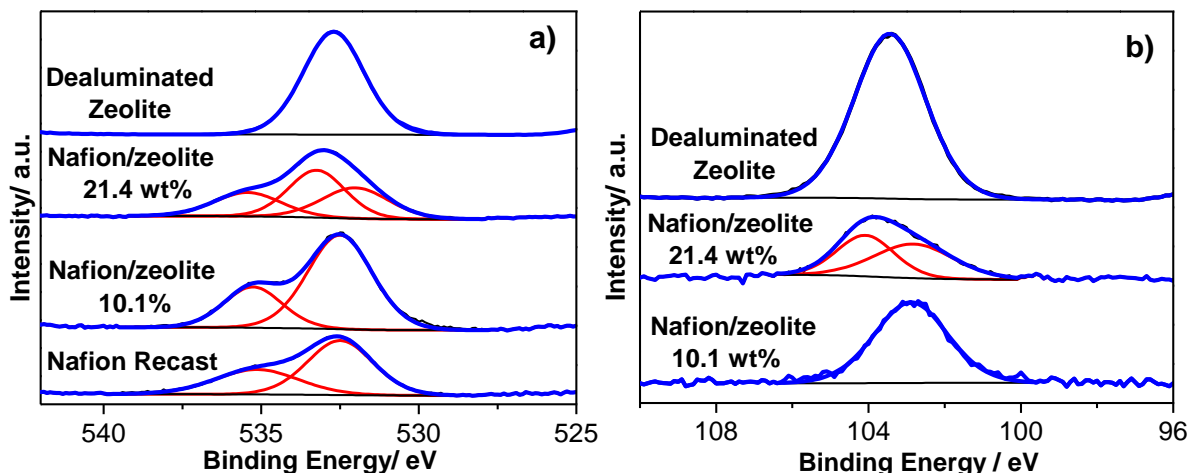


Figure 6.4: O1s (a) and Si2p (b) core level spectra of the dealuminated zeolite, recast Nafion and composite membranes N20_4 and N20_5.

Table 6.3 reports the (S/F), (O/F) and (Si/F), atomic ratios. As expected, the (O/F) and (Si/F) ratios increase with the zeolite content. A small decrease of (S/F) is observed for the composite membranes compared to the S/F in the unfilled Nafion, although this ratio should not vary with the zeolite content. This indicates a lower concentration of sulfonic acid groups on the surface of the composite membrane.

Table 6.3: (S/F), (O/F) and (Si/F) atomic ratios of recast Nafion and composite membranes with 10.1 wt% and 21.4 wt% zeolite from XPS.

Sample	S/F	O/F	Si/F
Nafion recast	0.021	0.221	-
N20_20	0.019	0.243	0.054
N20_40	0.015	0.269	0.068

The O1s spectrum of the composite membrane with the highest zeolite loading presents a third peak at 533.1 eV attributed to the oxygen ions from the zeolite network. In the Si2p spectra the presence of second peak at higher binding energy suggests an interaction between the zeolite surface and Nafion ionomer leading to a differentiation of the Si species. Such a new peak/shoulder is indicative of a strong depletion of the electron density around certain Si species, which means that the Si-O bonding became more ionic or that the Si species are surrounded by a more electronegative environment.

The shift of the O1s peak attributed to the zeolite network to higher binding energy values is consistent with the increase of the ionic character of the Si-O bond, and supports the hypothesis of the strong interaction between silanol groups and sulfonic acid groups.

A similar Si2p core level spectrum and peak separation was observed by Blanco-Brieva on a commercial fluorosulfonic acid Nafion® polymer on amorphous silica and on perfluorosulfonic acid-functionalized silica catalysts obtained from grafting 1,2,2-trifluoro-2-hydroxy-1-trifluoromethyl ethanesulfonic acid sultone onto the silica surface [8]. According to the authors this peak is indicative of an interaction between the Si and F atoms.

6.1.4. Water uptake, membrane porosity and ion exchange capacity

The water uptake of both the N5_n and N20_n series of the composite membranes was measured and the data is reported in Figure 6.5.

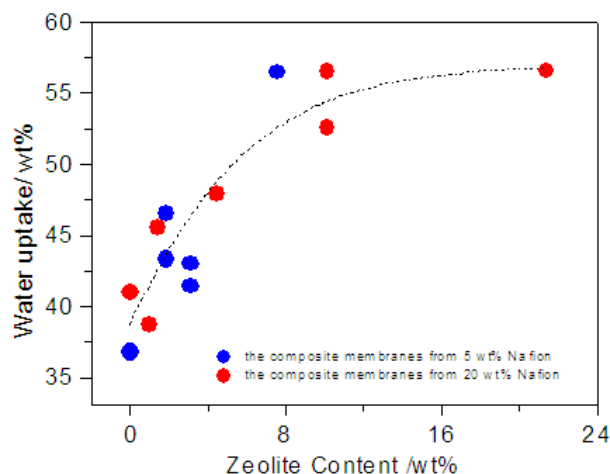


Figure 6.5: Water uptake (wt%) vs zeolite content.

The water uptake of the membranes increases linearly with the zeolite content up to 10 wt% where it reaches a maximum around 50 wt% and then it levels off.

The increase of water uptake of the composite is, in part, due to the introduction of an inorganic phase with an ionic character and a high water sorption capacity. In addition, the high water uptake is also due to the presence of defects and voids in the membrane, due to a non optimized interface between the zeolite and Nafion, and to the method used to fabricate the membranes (solution casting). The presence of defects and voids (which can accommodate a significant amount of water) was confirmed by SEM observations (Figure 6.6).

As shown in the figure, the membrane porosity is much higher when the zeolite is introduced in the matrix, and macropores in the μm range are easily seen for the membranes with the highest zeolite content. In order to estimate the contribution of the porosity of the composite and of the zeolite to the water uptake, a second and independent series of N20_n composite membranes was prepared by hot-pressing them before the activation procedure, as described in Section 2.5.2.4, Chapter 2.

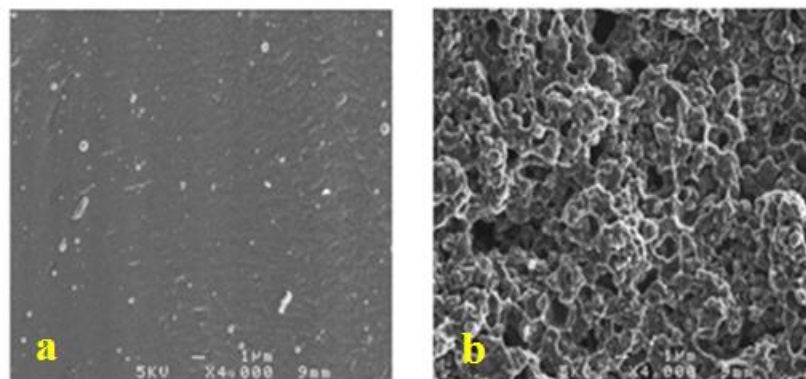


Figure 6.6: Cross-section SEM images of (a) reference Nafion (N20_0) and (b) composite Nafion and 40% zeolite (N20_40). The scale bar and the magnification in the SEM images are 1 μm and 4000 \times , respectively.

As expected, the water uptake was lower for the hot pressed composite membranes. A comparison between the water uptake of the membranes of the N20_n before and after hot-pressing is reported in Figure 6.7.

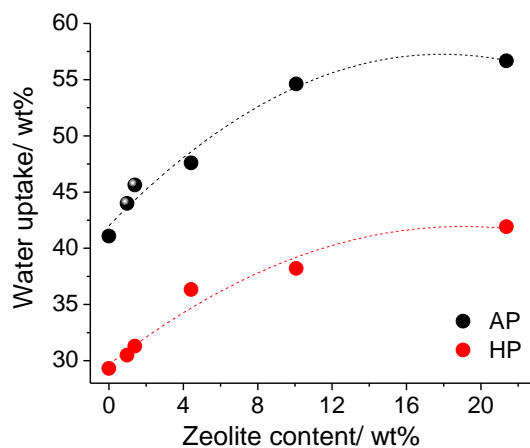


Figure 6.7: Water uptake of composite samples of the N20_n series, as prepared (AP) and after hot pressing (HP).

The loss of porosity of the composite membranes after hot-pressing was quantified from the variation of water uptake capacity as follows:

$$\% \text{ Pore loss} = \frac{(WU_b - WU_a)}{WU_b} \cdot 100$$

where WU_b and WU_a are the water uptake percentages of the composite membrane before and after hot pressing, respectively.

A pore loss between 24% and 31 % was observed for all the membranes, including the unfilled Nafion. Nevertheless, the variation of the water uptake with the zeolite content for the hot pressed membranes has the same trend as the corresponding samples before hot-pressing, with an initial increase and then leveling-off for at a zeolite content ≥ 10 wt% zeolite.

The increase of the water uptake should be proportional to the zeolite content but this is not the case for the composite membranes with the highest zeolite loading. The leveling-off at high zeolite content reflects the interaction between the zeolite hydroxyl groups and the sulfonic acid group of Nafion, as confirmed by TGA and XPS analysis. The $-\text{SO}_3\text{---H---O-Si-}$ interaction hinders the sulfonic acid groups from water coordination and the effect become significant for very high zeolite loadings in the Nafion composite membranes.

This trend was also confirmed by measuring the ion exchange capacity (IEC) of the composite membranes i.e. a measure of the number of protons available for the ion conduction. The IEC of the composite membranes as a function of the real zeolite content is reported in Figure 6.8.

As expected, a decrease of IEC was observed as a function of the zeolite content. IEC theoretical and experimental values are in good agreement, except for the highest loading of zeolite (21.4 wt%) where the experimental value (0.66 mmol g^{-1}) is lower than the theoretical value (0.76 mmol g^{-1}).

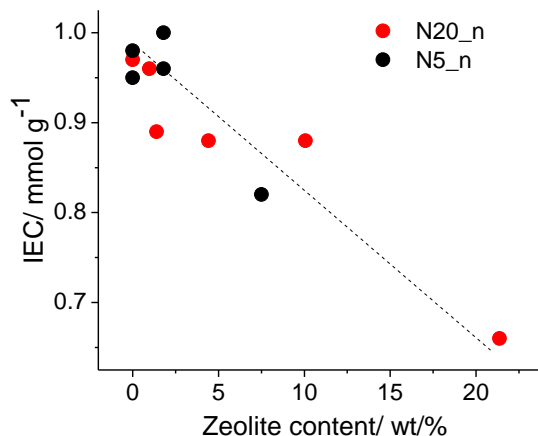


Figure 6.8: IEC as a function of the zeolite content.

The lower IEC value is in accordance with what is observed by TGA and XPS, i.e. with the fact that for a high loading of zeolite the fraction of sulfonic acid groups available is lower due to the strong interaction of the $-\text{SO}_3\text{H}$ and SiOH groups of the zeolite.

6.1.5 State of water and its mobility: DSC and DVS analysis

As already discussed in the introduction and in previous chapters, water plays an important role in the proton conduction mechanism in both Nafion and zeolites. Therefore, a high water uptake should improve the proton conductivity of composite membranes [9]. However, the different state of water, and consequently its different mobility, could contribute differently to the proton conductivity. For this reason, it is not only important to have a composite membrane with high a water uptake but also with a high percentage of mobile water. The state of water in the composite membranes was estimated both by a more classical approach, DSC (6.1.5.1), and from an analysis of the water sorption isotherms obtained by DVS (6.1.5.2).

6.1.5.1 DSC

The DSC thermograms of the unfilled Nafion and the composite membrane with 4.4 wt% of zeolite content (N20_10) are reported in Figure 6.9.

As shown in the figure, an endothermic peak attributed to freezable water (W_F) at

temperature lower than zero is present on both unfilled and composite membranes. It is also possible to notice a small difference between the melting temperatures of the two peaks. The melting temperature of freezable water for all composites of the N20_n series before and after hot-pressing is reported in Table 6.4. The melting temperature of water for the non hot-pressed membranes increases with the zeolite content. However, after hot pressing, the water melting temperature does not vary.

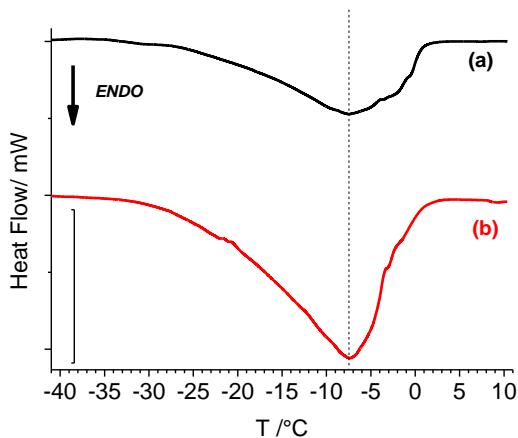


Figure 6.9: DSC thermograms of (a) unfilled Nafion and (b) composite at 4.4 wt% of zeolite content (N20_10).

Table 6.4: Melting temperature of freezable water for all composite of the N20_n series before (Non HP) and after (HP) hot-pressing.

Sample Name	Zeolite content after activation treatment / wt%	T melting / °C	
		Non HP	HP
N20_0	0	-6	-4
N20_2	1	-5	-5
N20_4	1.4	-3	-4
N20_10	4.4	-0.1	-4
N20_20	10.1	-0.2	-3
N20_40	21.4	0.01	-4

The trend observed for the not hot-pressed samples is a clear indication of the presence of non bound water trapped in the voids and defects of the composite membranes. The

contribution of this type of water almost disappears on DSC thermograms after hot-pressing due to the reduction of this macro porosity.

The freezable water content, W_F , in each sample was determined from the DSC thermograms, and it was normalized to the total water uptake (WU) as follows:

$$\theta_F = \frac{W_F}{WU} \times 100 \quad (\text{E6.1})$$

The % θ as a function of the zeolite content for the N20_n membranes before and after hot-pressing is reported in Figure 6.10.

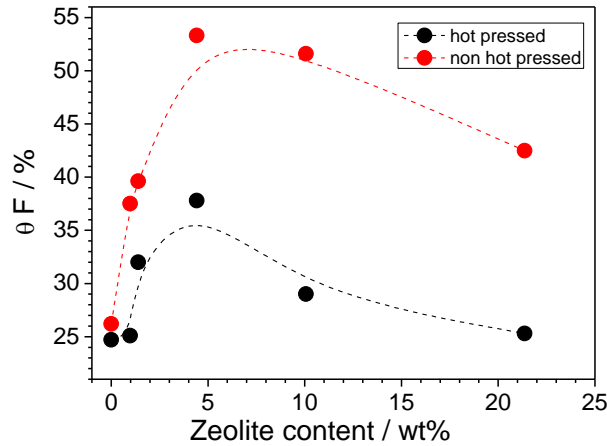


Figure 6.10: θ_F , as a function of the zeolite content for non and hot pressed membranes prepared from a 20% Nafion solution.

As shown in the figure, the $\theta_F\%$ of the non hot-pressed membranes is always higher than the $\theta_F\%$ of the hot-pressed membranes in accordance with the higher melting temperature of water found for the non hot-pressed samples. As already explained above, after hot-pressing, the macroporosity is reduced and all samples show similar water melting temperature and lower percentages of completely free water.

Figure 6.10 also shows that $\theta_F\%$ is always higher for the composite membranes with respect to Nafion with a maximum at 4.4 wt% of CBV780. Being more mobile than the other types of water in the membranes, the high percentage of freezable water is expected to promote the proton conduction, as also observed by other authors [10].

The reason for this trend of the freezable water with the zeolite content is not fully understood. Comparative DSC studies on the Faujasites and on Nafion composite membranes with the other Faujasites, other types of zeolites or fillers are necessary to better understand the role of the CBV780 on the state of water. In the meantime, water vapor sorption studies were done to complement the DSC results.

6.1.5.2 Dynamic Vapor Sorption measurements.

The different states of water in the composite membranes were also investigated by dynamic vapor sorption applying the Park model to the adsorption isotherms of the composites, as described in Paragraph 3.1.2.3, Chapter 3. The water adsorption isotherms recorded for the N20_n series, non-pressed and hot pressed are reported in Figure 6.11.

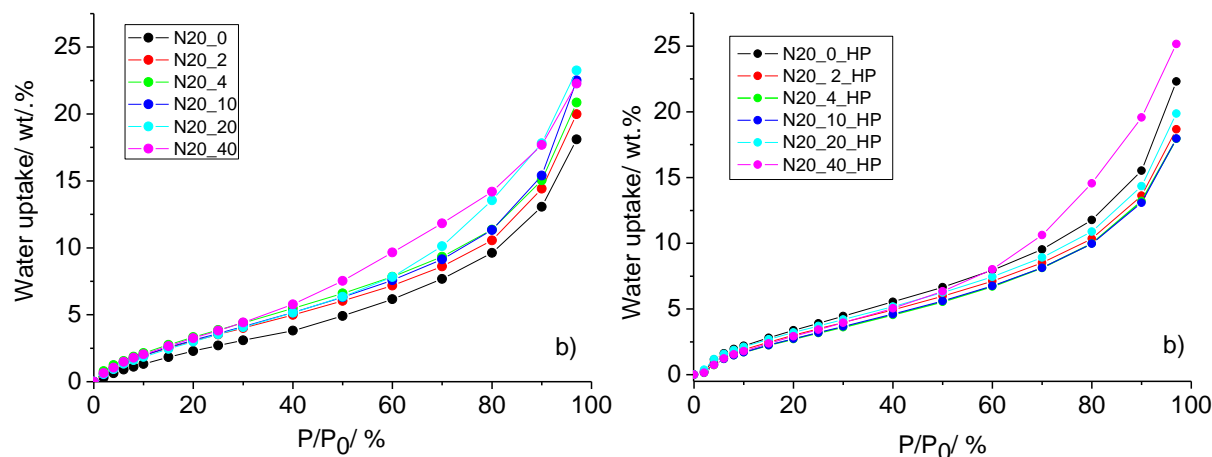


Figure 6.11: Water adsorption isotherms of N20_n composite membrane a) before and b) after hot-pressing.

By fitting the experimental data using the Park model, it was possible to determine the degree of non specific adsorbed water (θ_w [NSA]) characterized by a higher mobility, and therefore contributing more to the proton transport. Data for 97% RH is reported because this work is mainly concerned with DMFC applications requiring a high level of humidification, Figure 6.12. The θ_w [NSA] increased as a function of the zeolite content up to 1.4 wt.% and then a plateau is observed, confirming that the addition of the

CBV780 zeolite up to a certain amount increases the water mobility of the Nafion composite membranes.

For each membrane the water diffusion coefficient at 97% partial pressure was determined from the variation of the mass over time, as described in paragraph 3.1.2.2, Chapter 3. Figure 6.13 shows the diffusion coefficients as a function of the zeolite content for the hot pressed membranes.

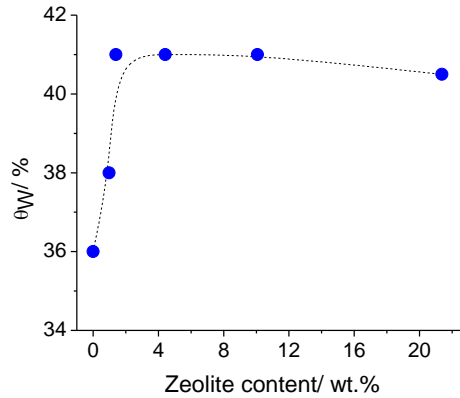


Figure 6.12: Non specific adsorbed water (θ_w [NSA]) as a function of the zeolite content at 97% P/P_0 .

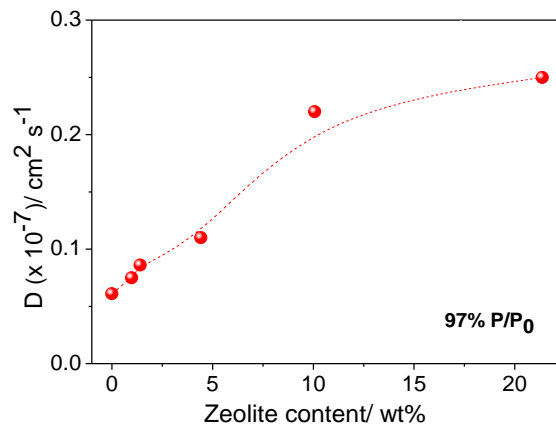


Figure 6.13: D values of Nafion/zeolite composite membranes as a function of zeolite content at 97% P/P_0 .

The diffusion coefficient values are on the order of $\sim 10^{-8} \text{ cm}^2 \text{ s}^{-1}$, in good agreement with values reported in literature for unmodified Nafion and composites determined from the vapor sorption technique [11,12]. As shown in the figure, the water diffusion coefficient

clearly increases with the zeolite content in the composite membranes, further confirming the positive effect of the introduction of this type of zeolite into the Nafion matrix.

6.1.6. Proton conductivity and fuel cell performances

The membrane proton conductivity was measured in two directions, through-plane and in-plane, and is reported in Figure 6.14a and Figure 6.14b, respectively.

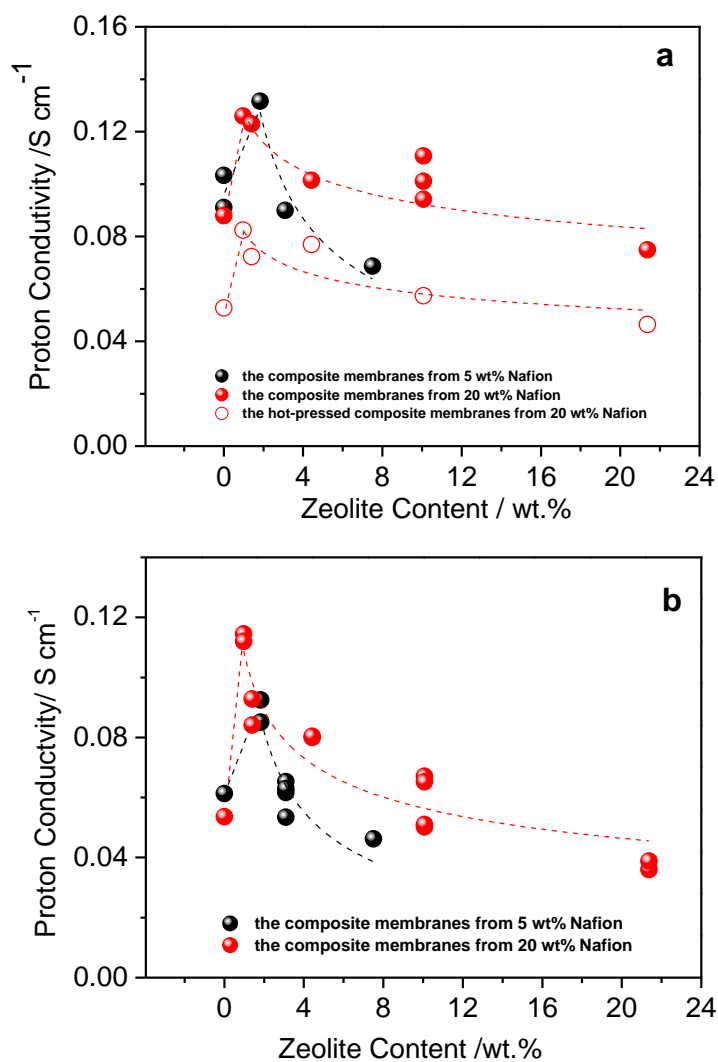


Figure 6.14: a) Through-plane and b) in-plane proton conductivity as a function of the zeolite content. The same values of in-plane proton conductivity were determined from both sides of the membranes.

The through-plane and in-plane proton conductivities show the same trend with the zeolite content, with a maximum at 1.4 wt% zeolite followed by a gradual decrease. The maximum through-plane and in-plane proton conductivity of the sample with 1.4 wt. % is 0.13 S cm^{-1} and 0.11 S cm^{-1} , respectively. These values are about 45% (TP) and 110% (IP) higher than the values measured for the unfilled Nafion membrane prepared by solution casting.

The increase of proton conductivity at low zeolite content can be ascribed to the increase of the water uptake and mobility in the membrane, as already discussed in the previous paragraphs. The decrease of the proton conductivity after the maximum can be related to the decrease of the IEC, and therefore of the proton concentration, with increasing zeolite concentration. Moreover, the interaction between $-\text{SO}_3\text{H}$ and $-\text{SiOH}$ also contributes to the reduction of the number of mobile protons available for charge transport.

Although the same trend is observed, the proton conductivity values of hot pressed membranes are lower compared to values found for the non hot pressed membranes. The decrease in proton conductivity is explained by the decrease of water uptake and mobility, after the reduction of porosity through the hot pressing procedure. Indeed, for all non hot pressed membranes, the in-plane proton conductivity is lower than the through-plane proton conductivity. Moreover, the discrepancy between through-plane and in-plane conductivity increases with the zeolite content as result of the porosity/voids in the Nafion-Faujasite membranes.

The two membranes of the N20_n series with the highest proton conductivity, N20_4 and N20_2_HP, were chosen to be tested in a DMFC, in addition to Nafion recast hot pressed and Nafion 115. The N20_4 sample was tested also before and after hot pressing. The fuel cell test of the two membranes with the same composition but different morphological characteristics aims to quantify the effect of the porosity on the DMFC performance. The DMFC tests were carried out at $40 \text{ }^\circ\text{C}$, with air at the cathode and for different methanol concentrations (between 1 and 10 M). The membrane thicknesses are reported in Table 6.5.

Table 6.5: Average membrane thickness.

Sample	Average thickness / μm
Commercial N115	130
N20_0_HP	145 \pm 10
N20_2_HP	135 \pm 10
N20_4	165 \pm 10
N20_4_HP	130 \pm 10

Figure 6.15 shows a selection of data recorded for the N20_4 membranes before and after hot-pressing: the open circuit voltage (OCV) as a function of the methanol concentration (C), the power density as a function of the current density for the two DMFCs, the cell voltage as a function of the current density, and the maximum power density as a function of the methanol concentration.

The OCV decreases with methanol concentration as expected from the high methanol crossover through Nafion-based membranes, Figure 6.15.a. In spite of its lower thickness, the cell equipped with the hot pressed membrane shows higher OCV and better performance compared to the one prepared with the non pressed membrane for all the methanol concentrations, Figure 6.15. In addition, the difference between the OCVs increases with the methanol concentration. This can be ascribed to the decreased methanol crossover [13] due to the more compact morphology of the hot pressed membrane. These results underline the importance of minimizing porosity and voids during the fabrication of composite membranes and the necessity of using a fabrication method different from solution casting. In fact, the commercial Nafion 115 prepared by extrusion has higher a OCV than the recast Nafion prepared by solution casting, Figure 6.16a.

However, the Nafion is extruded in its sulfonyl fluoride ($-\text{SO}_2\text{F}$) precursor form. When extruded, the conversion of the $-\text{SO}_2\text{F}$ into sulfonic acid groups is performed by treatment with a hot aqueous NaOH solution. This treatment would cause the dissolution of the Faujasite (Si-rich zeolite) and is therefore not applicable to these composites.

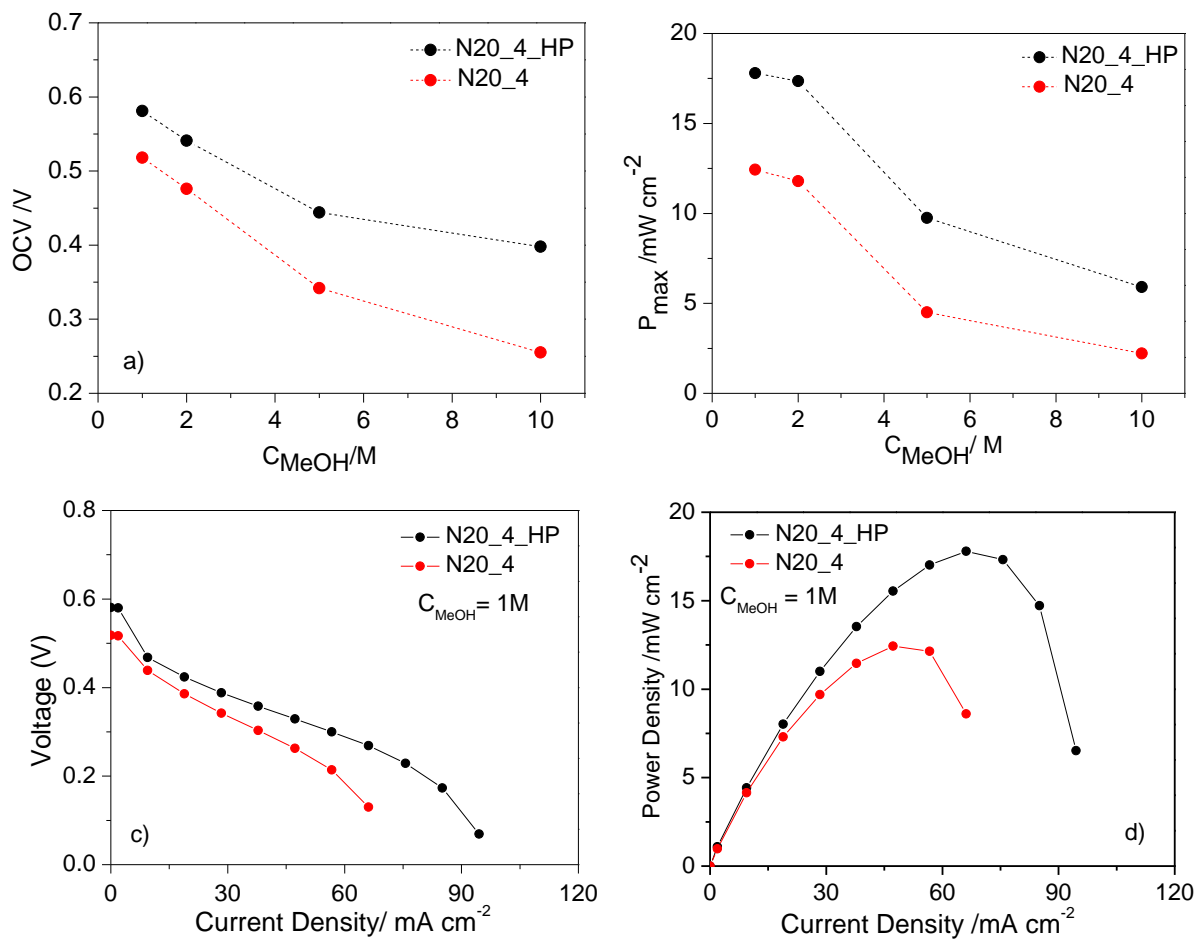


Figure 6.15: a) OCV as a function of the methanol concentration (C); b) maximum power density as a function of the methanol concentration, c) polarization curves and d) power density as a function of the current density of N20_4 before and after hot-pressing. $T = 40^{\circ}C$.

After the addition of zeolite, the OCV and performance of the fuel cells equipped with the N20_2_HP and N20_4_HP membranes improve significantly compared to the fuel cell based on the Nafion recast.

An improvement is observed in spite of the sub-optimal morphology of the composite membranes. It is believed that using a different fabrication procedure and/or by decreasing the zeolite particle size, it will be possible to achieve a better barrier to the

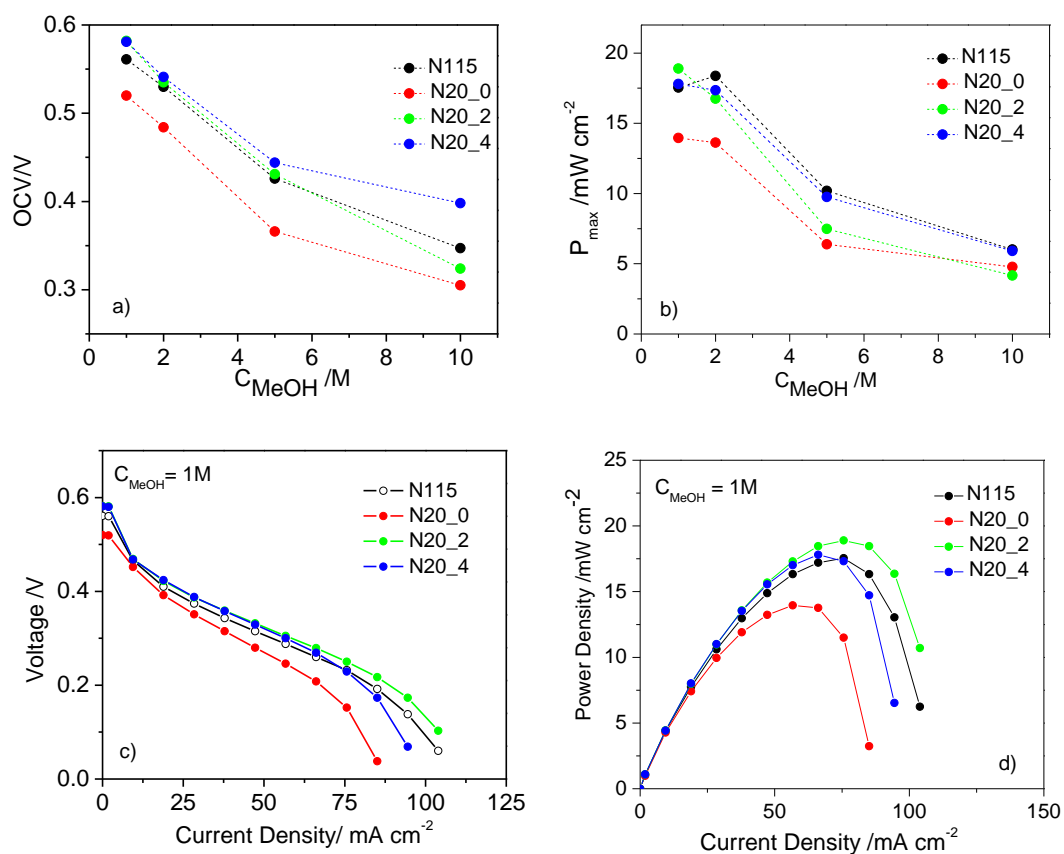


Figure 6.16: a) OCV as a function of the methanol concentration (C); b) maximum power density as a function of the methanol concentration; c) polarization curves, and d) power density as a function of the current density of commercial N115, N20_0, N20_2 and N20_4 hot-pressed. $T = 40^{\circ}\text{C}$.

methanol crossover without decreasing the proton conductivity. An alternative approach, which is being pursued, is the use of zeolites functionalized with sulfonic acid groups.

As reported in Chapter 5 there is an increase of proton conductivity of the zeolite following the introduction of sulfonic acid groups, therefore it is expected to further improve the fuel cell performance.

Nafion composite membranes were also prepared with functionalized CBV780 grafted with 70wt.% 3-MPTMS. The solution casting fabrication procedure of these membranes is described in Chapter 2. However, for the composites with functionalized zeolites it is very difficult to obtain homogeneous suspensions and membranes using the same

procedure as for Nafion-unmodified zeolite. Large agglomerates (mm size) of the zeolite particles on the recast membranes could be easily seen by eye. Some improvements in the quality of the dispersion were obtained by using dimethylacetamide (DMA) instead of isopropanol and by adding functionalized zeolite in the –SH form vs the –SO₃H form.

Table 6.6 reports the preliminary data on the physicochemical characterization (through-plane proton conductivity, σ_{TP} , water uptake, WU, and degree of freezable water, θ_F of composite membranes with 10 wt.% nominal content of functionalized zeolite. The Nafion –functionalized zeolite series was N20_Fn_HP (where N = Nafion, 20= D2021 Nafion solution, Fn the nominal wt% of functionalized zeolite, and HP is for hot pressed).

Table 6.6: Zeolite content, solvent used during the casting, zeolite - silane form during the cast procedure, through-plane proton conductivity (σ_{TP}), water uptake (%WU) and degree of freezable water (θ_F /%).

Sample name	Zeolite content	Solvent	CVB780 – silane form ¹	σ (S cm ⁻¹)	WU %	θ_F / %
N20_0_HP	0%	2-propanol	-	0.053	29.3	24.7
N20_10_HP	10%	2-propanol	-	0.077	36.3	38
N20_F10_1	10%	2-propanol	-SH	0.093	29.2	34.6
N20_F10_2	10%	DMA	-SO ₃ H	0.096	27.8	34.9
N20_F10_3	10%	DMA	-SH	0.098	28.2	39.4

¹ the conversion –SH to –SO₃H is done during the standard activation of Nafion with H₂O₂.

As seen from the data reported in Table 6.6, the zeolite functionalization improves the mobility of water and the proton conductivity of the composite membranes. In fact, the proton conductivity almost doubled with respect to unfilled recast Nafion membrane.

The membranes will be tested in DMFCs and compared with the performance obtained with the composite membranes prepared from non functionalized zeolites. Membranes with 2 wt% and 4 wt% are also under characterization.

6.1.7 Concluding remarks

Nafion – Faujasite (CBV 780) composite membranes were prepared by solution casting, and the effect of parameters such as zeolite content and final hot pressing treatment on the physicochemical properties and fuel cell performance was evaluated. The addition of the zeolite into the Nafion matrix improves the Nafion membrane properties:

1) there is a small **improvement of the thermal stability of Nafion** due to the interaction between Nafion's sulfonic acid groups and the hydroxyl groups of the zeolite, depending on the amount of filler.

2) there is an **increase of the proton conductivity** with a maximum (50-110% higher) between 1 and 4.4 wt% of zeolite content, due to the increase of the mobility of water in the fully hydrated membranes (as demonstrated by the higher water diffusion coefficient, and the higher degree of non specific adsorbed water and freezable water).

3) there is an increase of the open circuit voltage and an improvement of the DMFC performance for the membrane electrode assembly prepared with the composite membrane with 1.4 wt.% zeolite.

4) As shown by DMFC tests on composite membranes with 1.4 wt% zeolite before and after hot-pressing, **the porosity/morphology** of the membrane significantly affect the DMFC performance.. In this sense, the **solution casting procedure** is not the best because of the high porosity of the membranes. Extrusion is a preferable method, although in this specific case it was not possible to use it due to the dissolution of the zeolite in hot KOH.

5) Nafion-based composite membranes prepared with functionalized zeolites show an improvement of the water mobility and proton conductivity. The conductivity is indeed almost double. However, DMFC tests are needed to confirm the benefits of the addition of the functionalized zeolite.

6.2 Polymer-zeolite composite membranes

This part of the chapter is dedicated to the non ionomer – zeolite composite membranes. Several polymers were screened in an attempt to find the most suitable material for the fabrication of the zeolite based membrane for fuel cell applications. Other than being chemically and thermally stable at the temperature and chemical environment of DMFC operational conditions, the binders were also chosen for being impermeable to methanol. Other important considerations for the choice of a good material are its compatibility with zeolite, and its mechanical properties and processability, especially at high zeolite loadings as is desirable in this work.

6.2.1. Polyvinylidene fluoride-Zeolite composite membranes

Polyvinylidene fluoride (PVDF)-CBV780 composite membranes were fabricated by solution casting up to a zeolite loading of 80 wt%. Composite membranes with 5 wt% and 30 wt% of zeolite were also prepared using CBV780 functionalized with 12 mmol g⁻¹ of 3-MPTMS. TGA and water uptake were used to characterize the PVDF-zeolite samples.

The solution casting of the PVDF – CBV780 was difficult, due to a non-homogenous dispersion with a high tendency towards phase separation. As a consequence of the difficulty of the casting process, there was a significant loss of the inorganic phase during the composite fabrication, as confirmed by TGA analysis: about 90% and 50% of the zeolite is lost during the casting of films loaded with the as-received and functionalized CBV780, respectively. The lower loss in PVDF-functionalized zeolite composites is due to a better dispersion of the zeolite in the PVDF solution, probably favored by the higher compatibility between the alkyl chain of the silane and the hydrophobic backbone of PVDF.

The fabricated composites show poor mechanical properties mainly due to the poor adhesion between the inorganic phase and the polymer matrix. In fact, the membranes friability increases with the zeolite content. For this reason, only samples with a zeolite content between 5 wt% and 30 wt% showed adequate stiffness and could be

characterized. The water uptake of the composites before and after hot-pressing is shown in Figure 6.17.

The water uptake is, in fact, too high for a hydrophobic material as the main component. In fact, the expected contribution from the zeolite to the water uptake of the composite should be lower than 1 wt%. Clearly, the water uptake is due to the high concentration of defects and voids in the composite that make the material unsuitable for the DMFC applications, and further characterization on PVDF-zeolite composites were not carried out. Instead, a similar polymer, Teflon, and a different fabrication procedure were employed in order to increase the zeolite loading in the composites.

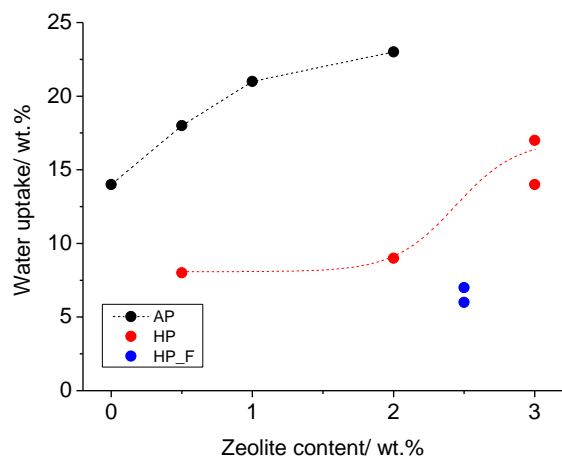


Figure 6.17: Water uptake of PVDF-zeolite composites; as-prepared (AP), after hot-pressing (HP) and hot-pressed with functionalized zeolite (F).

6.2.2 Zeolite-Teflon

Teflon-CBV780 composites were prepared using a zeolite content between 40 and 80 wt.% by mixing the zeolite with a Teflon suspension. Differently from PVDF-zeolite, the composite samples show stiffness and no loss of the inorganic phase occurs during the specific fabrication procedure. The water uptake and through-plane and in-plane proton conductivities were measured and are reported in Figure 6.18.a and Figure 6.18.b, respectively.

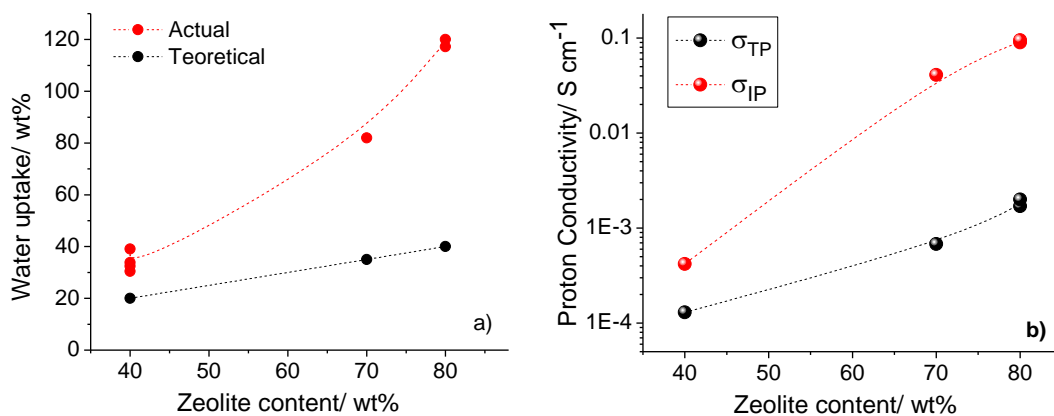


Figure 6.18: a) measured and estimated water uptake and b) through-plane and in-plane proton conductivity of the Teflon-zeolite composite as a function of the zeolite content.

As shown in Figure 6.18a, the water uptake of these membranes is very high, more than expected considering the contribution of the zeolite to the water uptake.

The significant discrepancy between the actual and theoretical values of water uptake is ascribed to the high porosity of the composites. This is also confirmed by the difference between through-plane and in-plane proton conductivity, as shown in Figure 6.18b, the former being more sensitive to the porosity. In fact, although showing a similar trend with the zeolite content, the in-plane proton conductivity is much lower than the proton conductivity measured through-plane, Figure 6.18b.

Nevertheless, there is an increase of proton conductivity with the zeolite content. Teflon is not a proton conductor and the effect of the zeolite contribution is clearly discernable in these measurements. The in-plane proton conductivity of the sample with 80 wt.% zeolite loading is of the order $10^{-3}\ cm^{-1}$, close to the proton conductivity of the zeolite powder (Chapter 5), although overestimated due to the porosity of the composite. Similar results were also obtained by Poltarzewski et al. [14] who reported a proton conductivity at room temperature on the order of $\sim 10^{-2}\ S\ cm^{-1}$ for a Teflon/ zeolite (Zeolon 100H) composite with a zeolite loading of 90 wt.%, although they observed very poor mechanical properties with this composite.

Due to the very high water uptake (120%) other composites with functionalized zeolites were not prepared.

PVDF and Teflon have similar polymer backbones and did not seem the best candidates to be used as binders for the zeolites. In addition to choosing a different binder, an alternative technique of composite membrane fabrication should be adopted to avoid the high percentage of defects and voids that would let the methanol pass through the membrane easily. For this reason, both the polymer type and the processing procedure were changed and SEBS and HDPE – zeolite composites were fabricated by a solvent-free method². The results are reported below.

6.2.3 HDPE based and SEBS based zeolite composite membranes

Two polymers, polyethylene and SEBS, were used to fabricate composite membranes with CBV780 up to a zeolite content of 60 wt%. The composites were fabricated by extrusion. A third series of composite membranes was fabricated by using a 50:50 wt% HDPE/SEBS blend. A blend of the two polymers was employed in order to achieve the optimal compromise between the rigidity of PE and the flexibility of Kraton. After a preliminary study with the as-received zeolite in order to determine the maximum zeolite content and optimal processing conditions, membranes with functionalized samples were also prepared for each series of composite, HDPE, SEBS and HDPE/SEBS.

The functionalized zeolite was mixed with the polymer in the –SH form in order to avoid the degradation of the sulfonic acid groups during the extrusion process. The –SH to –SO₃H conversion was carried out by treating the film in H₂O₂ at 50°C for 6h. Both high density polyethylene and Kraton are resistant to oxidizing agents, including H₂O₂. Nevertheless, films made of unfilled polymers, HDPE, SEBS and HDPE/SEBS were subjected to same treatment with H₂O₂. Water uptake at 97%RH, and in direct contact with liquid water, and the proton conductivity of the films before and after the treatment was measured and found to be unchanged, suggesting that the treatment does not significantly affect the polymer films.

² Although not prepared, it is not possible to exclude the possibility that the PVDF – CBV780 composite membranes prepared by extrusion would not have better properties than those obtained by solution casting.

- **High density polyethylene/ CBV780**

The high density polyethylene/CBV780 composite membranes show a very good consistency and compactness. As expected, the hydrophobic character of HDPE, its rigidity and the membranes compactness is reflected in the very low water uptake both at 97% P/P₀ and in direct contact with liquid water (Figure 6.19). In fact, the water uptake is significantly lower than that expected from the water sorption capacity of the CBV780. The result is a proton conductivity which is extremely low, much lower than the zeolite itself, even considering its proportion in the composites, 60% or lower, Figure 6.19 b. In order to improve the flexibility of the composites and their water uptake, composites with 50 wt% and 60 wt% zeolite were fabricated using SEBS and as-received and functionalized zeolites. Samples with a 50% loading of as-received and functionalized zeolites were also prepared by using a 50:50 blend of SEBS and HDPE.

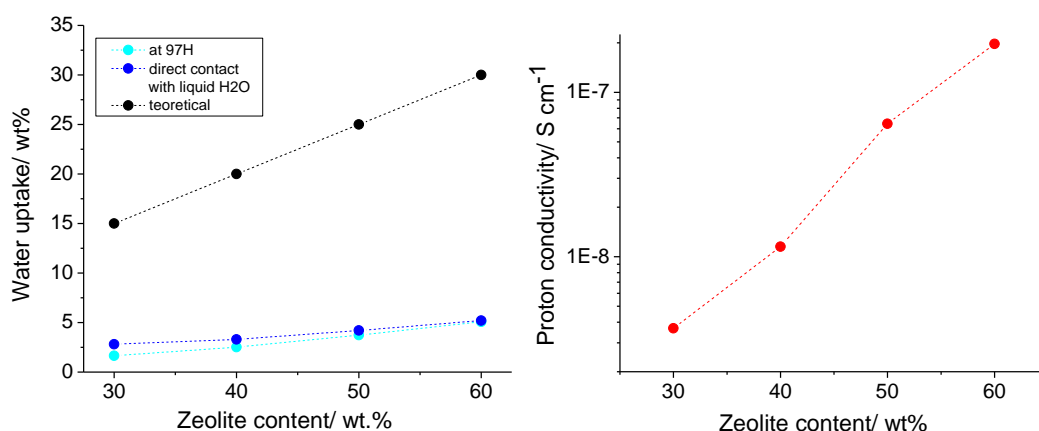


Figure 6.19: a) Water uptake of HDPE/CBV780 composite membranes measured after 48h at 97%P/P₀ and after 72h in direct contact with liquid water; estimated zeolite contribution for the water uptake is also included; b) Through-plane (TP) proton conductivity as a function of the zeolite content.

- **SEBS/ CBV780 and HDPE/SEBS/CBV780 composite membranes**

Compared to the composites with HDPE, SEBS based composites show a much higher flexibility and, similarly to the HDPE composites, they show a homogeneous dispersion

of the inorganic phase in the polymeric matrix. As expected the composite prepared with the 50:50 HDPE/SEBS blend shows an intermediate flexibility.

The water uptake at 97%RH, and in direct contact with liquid water, and the through-plane proton conductivity of HDPE, SEBS and HDPE/SEBS 50:50 composite membranes with 50% as-received and functionalized zeolite are compared in Figures 6.20, 6.21 and 6.22.

As expected, the water uptake both at 97%RH and in direct contact with liquid water of unfilled films is very low. After the addition of zeolite, the water uptake increases. The highest increase is observed for SEBS based composites and this can be explained by the higher polymer flexibility and therefore the higher capacity of the composite to accommodate water. However, the water uptake is still lower than expected from the zeolite water uptake and loading (50 wt% and 60 wt%; see Figure 6.18a).

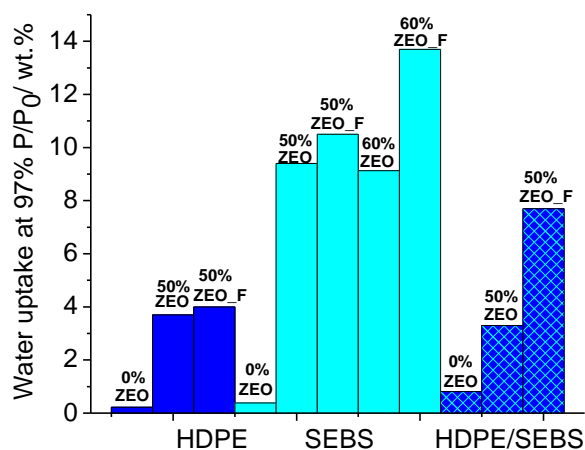


Figure 6.20: Water uptake at 97%P/P₀ of HDPE, SEBS and HDPE/SEBS composite membranes unfilled (0% ZEO) and prepared with 50 wt% and 60 wt% of unmodified and functionalized zeolite (ZEO_F).

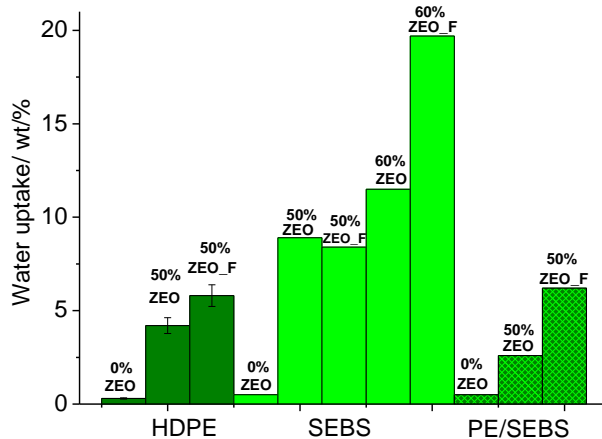


Figure 6.21: Water uptake from liquid water of HDPE, SEBS and HDPE/SEBS composite membranes unfilled (0% ZEO) and prepared with 50 wt% and 60 wt% of unmodified and of functionalized zeolite (ZEO_F).

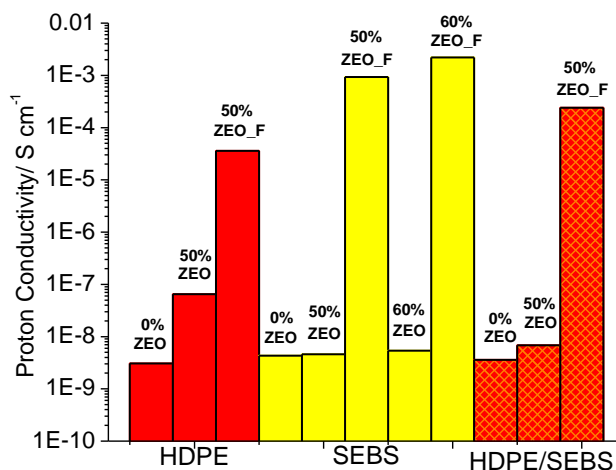


Figure 6.22: Through-plane proton conductivity of HDPE, SEBS and HDPE/SEBS composite membranes, unfilled (0% ZEO) and prepared with 50 wt% and 60 wt% of unmodified and functionalized zeolite (ZEO_F).

Therefore, the increase of water uptake with the zeolite loading in the composite membranes is ascribed to the zeolite rather than to a contribution of macroporosity or defects in the composites.

HDPE and SEBS composites with 50 wt% functionalized zeolites show comparable or slightly higher water uptakes than the composite with unmodified zeolite at equal

loading. More significant is the difference between the water uptake of composites with unmodified and functionalized zeolite at 60 wt% loading and the HDPE/SEBS blend. It has been shown that the water uptake at 97% P/P₀ of the functionalized zeolite is ~20% lower than the uptake measured for the unmodified zeolite (ZEO: 0.46 cc g⁻¹ vs ZEO_F: 0.36 cc g⁻¹; Chapter 5). Similarly to ionomers, the introduction of functional groups in a polymer matrix increases the osmotic pressure inside the film in contact with water and therefore increases the water uptake.

The proton conductivity of composites with HDPE, SEBS and HDPE/SEBS with 50% and 60% unmodified and functionalized zeolites is reported in Figure 6.22. The trend found for the proton conductivity of HDPE/zeolite and HDPE/SEBS/zeolite composites with the zeolite content and functionalization is the same as the trend observed for the water uptake, consistent with a transport of the proton assisted by the water molecules.

The effect of the functionalization on the proton conductivity is particularly significant: an improvement of almost three orders of magnitude and more than 4 orders of magnitude is found for HDPE and HDPE/SEBS composites, respectively. Although the conductivity values of the composites are of the same order of magnitude as the proton conductivity of the functionalized zeolite, such a significant increase compared to the composites with unmodified zeolite could raise the question of an overestimation of the proton conductivity due to defects in the composites.

The unmodified and functionalized zeolites have in fact a proton conductivity of the same order of magnitude. However, the water uptake data of the composites, Figures 6.20 and 6.21, exclude the hypothesis of an excessive presence of defects in the composites contributing to the increase of the proton conductivity.

The increase of proton conductivity due to the functionalization of the zeolite for the composites with SEBS is more marked than the increase of the water uptake. The addition of non-functionalized zeolite does not cause an increase of proton conductivity either at 50% or at 60% loading. However, SEBS membranes with functionalized zeolites have a much higher proton conductivity than composites with unmodified zeolites. In fact, the composite with 60 wt% of functionalized zeolite has a proton conductivity of $2.2 \times 10^{-3} \text{ S cm}^{-1}$. The effect of the sulfonic acid groups is very significant in increasing the osmotic pressure inside the composite films. The water accumulated at the interface

between the zeolite particles and the polymer matrix should be the preferred pathway for the proton conduction in the composite membranes.

6.2.4 Concluding remarks

PVDF and Teflon composites were prepared by solution casting and simple mixing of the components, respectively. These composites show however a poor mixing between components and a very high degree of porosity, as confirmed by excessively high water uptakes.

Composite membranes with HDPE, SEBS and HDPE/SEBS and a zeolite loading up to 60 wt% were prepared by extrusion. These composites are uniform and flexible. The water uptake and proton conductivity were found to vary consistently with the zeolite content, the zeolite functionalization and the nature of the binder. The highest proton conductivity, $2.2 \times 10^{-3} \text{ S cm}^{-1}$, was obtained with SEBS and 60 wt% functionalized CBV780 zeolite.

The results are promising, although further improvements and a more extensive characterization of the samples are required.

6.3 References

- [1] I. D. Stefanithis, K. A. Mauritz, 1990. "Microstructural evolution of a silicon oxide phase in a perfluorosulfonic acid ionomer by an in situ sol-gel reaction. 3. Thermal analysis studies". Macromolecules, Vol. 23 p. 2397-2402.
- [2] Q. Deng, R. B. Moore, K. A. Mauritz, 1998. "Nafion®/(SiO₂, ORMOSIL, and dimethylsiloxane) hybrids via in situ sol-gel reactions: Characterization of fundamental properties". Journal of applied Polymer Science, Vol. 68 p. 747-763.
- [3] V. Di Noto, R. Gliubizzi, E. Negro, G. Pace, 2006. "Effect of SiO₂ on Relaxation Phenomena and Mechanism of Ion Conductivity of [Nafion/(SiO₂)_x] Composite Membranes". Journal of Physical Chemistry B, Vol. 110 p. 24972-24986.
- [4] H. Park, Y. Kim, Y. S. Choi, W. H. Hong, D. Jung, 2008. "Surface chemistry and physical properties of Nafion/polypyrrole/Pt composite membrane prepared by chemical in situ polymerization for DMFC". Journal of Power Sources, Vol. 178 p. 610-619.

- [5] S. de Almeida, Y. Kawano, 1999. "Thermal behavior of Nafion membranes". Journal of Thermal Analysis and Calorimetry, Vol. 58 p. 569-577.
- [6] Q. Deng, C. A. Wilkie, R. B. Moore, K. A. Mauritz, 1998. "TGA-FTIR investigation of the thermal degradation of Nafion and Nafion/silicon oxide based nanocomposites". Polymer, Vol. 39 p. 5961-5972.
- [7] A. Collier, H. Wang, X. Yuan, J. Zhang, D. P. Wilkinson, 2006. "Degradation of polymer electrolyte membranes". International Journal of Hydrogen Energy, Vol. 31 p. 1838-1854.
- [8] G. Blanco-Brieva, J. M. Campos-Martin, M. P. de Frutos, J. L. G. Fierro, 2008. "Preparation, characterization and acidity evaluation of perfluorosulfonic acid-funzionalized silica catalysts" Industrial and Engineering Chemistry Research, Vol. 47 p. 8005-8010.
- [9] K.-D. Kreuer, A. Rabenau, W. Weppner, 1982. "Vehicle Mechanism. A new model for the interpretation of the conductivity of fast proton conductors". Angewandte Chemie International Edition, Vol. 21(3) p. 208-209.
- [10] A. Siu, J. Schmeisser, S. Holdcroft, 2006. "The Effect of Water on Low Temperature Conductivity of Polymer Electrolytes". Journal of Physical Chemistry B, Vol. 110 p. 6072-60.
- [11] D. J. Barnett, A.R. Garcia, F. Thielmann, 2006. "Measuring moisture sorption and diffusion kinetics on proton exchange membranes using a gravimetric vapor sorption apparatus". Journal of Power Sources, Vol. 160 p. 426-430.
- [12] P.W. Majsztzik, M. B. Satterfield, A. Bocarsly, J.B. Benziger, 2007. "Water sorption, desorption and transport in Nafion membranes". Journal of Membranes Science, Vol. 301, p. 93-106.
- [13] A. S. Arico, S. Srinivasan, V. Antonucci, 2001. "DMFCs: From fundamenta aspects to tecnology development". Fuel Cells, Vol. 1 p. 133-161.
- [14] Z. Połtarzewski, W. Wieczorek, J. Przyłuski, V. Antonucci, 1999. "Novel proton conducting composite electrolytes for application in methanol fuel cells". Solid State Ionics, Vol. 119 p. 301-304.

7. Conclusion

In this work, the feasibility of Faujasite-type zeolites as electrolytes for DMFC applications was evaluated as an alternative to Nafion, whose high methanol permeability significantly hampers the DMFC performance. Zeolites are solid acids with a well ordered pore system which could act as a selective barrier to the passage of methanol.

Several aspects were considered in this work, from the chemical stability of the zeolite in an acidic environment to its proton conductivity and shape selectivity. Additionally, two types of zeolite-based composite membranes, ionomer-zeolite and non ionomer -zeolite, were fabricated and characterized.

The study was carried out on three Faujasite-type zeolites differing in chemical composition (Si/Al=3.4, 16.3 and 48.7) and textural properties (530, 813 and 823 m²/g).

In order to evaluate the stability in an acidic environment, the zeolite was subjected to 6 mol dm⁻³ HCl treatment for extended times (up to 7000h). Faujasites showed a high resistance to acid attack, maintaining their crystal structure, although significant Al removal occurred. Dealumination occurred mainly during the first 24 h. As expected, the zeolite with a higher Si/Al ratio (CBV780) shows a higher stability in a strongly acidic environment, undergoing minor dealumination. Dealumination changed the textural properties of the parent zeolites, resulting in an increase of the surface area due to the formation of secondary micro- and mesoporosity. The extent of the textural modification was proportional to the extent of dealumination undergone by the zeolite. Therefore, minor changes occurred for CBV720 and CBV780. From N₂ sorption measurements, a partial collapse of the CBV600 zeolite's pore structure was observed for extended dealumination times (≥4500 h).

Dealumination, and therefore the chemical and textural modifications, significantly influenced the water sorption of the zeolites. At low relative humidity the water uptake decreases as the Al content decreases regardless of surface area, while the effect of specific surface area becomes predominant at high relative humidity. Moreover, at an equal Si/Al ratio and total pore volume, samples with a higher mesopore volume (20–60 Å) show a higher water adsorption at 90%RH. Understanding how the zeolite characteristics affect the water uptake is of great importance, due to the key role played

by water in the proton conduction mechanism in zeolites. In fact, a strong dependence of the proton conductivity of the Faujasites on the degree of hydration was found, and a difference of four orders of magnitude was observed between the proton conductivity of samples equilibrated at 10%RH and in direct contact with liquid water. In addition, samples with a higher water uptake show a higher proton conductivity at high RH, which represents a clear advantage for certain applications such as in DMFCs for which direct contact with a water/methanol solution is required. The proton conductivity was also found to depend on the textural properties of the zeolites, and a higher percentage of small pores seems to favor the proton conductivity, although the reasons for this are not clear at this point.

Differences in proton conductivity were also found between the three series of Faujasites. In spite of the lower Al content, CBV720 and CBV780 showed a proton conductivity two orders of magnitude higher than CBV600. This difference was ascribed to the higher specific surface area and capacity to accommodate water in CBV720 and CBV780, and hence to a higher proton mobility. The maximum proton conductivity measured for these zeolites was however still low ($\sim 10^{-4}$ S cm⁻¹) compared to the target value (Nafion ~ 0.1 S cm⁻¹). In order to increase the proton conductivity, the Faujasites were functionalized by the grafting of sulfonic acid groups using 3-mercaptopropyltrimethoxysilane as the coupling agent and a subsequent conversion of the mercapto groups into sulfonic acid groups by H₂O₂ treatment.

The functionalization was effective in improving the proton conductivity of the zeolites, but not to an equal extent for the three parent zeolites: while an increase of more than one order of magnitude was measured for CBV600 (high Al content, low specific surface area), the improvement for CBV720 and CBV780 was less significant. The explanation is the chemical composition of the starting zeolite. The Al in the zeolite framework seems to influence the grafting reaction by increasing the grafting yield, and also seems to stabilize the silane anchored onto the zeolite surface. Further investigation is however necessary to clarify this effect. The grafting yield seems to depend on the precursor concentration: when high concentrations of silane precursor are used, the tendency for self-polymerization of the silane could prevent the grafting onto the zeolite surface.

The surface coverage by the silane significantly reduces the zeolite porosity, decreasing the water and methanol sorption capacity. Nevertheless, sorption studies showed an appreciable increase of the selectivity towards water (vs methanol) for the functionalized samples. The silane grafting increases the barrier effect to methanol due to steric and chemical affinity constraints, without affecting to the same extent the adsorption of smaller water molecules.

Zeolite-based composite membranes were prepared with Nafion ionomer and also by dispersing the zeolite in different non-ionomer polymers impermeable to methanol. For the composite membrane fabrication a zeolite with a higher Si/Al ratio (CBV780) was chosen because it showed the highest proton conductivity and the highest chemical stability in an acidic environment.

When the zeolite was added to Nafion, an increase of the proton conductivity was measured for composite membranes with a zeolite content between 0.98 and 4.42 wt%. From DSC and DVS studies, it was observed that the zeolite addition causes an increase of the mobility of water in the fully hydrated membranes (higher water diffusion coefficient, higher degree of non specific adsorbed water and freezable water). Composite membranes also showed some suppression of the methanol crossover and consequently an improvement of the DMFC performance compared to the recast Nafion. However the improvement was not very significant compared to the commercial Nafion and this was explained in terms of the different porosity/morphology due to the different fabrication techniques. The solution casting procedure used in this work is not ideal because of the high porosity of the films due to solvent evaporation and a non-optimized Nafion/zeolite interface. Extrusion of Nafion sulfonyl fluoride precursor – zeolite composites would be a preferable method, although in this specific case it is not possible due to the dissolution of the zeolite in hot KOH.

Nafion-based composite membranes prepared with functionalized zeolites also show a higher water mobility and proton conductivity with respect to unfilled Nafion. The proton conductivity is almost double. However, DMFC tests are needed to fully confirm the benefits of the addition of the functionalized zeolite to Nafion.

In order to completely suppress the methanol crossover, and therefore to avoid Nafion or any other material permeable to methanol, several composites with non-ionomer polymers were studied:

- PVDF and Teflon composites were prepared by solution casting and simple mixing of the components, respectively. These composites show however a poor mixing between components due to the fabrication procedure, and very high values of water uptake. It is not excluded that the use of other method of fabrication could improve the properties of the composite.
- Composites membranes with HDPE, SEBS and HDPE/SEBS and a zeolite loading up to 60 wt% were prepared by extrusion. These composites are uniform and flexible. A consistent variation was found between the water uptake and proton conductivity as a function of the zeolite content, zeolite functionalization and the nature of the binder. The highest proton conductivity of $2.2 \times 10^{-3} \text{ S cm}^{-1}$ was obtained with SEBS and 60wt% functionalized CBV780 zeolite.

Although we have not attained the main objective, i.e. the fabrication of an “almost” zeolite membrane with high proton conductivity for DMFC applications, the present work was of fundamental importance to the establishment of a base line and a starting point for future work. It was shown that the zeolite can act as a selective barrier towards methanol through shape selectivity. The zeolite functionalization with sulfonic acid groups has to be fine-tuned in order to minimize the loss of surface area, the loss of water sorption capacity and the occlusion of the pore system.

Promising results were also obtained from the fabrication of composites with non-ionomer binders, although further improvements and a more extensive characterization of the samples are required.

It is really believed that an optimization of the functionalization procedure in combination with the fabrication of pinhole free, non-ionomer based composites with higher zeolite loadings (> 60wt%) could provide a novel membrane with a performance superior to Nafion 117 in a DMFC operating with concentrated methanol.

Several approaches are proposed to pursue this goal and presented as an outline for future work in the following paragraph.

7.1 Future work

The results on functionalized samples under the conditions used show that the silane grafting was not optimal, due to an excessive reduction of the surface area of the zeolite. Moreover, an increase of the number of sulfonic acid groups would be desirable.

In order to achieve this goal a different approach should be used. By performing the grafting reaction in anhydrous conditions and by replacing the trialkoxy silane used in this work with a silane with a single hydroxable group, it should be possible to preserve a higher specific surface area and larger pore size. In this way, the polymerization due to cross-linking between silane molecules and multi-layer formation should be avoided. Moreover, the use of a sulfonic acid group with a higher acidity such as phenyl sulfonic acid should also further increase the proton conductivity [1].

Two of the important aspects to be considered in future work are the optimization of the zeolite–polymer interface and an effort to further increase the zeolite loading (ideally up to 80-90 wt%). Extrusion is the preferable technique for the fabrication of pinhole free membranes, as is desirable for DMFC applications. The porosity of the current composite membranes needs to be quantified directly from gas porosity measurements. To further improve the zeolite – polymer interface and the zeolite loading, different proportions of HDPE/SEBS in the blend could be tested as well as the use of compatibilizers. The reduction of the zeolite particle size should also be explored as it is to be expected that the composites will be more compact [2] and have a higher proton conductivity (a lower percolation threshold for ion conductivity is anticipated).

7.2 References

- [1] J. C. McKeen, Y.S.Yan, M.E. Davis, 2008. “Proton conductivity of acid functionalized zeolite beta, MCM-41, and MCM-48: effect of acid strength”. Chemistry of Materials, Vol. 20, p. 5122-5124.

- [2] M. Lavorgna, L. Sansone, G. Scherillo, R. Gu, and A. P. Baker, 2011. "Transport Properties of Zeolite Na-X-Nafion Membranes: Effect of Zeolite Loadings and Particle Size". Fuel Cells, DOI: 10.1002/fuce.201000178.

Résumé

La consommation d'énergie et la dépendance aux combustibles fossiles ont crû de manière considérable au cours des ans. Des sources d'énergie alternatives sont requises pour répondre aux besoins d'énergie mondiaux et pour réduire cette dépendance aux énergies fossiles et l'émission de gaz à effet de serre. La recherche de sources d'énergie alternatives a encouragé le développement des piles à combustible qui sont des dispositifs électrochimiques qui convertissent directement l'énergie chimique d'un combustible en énergie électrique.

La pile à combustible consiste en une anode et une cathode séparées par un électrolyte. L'alimentation en combustible s'effectue à l'anode où il est oxydé, des électrons et des protons y sont produits. Les électrons sont conduits par un circuit externe jusqu'à la cathode tandis que les protons l'atteignent en traversant l'électrolyte. À la cathode, protons, électrons et O_2 (provenant d'un approvisionnement externe ou de l'air pour les dispositifs de type "air breathing") réagissent pour produire de l'eau.

L'apport de combustible s'effectuant de manière externe, la pile à combustible permet l'absence d'auto-décharge et un temps de recharge plus court en comparaison d'une batterie, tout en étant une alternative non polluante (de l'eau est produite lorsque H_2 est utilisé comme combustible) et plus efficace qu'un moteur à combustion interne [1,2,3]. Pour tous ces avantages elle a suscité beaucoup d'intérêt.

Il existe plusieurs types de piles à combustible, classés selon les types d'électrolyte et du combustible utilisé [1,2,4,5] qui trouvent des applications dans différents secteurs, depuis les véhicules spatiaux jusqu'aux petits appareils portables. Parmi les différents types, les piles à combustible à membrane échangeuse de protons (Proton Exchange Membrane Fuel Cell, PEMFC) ont reçu beaucoup d'intérêt, en particulier pour des applications portables ou dans le secteur automobile. Dans les PEMFCs, en effet, l'utilisation d'un polymère comme électrolyte représente un avantage par rapport à l'emploi d'un électrolyte liquide, en raison d'un assemblage, d'une manipulation et d'une sécurisation moins complexes et de l'absence de besoin de rechargement [1,6]. Les PEMFCs sont compactes et robustes et sont caractérisées par une importante densité de puissance, ce qui les rend idéales pour le secteur des transports. Conçues à l'origine pour

utiliser l'hydrogène comme combustible, les PEMFCs peuvent également fonctionner avec du méthanol, un combustible liquide avec une haute densité d'énergie d'ores-et-déjà disponible à bas coût. Une pile alimentée en méthanol directement à son anode est appelée une pile directe au méthanol (Direct Methanol Fuel Cell, DMFC).

L'utilisation d'un liquide comme le méthanol est beaucoup plus simple que celle de l'hydrogène et a attiré beaucoup d'intérêt vers ces dispositifs. Toutefois, la réaction d'oxydation du méthanol est plus lente et complexe que l'oxydation de l'hydrogène et la perte de combustible due à son passage de l'anode à la cathode au travers des membranes électrolytes utilisées actuellement est très significative pour ces dispositifs. Cette perméation du méthanol cause aussi, lorsque le méthanol atteint la cathode, un potentiel mixte diminuant ainsi la performance de la pile.

À l'heure actuelle l'électrolyte le plus utilisé pour les DMFCs est un ionomère d'acide perfluorosulfonique, connu par le nom sous lequel il est commercialisé par Du Pont, Nafion. De par sa structure chimique, le Nafion possède d'excellentes propriétés pour des applications en piles à combustibles : bonne stabilité chimique et thermique grâce à son squelette hydrophobe de tétrafluoroéthylène et importante conductivité protonique due à ses ramifications terminées par des groupements acides sulfoniques ($-\text{SO}_3\text{H}$)[7]. En revanche, le Nafion est très perméable au méthanol à cause de sa morphologie et du fait que le méthanol se mélange très bien à l'eau. L'eau a une place très importante dans le mécanisme de conduction des protons des membranes de Nafion, c'est pourquoi il est difficile de surmonter le problème de la perméabilité au méthanol sans affecter la conductivité protonique du Nafion.

Plusieurs solutions ont été proposées récemment pour résoudre ce problème de perméabilité du Nafion au méthanol, comme la fabrication de composites en incorporant au Nafion des charges inorganiques telles que SiO_2 [8-11], ZrO_2 [10], Al_2O_3 [10,12], TiO_2 [13,14] ou du phosphate de zirconium [15,16,17]. Toutefois, la plupart des membranes composites ont une conductivité protonique plus faible que le Nafion seul. L'utilisation d'un conducteur protonique comme charge devrait empêcher la chute de conductivité protonique du composite. Malgré cela, le passage de méthanol à travers la membrane n'est jamais complètement supprimé, le Nafion étant toujours le principal constituant de ce type de membranes composites.

Une approche plus innovante est l'utilisation d'un matériau inorganique comme conducteur protonique, créant une barrière sélective au méthanol par le contrôle de la taille des pores. Les zéolithes semblent être des matériaux adaptés à cette application. En effet, cette famille d'aluminosilicates cristallins offre de bonnes propriétés en terme de conduction ionique et un réseau de pores bien ordonnés qui pourrait agir comme barrière au passage du méthanol. Les propriétés des zéolithes dépendent de leur composition chimique (exprimée en terme de rapport Si/Al) et leur structure uniques.

Le réseau de la zéolithe peut être décrit comme des tétraèdres de AlO_4 et SiO_4 connectés les uns aux autres suivant quatre directions par la mise en commun des oxygènes. La présence d'aluminium au lieu de silicium, au centre du tétraèdre, introduit une charge négative dans le réseau. Les charges négatives sont neutralisées par un nombre adéquat de cations liés électrostatiquement au réseau et relativement libres de s'y déplacer, donnant lieu à de très bonnes propriétés d'échange d'ions et de conduction ionique [18]. En conséquence, la proportion d'aluminium dans le réseau détermine le nombre d'ions échangeables. Il affecte également l'hydrophilie et l'acidité de la surface de la zéolithe. En effet, pour chaque Al dans le réseau, un groupement de pontage hydroxyle (Al--OH--Si) est présent. Ce groupement est un site hydrophile et un acide de Brønsted [19,20]. Il détermine également la stabilité chimique de la zéolithe en environnement acide. Dans les solutions acides, l'aluminium peut être progressivement retiré du réseau d'aluminosilicate à cause de la liaison de protons aux sites basiques de Lewis [21-23]. Par conséquent la stabilité de la zéolithe envers l'attaque acide dépend fortement de sa teneur en aluminium et les zéolithes riches en Al sont ainsi moins stables en milieu acide. Au contraire, les zéolithes riches en Si sont moins stables en milieu basique. La structure des zéolithes est également unique.

Les tétraèdres d' AlO_4 et SiO_4 connectés à quatre directions sont assemblés en unités de construction secondaires qui peuvent être des polyèdres comme des cubes, des prismes hexagonaux ou des octaèdres. Ces polyèdres sont agencés pour former des structures plus complexes qui se répètent tridimensionnellement à grande échelle, créant une porosité ouverte faite de canaux et de vides de dimensions uniformes à l'échelle moléculaire. La taille de la fenêtre et des canaux représente une caractéristique importante de la zéolithe puisqu'elle contrôle la diffusion de certaines molécules plutôt que d'autres ce qui donne

lieu à une sélectivité de forme. La propriété de tamis moléculaire de la zéolithe peut jouer un rôle important pour son utilisation dans des électrolytes de piles à combustibles en bloquant le passage au méthanol sans affecter la diffusion de l'eau et par conséquent la mobilité des protons : le méthanol et l'eau ont des polarités et des diamètres moléculaires différents (0.27 nm pour l'eau et 0.38 nm pour le méthanol) [24].

Grâce à toutes ces propriétés, les zéolithes sont bien implantées dans de nombreux domaines allant de la catalyse à la détection de gaz. Ce n'est que récemment que les zéolithes ont été proposées comme matériaux pour les piles à combustibles. Différents types de zéolithes comme la mordénite, la chabazite, la clinoptilolite [25], la faujasite [26, 27] ou la H-ZSM5 [28] ont déjà été proposés comme additifs au Nafion®. Les zéolithes ont également été proposées en tant qu'électrolytes, mélangées avec un liant non ionomérique tel que le polytétrafluoroéthylène, des mélanges d'acide acrylique et oxyde de polyéthylène ou l'alcool de polyvinyle. Il a été reporté dans ces travaux de faibles diffusions du méthanol au travers des membranes composites. Bien que déjà bonne (jusqu'à 10^{-2} S cm⁻¹), la conductivité protonique de ces membranes composites est généralement inférieure à celle du Nafion [29-33]. Aucune de ces études n'a été focalisée sur l'établissement de critères de choix pour l'adaptation des propriétés de la zéolithe dans le but d'en maximiser ou augmenter la conductivité protonique, pour l'adaptation de sa sélectivité de forme et pour trouver le liant le plus compatible et le plus adéquat pour la préparation de films avec la zéolithe pour l'assemblage en pile à combustible. De plus, il est important de vérifier la stabilité chimique de la zéolithe dans l'environnement acide d'opération en pile à combustible en fonction de leur composition chimique. Bien qu'elles présentent de bonnes propriétés pour la conduction des ions, les zéolithes ont une conductivité protonique allant de 10^{-8} S cm⁻¹ en atmosphère sèche jusqu'à 10^{-3} - 10^{-2} S cm⁻¹ à température ambiante pour des matériaux complètement hydratés [34], ce qui n'est pas suffisant pour concurrencer le Nafion (0,1 S cm⁻¹ à 25°C).

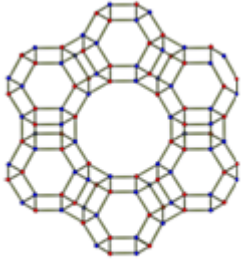
Le mécanisme de conduction ionique des zéolithes est contrôlé par différents paramètres, tels que le nombre de porteurs et leur mobilité, dépendant des propriétés chimiques de la surface de la zéolithe, du taux d'hydratation du matériau, de sa porosité [34, 35-40] et de l'interaction entre tous ces facteurs.

De plus les membranes de zéolithes elles-mêmes ont de faibles propriétés mécaniques et l'emploi d'un liant est nécessaire à l'obtention de films capables de supporter la pression et les contraintes mécaniques au cours de la préparation de l'assemblage électrodes-membrane et de l'opération de la pile à combustible. Le choix du liant, les proportions du mélange et le procédé de fabrication du composite sont autant d'aspects importants à considérer afin d'obtenir de bonnes propriétés mécaniques tout en préservant la conductivité protonique et la non-perméabilité au méthanol.

Plus de 200 types de zéolithes sont connus, naturels ou synthétiques, caractérisés par différentes structures et compositions et, par conséquent, différentes propriétés [18]. Le choix de la zéolithe la plus appropriée pour des applications en pile à combustible doit être dicté par des critères spécifiques reliés à son endurance, sa sélectivité envers le méthanol et ses propriétés de transport des protons. Une partie de ce travail de recherche a visé l'établissement de ces critères, ce qui a également contribué à le diriger vers une étude plus ciblée sur la fonctionnalisation de la surface de la zéolithe avec des groupements acides sulfoniques et sur la fabrication et la caractérisation de membranes composites.

La zéolithe de type faujasite (FAU) a été choisie comme matériau de départ pour ce travail de recherche. La structure de la FAU est caractérisée par des cages sphériques de 1,3 nm de diamètre avec quatre (plus petites) ouvertures circulaires de 0,74 nm de diamètre. Le choix des FAU plutôt qu'un autre type de zéolithe a été déterminé par leur importante taille de pores, leur surface spécifique élevée, leur réseau tridimensionnel de porosité ouverte qui permet une diffusion intra-cristalline plus rapide et par leur disponibilité commercialement en une vaste gamme de compositions chimiques [18]. Trois FAU commerciales dans la forme H^+ , CBV600, CBV720 et CBV780, (fournies par Zeolyst International) ont été étudiées. Leurs caractéristiques sont reportées dans le Tableau I.

Tableau I: Ratio molaire Si/Al, surface spécifique (S_{BET}), dimension de la cellule unitaire, volume de micropores et volume de mésopores des trois faujasites de forme H+ commerciales.

 Faujasite	FAU	Si/Al ^I	S_{BET}^{II} m ² g ⁻¹	Volume de micropores ^{II} ($< 20\text{\AA}$) cc g ⁻¹	Volume de mésopores ^{II} ($20\text{-}60\text{\AA}$) cc g ⁻¹
	CBV600	3.4	530	0.163	0.052
	CBV720	16.3	813	0.247	0.118
	CBV780	48.7	823	0.238	0.132

I : obtenu par analyse par activation neutronique; II: obtenu par adsorption de N₂

Dans ces travaux, la désalumination a été effectuée par lixiviation par du HCl 6 molaire. Le traitement acide permet de tester l'endurance des faujasites en milieu acide et, par conséquent, la faisabilité de membranes pour des PEMFCs ou des DMFCs avec ces matériaux. En outre, lorsque l'aluminium est retiré du réseau et dissous dans la solution, une modification des propriétés de texture se produit [41-43, 37]. La désalumination a ainsi pu être également employée comme moyen d'ajuster la porosité des zéolithes et d'obtenir des échantillons sur une large gamme de compositions chimiques et de propriétés texturales.

Afin d'évaluer son endurance en environnement acide, la zéolithe a été soumise à un traitement dans HCl à 6 mol dm⁻³ pour des temps prolongés (jusqu'à 7000h). Les faujasites ont montré une forte endurance à l'attaque acide en conservant leur structure cristalline, bien qu'une quantité significative d'Al en ait été retirée. La désalumination s'est produite principalement au cours des 24 premières heures et, comme il était attendu, la zéolithe avec le rapport Si/Al le plus élevé (CBV780) présente la plus importante stabilité en environnement acide fort, subissant la désalumination dans une moindre mesure. La désalumination a changé les propriétés texturales du matériau de départ : une augmentation de la surface spécifique due à la formation de micro- et mésoporosités secondaires a été observée et l'ampleur des modifications de textures a été proportionnelle

à l'ampleur de la désalumination subie par la zéolithe. Ainsi des changements mineurs se sont produits pour les zéolithes CBV720 et CBV780. D'après des mesures d'adsorption de N₂, un effondrement partiel de la structure de pores de la zéolithe CBV600 n'a été observé que pour des temps de désalumination prolongés (≥ 4500 h).

L'exposition à l'acide et par conséquent les modifications chimiques et texturales a également influencé de manière significative la sorption d'eau par la zéolithe. Il a été possible d'observer qu'à faible humidité relative la sorption d'eau diminue lorsque la proportion d'Al augmente et ce quelle que soit la surface spécifique, alors que l'effet de la surface spécifique devient prédominant à haute humidité relative. De plus, à ratio Si/Al et volume de pores total équivalents, les échantillons avec le plus haut volume mésoporeux (20–60 Å) ont la plus importante sorption d'eau à 90% RH. La compréhension de la manière dont les caractéristiques de la zéolithe affectent ses propriétés de sorption est de grande importance à cause du rôle que joue l'eau dans le mécanisme de conduction des protons dans les zéolithes, comme il a également été observé au cours de ces travaux. En effet, à partir de mesures à différents taux d'humidité relative, il a été possible d'observer une forte dépendance entre la conductivité protonique et le taux d'hydratation des échantillons de faujasite. Une différence de conductivité protonique de quatre ordres de grandeur a été mesurée entre des échantillons équilibrés à 10% d'humidité relative et en contact direct avec l'eau en phase liquide et les échantillons ayant une sorption d'eau élevée présentent une plus haute conductivité protonique à forte humidité relative. Ce comportement représente clairement un avantage pour certaines applications comme les DMFCs pour lesquelles un contact direct avec une solution d'eau et méthanol est requis. De plus, une dépendance de la conductivité protonique en fonction des propriétés structurales des zéolithes a également été trouvée et un fort pourcentage de petits pores semble favoriser la conductivité protonique, bien que les raisons n'en soient pas claires à l'heure actuelle.

Des différences de conductivité protonique ont également été observées entre la CBV600 et les CBV720 et CBV780. Bien qu'ayant une teneur en Al plus faible, les CBV720 et 780 ont une conductivité protonique plus élevée de deux ordres de grandeur que la CBV600 et cette différence a été attribuée à la plus grande surface spécifique, à une capacité d'absorption de l'eau supérieure et ainsi une plus grande mobilité pour les

protons. Le maximum de conductivité protonique qui a été mesuré pour ces zéolithes reste toutefois bas ($\sim 10^{-4}$ S cm⁻¹) en regard de l'objectif (Nafion $\sim 0,1$ S cm⁻¹).

Afin d'augmenter la conductivité protonique, les faujasites ont été fonctionnalisées par greffage de groupements acides sulfoniques par utilisation du 3-mercaptopropyltriméthoxysilane comme agent de couplage suivi d'une conversion du groupe mercapto- en groupe acide sulfonique. Les agents de couplage silaniques peuvent former des liaisons covalentes durables entre des matériaux organiques et inorganiques tout en intégrant le groupe fonctionnel désiré [44].

Des fonctionnalisations par greffage d'alkyl- et aryl-organosilanes ont déjà été reportées sur l'alumine [45] et la silice afin de les employer comme catalyseurs pour des applications industrielles [46-55], d'améliorer leur compatibilité avec les autres constituants de composites ou pour les employer comme conducteurs protoniques [56-50] avec un accroissement de la conductivité des protons allant jusqu'à deux ordres de grandeur. Plus récemment, la procédure de fonctionnalisation a également été appliquée aux zéolithes [60,61], afin d'améliorer leurs propriétés catalytiques [62,63], leurs propriétés mécaniques lorsqu'elles sont associées à des polymères dans des composites [64-69] ou bien afin de les employer dans des membranes de perméation gazeuse et des applications pour l'environnement [69-70]. Seuls quelques travaux font état de l'utilisation de zéolithes organofonctionnalisées comme électrolytes pour des piles à combustible. Bien qu'une augmentation significative de la conductivité protonique des poudres de zéolithe fonctionnalisées (par rapport à celles non modifiées) ait été reportée, des progrès supplémentaires sont requis pour que ces matériaux soient suffisamment conducteurs pour concurrencer le Nafion. Jusqu'à présent, aucun des travaux reportés dans la littérature n'a porté sur l'optimisation des conditions de fonctionnalisation et leur influence sur les propriétés de texture des zéolithes, la prise et la diffusion de solvants et leur corrélation avec la conductivité protonique et la sélectivité envers le méthanol. Afin d'établir la corrélation entre le recouvrement de la surface par les silanes et les propriétés de l'échantillon fonctionnalisé (conductivité protonique et sélectivité envers le méthanol), des paramètres tels que les propriétés chimiques de la surface du matériau initial, ses propriétés de textures et la concentration du précurseur de silane ont été contrôlés au

cours de ce travail afin d'obtenir un recouvrement maximum. Cette partie de l'étude vise à identifier les conditions de fonctionnalisation les plus adéquates à l'obtention d'un électrolyte à base de faujasite ayant une bonne conductivité protonique et une forte sélectivité de l'eau par rapport au méthanol.

L'agent de couplage silanique choisi est le 3-mercaptopropyltriméthoxysilane (3-MPTMS). Son groupe fonctionnel est le groupe mercapto (-SH) tandis qu'à l'autre extrémité de la chaîne se trouvent trois alkoxy-silanes attachés au silicium. Les groupes silanols réactifs formés par hydrolyse des groupements alkoxy-silanes condensent avec les groupes silanols à la surface des zéolithes pour former des liens covalents. Le groupe mercapto ainsi ancré à la surface de la zéolithe est alors converti en groupement acide sulfonique par oxydation par H_2O_2 [48, 71-74].

Plusieurs échantillons ont été préparés avec différentes quantités de précurseur de silane pendant 6h. La conversion de -SH en $-SO_3H$ a été effectuée par traitement dans H_2O_2 à 30% à 50°C pendant 6h. Ces conditions ont été établies par une étude préliminaire sur un échantillon greffé avec 41 mmol g^{-1} de 3-MPTMS en faisant varier le temps d'oxydation de 1h30 à 9h et la température (50°C ou température ambiante).

La fonctionnalisation a été efficace pour améliorer la conductivité protonique de la zéolithe mais pas dans des mesures équivalentes pour les trois zéolithes mères : alors qu'une augmentation de plus d'un ordre de grandeur a été mesurée pour la CBV600 (haute teneur en Al, faible surface spécifique), l'amélioration pour les CBV720 et CBV780 n'a pas été significative. La première considération concerne le choix du matériau de départ. La teneur en Al du réseau de la zéolithe semble en effet jouer un rôle dans le greffage en augmentant le rendement et aussi probablement en stabilisant l'ancrage du silane à la surface de la zéolithe, toutefois une étude supplémentaire est nécessaire.

En second rang, le rendement du greffage à la surface de la zéolithe semble dépendre de la concentration du précurseur: lorsque de fortes concentrations de précurseur de silane sont utilisées, la tendance à l'autopolymérisation du silane pourrait prévenir le greffage à la surface de la zéolithe.

Le recouvrement de la surface par le silane diminue également de manière significative la porosité de la zéolithe, affectant la sorption d'eau et de méthanol. Des études de sorption

sur des échantillons bruts tel que reçus et fonctionnalisés menées au cours de ce travail ont montré une sensible sélectivité envers l'eau et le méthanol. Le recouvrement de la surface par le silane augmente l'effet de barrière au méthanol par des contraintes stériques et d'affinité chimique, sans affecter dans la même mesure l'adsorption de molécules d'eau plus petites.

Bien que l'emploi de la zéolithe seule serait souhaitable pour mieux contrôler le flux de méthanol à travers l'électrolyte et surmonter les problèmes de stabilité thermique, ses propriétés mécaniques ne sont pas idéales pour ce type d'applications. En effet, en pile une membrane ou pastille faite de zéolithe serait trop cassante pour soutenir une quelconque contrainte. C'est pourquoi il est nécessaire d'utiliser un composite constitué de la poudre de zéolithe mélangée à un liant polymère ou un ionomère et dans lequel une synergie entre les deux composants devrait produire un matériau ayant les caractéristiques requises.

Le choix d'une bonne matrice polymère pour le composite est dicté par plusieurs exigences : naturellement, il doit être stable chimiquement et thermiquement aux conditions d'opération des PEMFCs ou DMFCs et, idéalement, il devrait être un matériau permettant la mobilité des protons mais non perméable au méthanol. Une partie du travail a également été dédiée à la fabrication de composites de faujasite avec différents matériaux (ionomère Nafion et liants polymériques) afin d'obtenir des films adaptés mécaniquement à l'utilisation dans une pile à combustible. Pour la fabrication des composites, la zéolithe ayant le ratio Si/Al le plus élevé (CBV780) a été choisie puisqu'elle avait présenté la conductivité protonique la plus élevée et la plus haute stabilité chimique en milieu acide. Plusieurs composites de Nafion ont été préparés avec la zéolithe brute telle que reçue et fonctionnalisée.

Quelques travaux reportés dans la littérature portent sur des composites de Nafion fabriqués avec des zéolithes brutes et fonctionnalisées mais la majorité de ces travaux sont focalisés sur les performances en piles à combustible. Bien que l'utilisation du Nafion ne soit pas l'objectif principal de ce travail, le Nafion reste le matériau de référence. C'est pourquoi des composites de Nafion et faujasite ont également été

préparés et caractérisés mais une attention particulière a été portée à l'étude de l'influence de la zéolithe sur la mobilité de l'eau dans les membranes composites.

Lorsqu'elle est additionnée au Nafion, une augmentation de la conductivité protonique a été mesurée pour des membranes composites avec une teneur en zéolithe entre 0,98 et 4,42% en masse. D'après les mesures par DSC et DVS, il est en effet observé que l'ajout de la zéolithe cause une augmentation de la mobilité de l'eau pour les membranes totalement hydratées (coefficient de diffusion de l'eau plus élevé, plus haut degré d'eau non spécifique adsorbée et d'eau libre congelable par mesures par DVS et DSC). Les membranes composites à base de Nafion préparées avec des échantillons fonctionnalisés montrent une évidente amélioration de la mobilité de l'eau et de la conductivité protonique. La conductivité est en effet presque doublée. Toutefois des tests en DMFC sont nécessaires pour confirmer l'intérêt de l'addition de zéolithe fonctionnalisée.

Les échantillons de composites présentent également une atténuation de la perméabilité au méthanol et par conséquent une amélioration des performances en DMFC par comparaison avec le Nafion préparé par moulage. Toutefois l'amélioration n'a pas été significative par comparaison avec le Nafion commercial et ceci a été expliqué par des différences de porosité et morphologie dues à une technique de fabrication différente. Le procédé de moulage à partir de solutions utilisé pour ce travail n'est pas idéal à cause de l'importante porosité des membranes obtenues. L'extrusion est donc une méthode préférable bien qu'elle n'ait pas été possible dans ce cas spécifique à cause de la dissolution de la zéolithe dans le KOH chaud.

L'approche plus innovatrice visée dans ce travail consiste à utiliser la zéolithe comme principal constituant du composite et un polymère non conducteur protonique et imperméable au méthanol (bien que plutôt hydrophobe également). Idéalement, la quantité de polymère devrait être aussi faible que possible. Toutefois, la préparation d'un composite où la matrice polymère est en faible proportion est souvent malaisée. Il est donc important de considérer plusieurs aspects, comme la compatibilité entre les constituants organique et inorganique; l'homogénéité du composite, ce qui implique une bonne dispersion du constituant inorganique dans la matrice polymère ; la porosité, qui est une caractéristique particulièrement importante pour les applications en pile à

combustible en affectant la séparation des réactifs. En tenant compte de ces différents points, la sélection du polymère et la méthode de fabrication peuvent jouer un rôle très important. Au cours de ce travail, plusieurs polymères ont été utilisés.

Plusieurs polymères non conducteurs protoniques ont été évalués en tant que liant pour la zéolithe. Le polytétrafluoroéthylène (PTFE), le polyfluorure de vinylidène (PVDF), le polyéthylène à haute densité (HDPE) et le polystyrène-co-éthylène-butadiène-styrène (un copolymère constitué de blocs de polystyrène et de blocs de caoutchouc).

Les composites de PVDF et Teflon ont été préparés par moulage de solutions et simple mélange des constituants, respectivement. Ces composites présentent un faible mélange entre les différents constituants du fait du procédé de fabrication. Il n'est pas exclu que l'emploi d'une autre méthode de fabrication puisse en améliorer les propriétés des membranes composites avec du HDPE et du SEBS avec un taux de zéolithe allant jusqu'à 60% en masse et préparées par extrusion présentent de meilleures consistance et flexibilité. Un composite avec un mélange 50:50 des deux polymères a également été préparé afin de trouver un compromis entre la haute rigidité du PE et la haute flexibilité du SEBS. La conductivité protonique la plus élevée de $2.2 \times 10^{-3} \text{ S cm}^{-1}$ a été obtenue avec le SEBS et 60% de zéolithe CBV780 fonctionnalisée.

Bien que nous n'ayons pas atteint notre principal objectif, c'est-à-dire la fabrication d'une membrane quasi-totalement constituée de zéolithe avec une conductivité protonique élevée pour des DMFCs, le présent travail a été d'une importance fondamentale pour établir une ligne de base et le point de départ pour de futurs travaux. Il a été montré que la zéolithe peut agir comme barrière sélective au méthanol de par une sélectivité de forme. La fonctionnalisation de la zéolithe avec des groupements acides sulfoniques doit être ajustée finement afin de minimiser la perte de surface spécifique, la perte de capacité de sorption d'eau et l'occlusion complète du système de pores.

Des résultats prometteurs ont été obtenus de la fabrication de composites avec des liants non ionomériques, bien qu'une amélioration supplémentaire et une caractérisation plus intensive des échantillons soient requises.

On peut tout-à-fait croire qu'une optimisation de la procédure de fonctionnalisation conjointement à la fabrication de composites à base non ionomérique avec un taux de zéolithe plus important (>60% en masse) et sans porosité pourraient aboutir à une nouvelle membrane ayant des performances supérieures à celles du Nafion 117 dans une DMFC fonctionnant avec du méthanol concentré.

Plusieurs approches sont proposées pour la poursuite de cet objectif et présentées comme une vue d'ensemble de travaux futurs dans le paragraphe suivant.

Les résultats obtenus sur les échantillons fonctionnalisés dans les conditions utilisées montrent que le recouvrement de la surface par greffage de silane n'est pas optimal, à cause d'une réduction excessive de la surface spécifique de la zéolithe. De plus, une augmentation du nombre de groupements acides sulfoniques serait souhaitable.

Afin de parvenir à cet objectif, une approche différente devrait être employée. En effectuant la réaction de greffage en conditions anhydres et en remplaçant le trialkoxy silane utilisé pendant ces travaux par un silane ayant un seul groupe hydrolysable, il devrait être possible de préserver une surface spécifique plus élevée et une plus grande taille de pores. De cette manière, la polymérisation due à des liaisons entre les molécules de silane et la formation de multicouches devraient être évitées. De plus, l'utilisation de groupes acides sulfoniques ayant une acidité plus élevée comme les groupements acides phénylesulfoniques devrait également augmenter encore la conductivité protonique [75].

Deux autres aspects importants à prendre en compte dans des travaux futurs sont l'optimisation de l'interface entre la zéolithe et le polymère et, simultanément, l'accroissement du taux de zéolithe (idéalement jusqu'à 80-90% en masse). L'extrusion est la technique préférable pour la fabrication de membranes sans porosité, comme il est souhaitable pour l'application en DMFC. Tout d'abord la porosité des membranes composites actuelles doit être quantifiée directement par des mesures de perméabilité à des gaz. Afin d'améliorer encore l'interface entre la zéolithe et le polymère et le taux de zéolithe, différentes proportions de HDPE et SEBS pourraient être testées dans le mélange, ainsi que l'emploi d'agents compatibilisants. La réduction de la taille des particules de zéolithe devrait également être explorée puisqu'il est attendu que les

composites seraient plus compacts [76] et auraient une conductivité protonique plus élevée (un seuil de percolation plus faible pour la conductivité ionique est escompté).

References

- [1] J. Larminie and A. Dicks, 2003. Fuel cell Systems Explained. 2nd Edition, England, John Wiley & Sons Ltd.
- [2] Fuel Cell Handbook. 7 ed. 2004. Morgantown: EG&G Technicals Services, Inc., Science Applications International Corporation.
- [3] M. Winter and R. J. Brodd, 2004. «What Are Batteries, Fuel Cells, and Supercapacitors?». Chemical Reviews, Vol. 104, p. 4245-4269.
- [4] J. M. Andu´ jar and F. Segura, 2009. «Fuel cells: History and updating. A walk along two centuries». Renewable and Sustainable Energy Reviews, Vol. 13, p. 2309–2322.
- [5] A. Kirubakaran , Shailendra Jain and R.K. Nema, 2009. «A review on fuel cell technologies and power electronic interface». Renewable and Sustainable Energy Reviews, Vol. 13, p. 2430-2440.
- [6] L. Carrette, K. A. Friedrich and U. Stimming, 2001. «Fuel Cells-Fundamental and Applications». Fuel Cells, Vol. 1 (1), p. 5-39.
- [7] K. A. Mauritz and R. B. Moore, 2004. «State of Understanding of Nafion». Chemical Reviews, Vol. 104, p. 4535-4585.
- [8] A. M. Herring, 2006. «Inorganic-Polymer Composite Membranes for Proton Exchange Membrane Fuel Cells». Polymer Reviews, Vol. 46 (3), p. 245-296
- [9] B. Baradie, J. P. Dodelet and D. Guay, 2000. «Hybrid Nafion-inorganic membrane with potential applications for polymer electrolyte fuel cells». Electroanalytical Chemistry, Vol. 489, p. 101-105.
- [10] A. S. Arico, V. Baglio, A. Di Blasi, P. Creti, P. L. Antonucci and V. Antonucci, 2003. «Influence of the acid-base characteristics of inorganic fillers on the high temperature performance of composite membranes in direct methanol fuel cells». Solid State Ionics, Vol. 161, p. 251-265.
- [11] W. L. Xu, T. H. Lu, C. P. Liu and W. Xing, 2005. «Low methanol permeable composite Nafion/silica/PWA membranes for low temperature direct methanol fuel cells». Electrochimica Acta, Vol. 50, p. 3280-3285.

- [12] K. A. Mauritz, 1998. «Organic-inorganic hybrid materials: perfluorinated ionomers as sol-gel polymerization templates for inorganic alkoxides». Materials Science and Engineering: C, Vol. 6, p. 121-133.
- [13] H. Uchida, Y. Ueno, H. Hagihara, M. Watanabe, 2003. «Self-Humidifying Electrolyte Membranes for Fuel Cells». Journal of Electrochemical Society, Vol. 150, p. A57-A62.
- [14] A. Sacca, A. Carbone, E. Passalacqua, A. D'Epifanio, S. Licoccia, E. Traversa, E. Sala, F. Traini and R. Ornelas, 2005. «Nafion-TiO₂ hybrid membranes for medium temperature polymer electrolyte fuel cells (PEFCs)». Journal of Power Sources, Vol. 152, p. 16-21.
- [15] F. Damay and L. C. Klein, 2003. «Transport properties of Nafion(TM) composite membranes for proton-exchange membranes fuel cells». Solid State Ionics, Vol.162-163, p. 261-267.
- [16] H. C. Kuan, C. S. Wu, C. Y. Chen, Z. Z. Yu, A. Dasari and Y. W. Mai, 2006. «Preparation of Exfoliated Zirconium Phosphate/Nafion Organic-Inorganic Hybrid Proton Exchange Membranes». Electrochemical and Solid-State Letters, Vol. 9, p. A76-A79.
- [17] A. K. Sahu, S. Pitchumani, P. Sridhar and A. K. Shukla, 2009. «Co-assembly of a Nafion-Mesoporous Zirconium Phosphate Composite Membrane for PEM Fuel Cells». Fuel Cells, Vol. 9, p. 139-147.
- [18] H. van Bekkum, E. M. Flanigen, J. C. Jansen, “Introduction to Zeolite Science and Practice”, Elsevier Science Publishers B. V., 1991, p. 18.
- [19] A.L. Blumenfeld, J.J. Fripiat, 1999. «Characterization of Brønsted and Lewis acidity in zeolites by solid-state NMR and the recent progress in the REDOR technique». Magnetic Resonance in Chemistry, Vol. 37, p. S118-S125.
- [20] R.A. Van Santen, 1994. «Theory of Brønsted acidity in zeolites». Advanced Zeolite Science and Applications, Vol. 85, p. 273-294.
- [21] M. Rožić, Š. Cerjan-Stefanović, S. Kurajica, M. Rožmarić Mačefat, K. Margeta and A. Farkaš, 2005. «Decationization and dealumination of clinoptilolite tuff and ammonium exchange on acid-modified tuff». Journal of Colloid and Interface Science, Vol. 284, p. 48-56.
- [22] A. De Lucas, P. Canizares, A. Durán and A. Carrero, 1997. «Dealumination of HZSM-5 zeolites: Effect of steaming on acidity and aromatization activity». Applied Catalysts A: General, Vol. 154 (1-2,) p. 221-240.
- [23] R. M. Ravenelle, F. Schüßler, A. D'Amico, N. Danilina, J. A. Van Bokhoven, J. A.

- Lercher, C. W. Jones, C. Sievers, 2010. «Stability of zeolites in hot liquid water». *Journal of Physical Chemistry C*, Vol. 114, p. 19582-19595.
- [24] E. P. Ivanova, M.A. Kostova, B.K. Koumanova, 2010. «kinetics of water and alcohol vapors adsorption on natural zeolite». *Asia-Pacific Journal of Chemical Engineering*, Vol. 5, p. 869-881.
- [25] V. Baglio, A. S. Aricò, A. Di Blasi, P. L. Antonucci, F. Nannetti, V. Tricoli and V. Antonucci, 2005. «Zeolite-based Composite Membranes for High Temperature Direct Methanol Fuel Cells». *Journal of Applied Electrochemistry*, Vol. 35, p. 207-212.
- [26] P. Kongkachuichay and S. Pimprom, 2010. «Nafion/Analcime and Nafion/Faujasite Composite Membranes for Polymer Electrolyte Membrane Fuel Cells». *Chemical Engineering Research and Design*, Vol. 88, p. 496.
- [27] Z. Zhang, F. Desilets, V. Felice, B. Mecheri, S. Licoccia, A. C. Tavares, 2011. «On the Proton Conductivity of Nafion-Faujasite Composite Membranes for Low Temperature Direct Methanol Fuel Cells». *Journal of Power Sources*, Vol. 196 (22), p. 9176-9187.
- [28] M. H. Yildirim, A. Roca Curo, J. Motuzas, A. Julbe, D. F. Stamatialis and M. Wessling, 2009. «Nafion/H-ZSM-5 Composite Membranes with Superior Performance for Direct Methanol Fuel Cells». *Journal of Membrane Science*, Vol. 338, p. 75-83.
- [29] Z. Połtarzewski, W. Wieczorek, J. Przyłuski and V. Antonucci, 1999. «Novel Proton Conducting Composite Electrolytes for Application in Methanol Fuel Cells». *Solid State Ionics*, Vol. 119, p. 301-304.
- [30] B. Libby, W.H. Smyrl and E.L. Cussler, 2003. «Polymer-Zeolite Composite Membranes for Direct Methanol Fuel Cells». *AIChE Journal*, Vol. 49, p. 991-1001.
- [31] J. Kjær, S. Yde-Andersen, N. A. Knudsen and E. Skou, 1991. «Solid State Electrolyte Membranes for Direct Methanol Fuel Cells». *Solid State Ionics*, Vol. 46, p. 169-173.
- [32] N. Rao, T. P. Andersen and P. Ge, 1994. «Tin mordenite membranes for direct methanol fuel cells ». *Solid State Ionics* Vol. 72, p. 334-337.
- [33] T. Sancho, J. Lemus, M. Urbiztondo, J. Soler and M. P. Pina, 2008. «Zeolites and Zeotype Materials as Efficient Barriers for Methanol Cross-over in DMFCs». *Microporous and Mesoporous Materials*, Vol. 115, p. 206-213.

- [34] S.D.Mikhailenko, S.Kaliaguine, E.Ghali, 1997. «Water-assisted ionic conductance of zeolites with ZSM-5 structure». Microporous Materials, Vol.11, p. 37-44.
- [35] M.E. Franke, U. Simon, 1999. «Proton mobility in H-ZSM5 studied by impedance spectroscopy». Solid State Ionics, Vol. 118, p. 311-316.
- [36] P. Nischwitz, P. Amels, F. Fetting 1994. «Studies on the ionic conductivity of zeolitic solids». Solid State ionics, Vol. 73, p. 105-118.
- [37] V. Felice, A.C.Tavares, 2011. «Faujasite zeolite as solid electrolyte for low temperature fuel cells». Solid State Ionics, Vol. 194 (1), p. 53-61.
- [38] M. S. Whittingham, A.J. Jacobson, *Intercalation chemistry* 1982, Academic Press, New York.
- [39] M. Dekker, I. 't Zand, J. Schram, J. Schoonman, 1989. «NH₄Y and HY zeolites as electrolytes in hydrogen sensors». Solid State Ionics, Vol. 35, p. 157-164.
- [40] N. H. Mogensen, E. Skou, 1995. «Effect of salvation of charge carriers in hydrated zeolites». Solid State Ionics, Vol. 77, p. 51-54.
- [41] J. Lynch, F. Raatz, P. Dufresne, 1987. «Characterization of the textural properties of dealuminated HY forms». Zeolite, Vol. 7, p. 333-338.
- [42] A. Zukal, V. Patzelova, U. Lohse, 1986. «Secondary porous structure of dealuminated Y zeolites». Zeolites, Vol. 6 (2), p. 133-136.
- [43] T. Kawai and K. Tsutsumi, 1999. «A Study on the Surface Silanol Groups Developed by Hydrothermal and Acid Treatment of Faujasite Type Zeolites». Journal of Colloid and Interface Science, Vol. 212, p. 310-316.
- [44] B. Arkles, G.Larson, *Silicon compounds: Silanes and Silicones* 2004, Morrisville, PA, Gelest, Inc.
- [45] V. Smuleac, D.A. Butterfield, S.K. Sikdar, R. S. Varma, D. Bhattacharyya, 2005. «Polythiol-functionalized alumina membranes for mercury capture». Journal of Membrane Science, Vol. 251, p. 169-178.
- [46] S.-E. Park, Sujandi, 2008. «Green approaches via nanocatalysis with nanoporous materials: Functionalization of mesoporous materials for single site catalysis». Current Applied Physics, Vol. 8, p. 664-668.
- [47] B. Sow, S. Hamoudi, M.H. Zahedi-Niaki, S. Kaliaguine, 2005. «1-Butanol etherification over sulfonated mesoporous silica and organo-silica». Microporous and Mesoporous Materials, Vol.79, p. 129-136.

- [48] S. Sreevardhan Reddy, B. D. Raju, V.Siva Kumar, A.H. Padmasri, S. Narayanan, K. S. Rama Rao, 2007. «Sulfonic acid functionalized mesoporous SBA-15 for selective synthesis of 4-phenyl-1,3-dioxane». Catalysis Communications, Vol. 8, p. 261-266.
- [49] C. S.Gill, B.A.Price, C.W.Jones, 2007. «Sulfonic acid-functionalized silica-coated magnetic nanoparticle catalysts». Journal of Catalysis, Vol. 251, p. 145-152.
- [50] I. Diaz, C. Marquez-Alvarez, F. Mohino, J. Perez-Pariente, E. Sastre, 2000. «Combined alkyl and sulfonic acid functionalization of MCM-41-Type silica: Part 1. Synthesis and Characterization». Journal of Catalysis, Vol. 193, p. 283-294.
- [51] M. Boveri, J. Aguilar-Pliego, J. Pérez-Periente, E. Sastre, 2005. «Optimization of the preparation method of HSO₃-functionalized MCM-41 solid catalysts». Catalysis Today, Vol. 107-108, p. 868-873.
- [52] B. Rác, M. Nagy, I. Pálinkó, Á. Molnár, 2007. «Application of sulfonic acid functionalized MCM-41 materials—Selectivity changes in various probe reactions». Applied Catalysis A: General, Vol. 316, p. 152-159.
- [53] W. D. Bossaert, D.E. DeVos, W. M. Van Rhijn, J. Bullen, P.J. Grobet, P.A. Jacobs, 1999. «Mesoporous Sulfonic Acids as selective heterogeneous catalysts for synthesis of monoglycerides». Journal of Catalysis, Vol. 182, p. 156-164.
- [54] E. Cano-Serrano, G. Blanco-Brieva, J. M. Campos-Martin, J. L. G. Fierro, 2003. «Acid-Functionalized amorphous silica by chemical grafting-quantitative oxidation of thiol groups». Langmuir, Vol. 19, p. 7621-7627.
- [55] W. M. Van Rhijn, D. E. De Vos, B. F. Sels, W. D. Bossaert, P. A. Jacobs, 1998. «Sulfonic acid functionalised ordered mesoporous materials as catalysts for condensation and esterification reactions». Chemical Communications, p. 317-318.
- [56] S. Mikhailenko, D. Desplandier-Giscard, C. Danumah, S. Kaliaguine, 2002. «Solid electrolyte properties of sulfonic acid functionalized mesostructured porous silica». Microporous and Mesoporous Materials, Vol. 52, p. 29-37.
- [57] H. Munakata, H. Chiba, K. Kanamura, 2005. «Enhancement on proton conductivity of inorganic-organic composite electrolyte membrane by addition of sulfonic acid group». Solid State Ionics, Vol. 176, p. 2445-2450.
- [58] R. Marschall, I. Bannat, J. Caro, M. Wark, 2007. «Proton conductivity of sulfonic acid functionalized mesoporous materials». Microporous and Mesoporous Materials, Vol. 99, p. 190-196.

- [59] S. Hamoudi, S. Royer, S. Kaliaguine, 2004. «Propyl- and arene-sulfonic acid functionalized periodic mesoporous organosilicas». Microporous and Mesoporous Materials, Vol. 71, p. 17-25.
- [60] W. Song, J. F. Woodworth, V. H. Grassian, S.C. Larsen, 2005. «Microscopic and Macroscopic Characterization of Organosilane-Functionalized Nanocrystalline NaZSM-5». Langmuir, Vol. 21, p. 7009-7014.
- [61] B.-Z. Zhan, M.A. White, M. Lumsden, 2003. «Bonding of organic amino, vinyl, and acryl groups to nanometer-sized NaX zeolite crystal surfaces ». Langmuir, Vol. 19, p. 4205-4210.
- [62] J. C. McKeen, Y. S. Yan, M.E. Davis, 2008. «Proton Conductivity of Acid-Functionalized Zeolite Beta, MCM-41, and MCM-48: Effect of Acid Strength». Chemistry of Materials, Vol. 20, p. 5122-5124.
- [63] C.W. Jones, K. Tsuji, M. E. Davis, 1998. «Organic-functionalized molecular sieves as shape-selective catalysts». Nature, Vol. 393, p. 52.
- [64] D. Metin, F. Tihminlioglu, D. Balköse, S. Ülkü, 2004. «The effect of interfacial interactions on the mechanical properties of polypropylene/natural zeolite composites». Composite Part A, Vol. 35, p. 23-32.
- [65] X. Li, E. P. L. Roberts, S. M. Holmes, V. Zholobenko, 2007. «Functionalized zeolite A-nafion composite membranes for direct methanol fuel cells». Solid State Ionics, Vol. 178, p. 1248-1255.
- [66] B. A. Holmberg, X. Wang, Y. Yan, 2008. «Nanocomposite fuel cell membranes based on Nafion and acid functionalized zeolite beta nanocrystals». Journal of Membranes Science, Vol. 320, p. 86-92.
- [67] Y. Li, H. M. Guan, T.-S. Chung, S. Kulprathipanja, 2006. «Effects of novel silane modification of zeolite surface on polymer chain rigidification and partial pore blockage in polyethersulfone (PES)–zeolite. A mixed matrix membranes». Journal of Membranes Science, Vol. 275, p. 17-28.
- [68] Z. Chen, B. Holmberg, W. Li, X. Wang, W. Deng, R. Munoz, Y. Yan, 2006. «Nafion/Zeolite nanocomposite membrane by in Situ Crystallization for a direct methanol fuel cell». Chemistry of Materials, Vol. 18, p. 5669-5675.
- [69] P. Huttenloch, K. E. Roehl, K. Czurda, 2001. « Sorption of nonpolar aromatic contaminants by chlorosilane surface modified natural minerals». Environmental Science and Technology, Vol. 35 (21), p. 4260-4264.

- [70] W. Song, G. Li, V. H. Grassian, S. C. Larsen, 2005. «Development of Improved materials for environmental applications: Nanocrystalline NaY zeolites». Environmental Science and Technology, Vol. 39, p. 1214-1220.
- [71] M.Chidambaram, C.Venkatesan, A.P. Singh, 2006. «Organosilanesulfonic acid functionalized Zr-TMS catalysts: Synthesis, characterization and catalytic applications in condensation reactions». Applied Catalysis A: General, Vol. 310, p.79–90.
- [72] T.J. Horr, P.S. Arora, 1997. «Determination of the acid-base properties for 3-amino 3-chloro and 3-mercaptopropyltrimethoxysilane coatings on silica surfaces by XPS». Colloids and Surfaces A: Physicochemical and Engineering Aspects, Vol. 126 (2-3), p. 113.
- [73] C. Wu, T. Xu, W. Yang, 2003. «A new inorganic–organic negatively charged membrane: membrane preparation and characterizations». Journal of Membrane Science Vol. 224, p.117-125.
- [74] B. Rać, A. Molnar, P. Forgo, M. Mohai, I. Bertóti, 2006. «A comparative study of solid sulfonic acid catalysts based on various ordered mesoporous silica materials». Journal of Molecular Catalysis A: Chemical, Vol. 244, p. 46–57.
- [75] J.C. McKeen, Y.S. Yan, M.E. Davis, 2008. «Proton conductivity of acid-functionalized zeolite beta, MCM-41, and MCM-48: effect of acid strength». Chemistry of Materials, Vol. 20, p. 5122-5124.
- [76] M. Lavorgna, L. Sansone, G. Scherillo, R. Gu, and A. P. Baker, 2011. «Transport Properties of Zeolite Na-X–Nafion Membranes: Effect of Zeolite Loadings and Particle Size». Fuel Cells, DOI: 10.1002/fuce.201000178.